

# Elastic and Inelastic Pion Reactions on Few Nucleon Systems

Dissertation

zur Erlangung des Doktorgrades (Dr. rer. nat.)  
der Mathematisch–Naturwissenschaftlichen Fakultät  
des Rheinischen Friedrich-Wilhelms–Universität Bonn

Vorgelegt von  
Vadim Lensky  
aus Moskau

Bonn 2007

Angefertigt mit Genehmigung der Mathematisch–Naturwissenschaftlichen Fakultät  
der Rheinischen Friedrich-Wilhelms–Universität Bonn

1. Referent: Dr. rer. nat. Christoph Hanhart
2. Referent: Prof. Dr. rer. nat. Ulf-G. Meißner

Tag der Promotion: 21.06.2007

Diese Dissertation ist auf dem Hochschulschriftenserver der ULB Bonn  
[http://hss.ulb.uni-bonn.de/diss\\_online](http://hss.ulb.uni-bonn.de/diss_online) elektronisch publiziert.  
Das Erscheinungsjahr ist 2007.





# Contents

<b>Introduction</b>	<b>1</b>
<b>1 Chiral Effective Theory for Few–Nucleon Systems</b>	<b>5</b>
1.1 Chiral symmetry of QCD . . . . .	5
1.2 ChPT in mesonic sector . . . . .	8
1.3 Inclusion of baryons . . . . .	13
1.4 ChPT for few–nucleon systems . . . . .	16
<b>2 Pion Production in Nucleon–Nucleon Collisions</b>	<b>20</b>
2.1 Introduction . . . . .	20
2.2 Power counting and the concept of reducibility . . . . .	22
2.3 Evaluation of loops . . . . .	26
2.4 Effect of Delta isobar . . . . .	31
2.5 Results . . . . .	33
2.6 Summary of Chapter 2 . . . . .	37
<b>3 Pion Photoproduction off the Deuteron: <math>\gamma d \rightarrow \pi^+ nn</math></b>	<b>39</b>
3.1 Introduction . . . . .	39
3.2 Remarks on the $\pi d$ system . . . . .	43
3.3 The role of the $\pi NN$ cuts . . . . .	45
3.4 The reaction $\gamma d \rightarrow \pi^+ nn$ . . . . .	48
3.5 Results and discussion . . . . .	52
3.6 Summary of Chapter 3 . . . . .	58
<b>4 Neutron–Neutron Scattering Length</b>	<b>60</b>
4.1 Introduction . . . . .	60
4.2 ChPT calculation for $\gamma d \rightarrow \pi^+ nn$ . . . . .	61
4.3 Differential cross sections: relevant features . . . . .	62
4.4 Extraction of $a_{nn}$ and theoretical uncertainty . . . . .	65
4.5 Summary of Chapter 4 . . . . .	70
<b>5 Corrections to <math>a_{\pi d}</math></b>	<b>72</b>
5.1 Introduction . . . . .	72
5.2 Power counting . . . . .	74
5.3 Results . . . . .	78
5.4 Discussion . . . . .	80

5.5 Summary of Chapter 5 . . . . .	81
<b>Summary and Outlook</b>	<b>83</b>
<b>Acknowledgements</b>	<b>89</b>
<b>A Lagrangian Densities</b>	<b>90</b>
<b>B Diagram Technique</b>	<b>93</b>
B.1 Application of projectors to $NN$ system . . . . .	93
B.2 Rules of the diagram technique . . . . .	98
<b>C Projectors</b>	<b>103</b>
C.1 Spin-angular projectors . . . . .	103
C.2 Isospin projectors . . . . .	111
<b>D One-pion exchange <math>NN \rightarrow N\Delta</math></b>	<b>113</b>
<b>E Matrix Elements and Observables</b>	<b>116</b>
E.1 General definitions . . . . .	116
E.2 Reaction $\gamma d \rightarrow \pi^+ nn$ . . . . .	117
E.3 Reaction $pp \rightarrow d\pi^+$ . . . . .	126
E.4 Corrections to $a_{\pi d}$ . . . . .	130
<b>F Loops for <math>NN \rightarrow NN\pi</math></b>	<b>132</b>
<b>Bibliography</b>	<b>148</b>

# Introduction

Low-energy meson reactions on few-nucleon systems are of great interest for they are one of the best tools to deepen our understanding of the nuclear few-body problem. In particular, reactions involving the lightest meson, *i.e.* the pion, are subject of special experimental and theoretical efforts since they can provide us with very important information on various aspects of low-energy hadron dynamics.

One can say that the special role of the pion was conjectured even before the pion itself was experimentally discovered. In fact, the interaction of nucleons by means of exchanging mesons consisted the basis of the first theory of nuclear forces formulated by Yukawa in 1930's, which gave rise to the meson theory of nuclear forces. The experimental discovery of the pion in 1948 [1, 2] stimulated a rapid development of Yukawa's theory of nuclear forces. For the initial developments on meson theory we refer to Refs. [3, 4] and references therein. Although the meson theory of nuclear forces has undergone many developments and modifications since the works of Yukawa, his original idea on mesonic origin of nuclear forces is still valid. A more detailed historical review together with the recent developments can be found in Ref. [5].

This special role of the pion becomes even more important in the framework of chiral perturbation theory (ChPT), which had its foundation in the work of Weinberg [6], and received initial development in the works of Gasser and Leutwyler [7, 8]. This theory is a low-energy effective theory of the quantum chromodynamics (QCD), which has been proven as the theory of the strong interactions for its predictions in the high energy region are in a brilliant agreement with the experiment. However, the mathematical structure of the QCD is drastically different at high and at low energies: the coupling constant of the theory gets small at high energies, thus allowing for perturbation theory, and grows at low energies, making the conventional expansion in the powers of coupling constant inapplicable. Remarkably, this difficult situation with the low-energy spectrum of the theory, which we are interested in, has an elegant solution—namely the treatment of low-energy hadron interactions within an effective theory—ChPT. The main idea that underlies ChPT is the idea of symmetry violation. The symmetry of the fundamental theory—in this case the chiral symmetry of the QCD—should have its reflection in the properties of the effective theory, which is the theory of interactions of the effective degrees of freedom, the hadrons, rather than quarks and gluons that are degrees of freedom of the underlying theory. The chiral symmetry of the QCD appears to be spontaneously broken in nature, and the pion (along with other lightest pseudoscalars—the kaons and eta meson) is identified with the Goldstone boson of the spontaneously broken symmetry. The Goldstone theorem states that the Goldstone bosons do not participate in any interaction in the low-energy limit. This allows one to expand the

observables in powers of small energies of interacting particles. The fact that the pion is not massless as is mandatory for Goldstone bosons means that the chiral symmetry is broken also explicitly rather than only spontaneously. However, the smallness of pion masses allows one to treat the mass terms as a small perturbation as well. Thus, the theory is expanded in powers of small energies and momenta of interacting particles. The small expansion parameter, which is a measure of interactions amongst the particles of the theory, in this case is the ratio of small momenta of order of pion mass  $m_\pi$  to the scale of chiral symmetry breaking, which is of order of the nucleon mass  $M$  (and is often identified with this large mass). The inclusion of baryons into this scheme causes some difficulties because of their large mass, but this problem is solved within the heavy-baryon formalism [9, 10], the idea of which is to integrate the "heavy" baryon component out. We refer to the work of Bernard, Kaiser, and Meißner [11] for a review of various aspects of chiral perturbation theory. Since the pion is the lightest member of the Goldstone octet, it appears to be possible to describe the interaction of pions among themselves [6, 7, 12], pions and nucleons [13], and also few-nucleon systems [14–20], in terms of chiral Lagrangians that contain only pion and nucleon fields. In Chapter 1 we will review the formalism of chiral perturbation theory for the processes in few-nucleon systems in more detail. We should mention here the two advantages of the ChPT expansion: this technique allows for a systematic—order-by-order—approach to the calculation of observables, and also allows for an overall error estimate of the calculated quantities, which is usually based on the so-called "naturalness" assumption. The word "naturalness" means that one expects the numerical values of the terms, that enter the expansion at some given order  $n$ , to be equal  $\mathcal{C}_n \chi^n$ , where  $\chi \sim m_\pi/M$  is the expansion parameter, and  $\mathcal{C}_n$  is a number of order unity.

In this work we consider two specific reactions involving pions on few-nucleon systems, namely pion production in nucleon–nucleon collisions—the reaction  $NN \rightarrow NN\pi$ , and pion photoproduction on the deuteron in the reaction  $\gamma d \rightarrow \pi^+ nn$ . These two reactions are closely related to the issue of dispersive and absorptive corrections to the pion–deuteron scattering length, which we also consider in our analysis. The reaction  $\gamma d \rightarrow \pi^+ nn$  is also considered as the possible source for a high-precision determination of the neutron–neutron scattering length.

The production of pions in nucleon–nucleon collisions near threshold—the reaction  $NN \rightarrow NN\pi$ —is of special importance. It is the first hadronic inelasticity of  $NN$  scattering, therefore understanding of pion production leads to more profound understanding of the properties of the  $NN$ -system. Understanding of the reaction  $NN \rightarrow NN\pi$  is also a prerequisite to the study of isospin violation. Recently the forward-backward asymmetry of the reaction  $np \rightarrow d\pi^0$  [21] was measured. In this reaction, the isospin violating effects appear as a result of interference of isospin violating and isospin conserving amplitudes, therefore it is necessary to have isospin symmetric part well under control. The understanding of  $NN \rightarrow NN\pi$  also allows one to include the dispersive corrections to the pion–deuteron scattering length in a chiral perturbation theory analysis. This quantity is necessary for an accurate extraction of the isoscalar pion–nucleon scattering length from deuteron reactions, which are otherwise difficult to access. Another interesting issue that is related to the reaction  $NN \rightarrow NN\pi$  is the presence of large transfer momentum of order of  $\sqrt{Mm_\pi} \gg m_\pi$ , needed to produce a pion already



at threshold. This large scale has to be taken into account, and leads to modifications of the ChPT expansion and of the corresponding counting scheme. This research is still in progress, and we will report in this work on the first reliable quantitative results we obtained in this scheme. For a recent review of various aspects of pion production in nucleon–nucleon collisions near the threshold we refer to the review by Hanhart [22].

As concerning the reaction  $\gamma d \rightarrow \pi^+ nn$ , the calculation of this reaction is of high theoretical interest, because it also provides an important test for our understanding of those aspects of  $\pi NN$  dynamics that are relevant for pion production reactions on the deuteron. The first aspect of this interest is related to the possibility to obtain information on the elementary pion photoproduction amplitude on the neutron by using the deuteron as an effective neutron target. The second one is the determination of the  $nn$  scattering length from  $\pi^+$  production data. Pion photoproduction on the deuteron has been studied quite extensively over the past fifty years. Here we refer to the review of Laget [23], which has a broad coverage of earlier works. We should mention that in this work we will consider the near threshold pion photoproduction, *i.e.* excess energies below 20 MeV, in contrast to most phenomenological studies that were concentrated on the Delta isobar region, cf. Ref. [24] and references therein; for a recent review see also Refs. [25–27].

The structure of this thesis is as follows. In Chapter 1 we review the ChPT framework as applied to the reactions in few–nucleon systems. In particular, we examine Weinberg’s hybrid approach to the reactions in few–nucleon systems, which is based on the concepts of reducibility and power counting.

In Chapter 2 we consider the reaction  $NN \rightarrow NN\pi$ . We start with the formulation of the modified counting, which is needed in order to take into account the relatively large momentum transfer of order of  $\sqrt{Mm_\pi}$  typical for this reaction [28–30]. The expansion parameter in this case is  $\chi_\pi = \sqrt{m_\pi/M}$  rather than  $\chi$ . Then we survey the recent developments of Kaiser and Hanhart [30] who calculated all loop diagrams for the reaction  $NN \rightarrow NN\pi$ , where the pion is in an  $s$ -wave with respect to the  $NN$  system, up to next-to-leading order (NLO) in the modified expansion. We show that the proper treatment of the naively reducible loop diagrams gives rise to genuinely irreducible pieces of these loops. This results, in turn, in a complete cancellation of all NLO loops for  $NN \rightarrow NN\pi$ , solving thus the problem concerning the  $s$ -wave pion production stated recently by Gårdestig, Phillips, and Elster [31]. We show that this treatment simultaneously leads to the enhancement of the leading isovector rescattering amplitude by a factor of 4/3 compared to what was used commonly in the previous works. The outcome is a theoretical prediction for the total cross–section of the reaction  $pp \rightarrow d\pi^+$  near the threshold that is in good agreement with experimental data—the first time within ChPT. We also calculate the  $p$ -wave pion production cross–section near the threshold, providing thus the complete calculation for the total cross–section of the reaction  $pp \rightarrow d\pi^+$  up to NLO in ChPT expansion in  $\chi_\pi$ . Our result shows good agreement with experimental data near the reaction threshold.

In Chapter 3 we perform a calculation for the reaction  $\gamma d \rightarrow \pi^+ nn$ , which is a reaction with typical momentum transfer of order of  $m_\pi$ . Consequently, the usual Weinberg’s counting and expansion in powers of  $\chi$  is applied to this reaction. We survey the assumptions commonly done in calculations for this reaction. In particular, we consider the

nucleon recoil corrections that are commonly neglected in few-body calculations. These corrections were recently shown by Baru et al. [32] to give contributions non-analytic in  $\chi$  when taken into account explicitly, *i.e.* without expanding the corresponding propagators. We calculate these corrections explicitly and show that the static approximation (that neglects the recoil correction) fails in this case. We calculate the transition operator for  $\gamma d \rightarrow \pi^+ nn$  up to  $\chi^{5/2}$  in Weinberg's counting, where non-integer powers of  $\chi$  stem from the recoil corrections. The value of the leading pion photoproduction multipole  $E_{0+}$ , which is the only free parameter entering our calculation, is fixed from the ChPT calculation at N<sup>3</sup>LO [33]. We show that our results for the total cross-section agree with experimental data within the uncertainty up to excess energies of 20 MeV. At the same time we argue that the results of previous calculations that correspond to our calculation up to NLO in the expansion in  $\chi$  significantly underestimate the data.

In Chapter 4 we discuss the possibility to determine the neutron-neutron scattering length from the reaction  $\gamma d \rightarrow \pi^+ nn$ . We use the transition operator for this reaction calculated in Chapter 3. In addition, we employ the  $NN$  wave functions evaluated in the ChPT framework in order to have a fully consistent calculation that allows for a reliable uncertainty estimate. We use wave functions corresponding to N<sup>2</sup>LO (*i.e.* up to terms  $\mathcal{O}(\chi^2)$ ) calculation developed in Refs. [18, 34]. We show that for a proper choice of kinematics and momenta region to be considered, the theoretical uncertainty for the extraction of neutron-neutron scattering length does not exceed 0.1 fm. The estimate of uncertainty is performed very conservatively by evaluating the effect of the calculated NLO and N<sup>2</sup>LO+ $\chi^{5/2}$  corrections on the momentum spectra in the five-fold differential cross-section. In Appendix E.2.4 we provide a simple analytic expression for the shape of the differential cross-section we consider. This expression can be used in the Monte-Carlo simulations for the analysis of possible experimental setup.

In Chapter 5 we turn to the dispersive and absorptive corrections to the pion-deuteron scattering length. We provide a calculation of these corrections—the first time within ChPT. In this calculation we apply two counting schemes—the expansion in  $\chi_\pi$  for the hadronic part of these corrections and the expansion in  $\chi$  for the electromagnetic one. The estimate of order of magnitude of the corrections being considered here is  $\chi^{3/2}$ . We show that our result for the absorptive corrections agrees well with the experimental result for the width of pionic deuterium. As concerning the dispersive corrections, our result is smaller than in previous works, due to cancellations of individually sizable terms. We argue that a consistent calculation of the dispersive corrections to the pion-deuteron scattering length should include several effects that are commonly disregarded in phenomenological calculations.

We close the discussion with a brief summary of our findings.

# Chapter 1

## Chiral Effective Theory for Few–Nucleon Systems

In this chapter we review the formalism which we are working in, that is the chiral effective theory, to be more specific—its application to the few–nucleon sector. We aim at a general outline of the formalism rather than at a profound and detailed description. For the details and further references we refer the reader to the review of Bernard, Kaiser, and Meißner [11], and the lectures of Leutwyler [35, 36]. The recent developments of ChPT concerning the nuclear forces along with a vast list of references can be found in Refs. [19, 37], and a review of the issues related to the effective field theory treatment of the reaction  $NN \rightarrow NN\pi$  is contained in Ref. [22] (we also survey these issues in Chapter 2).

### 1.1 Chiral symmetry of QCD

Quantum ChromoDynamics (QCD), which describes the strong interactions, is a non-Abelian gauge theory. The gauge group of the QCD is  $SU(3)$ , and the QCD Lagrangian is given by

$$\mathcal{L}_{\text{QCD}} = -\frac{1}{4}\mathcal{G}_{\mu\nu}^a\mathcal{G}_a^{\mu\nu} + \bar{q}\left(i\not{D} - \hat{M}\right)q, \quad (1.1)$$

where  $q$  stand for the quark fields that transform under the fundamental representation of  $SU(3)$ ,  $\hat{M}$  is the  $N_f \times N_f$  quark mass matrix with  $N_f$  being the number of different quark flavours, and  $\mathcal{G}_{\mu\nu}^a$  is the gluon field strength tensor which is related to the gauge (gluon) field  $G_\nu^a$  that belongs to the adjoint representation of  $SU(3)$  via

$$\mathcal{G}_{\mu\nu}^a = \partial_\mu G_\nu^a - \partial_\nu G_\mu^a - g f^{abc} G_\mu^b G_\nu^c, \quad a, b, c = 1 \dots 8. \quad (1.2)$$

Here,  $f^{abc}$  are the structure constant of  $SU(3)$  specifying the  $SU(3)$  Lie algebra:

$$[T^a, T^b] = i f^{abc} T^c \quad (1.3)$$

with  $T^a$  being the  $SU(3)$  hermitian generators related to the conventional Gell-Mann matrices  $\lambda^a$  as  $T^a = \lambda^a/2$ , and  $g$  is the gauge coupling constant. The quark covariant derivative is given by

$$D_\mu q = \partial_\mu q - ig T^a G_\mu^a q. \quad (1.4)$$

Note that the quark field  $q$  is also a flavour  $SU(N_f)$  multiplet:  $q^T = (u, d, s, \dots)$ . We will assume the mass matrix  $\hat{M}$  to be diagonal (which is achieved in general by an appropriate transformation of quark fields).

In the limit of massless quarks, the Lagrangian of QCD can be written as

$$\mathcal{L}_{\text{QCD}} = -\frac{1}{4}\mathcal{G}_{\mu\nu}^a\mathcal{G}_a^{\mu\nu} + \bar{q}_R i\not{D}q_R + \bar{q}_L i\not{D}q_L, \quad (1.5)$$

where  $q_{R,L}$  are the right- and left-handed components of the quark fields, defined as

$$q_R = \frac{1}{2}(1 + \gamma^5)q \equiv P_R q, \quad q_L = \frac{1}{2}(1 - \gamma^5)q \equiv P_L q. \quad (1.6)$$

We have introduced here the left- and right-handed projectors  $P_{R,L} = (1 \pm \gamma^5)/2$  with  $\gamma^5$  being the usual product of the four Dirac matrices:  $\gamma^5 = i\gamma^0\gamma^1\gamma^2\gamma^3$ ,  $(\gamma^5)^2 = 1$ . These projectors have the following properties:

$$P_R^2 = P_R, \quad P_L^2 = P_L, \quad P_R P_L = P_L P_R = 0, \quad P_R + P_L = 1.$$

We see that the QCD Lagrangian in the massless limit, besides its invariance with respect to the gauge  $SU(3)$  group, appears to be invariant under additional global *independent* transformations of the left- and right-handed components of the quark. These transformations mix the flavour components of the left- and right-handed quark fields:

$$q'_R = T_R q_R, \quad q'_L = T_L q_L, \quad T_R, T_L \in U(N_f) \implies \mathcal{L}'_{\text{QCD}} = \mathcal{L}_{\text{QCD}}. \quad (1.7)$$

Here  $T_R$  and  $T_L$  are *independent* matrices belonging to  $U(N_f)$ . They can be parameterized as

$$T_R = \exp(i\boldsymbol{\theta}_R \cdot \mathbf{t} P_R), \quad T_L = \exp(i\boldsymbol{\theta}_L \cdot \mathbf{t} P_L),$$

where  $\mathbf{t} = \{t_i\}$ ,  $i = 1, \dots, N_f^2$  are the generators of  $U(N_f)$ , and  $\boldsymbol{\theta}_{R,L} = \{\theta_{R,L}^i\}$ ,  $i = 1, \dots, N_f^2$  are the corresponding unitary rotation angles.

Since  $T_R$  and  $T_L$  act independently on the quark field, the symmetry group of the massless QCD Lagrangian is

$$U(N_f)_R \times U(N_f)_L \longrightarrow U(1)_A \times SU(N_f)_R \times U(1)_V \times SU(N_f)_L, \quad (1.8)$$

where we put explicit labels  $R$ ,  $L$  on the groups that transform the corresponding components of  $q$ , and used the fact that  $U(N)$  is isomorphic to  $U(1) \times SU(N)$ , and also  $U_R(N) \times U_L(N)$  is isomorphic to  $U_V(N) \times U_A(N)$ , where now labels  $V$  and  $A$  denote the vector and axial transformations parameterized as

$$T_V = \exp(i\boldsymbol{\theta}_V \cdot \mathbf{t}), \quad T_A = \exp(i\boldsymbol{\theta}_A \cdot \mathbf{t}\gamma^5),$$

where  $\boldsymbol{\theta}_{V,A} = (\boldsymbol{\theta}_R \pm \boldsymbol{\theta}_L)/2$ . The vector  $U(1)_V$  symmetry corresponds to the conservation of baryon number. As concerning the axial  $U(1)_A$  symmetry, it turns to be broken due to the Abelian anomaly at the quantum level [38, 39], resulting, for instance, in the decay  $\pi^0 \rightarrow \gamma\gamma$ . The remaining  $SU(N_f)_R \times SU(N_f)_L$  global symmetry group is called the chiral group. The Noether currents that correspond to this symmetry are given by

$$\mathcal{J}_{R,L}^{\mu a} = \bar{q}\gamma^\mu P_{R,L} q, \quad a = 1, \dots, N_f^2 - 1. \quad (1.9)$$

In reality, the quark masses differ from zero, therefore the chiral symmetry is broken. However, the masses of the up ( $u$ ) and down ( $d$ ) quarks are small compared to the typical hadronic scales of order of 1 GeV:  $m_u = 1.5 \dots 3.0$  MeV,  $m_d = 3 \dots 7$  MeV<sup>#1</sup>. This smallness allows for perturbative treatment of the quark mass effects, as is discussed below. The strange quark ( $s$ ) plays an intermediate role with its mass  $m_s = 70 \dots 120$  MeV, and the remaining three quarks are a lot heavier:  $m_c \approx 1.25$  GeV,  $m_b \approx 4$  GeV,  $m_t \approx 170$  GeV. In what follows we will consider only the case of two quark flavours:  $q^T = (u, d)$ .

### 1.1.1 Spontaneous chiral symmetry breaking

Suppose we have a theory that possesses a certain global continuous symmetry, for instance, the chiral symmetry of massless QCD. There are two distinct ways how this symmetry can be realized. The first one that is called the Wigner mode implies that not only the Lagrangian of the system is invariant under some group of transformations  $G$ , but also the ground state is invariant under the same group. The second way, called the Goldstone mode, corresponds to the situation when only a subgroup  $H \subset G$  leaves the ground state invariant. The necessary condition for  $H$  to leave the ground state invariant is that the generators of  $H$  annihilate the ground state. Those generators of  $G$  that do not turn the ground state to zero are called broken generators. As stated by the Goldstone theorem [41, 42], in this case there should be exactly  $N_G - N_H$  massless bosons in the theory spectrum, where  $N_G(N_H)$  is the dimension of  $G(H)$ , respectively (or, stated differently, one boson corresponds to each broken generator of  $G$ ). These bosons are called Goldstone bosons<sup>#2</sup>. Goldstone bosons have zero spin, and the remaining quantum numbers of the Goldstone bosons have to be the same as the corresponding numbers of broken generators of  $G$ .

### 1.1.2 Isospin symmetry

There is another symmetry that is nearly obeyed in the strong interactions and that was discovered long ago—the isospin symmetry, which is expressed in the existence of almost degenerate multiplets. For instance, the nucleon doublet ( $p, n$ ) as well as the pion triplet ( $\pi^+, \pi^0, \pi^-$ ) are characterized by a very small mass splitting between the components of each multiplet:  $M_n - M_p = 1.3$  MeV,  $m_{\pi^\pm} - m_{\pi^0} = 4.6$  MeV. These values are so small that the isospin symmetry was believed for a long time to be an exact symmetry of the strong interactions. Mathematically, isospin symmetry means that the QCD Lagrangian is invariant under  $SU(2)_V$  subgroup of the chiral group that mixes the up and down quarks. This symmetry would be exact given the masses of  $u$ - and  $d$ -quarks were equal. We know nowadays that this symmetry is broken since the masses of up and down quarks are different. However, the values of  $m_u$  and  $m_d$  are small compared with the typical hadronic scale of order of 1 GeV, therefore the isospin breaking effects in the nucleon doublet are small. On the other hand, one could expect

<sup>#1</sup>These estimates were obtained at the renormalization scale  $\mu \approx 2$  GeV [40].

<sup>#2</sup>The situation is somewhat more complicated when a gauge symmetry is broken; in this case the Goldstone bosons appear as components of the gauge field rather than as independent particles—see, *e.g.* Ref. [43] and references therein.

these effects to be large for pions. However, as we will see below, these effects for pions are suppressed.

## 1.2 ChPT in mesonic sector

### 1.2.1 Non-linear realization of chiral symmetry

The main ideas of ChPT for pions were formulated in the fundamental work of Weinberg [6]. The concept is very general and allows for the description of the effective degrees of freedom dynamics, starting from the symmetry properties of the underlying theory. The way how to implement the transformation properties of the broken symmetry group on the Goldstone boson fields was first discussed by Weinberg [44] on an example of  $SU(2)_V \times SU(2)_A$  symmetry group broken to  $SU(2)_V$ , and was generalized by Coleman, Callan, Wess and Zumino [45, 46]. The symmetry group  $G$  acts on the quark fields according to Eq. (1.7). The action of  $G$  on the effective field is given by the following representation:

$$\pi^a \xrightarrow{g} \varphi^a(g, \pi), \quad (1.10)$$

where  $g$  is a transformation from  $G$ . The explicit expression for the corresponding Noether currents is determined by the form of the function  $\varphi^a(g, \pi)$ . The representation property

$$\varphi(g_1, \varphi(g_2, \pi)) = \varphi(g_1 g_2, \pi) \quad (1.11)$$

fixes the mapping uniquely (up to an isomorphism—see below).

To show this, let us consider the image of the zero,  $\varphi(g, 0)$ . It is straightforward to demonstrate that the composition law of Eq. (1.11) dictates that the set of elements  $h$  which map the zero onto itself forms a subgroup  $H \subset G$ . Moreover,  $\varphi(gh, 0)$  coincides with  $\varphi(g, 0)$  for any  $g \in G$ ,  $h \in H$ . Hence the function  $\varphi(g, 0)$  takes values on the space  $G/H$ , which is obtained from  $G$  by identifying elements  $g, g'$  differing only by right multiplication by an element of  $H$ ,  $g' = gh$ , that is, on the factor group  $G/H$ . The function  $\varphi(g, 0)$  thus maps the elements of  $G/H$  into the space of effective (pion) field variables. The mapping is reversible, since from  $\varphi(g_1, 0) = \varphi(g_2, 0)$  follows  $g_1^{-1}g_2 \in H$ . Thus, the pion fields  $\pi^a$  can be considered as the coordinates of the factor group  $G/H$ .

Let us choose a representative element  $a$  in each of the equivalence classes  $\{gh, h \in H\}$ . This representative element sets a unique decomposition of every group element given by  $g = ah$ . The composition law given by Eq. (1.11) shows that the image  $a'$  of the element  $a$  under the action of  $g \in G$  is obtained by decomposing the product  $ga$  into equivalence classes  $a'h$ —this is the standard action of  $G$  on the (homogeneous) space  $G/H$ . Therefore the geometry fully fixes the transformation law of the pion field, except for the freedom in the choice of coordinates on the manifold  $G/H$ .

In the case of  $G = SU(2) \times SU(2)$  and  $H = SU(2)$ , the factor group  $G/H$  is the group  $SU(2)$ . The pion field may be represented as an element of this group, *i.e.*, as a  $2 \times 2$  matrix field  $U(x) \in SU(2)$ . Alternatively, we can identify the pion field with the three coordinates  $\pi^1, \pi^2, \pi^3$  that are needed to parameterize the group  $SU(2)$ . The choice of coordinates is not unique. Using conventional exponential coordinates, the

relation between the matrix field  $U(x)$  and the pseudoscalar fields  $\pi^a(x)$  takes the form

$$U(x) = \exp\left[i\frac{\vec{\pi}(x)}{f_\pi}\right], \quad \pi(x) = \vec{\tau}\vec{\pi}(x) \quad (1.12)$$

where  $\vec{\tau} = \{\tau_1, \tau_2, \tau_3\}$  are the Pauli matrices, and  $f_\pi$  is the pion decay constant in the chiral limit. Note that the specific expression of  $U(x)$  in terms of  $\pi^a$  is unimportant for our considerations in this chapter; however, in the concrete calculations we use the so-called sigma representation, where the relation between the pion field and the matrix  $U(x)$  reads

$$U(x) = \sqrt{1 - \frac{\vec{\pi}^2(x)}{f_\pi^2}} + i\frac{\vec{\tau}\vec{\pi}(x)}{f_\pi}. \quad (1.13)$$

Of course, the physical results do not depend on the parameterization of the field.

As noted above, the action of  $g \in G$  on the element  $a \in G/H$  is given by  $ga = a'h$ . In the case under consideration,  $G$  consists of pairs of elements  $g = (T_R, T_L)$ , while  $H$  contains the equal pairs,  $T_R = T_L$ . As representative elements of the equivalence classes, we may choose  $a = (U, \mathbf{1})$ . The transformation law then amounts to

$$ga = (T_R, T_L)(U, \mathbf{1}) = (T_R U, T_L) = (T_R U T_L^\dagger, \mathbf{1})(T_L, T_L) = a'h \quad (1.14)$$

Therefore the transformation law of the pion field reads

$$U'(x) = T_R U(x) T_L^\dagger. \quad (1.15)$$

The matrix  $U(x)$  thus transforms linearly. Note, however, that the corresponding transformation law for the pion field  $\pi^a(x)$  is nonlinear. The above general discussion indicates that the occurrence of nonlinear realizations of the symmetry group is a characteristic feature of the effective Lagrangian technique.

## 1.2.2 Effective Lagrangian

Now we are at the position to construct the most general Lagrangian corresponding to the theory describing the dynamics of the Goldstone bosons associated with the spontaneous symmetry breakdown in QCD. Following the general argument that the effective Lagrangian should be a Lorentz scalar, and recalling that in the chiral limit we want the Lagrangian to be invariant under  $SU(2)_L \times SU(2)_R \times U(1)_V$ , and taking into account that due to the spontaneous symmetry breaking the ground state should only be invariant under  $SU(2)_V \times U(1)_V$ , we straightforwardly get the following expression for the lowest order effective Lagrangian:

$$\mathcal{L}_{\text{eff}}^{(2)} = \frac{f_\pi^2}{4} \text{Tr} (\partial_\mu U \partial^\mu U^\dagger), \quad (1.16)$$

where  $U = U(x)$  is given by Eq. (1.12), and the trace is performed in flavour space. The label "2" stands for the lowest order of  $\pi^a(x)$  in the expansion of this Lagrangian. It is easy to show that the Lagrangian given by Eq. (1.16) has the following properties:

- The Lagrangian is invariant under global  $SU(2)_R \times SU(2)_L \times U(1)_V$  transformations:

$$\mathcal{L}_{\text{eff}}^{(2)'} = \frac{f_\pi^2}{4} \text{Tr} \left( T_R \partial_\mu U T_L^\dagger T_L \partial^\mu U^\dagger T_R^\dagger \right) = \mathcal{L}_{\text{eff}}^{(2)} \quad (1.17)$$

(the invariance under  $U(1)_V$  is trivial because this transformation does not change the Goldstone boson field, since its baryon charge equals to zero);

- The Lagrangian has even intrinsic parity, *i.e.* is a scalar rather than a pseudoscalar, which is also a criterion that can rule out some terms—see below. One can check whether an expression constructed from  $U$  and  $\partial_\mu U$  is a scalar, by substituting  $\pi^a(t, \vec{x}) \rightarrow -\pi^a(t, -\vec{x})$  or, equivalently,  $U(t, \vec{x}) \rightarrow U^\dagger(t, -\vec{x})$ . The result for the Lagrangian should read  $\mathcal{L}_{\text{eff}}^0(t, \vec{x}) \rightarrow \mathcal{L}_{\text{eff}}^0(t, -\vec{x})$ . Note that the expansion of the Lagrangian proceeds thus in even powers of  $\pi^a(x)$ ;
- The Lagrangian of Eq. (1.16) is the only possible Lagrangian with minimal number of derivatives, since other possible terms like  $\text{Tr}(\partial_\mu U U^\dagger) \text{Tr}(U \partial^\mu U^\dagger)$ ,  $\text{Tr} U^\dagger U$ ,  $\text{Tr}(\partial^\mu U U^\dagger)$  either give zero or result in a constant, or can be reduced to the expression of Eq. (1.16) up to a total derivative.

With the definition of fields  $\pi^a(x)$  of Eq. (1.12) (or of Eq. (1.13)) and the Lagrangian of Eq. (1.16), we get, expanding the exponential matrix  $U(x)$ :  $U = 1 + i\pi/f_\pi + \dots$ ,  $\partial_\mu U = i\partial_\mu \pi/f_\pi + \dots$ , resulting in

$$\mathcal{L}_{\text{eff}}^{(2)} = \frac{f_\pi^2}{4} \text{Tr} \left[ \frac{i\partial_\mu \pi}{f_\pi} \left( -\frac{i\partial^\mu \pi}{f_\pi} \right) \right] + \dots = \frac{1}{4} \text{Tr}(\tau_a \partial_\mu \pi^a \tau_b \partial^\mu \pi^b) + \dots = \frac{1}{2} \partial_\mu \pi^a \partial^\mu \pi^a + \mathcal{L}_{\text{int}}, \quad (1.18)$$

thus reproducing the standard form for the kinetic term of a (pseudo)scalar field.

The Lagrangian of fourth order in momenta reads [6, 8]

$$\mathcal{L}_{\text{eff}}^{(4)} = \frac{l_1}{4} (\text{Tr}(\partial_\mu U \partial^\mu U^\dagger))^2 + \frac{l_2}{4} \text{Tr}(\partial_\mu U \partial^\nu U^\dagger) \text{Tr}(\partial^\mu U \partial_\nu U^\dagger). \quad (1.19)$$

The quantities  $l_i$  are the so-called low-energy constants. They can not be determined by the symmetry arguments, and should be taken from somewhere—either from comparison with the experiment, or from lattice calculations, or from some model calculations.

### 1.2.3 Chiral symmetry breaking due to quark masses

It is interesting to see how one deals with the mass terms that break the chiral symmetry. The term in the QCD Lagrangian that breaks the chiral symmetry reads:

$$\mathcal{L}_M = -\bar{q}_R \hat{M} q_L - \bar{q}_L \hat{M}^\dagger q_R, \quad (1.20)$$

where  $\hat{M}$  is the quark mass matrix defined in Eq. (1.1). The idea underlying the treatment of these chiral symmetry breaking terms is that one knows explicitly the law under which they are transformed by chiral rotations. Therefore one should also write down in the effective Lagrangian such non-invariant terms, the choice of which, however, is restricted by the symmetry. This treatment was suggested in the work of Weinberg [6].



We will, however, follow the equivalent approach by Gasser and Leutwyler [7]. Namely, we will treat the mass matrix  $\hat{M}$  as an external (spurious, *i.e.* not dynamical) field, which interacts with quarks, and transforms under the chiral group as

$$\hat{M}' = T_R \hat{M} T_L^\dagger. \quad (1.21)$$

This transformation law makes the quark mass term given by Eq. (1.20) to be invariant under chiral transformations. Now we have to write down general chirally invariant Lagrangians that contain mass insertions. At lowest order in  $\hat{M}$  one obtains

$$\mathcal{L}_{\chi\text{sb}} = \frac{f_\pi^2 B_0}{2} \text{Tr}(\hat{M} U^\dagger + U \hat{M}^\dagger), \quad (1.22)$$

where  $B_0$  is a constant with dimension of mass, and the subscript  $\chi\text{sb}$  refers to symmetry breaking. This Lagrangian is the lowest-order mass insertion that is consistent with all required symmetries; for instance, the term  $\text{Tr}(\hat{M} U^\dagger - U \hat{M}^\dagger)$  transforms as a pseudoscalar under parity transformation and therefore is not allowed (since the strong interactions are known to conserve parity with high accuracy). Notice that because  $\hat{M} = \hat{M}^\dagger$ ,  $\mathcal{L}_{\chi\text{sb}}$  contains only terms even in  $\pi$ . Note also that there is also term containing two traces like  $\text{Tr} \hat{M} \text{Tr}(U + U^\dagger)$  which is not chirally invariant in general, however, for the case of chiral  $SU(2)_R \times SU(2)_L$  symmetry this latter term appears to be proportional to  $\mathcal{L}_{\chi\text{sb}}$ . Indeed, since an  $SU(2)$  matrix  $U$  can be parameterized by two complex numbers  $a$  and  $b$  such that  $|a|^2 + |b|^2 = 1$  as

$$U = \begin{pmatrix} a & b \\ -b^* & a^* \end{pmatrix},$$

one can write  $U + U^\dagger = (\text{Tr } U) \mathbf{1}$ . We can rewrite therefore

$$\mathcal{L}_{\chi\text{sb}} = \frac{f_\pi^2 B_0}{2} \text{Tr}(\hat{M}) \text{Tr}(U). \quad (1.23)$$

Expressing  $U$  in terms of the pion field  $\pi$ , one gets

$$\mathcal{L}_{\chi\text{sb}} = f_\pi^2 B_0 (m_u + m_d) - \frac{B_0}{2} (m_u + m_d) \vec{\pi}^2 + \mathcal{O}(\vec{\pi}^4). \quad (1.24)$$

Although the first term of this equation is constant and therefore does not contribute to the scattering matrix elements, it contains some information about the structure of the vacuum. For instance, it can be demonstrated [7] that the value of  $B_0$  can be related to the value of quark condensate as

$$\langle 0 | \bar{u}u | 0 \rangle = \langle 0 | \bar{d}d | 0 \rangle = -f_\pi^2 B_0 + (\text{symmetry breaking corrections of higher orders}). \quad (1.25)$$

As concerning the second term, it can be identified with the pion mass term  $-m_\pi^2 \vec{\pi}^2 / 2$ , where  $m_\pi^2$  is given by

$$m_\pi^2 = B_0 (m_u + m_d).$$

Remarkably, the isospin breaking corrections that are proportional to  $m_u - m_d$  start to contribute only at higher orders.

Using the relation between  $B_0$  and the quark condensate, it is straightforward to obtain the well-known Gell-Mann–Oakes–Renner relation [47]:

$$m_\pi^2 = -\frac{(m_u + m_d)}{f_\pi^2} \langle 0 | \bar{u}u | 0 \rangle + \mathcal{O}(m_{u,d}^2). \quad (1.26)$$

### 1.2.4 Counting with pions

As we have seen in the discussion above, the symmetry arguments tell one how to construct the effective Lagrangians describing the low-energy dynamics of QCD. Along with the notion of chiral symmetry, there is another very important concept, namely—the possibility for a systematic expansion in a perturbative series. These ideas are the cornerstones of chiral effective field theory. Weinberg [6] showed how to truncate the series in order to achieve the desired accuracy. In the discussion on how to construct the effective Lagrangians, we have seen that the chirally symmetric Lagrangian of order  $d$  contributes a factor of  $Q^d$ , where  $Q$  stands for small momentum scale. Analogously, the chiral symmetry breaking Lagrangian of order  $d$  contributes a factor of  $m_\pi^d$ , and we count  $m_\pi \sim Q$ . Analogously, an internal pion propagator contributes a factor  $Q^{-2}$ , and each loop integration gives a factor of  $Q^4$ . Using the usual topological identities relating the number of loops to the one of internal lines and vertices, Weinberg showed the chiral dimension of an arbitrary Feynman graph with  $L$  loops and  $N_d$  vertices from  $\mathcal{L}_{\text{eff}}^{(d)}$  to be

$$D = 2 + \sum_d N_d(d - 2) + 2L. \quad (1.27)$$

The important thing is that the  $\mathcal{L}_{\text{eff}}$  starts from chiral dimension two, therefore the right hand side of this equation is bounded from below. Furthermore, since the loops as well as the vertices from Lagrangians of higher orders lead to a suppression of the corresponding Feynman graph, there is only finite number of diagrams that give contributions at any given order. According to Eq. (1.27), at the leading order ( $D = 2$ ) only tree diagrams contribute, whereas loops diagrams start to appear only at order  $Q^4$ . Notice that the loop diagrams may introduce non-analytic terms in the expansion.

An important property, in which the so obtained expansion in powers of small momenta  $Q$  differs from usual renormalizable perturbation theory, is the order-by-order renormalization. This means that new parameters—the low-energy constants—appear at each new order in the expansion in  $Q$ , opposite to usual renormalizable theories. These new parameters should be fixed from a comparison with experimental data, or from lattice calculations *etc.*

Let us now discuss what should be meant under "small" momentum scale. We suppose that small momenta are much less than some typical hadronic scale, denoted  $\Lambda_\chi$ , at which spontaneously broken chiral symmetry is not a good approximation anymore. For instance, the lightest meson that has quantum numbers different from those of Goldstone bosons, the  $\rho$ -meson with mass  $m_\rho = 770$  MeV, corresponds to a resonance in  $\pi\pi$  scattering, therefore this is a natural barrier to the derivative expansion of the Goldstone mesons. This implies  $Q \ll \Lambda_\chi \sim 770$  MeV. From the other hand, Georgi and Manohar [48], based on the renormalization scale independence arguments, have argued that a consistent chiral expansion is possible if  $\Lambda_\chi \leq 4\pi f_\pi \approx 1$  GeV. In what follows, we will assign  $\Lambda_\chi \sim 4\pi f_\pi$ . This choice is more convenient when dealing with baryons, since there are two expansion parameters in this case, namely  $Q/\Lambda_\chi$  and  $Q/M$ , where  $M$  is the nucleon mass, and it appears to be convenient to put them on the same footing (as we will show in the next section). Anyway, the two ways of reasoning—the meson-resonance barrier and the renormalization scale independence—give similar estimates for  $\Lambda_\chi$ .

## 1.3 Inclusion of baryons

In the previous section we have considered the purely mesonic sector involving the interaction of Goldstone bosons (pions) with each other. In this section we will outline, how ChPT can be extended to describe the dynamics of baryons at low energies.

### 1.3.1 Transformation properties of baryons

Let us consider how the baryons (we consider here the nucleon doublet) transform accordingly to the chiral symmetry of the QCD Lagrangian. For the details we refer to works of Refs. [44–46]. We assume the fields entering the Lagrangian to transform under irreducible representations of the subgroup  $H$  which leaves the vacuum invariant, whereas the symmetry group  $G$  of the Hamiltonian or Lagrangian is nonlinearly realized, as we saw in the previous section on an example of Goldstone bosons. We aim at a description of the interaction of baryons with the Goldstone bosons at low energies, therefore we need to specify the transformation properties of the baryon fields entering the Lagrangian.

We associate with the neutron and the proton a complex, four-component Dirac field which we arrange in an isospinor:

$$\Psi = \begin{pmatrix} p \\ n \end{pmatrix} \quad (1.28)$$

denotes the nucleon field with two four-component Dirac fields for the proton and the neutron. For the pion fields, we have already showed that the mapping  $U \rightarrow T_R U T_L^\dagger$ , where  $U = U(x)$  is the matrix of pion fields, defines a nonlinear realization of  $G$ . Let us denote the square root of  $U(x)$  by  $u(x)$ ,  $u^2(x) = U(x)$ , and define the  $SU(2)$ -valued matrix function  $K(T_R, T_L, U)$  by

$$u(x) \rightarrow u'(x) = \sqrt{T_R U T_L^\dagger} \equiv T_R u K^{-1}(T_R, T_L, U), \quad (1.29)$$

*i.e.*

$$K(T_R, T_L, U) = u'^{-1} T_R u = \sqrt{T_R U T_L^\dagger}^{-1} T_R \sqrt{U}. \quad (1.30)$$

The following homomorphism defines an action of  $G$  on the set  $\{(U, \Psi)\}$ :

$$\varphi(g) : \begin{pmatrix} U' \\ \Psi' \end{pmatrix} = \begin{pmatrix} T_R U T_L^\dagger \\ K(T_R, T_L, U) \Psi \end{pmatrix}. \quad (1.31)$$

This action is consistent with the group properties. Let us demonstrate that. First, the identity leaves  $(U, \Psi)$  invariant. Then, since Eq. (1.30) results in that

$$K(T_{L_1}, T_{R_1}, T_{R_2} U T_{L_2}^\dagger) K(T_{L_2}, T_{R_2}, U) = K((T_{L_1} T_{L_2}), (T_{R_1} T_{R_2}), U), \quad (1.32)$$

we have

$$\begin{aligned} \varphi(g_1) \varphi(g_2) \begin{pmatrix} U \\ \Psi \end{pmatrix} &= \varphi(g_1) \begin{pmatrix} T_{R_2} U T_{L_2}^\dagger \\ K(T_{L_2}, T_{R_2}, U) \Psi \end{pmatrix} = \begin{pmatrix} T_{R_1} T_{R_2} U T_{L_2}^\dagger T_{L_1}^\dagger \\ K(T_{L_1}, T_{R_1}, T_{R_2} U T_{L_2}^\dagger) K(T_{L_2}, T_{R_2}, U) \Psi \end{pmatrix} \\ &= \begin{pmatrix} T_{R_1} T_{R_2} U (T_{L_1} T_{L_2})^\dagger \\ K(T_{L_1} T_{L_2}, T_{R_1} T_{R_2}, U) \Psi \end{pmatrix} = \varphi(g_1 g_2) \begin{pmatrix} U \\ \Psi \end{pmatrix}, \end{aligned}$$

thus proving the concurrence with the group structure. Note that for a general group element  $g = (T_L, T_R)$  the transformation behavior of  $\Psi$  depends on  $U$ . For the special case of an isospin transformation,  $T_R = T_L = T_V$ , one obtains  $u' = T_V u T_V^\dagger$ , since

$$U' = u'^2 = T_V u T_V^\dagger T_V u T_V^\dagger = T_V u^2 T_V^\dagger = T_V U T_V^\dagger.$$

Comparing with Eq. (1.29) yields  $K^{-1}(T_V, T_V, U) = T_V^\dagger$  or  $K(T_V, T_V, U) = T_V$ , *i.e.*,  $\Psi$  transforms linearly as an isospin doublet under the isospin subgroup  $SU(2)_V$  of  $SU(2)_L \times SU(2)_R$ . A general feature here is that the transformation behavior under the subgroup which leaves the ground state invariant is independent of  $U$ . Moreover, as one can see directly from Eq. (1.15), the Goldstone bosons  $\pi$  transform according to the adjoint representation of  $SU(2)_V$ , *i.e.*, as an isospin triplet.

### 1.3.2 Baryonic effective Lagrangian

We will now discuss the most general effective baryonic Lagrangian at lowest order. Let us start with the construction of the  $\pi N$  effective Lagrangian  $\mathcal{L}_{\text{eff}, \pi N}^{(1)}$ . Since the transformation of the nucleon field depends not only on  $T_R$  and  $T_L$  but also on  $U(x)$ , which is a function of coordinates, it is natural then to demand the  $SU(2)_L \times SU(2)_R$  symmetry to be local. Recall that the nucleon doublet and  $U$  transform as

$$\begin{pmatrix} U'(x) \\ \Psi'(x) \end{pmatrix} = \begin{pmatrix} T_R(x)U(x)T_L^\dagger(x) \\ K[T_L(x), T_R(x), U(x)]\Psi(x) \end{pmatrix}, \quad (1.33)$$

where we assume the matrices  $T_{R,L}$  to be explicitly dependent on  $x$ . The local character of the transformation means that we need to introduce a covariant derivative  $D_\mu \Psi$  which should transform in the same way as  $\Psi$ :

$$[D_\mu \Psi(x)]' = K[T_L(x), T_R(x), U(x)]D_\mu \Psi(x). \quad (1.34)$$

Since  $K$  not only depends on  $T_L$  and  $T_R$  but also on  $U$ , the covariant derivative will contain  $u$  and  $u^\dagger$  and their derivatives, as will be shown below.

Let us introduce the so-called chiral connection

$$\Gamma_\mu = \frac{1}{2} [u^\dagger \partial_\mu u + u \partial_\mu u^\dagger]. \quad (1.35)$$

Using the properties of matrices  $u$  and  $K$  given by Eq. (1.29), it is easy to show that the chiral connection transforms as

$$\Gamma'_\mu = K \Gamma_\mu K^\dagger - (\partial_\mu K) K^\dagger, \quad (1.36)$$

therefore the covariant derivative of the nucleon doublet given by

$$D_\mu \Psi = (\partial_\mu + \Gamma_\mu) \Psi \quad (1.37)$$

indeed transforms covariantly, that is

$$D'_\mu \Psi' = [\partial_\mu + \Gamma'_\mu] K \Psi = K (\partial_\mu + \Gamma_\mu) \Psi. \quad (1.38)$$

There exists another Hermitian building block, the so-called vielbein,

$$u_\mu \equiv i [u^\dagger \partial_\mu u - u \partial_\mu u^\dagger], \quad (1.39)$$

which transforms accordingly to

$$u'_\mu = K u_\mu K^\dagger, \quad (1.40)$$

and under parity transforms as an axial vector:

$$u_\mu \xrightarrow{P} i [u \partial_\mu u^\dagger - u^\dagger \partial_\mu u] = -u_\mu.$$

The transformation property of the field  $\Psi$  under the chiral rotations tells us that the most general effective  $\pi N$  Lagrangian describing processes with a single nucleon in the initial and final states has the form  $\bar{\Psi} \hat{O} \Psi$ , where  $\hat{O}$  is an operator acting in Dirac spinor and flavor space, transforming under  $SU(2)_L \times SU(2)_R$  as  $\hat{O}' = K \hat{O} K^\dagger$ . As in the mesonic sector, the Lagrangian must be a Hermitian Lorentz scalar and be even under the parity, charge conjugation and time reversal transformations.

The most general such Lagrangian with the smallest number of derivatives is given by [49]

$$\mathcal{L}_{\text{eff}, \pi N}^{(1)} = \bar{\Psi} \left( i \not{D} - M + \frac{g_A}{2} \gamma^\mu \gamma_5 u_\mu \right) \Psi. \quad (1.41)$$

It contains two parameters not determined by chiral symmetry: the nucleon mass  $M$  and the axial-vector coupling constant  $g_A$ . The overall normalization of the Lagrangian is chosen such that in the case of no external fields and no pion fields it reduces to that of a free nucleon of mass  $M$ .

### 1.3.3 Heavy baryon formalism

In a fully relativistic formulation of low-energy theory of interacting nucleons and pions one loses the one-to-one correspondence between the number of loops and the power of small external momenta. The origin of this is the large mass of nucleons. The scale introduced by this mass can not be regarded small and does not vanish in the chiral limit. A solution of this problem has been proposed by Jenkins and Manohar [9], see also Bernard et al. [10]. The idea is to expand the amplitudes around the infinitely heavy nucleons' limit. This implies a simultaneous expansion in powers of  $Q/\Lambda_\chi \sim Q/(4\pi f_\pi)$  and  $Q/M$ . We outline here how this expansion is done. For a heavy nucleon it is convenient to parameterize its four-momentum  $p$  as

$$p_\mu = M v_\mu + q_\mu, \quad (1.42)$$

where  $v_\mu$  is the nucleon four-velocity satisfying  $v^2 = 1$ , and  $q_\mu$  is a small residual momentum such that  $v_\mu q^\mu \ll M$ . The trivial kinematic dependence of  $p_\mu$  on the large term  $M v_\mu$  is now explicit. In the rest frame with  $v_\mu = (1, 0, 0, 0)$  the three-momentum is given by  $\vec{q}$ , and  $p = (\sqrt{M^2 + q^2}, \vec{q})$ . To get rid of the nucleon mass term in the Lagrangian for the free nucleon field, one can introduce the velocity projected components  $N$  and  $h$  of the nucleon field via

$$N = e^{iMv \cdot x} P^+ \Psi, \quad h = e^{iMv \cdot x} P^- \Psi, \quad (1.43)$$

where  $P^\pm$  are the four-velocity projector operators defined as

$$P^\pm = \frac{1}{2}(1 \pm \not{v}). \quad (1.44)$$

They have the property  $\not{v}P^\pm = \pm P^\pm$ . The exponential factor in Eq. (1.43) eliminates the dependence of the nucleon field on the large momentum  $Mv_\mu$ . The quantities  $N$  and  $h$  are usually called the large and small nucleon components, respectively. We can now express the Lagrangian that in terms of  $N$  and  $h$  as

$$\mathcal{L}_{\text{nuc}} = \bar{\Psi}(i\not{\partial} - M)\Psi = \bar{N}i(v \cdot \partial)N - \bar{h}(iv \cdot \partial + 2M)h + \bar{N}i\not{\partial}h + \bar{h}i\not{\partial}N. \quad (1.45)$$

The equations of motions for  $N$  and  $h$  obtained from this Lagrangian read

$$\begin{aligned} (v \cdot \partial)N &= -P^+\not{\partial}h, \\ (v \cdot \partial)h &= 2iMh + P^-\not{\partial}N. \end{aligned} \quad (1.46)$$

From the second equation one sees that  $h = iP^-\not{\partial}N/2M$  up to corrections of order  $1/M$ . Therefore, the large component  $N$  obeys the free equation of motion

$$(v \cdot \partial)N = 0 \quad (1.47)$$

up to  $1/M$  corrections. The nucleon mass does not enter this equation of motion to leading order. The small component  $h$  can now be completely eliminated from the Lagrangian with the help of the equations of motion. An analogous procedure can be done for the nucleon field interacting with the pion field, leading to the counting scheme analogous to that for the pions. The expansion in this case is performed in powers of  $Q/\Lambda_\chi$  and  $Q/M$  simultaneously, and it is convenient to treat these two numbers on an equal footing. For the details we refer to the review by Bernard, Kaiser, and Meißner [11] and references therein. We should mention also the works of Weinberg [50, 51] where an equivalent way to get rid of the nucleon time derivatives by using the equation of motion was suggested.

## 1.4 ChPT for few–nucleon systems

In the previous sections we examined the method how the low-energy interactions of pions and nucleons can be described. These ideas proved to be a powerful tool for investigations of  $\pi\pi$  [12] and  $\pi N$  [13] systems. However, the boundstates of few–nucleon systems question already by their existence the possibility to treat them along the very same guidelines. Indeed, a bound state corresponds to a singularity in the scattering matrix and therefore can be obtained only as a sum of an infinite number of a perturbation theory series. The method how to treat few–nucleon systems in ChPT was suggested by Weinberg [50–52]. The idea was to use a general chirally invariant Lagrangian describing the interaction among nucleons and pions, which at leading order in small momenta has the form [50]

$$\begin{aligned} \mathcal{L} &= \frac{1}{2}D^{-2}\partial^\mu\vec{\pi}\partial_\mu\vec{\pi} - \frac{1}{2}D^{-1}m_\pi^2\vec{\pi}^2 \\ &+ \bar{N}[i\partial_0 - D^{-1}f_\pi^{-2}\vec{\tau} \cdot (\vec{\pi} \times \partial_0\vec{\pi}) - M - D^{-1}\vec{\tau} \cdot (\vec{\sigma} \cdot \nabla)\vec{\pi}]N \\ &- \frac{1}{2}C_S(\bar{N}N)(\bar{N}N) - \frac{1}{2}C_T(\bar{N}\vec{\sigma}N) \cdot (\bar{N}\vec{\sigma}N) \end{aligned} \quad (1.48)$$

(here the pion field is parameterized by the stereographic coordinates [44],  $D = 1 + \vec{\pi}^2/f_\pi^2$ , and  $C_S$ ,  $C_T$  are the low-energy constants characterizing the nucleon–nucleon interaction) and to develop counting and the corresponding chiral expansion. Then, in order to avoid large factors arising from the nucleon time derivatives, Weinberg suggested to replace the time derivative according to the nucleon equation of motion that reads

$$[i\partial_0 - D^{-1}f_\pi^{-2}\vec{\tau} \cdot (\vec{\pi} \times \partial_0\vec{\pi})]N = [M + D^{-1}\vec{\tau} \cdot (\vec{\sigma} \cdot \nabla)\vec{\pi} + \dots]N; \quad (1.49)$$

since this procedure reduces to merely the change of the coefficients of the terms that do not contain nucleon time derivatives, it was then argued that one can regard the Lagrangian as if there were no nucleon time derivatives. Of course this approach should be equivalent to the heavy-baryon formalism. The counting rules are derived from the Lagrangian as follows:

- The propagator of a nucleon with four-momentum  $Mv + q$  is

$$\frac{P^+}{q_0 + i\gamma}, \quad \gamma \rightarrow 0+$$

hence each nucleon propagator contributes a factor  $Q^{-1}$  to the matrix element;

- Each pion propagator contributes a factor  $Q^{-2}$ ;
- Each derivative (or pion mass) in any interaction contributes a factor  $Q$ . Recall that we got rid of nucleon time derivatives that would contribute large factors spoiling the counting;
- Each four-momentum integration contributes a factor  $Q^4$ .

The total index  $\mathcal{V}$  of a diagram with  $L$  loops,  $N_E$  external nucleon lines,  $V_i$  vertices of type  $(d_i, n_i)$ , where  $d_i$  is the number of derivatives and  $n_i$  is the number of nucleon fields in  $i$ th vertex, is obtained using usual topological arguments, and the resulting expression reads

$$\mathcal{V} = 2 - \frac{1}{2}N_E + 2L + \sum_i V_i [d_i + \frac{1}{2}n_i - 2]. \quad (1.50)$$

As in the case of purely pionic systems, the chiral symmetry bounds the number  $\mathcal{V}$  from below (for each given number of external nucleon lines). In particular, the numbers  $[d_i + \frac{1}{2}n_i - 2]$  are bounded by zero, which is reached for terms written in Eq. (1.48).

As it was already noted, the power counting arguments as given above can be applied directly only for calculating processes in the pure pionic and in the single-nucleon sectors. Moreover, there are graphs that are divergent. An example of such a graph is shown in Fig. 1.1. The matrix element corresponding to this graph is proportional to

$$\int d^4q \frac{\mathcal{R}(q)}{(q_0 + i\gamma)(q_0 - i\gamma)(q^2 - m_\pi^2)^2},$$

where  $\mathcal{R}(q)$  contains terms non-vanishing in the limit  $q_0 \rightarrow 0$ . Thus, the integral over  $d_0$  has a pinch singularity:

$$\int dq_0 \frac{1}{(q_0 + i\gamma)(q_0 - i\gamma)},$$

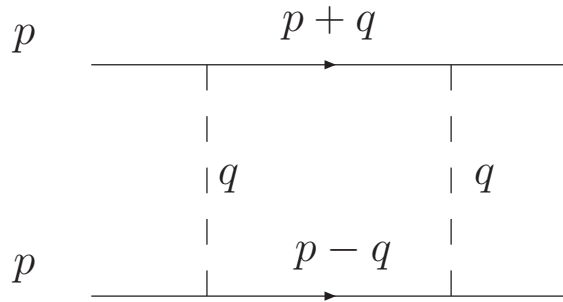


Figure 1.1: Example of an "infrared divergent" graph for nucleon–nucleon scattering.

which can not be avoided by shifting the integration contour. This infrared divergency forces one to include the nucleon kinetic energy term

$$\mathcal{L}_{\text{kin}} = \bar{N} \frac{\nabla^2}{2M} N \quad (1.51)$$

in the Lagrangian. These corrections make the integral over  $q_0$  finite, however, this integral appears to be larger by a factor of order of  $M/Q$  than is given by the counting. Thus, the perturbation theory fails to describe the nuclei, one has to sum an infinite series of diagrams that are not suppressed. Weinberg suggested how to cope with this, using the concept of reducibility. In doing the expansion it is convenient firstly to turn to the conventional time-ordered perturbation theory (TOPT). The idea is to classify all TOPT graphs accordingly with their reducibility. The (two-nucleon) reducible graphs are those graphs that contain a purely two-nucleon intermediate state. Those graphs, which do not contain such a state, are irreducible. These are namely reducible diagrams that violate the counting, whereas irreducible graphs respect the counting rules. The way how to sum over the reducible graphs has been known long ago: they are summed by solving the Lippmann-Schwinger equation. Thus, Weinberg's approach to few-nucleon systems is:

- The (TOPT) graphs that do not contain  $N$ -nucleon intermediate state are classified as irreducible ones;
- The irreducible graphs are assigned with their chiral order according to the counting rules;
- The sum of irreducible graphs up to a certain order gives the effective potential;
- The sum of reducible graphs is obtained by solving the  $N$ -particle Lippmann-Schwinger equation, using the effective potential as the kernel.

This approach was also expanded by Weinberg to processes in few-nucleon systems with external probes—in his work [52] Weinberg calculated the corrections to the pion-deuteron scattering length. The only modification of the framework in this case is that it is the transition operator describing the interaction of nucleons with external particles that is constructed according to the counting rules. This transition operator is then



convoluted with the few-nucleon wave functions, obtained by solving the Lippmann–Schwinger equation. This approach is known as ”hybrid approach“ since in its initial formulation the transition operator obtained using ChPT should be convoluted with the few-nucleon wave functions obtained from model calculations (reliable wave functions constructed within the ChPT framework appeared only very recently, see Ref. [19] and references therein; however, there is still a lot of work to be done, for instance, it is of a great importance to get a reasonable description of the  $NN$  forces at energies close to the pion production threshold). This approach is closely related with the phenomenological distorted-wave approximation. In fact, the crucial difference between the DWA and the hybrid approach is that the latter allows for a systematic expansion and for an error estimate, which should be considered advantages of the ChPT calculations over the phenomenology—this point has received numerous confirmations in our work.

# Chapter 2

## Pion Production in Nucleon–Nucleon Collisions

In this chapter we consider pion production in nucleon-nucleon collisions close to threshold. We review current theoretical developments concerning the treatment of these reactions within ChPT. We present our results for the total cross-section of the reaction  $pp \rightarrow d\pi^+$  near threshold to next-to-leading order (NLO). Already at this order loops start to contribute.

### 2.1 Introduction

The production of pions in nucleon–nucleon collisions near threshold — the reaction  $NN \rightarrow NN\pi$  — is of special importance. It is the first hadronic inelasticity of  $NN$  scattering, therefore understanding of pion production leads to more profound understanding of the properties of the  $NN$ -system. Understanding of reaction  $NN \rightarrow NN\pi$  is also prerequisite to the study of isospin violation. Recently the forward-backward asymmetry of the reaction  $np \rightarrow d\pi^0$  [21] as well as total cross-section of the reaction  $dd \rightarrow \alpha\pi^0$  [53] were measured. In the former reaction, the isospin violating effects appear as a result of interference of isospin violating and isospin conserving amplitudes, therefore it is necessary to have isospin symmetric part well under control. Recent theoretical developments considering these issues can be found in Refs. [54, 55]. Quantitative description of pion production near threshold also gives a key to calculation of absorptive and dispersive corrections to the pion-deuteron scattering length—we consider this issue in detail in Chapter 5.

The first attempts to understand  $NN \rightarrow NN\pi$  quantitatively were made in the sixties. In the work of Koltun and Reitan [56], the production of pions in the  $s$ -wave with respect to the  $NN$  pair in the reactions  $pp \rightarrow pp\pi^0$  and  $pp \rightarrow d\pi^+$  was investigated.

The authors of Ref. [56] worked in the distorted wave Born approximation. The diagrams that were included in their calculation are shown on Fig. 2.1. The diagram (*i*) corresponds to the direct pion production on one of the nucleons, and the diagram (*ii*) to the rescattering of pion off the second nucleon. The strengths of the corresponding pion–nucleon interactions were defined from  $\pi N$  scattering lengths. The values of the total cross-sections they obtained showed an agreement with the existing experimental

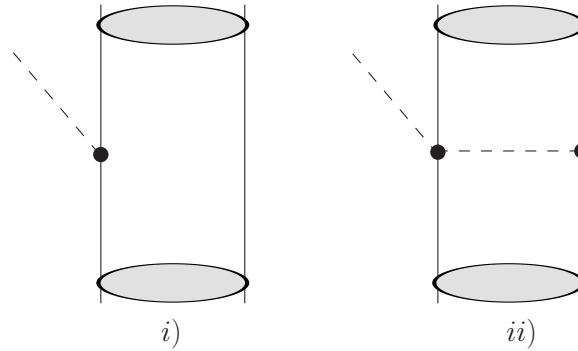


Figure 2.1: Diagrams included in the calculation of Koltun and Reitan [56]. Diagram (i) corresponds to direct production, diagram (ii) — to  $\pi N$  rescattering. Blobs denote  $NN$  interaction in the initial and final states.

near-threshold data.

However, highly accurate data close to the production threshold became possible only quite recently with the advent of cooler synchrotrons. When the first close to threshold data for the total cross section of the reaction  $pp \rightarrow pp\pi^0$  appeared in 1990 [57], it had been a big surprise that the model of Ref. [56] (which was revisited in [58]) fell short by a factor of 5–10. At the same time, the observed energy dependence of the total  $pp \rightarrow pp\pi^0$  cross-section was correctly reproduced. This was shown [58] to be due to effects of  $NN$  interaction in  $^1S_0$  final state (including Coulomb interaction).

To cure the discrepancy between theory and experiment, many different mechanisms were proposed. For a recent review of these issues see Ref. [22]. The inclusion of the Delta isobar resulted in an enhancement [59], however not sufficient — the cross-section was still by a factor of approximately three smaller. The role of Delta isobar was reinvestigated later in [60], where its importance was confirmed. The papers [61, 62] suggested to use heavy meson exchanges to enhance the cross-section, and showed that the inclusion of the corresponding contributions can lead to a satisfactory description of experimental data. However, in Ref. [63] it was demonstrated that taking into account offshell effects in  $\pi N$  rescattering also leads to an enhancement of the theoretical number for  $pp \rightarrow pp\pi^0$  total cross-section and may even lead to an overestimated cross-section depending on parameterization of  $\pi N$  amplitude used. This issue was further discussed in Refs. [60, 64–66].

Also meson exchange currents were considered, where pion is emitted from an exchanged meson [67], as well as resonance contributions [68]. These effects, however, seemed to be smaller compared to the effects of heavy meson exchanges and offshell  $\pi N$  rescattering.

The total cross sections for the reactions  $np \rightarrow d\pi^0$  and  $pp \rightarrow d\pi^+$  on the other hand could be described by the calculation of Koltun and Reitan within a factor of two, and the inclusion of heavy meson exchanges brought the number into an agreement with the experiment [69], see also [70]. Such a difference between the reactions  $pp \rightarrow pp\pi^0$  and  $pp \rightarrow d\pi^+$  is a consequence of the fact that the isovector rescattering that dominates the charged pion production in  $pp \rightarrow d\pi^+$ , does not contribute to  $pp \rightarrow pp\pi^0$  [56]. Thus, the pion production in this latter reaction goes through many different concurring

mechanisms and the resulting pattern becomes hard to reveal.

To resolve the situation, various groups started to investigate  $NN \rightarrow NN\pi$  using ChPT. As an effective field theory it is to be free of any ambiguities and people expected that now the relevant physics of  $NN \rightarrow NN\pi$  could be identified. As a big surprise to many, however, it turned out that, when naively using the original power counting by Weinberg [52], the discrepancy between theory and data became even larger at next-to-leading order (NLO) for  $pp \rightarrow pp\pi^0$  [28, 71] as well as for  $pp \rightarrow d\pi^+$  [65]. The authors of these works showed, in particular, that the pion rescattering diagram for the reaction  $pp \rightarrow pp\pi^0$  interferes with the direct production diagram destructively when one calculates the corresponding matrix element according to the rules of ChPT, contrary to the phenomenological calculations (see, *e.g.*, Ref. [63]). In Ref. [65] it was stressed that one should include higher orders in ChPT (*i. e.* loop diagrams) to understand the origin of this opposite sign.

In addition, the corrections at one-loop order (next-to-next-to-leading order (N<sup>2</sup>LO) in the standard counting) were calculated for  $pp \rightarrow pp\pi^0$  and turned out to be much larger than the NLO tree corrections [72, 73], thus questioning the convergence of chiral expansion.

At the same time it was already realized that a modified power counting is necessary to properly take care of the large momentum transfer characteristic for pion production in  $NN$  collisions. This was suggested in Ref. [28]. However, this modified counting scheme in its original formulation did not change the results neither for neutral [28] nor for charged pions [29].

Recently there were two developments: one that focused on some technical aspects related to the evaluation of the matrix elements [74–77] and another regarding the power counting for the large momentum transfer reactions. Formal inconsistencies of the naive power counting using the heavy baryon scheme were pointed out in Ref. [78]. Especially it was noted there that one cannot neglect the nucleon kinetic energy in the nucleon propagator as it is commonly done in the heavy baryon formalism. The reason for this is that in the reactions  $NN \rightarrow NN\pi$  the production of a pion is provided by kinetic energies of colliding nucleons and therefore one cannot expand the nucleon propagator in tree level diagrams.

The ideas concerning a modification of the counting scheme formulated in Refs. [28, 29] were further developed and improved — it was especially recognized how to properly estimate loop contributions. This modified scheme was implemented in Refs. [30, 79] — the essential features are described in detail below. The basic conclusion was that an ordering scheme exists for the reactions  $NN \rightarrow NN\pi$  that can lead to a convergent series. However, so far full calculations (including the distortions due to the  $NN$  interactions) within this scheme existed only for the production of  $p$ -wave pions [79], where the series was demonstrated to converge and an agreement with experimental data was achieved.

## 2.2 Power counting and the concept of reducibility

In this section we discuss the modifications of the counting scheme necessary to properly treat the large transfer momentum. We also remind the reader of the concept of

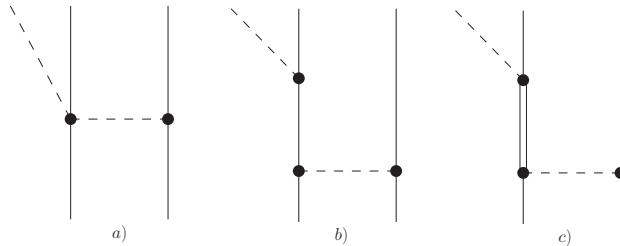


Figure 2.2: Tree level diagrams that contribute at leading ((a) and (b)) and next-to-leading order (c) to  $NN \rightarrow NN\pi$ . The double line denotes a  $\Delta$ -isobar. Note, in diagrams (b) and (c)—for illustration—with the one-pion exchange only one part of the  $NN$  and  $NN \rightarrow N\Delta$  potential is shown.

reducibility, which is one of the basic ideas of ChPT treatment for few nucleon systems. Here we follow Ref. [30], where it was demonstrated by explicit evaluation of the leading loop contributions how the presence of the large momentum scale influences loops. The central findings of that work were that it is possible to define an ordering scheme for  $NN \rightarrow NN\pi$ , but some loops are to be promoted to significantly lower orders compared to what is expected from Weinberg's original counting.

As mentioned in the previous section, the power counting needs to be modified in order to be applicable for  $NN \rightarrow NN\pi$ . The reason for this necessity is the magnitude of the nucleon center-of-mass momentum  $\vec{p}$  required to produce even a pion at rest in  $NN$  collisions. It is given by

$$p = \sqrt{m_\pi(M + m_\pi/4)}. \quad (2.1)$$

Eq. (2.1) exhibits the important feature of the reaction  $NN \rightarrow NN\pi$ , namely the large momentum mismatch between the initial and the final nucleon-nucleon state. This leads to a large invariant (squared) momentum transfer  $t \sim -Mm_\pi$  between in- and outgoing nucleons. In addition, it seems compulsory to include the Delta isobar as an explicit degree of freedom, since the Delta-nucleon mass difference  $\delta = M_\Delta - M = 293 \text{ MeV}$  is comparable to the external momentum  $p \simeq \sqrt{Mm_\pi} = 362 \text{ MeV}$ . The hierarchy of scales

$$m_\pi \ll p \simeq \delta \ll M, \quad (2.2)$$

suggested by this feature is in line with findings within meson exchange models where the Delta isobar gives significant contributions even close to the threshold [60, 70]<sup>#1</sup>. Thus, it is more natural to take as expansion parameter the quantity

$$\chi_\pi = \frac{p}{M} = \sqrt{\frac{m_\pi}{M}}. \quad (2.3)$$

As a result at leading order only tree level diagrams contribute to the transition operator (diagrams (a) and (b) of Fig. 2.2).

<sup>#1</sup>For the channel  $pp \rightarrow pp\pi^0$  strong support for an important role played by the Delta isobar was given by a partial wave analysis [80].

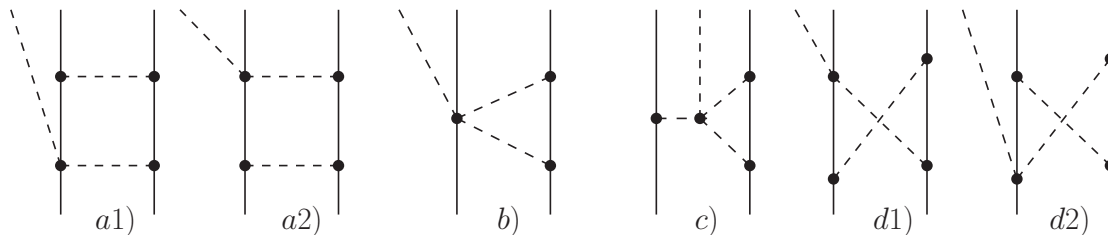


Figure 2.3: Leading loop diagrams for  $NN \rightarrow NN\pi$ . Here dashed lines denote pions and solid lines denote nucleons.

Already at next-to-leading order—in addition to the first diagram that involves a Delta isobar (diagram (c) of Fig. 2.2)—the first loops appear (see Fig. 2.3). As a consequence of the two scales  $p$  and  $m_\pi$  given in Eq. (2.2) there exists a dimensionless parameter that is of order  $\chi_\pi$ , namely  $m_\pi/p$ , that can appear as the argument of non-analytic functions as a result of the evaluation of loop integrals. Thus, each loop now contributes not only to a single order, but to all orders higher than the one where it starts to contribute [22]. In this work we only consider the leading parts of the loops in Fig. 2.3 that start to contribute at NLO.

Let us now turn to the concept of reducibility in describing few-nucleon systems. Already the existence of nuclei—the deuteron in particular—shows that perturbation theory is insufficient to properly describe two-nucleon systems: only an infinite sum of diagrams can produce a pole in the  $S$ -matrix. To bring this observation in line with power counting, Weinberg proposed to classify all possible diagrams according to the concept of reducibility [14, 15, 17, 50, 51]: those diagrams that have a two nucleon cut are called reducible. Those which do not are called irreducible. The latter constitute the potential that is to be constructed according to the rules of ChPT. The former are then generated by solving the Schrödinger equation, using the mentioned potential as kernel. This scheme acknowledges that the two nucleon cut contributions are enhanced compared to the irreducible parts.

It was also Weinberg who gave a recipe how to calculate processes on few nucleon systems with external probes [52]: here the transition operators are to be calculated using ChPT. Then those transition operators must be convoluted with the appropriate  $NN$  wave functions—in full analogy to the so-called distorted wave Born approximation traditionally used in phenomenological calculations [56], however supplemented with a power counting.

Therefore it is necessary to disentangle those diagrams that are part of the transition operator from those that are the result of a convolution of the transition operator with the wave functions. In complete analogy to  $NN$  scattering described above, the former are called reducible and the latter irreducible. Also here the distinction stems from whether or not the diagram shows a two nucleon cut. Thus, in accordance to this rule, the one loop diagrams shown in Fig. 2.3 (b)–(d) are irreducible, whereas diagrams (a) seem to be reducible.

Following these guidelines, the authors of work [30] obtained the following important results:

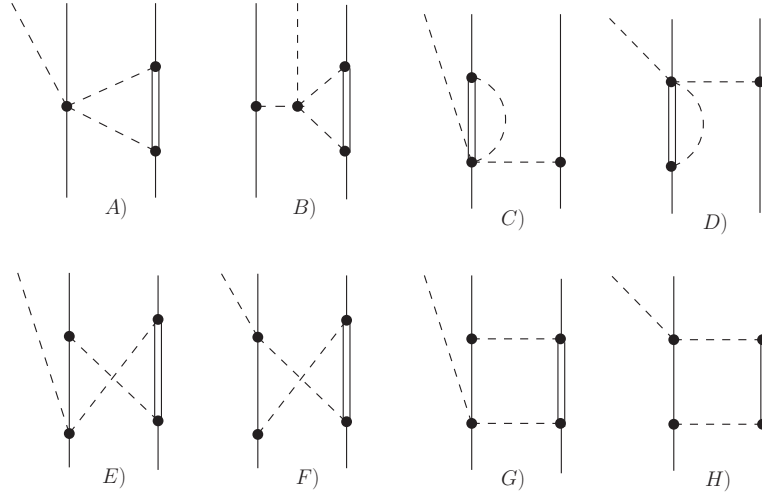


Figure 2.4: Leading loop diagrams with Delta isobar for  $NN \rightarrow NN\pi$ . Here dashed lines denote pions and solid lines denote nucleons. Double line denote Delta isobars.

- There are several loops with Delta isobar that also start to contribute at NLO—they are shown in Fig. 2.4. The sum of all NLO contributions of these loops canceled both for the reaction channels  $pp \rightarrow pp\pi^0$  and  $pp \rightarrow d\pi^{+\#2}$ . The reason of this cancellation was explained to be the following: the contribution of each of these loops with Delta isobar is divergent, and there is no counterterm at this order that would absorb these divergences. Therefore this cancellation was considered to be an evidence for the consistency of the counting scheme;
- The sum of NLO contributions of leading loops with nucleons (diagrams of Fig. 2.3 (b)–(d)) canceled for the reaction channel  $pp \rightarrow pp\pi^0$ . However, the origin of this cancellation could not be identified;
- The sum of NLO contributions of diagrams of Fig. 2.3 (b)–(d) for the channel  $pp \rightarrow d\pi^+$  gave a finite answer. However, as pointed out in Ref. [31], the amplitude that corresponds to this sum grows linearly with increasing final  $NN$ -relative momentum. This behavior leads to a large sensitivity to the final  $NN$  wavefunction, once the convolution of those with the transition operators is evaluated as demanded by the non-perturbative nature of the  $NN$  interaction. The solution to this problem proposed in Ref. [31] is to include a new counter term at leading order to absorb this unphysical behavior. However, chiral symmetry does not allow for such a structure (see below for the details).

Thus, two important questions were left unanswered: why there is an exact cancellation of the NLO contributions from nucleon loops for  $pp \rightarrow pp\pi^0$  and how to avoid the wave function sensitivity in  $pp \rightarrow d\pi^+$ . We address these questions below in this chapter. As we will show, the solutions to both questions are related and at the same

<sup>#2</sup>Note that some of these loops were found in Ref. [70] to give large contribution in  $pp \rightarrow d\pi^+$ ; see the corresponding discussion in Sections 2.4, 2.5.

time shed some light on the concept of reducibility in pion reactions on few–nucleon systems. Particularly, we mentioned above that in accordance to the rule that the diagrams that have a two nucleon cut are called reducible, the one loop diagrams (a) on Fig. 2.3 seem to be reducible. However, we will show that diagrams (a) contain a genuine irreducible piece due to the energy dependence of the leading  $\bar{N}N\pi\pi$ –vertex, the so–called Weinberg–Tomozawa term (WT) — see Ref. [81]. Specifically, the energy–dependent part of the WT vertex cancels one of the intermediate nucleon propagators, resulting in the irreducible part of diagrams (a).

We further demonstrate that the net effect of the inclusion of the NLO loops, shown in Fig. 2.3, is to enhance the leading rescattering amplitude by a factor of 4/3, bringing its contribution to the cross section for  $pp \rightarrow d\pi^+$  close to the experimental value.

## 2.3 Evaluation of loops

Let us consider the relevant production amplitudes for  $s$ -wave pion production (for further details see Appendix E). At threshold only two amplitudes are allowed to contribute to the reaction  $NN \rightarrow NN\pi$ , namely  $A_{11}$  and  $A_{10}$ , where we used the notation  $A_{T_i T_f}$  to label the total isospin of the initial ( $T_i$ ) and final ( $T_f$ )  $NN$ –pair. The third amplitude allowed by the standard selections rules —  $A_{01}$  — has to have at least one  $p$ -wave in one of the final subsystems. To the reactions  $pp \rightarrow pp\pi^0$  and  $pn \rightarrow pp\pi^-$  only  $A_{11}$  and to  $NN \rightarrow d\pi$  only  $A_{10}$  contribute at threshold, whereas both  $A_{11}$  and  $A_{10}$  contribute to the reaction  $pp \rightarrow pn\pi^+$ .

The only transitions that are allowed to contribute near threshold are  ${}^3P_0 \rightarrow {}^1S_0s$  for  $A_{11}$  and  ${}^3P_1 \rightarrow {}^3S_1s$  for  $A_{10}$ , where small letters denote the pion angular momentum with respect to the  $NN$  system and the  $NN$  partial waves are labeled with the standard notation  ${}^{2S+1}L_J$ . Those lead to the following transition amplitude structures [22]

$$\mathcal{T} = iA_{11} \left( (\vec{S} \cdot \vec{p}) \mathcal{I}' \right) + A_{10} \left( [\vec{S} \times \vec{p}] \cdot \vec{S}' \right) \quad (2.4)$$

with  $\mathcal{I}' = (\chi_{1'}^\dagger \sigma_2 \chi_{2'}^*) / \sqrt{2}$  and  $\vec{S} = (\chi_2^t \sigma_2 \vec{\sigma} \chi_1) / \sqrt{2}$  and  $\vec{S}' = (\chi_{1'}^\dagger \vec{\sigma} \sigma_2 \chi_{2'}^*) / \sqrt{2}$ , where the  $\chi_{1,2}$  ( $\chi_{1',2'}$ ) denote spinors for the incoming (outgoing) nucleons, and  $\chi^t$  stands for transposed spinors. For a deuteron in the final state we need to use

$$\mathcal{T} = A_{10} \left( [\vec{S} \times \vec{p}] \cdot \vec{\epsilon}_d^* \right) , \quad (2.5)$$

where now  $\vec{\epsilon}_d^*$  denotes the deuteron polarization vector. The transition amplitudes  $A$  are to be convoluted with the corresponding initial and final  $NN$  wave functions in order to obtain matrix elements. We come back to the evaluation of the deuteron cross section in section 2.5.

If we neglect all  $NN$  distortions, we get for the leading rescattering contribution (Fig. 2.2 (a)) at threshold [30]

$$A_{11}^{2a} = 0, \quad A_{10}^{2a} = 2 \left( \frac{2m_\pi M}{2f_\pi^2} \right) \frac{1}{p_\mu^2 - m_\pi^2} \left( \frac{g_A M}{f_\pi} \right) = -\frac{2g_A m_\pi M^2}{p^2 f_\pi^3} (1 + \mathcal{O}(\chi_\pi)) , \quad (2.6)$$



where we used that the  $\pi N \rightarrow \pi N$  amplitude to leading order contains not only the standard WT term that scales as the sum of the incoming and outgoing pion energies, here equal to  $m_\pi$  and  $m_\pi/2$ , respectively, but also its recoil correction equal to  $p^2/2M = m_\pi/2$ . We also use here and below the shorthand  $p_\mu^2 = p^\mu p_\mu$  for the square of a four-vector. The relevant terms of the underlying Lagrangian density are given in Appendix A. Note that with a value of  $2m_\pi M/2f_\pi^2$  the WT vertex including the recoil correction as it appears in the  $NN \rightarrow NN\pi$  amplitude takes exactly the value it has for elastic  $\pi N$  scattering at threshold.

In the reaction  $NN \rightarrow NN\pi$  the energies of the initial nucleons are of order  $p^2/2M \sim m_\pi$  and the momenta are of order  $p$ . In irreducible loops, on the other hand, both energies and momenta are of order  $p$  (see Appendix F for the details). As a consequence in the evaluation of diagrams (b), (c), and (d) of Fig. 2.3 the nucleon recoil terms (*i.e.* the nucleon kinetic energies) can be neglected in the nucleon propagators, since they scale as  $m_\pi$ . At first glance this seems to be at variance with the recent finding that three body  $NN\pi$  cuts that originate from the nucleon recoils play an essential role in pion reactions on few nucleon systems [32, 82]. However, the reactions studied in these references had very different kinematics, as they were small momentum transfer reactions, where in typical kinematics the  $\pi NN$  state was near on-shell. Here, on the other hand, we are faced with a large momentum transfer reaction: for typical kinematics a  $\pi NN$  intermediate state is far off-shell. In addition, here there is an additional kinematical suppression for the  $\pi NN$  cuts: at the cut the typical pion momentum, which sets the scale for the typical loop momentum, is that of the external pion of order of at most  $m_\pi$ . As a consequence the  $\pi NN$  cuts do not contribute before N<sup>5</sup>LO to the reaction  $NN \rightarrow NN\pi$  [22].

By comparison to the full results of Ref. [72], in Ref. [30] it was shown that it is allowed to expand the integrand of the loop integrals before evaluation in powers of  $\sqrt{m_\pi/M}$ . As a consequence it was possible to express the leading contribution of all loops corresponding to diagrams (b)–(d) of Fig. 2.3 in terms of a single integral

$$I_0(p_0, \vec{p}) = \frac{1}{i} \int \frac{d^4 l}{(2\pi)^4} \frac{1}{(l_0 - i\gamma)(l_\mu^2 - m_\pi^2)((l+p)_\mu^2 - m_\pi^2)}. \quad (2.7)$$

One finds  $I_0(p_0, \vec{p}) = I_0(\vec{p}^2) (1 + \mathcal{O}(\chi_\pi)) = 1/(16\sqrt{\vec{p}^2}) (1 + \mathcal{O}(\chi_\pi))$ . The assumption of threshold kinematics (all outgoing momenta vanish) simplifies the operator structure significantly and we can write — neglecting for the moment the distortions from the  $NN$  interaction — in order [30]

$$\begin{aligned} A_{10}^{3b+3c+3d} &= \frac{g_A^3 M^2}{4f_\pi^5} (-2 + 3 + 0) p^2 I_0(\vec{p}^2) = \frac{g_A^3 M^2 p}{64f_\pi^5} \\ A_{11}^{3b+3c+3d} &= \frac{g_A^3 M^2}{4f_\pi^5} (-2 + 3 - 1) p^2 I_0(\vec{p}^2) = 0. \end{aligned} \quad (2.8)$$

Note, here and in what follows we write equalities although we dropped terms of higher order in  $\chi_\pi$ . As mentioned in the introduction to this chapter, the sum of the NLO loops vanishes in case of  $A_{11}$ . We will give an explanation for this cancellation below. Let us now concentrate on  $A_{10}$ . In order to obtain matrix elements and thus compare

the result of Eq. (2.8) to data, the transition operators need to be convoluted with appropriate  $NN$  wave functions. The convolution integrals that arise necessarily involve non-vanishing  $\vec{p}'$ , denoting the outgoing  $NN$  relative momenta, even if we still work at threshold. However, the structure of the loop integral  $I_0$  is such that — to leading order — only  $\vec{p} - \vec{p}'$  appears in the integrals and thus one can directly generalize the expressions of Eqs. (2.8) (see also Appendix F). As was argued in Ref. [31], this implies that for large  $p'$  the contributions from the loops grows linearly with  $p'$ . When it then comes to the convolution of those operators with the  $NN$  wave function, this linear growth of the transition operators leads to a large sensitivity to the deuteron wave functions. Indeed, already with a constant transition operator one would have obtained the coordinate wave function at origin as a result of convolution, which is not well defined (see discussion in Ref. [83]); in the case under consideration the result would behave even worse. However, there should be no sensitivity to the particular wave functions used, for off-shell quantities are not observable [84, 85]. On the other hand, the chiral Lagrangian does not allow for a counter term to compensate this linear growth. From Eqs. (2.4), (2.8) one sees that a counterterm that would absorb this unwanted behaviour would couple the pion field to the nucleon field neither via a derivative of pion field nor via pion mass. Therefore, this counterterm would not vanish in chiral limit, violating the chiral symmetry. The solution given in Ref. [31], namely the inclusion of such a counter term at leading order, is therefore not consistent with the effective field theory used. However, as we will show, the loops with the unwanted behavior will be canceled exactly by the irreducible pieces of diagrams (a) of Fig. 2.3. We proceed as follows: we first show this cancellation to one loop order without distortions. Then we generalize the result to the inclusion of the full  $NN$  wave functions.

We still assume threshold kinematics and now turn to the evaluation of diagrams (a) of Fig. 2.3. In doing so one first has to realize that in contrast to the irreducible diagrams discussed in the beginning of this section, energies in the diagrams with a two-nucleon cut are of the order of the external energies ( $l_0 \sim p^2/2M \sim m_\pi$ ). Therefore, there is a priori no reason to neglect the nucleon recoils that are of the order of  $m_\pi$ . We thus get for the full expression for the first diagram of Fig. 2.3 (a), up to higher orders,

$$A_{10}^{3a1} = i \frac{3g_A^3 M^2}{8f_\pi^5} \int \frac{d^4 l}{(2\pi)^4} \frac{[l_0 + m_\pi - (2\vec{p} + \vec{l}) \cdot \vec{l} / (2M)]}{(l_0 - \frac{m_\pi}{2} - \frac{(\vec{l} + \vec{p})^2}{2M} + i\gamma)(-l_0 + \frac{m_\pi}{2} - \frac{(\vec{l} + \vec{p})^2}{2M} + i\gamma)} \times \frac{(\vec{l} \cdot (\vec{l} + \vec{p}))}{(l_\mu^2 - m_\pi^2)((l + p)_\mu^2 - m_\pi^2)},$$

$$A_{11}^{3a1} = 0, \tag{2.9}$$

where we included the recoil correction to both the WT term in the numerator as well as the nucleon energies in the denominator, in line with the discussion above. The vanishing  $A_{11}^{1a1}$  reproduces the well known result that the WT interaction does not contribute to the leading rescattering diagram in  $pp \rightarrow pp\pi^0$ .

In order to proceed we rewrite the first term in the numerator of the above integral as

$$\left[ l_0 + m_\pi - \frac{(2\vec{p} + \vec{l}) \cdot \vec{l}}{2M} \right] = \left[ \left( l_0 - \frac{m_\pi}{2} - \frac{(\vec{p} + \vec{l})^2}{2M} \right) + 2m_\pi \right],$$

where we used that at threshold  $p^2/M = m_\pi$ . The first term now exactly cancels the first nucleon propagator and we are left with an expression that no longer has a two nucleon cut — it is irreducible. In this irreducible piece we can neglect the recoil corrections in the remaining nucleon propagator — cf. the discussion at the beginning of this section — and get

$$A_{10}^{3a1} = i \frac{3g_A^3 M^2}{8f_\pi^5} \int \frac{d^4 l}{(2\pi)^4} \left\{ \frac{(\vec{l} \cdot (\vec{l} + \vec{p}))}{(-l_0 + i\gamma)(l_\mu^2 - m_\pi^2)((l+p)_\mu^2 - m_\pi^2)} + \frac{2m_\pi}{(l_0 - \frac{m_\pi}{2} - \frac{(\vec{l} + \vec{p})^2}{2M} + i\gamma)(-l_0 + \frac{m_\pi}{2} - \frac{(\vec{l} + \vec{p})^2}{2M} + i\gamma)} \frac{(\vec{l} \cdot (\vec{l} + \vec{p}))}{(l_\mu^2 - m_\pi^2)((l+p)_\mu^2 - m_\pi^2)} \right\}. \quad (2.10)$$

Up to higher orders the first term gives

$$A_{10}^{3a1(\text{irr})} = - \left( \frac{3}{4} \right) \frac{g_A^3 M^2}{4f_\pi^5} p^2 I_0(\vec{p}^2) = - \frac{3}{4} \frac{g_A^3 M^2 p}{64f_\pi^5}, \quad (2.11)$$

where the label (irr) indicates that this is only the irreducible piece of the diagram. Analogous considerations for the second diagram of diagrams (a) of Fig. 2.3 give

$$A_{10}^{3a2} = i \frac{g_A^3 M^2}{8f_\pi^5} \int \frac{d^4 l}{(2\pi)^4} \left\{ \frac{(\vec{l} \cdot (\vec{l} + \vec{p}))}{(-l_0 + i\gamma)(l_\mu^2 - m_\pi^2)((l+p)_\mu^2 - m_\pi^2)} - \frac{2m_\pi}{(l_0 + \frac{m_\pi}{2} - \frac{(\vec{l} + \vec{p})^2}{2M} + i\gamma)(-l_0 + \frac{m_\pi}{2} - \frac{(\vec{l} + \vec{p})^2}{2M} + i\gamma)} \frac{(\vec{l} \cdot (\vec{l} + \vec{p}))}{(l_\mu^2 - m_\pi^2)((l+p)_\mu^2 - m_\pi^2)} \right\}. \quad (2.12)$$

The leading piece of the first term gives

$$A_{10}^{3a2(\text{irr})} = - \left( \frac{1}{4} \right) \frac{g_A^3 M^2}{4f_\pi^5} p^2 I_0(\vec{p}^2) = - \frac{1}{4} \frac{g_A^3 M^2 p}{64f_\pi^5}. \quad (2.13)$$

Thus we get

$$A_{10}^{3a1(\text{irr})+3a2(\text{irr})+3b+3c+3d} = \frac{g_A^3 M^2}{4f_\pi^5} \left( -\frac{3}{4} - \frac{1}{4} - 2 + 3 + 0 \right) p^2 I_0(\vec{p}^2) = 0$$

$$A_{11}^{3a1(\text{irr})+3a2(\text{irr})+3b+3c+3d} = \frac{g_A^3 M^2}{4f_\pi^5} ( 0 + 0 - 2 + 3 - 1 ) p^2 I_0(\vec{p}^2) = 0, \quad (2.14)$$

where we repeat the results for  $A_{11}$  from above for comparison. Thus, in both channels that contribute at the production threshold the sum of all irreducible loops that appear at NLO cancels. On the other hand the remaining pieces in the expressions for  $A_{10}^{1a}$  exactly agree to the convolution of the leading rescattering contribution with the one pion exchange, however, with the  $\bar{N}N\pi\pi$  WT vertex put on-shell. Thus the WT vertex takes the value  $2m_\pi M/(2f_\pi^2)$ —cf. Eq. (2.6). The two-nucleon propagators in these integrals have a unitarity cut and it is this cut contribution that should dominate the

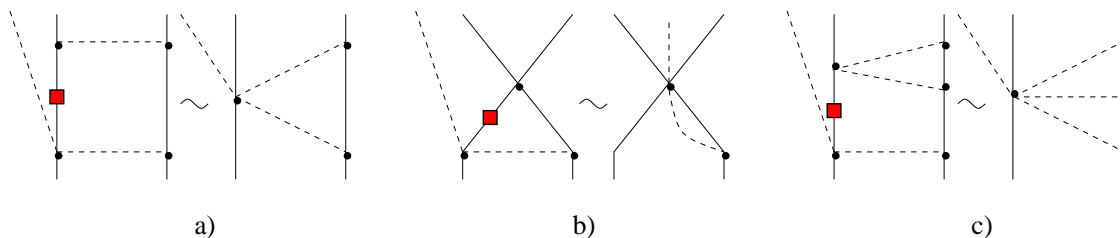


Figure 2.5: Illustration of the kind of topologies that corresponds to the irreducible structures (denoted by the filled box on the propagator that gets canceled by the energy dependence of the  $\pi N \rightarrow \pi N$  vertex) that emerge from the convolution of the energy dependent rescattering term with various contributions to the  $NN$  potential.

integral—in line with Weinberg’s original classification as reducible and irreducible. In other words, these pieces are indeed dominated by the reducible piece<sup>#3</sup>.

Next we show that for all ingredients of the  $NN$  potential but the one–pion exchange the choice of an on–shell  $\bar{N}N\pi\pi$  vertex is of sufficient accuracy. To this end we remind the reader that the integral corresponding to the irreducible pieces of this first diagram of Fig. 2.3 (a) had a structure like diagram (b) of that figure. This is illustrated in part (a) of Fig. 2.5. At leading order in the  $NN$  potential there is besides the one pion exchange also a contact interaction. The convolution of the rescattering diagram with the WT vertex (diagram (a) in Fig. 2.2) with this part of the  $NN$  potential we can again decompose into a reducible piece with the  $\pi N \rightarrow \pi N$  vertex on–shell and an irreducible piece that takes a structure of an integral with one nucleon less (see part (b) of Fig. 2.5); this diagram, however, does not contribute below N<sup>4</sup>LO and is therefore irrelevant to the order we are working. Thus, all that is to be kept is the convolution of the on–shell rescattering contribution with the contact  $NN$  interaction — in line with the findings of Ref. [74]. At NLO in the  $NN$  potential there are pion loops. Then the irreducible piece of the convolution of the leading rescattering contribution with this piece results in a two loop diagram (for a particular example see part (c) of Fig. 2.5) that does not contribute up to N<sup>3</sup>LO. Thus, to the order we are working we can safely put the WT vertex on–shell for the convolution of any piece of the  $NN$  potential with the leading rescattering contribution.

What remains to be shown is that the cancellation of Eq. (2.14) survives (to the given order) the convolution with the full wave functions. This generalization is straightforward. The corresponding diagrams are shown in Fig. 2.6 for the inclusion of the final state interaction that we want to discuss in detail. The argument in case of the initial state interaction is completely analogous and will not be given. Note that only the irreducible parts of the diagrams (a) are to be included — the reducible pieces get absorbed into the wave functions. Let  $k_\mu$  denote the integration variable of the convolution integral that we chose equal to the four momentum of one of the nucleons. As argued

<sup>#3</sup>In addition, the relative strength as well as sign in these terms equal to  $-3$  for the pion exchange in the final  $T_f = 0$  channel compared to  $+1$  for the pion exchange in the initial  $T_i = 1$  channel equal to the expectation values of the isospin parts of the one pion exchange in the relevant isospin channel, since  $\langle TT_3 | \vec{\tau}_1 \cdot \vec{\tau}_2 | TT_3 \rangle = 2T(T+1) - 3$ .

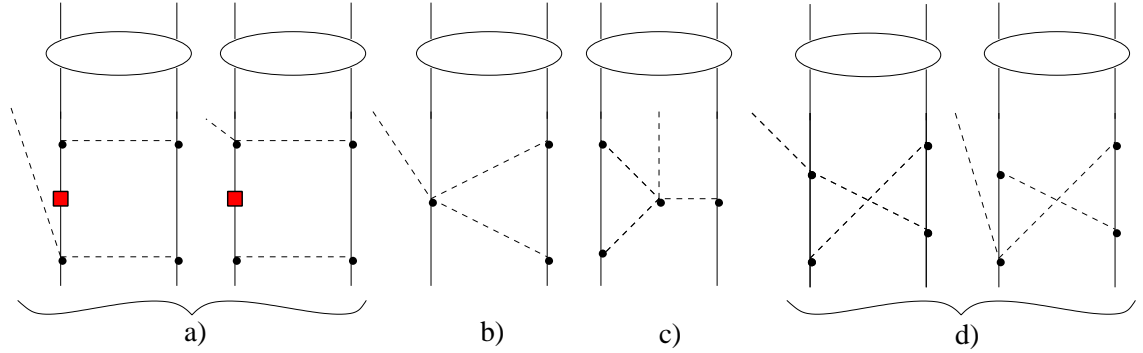
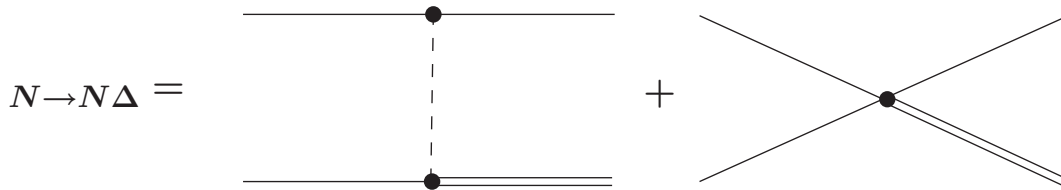


Figure 2.6: Leading loop diagrams for  $NN \rightarrow NN\pi$ , convoluted with the  $NN$   $T$ -matrix, denoted by the ellipse. Here dashed lines denote pions and solid lines denote nucleons. The filled box on the nucleon propagators of the diagrams (a) indicate that only the irreducible piece is to be taken. The reducible part gets absorbed into the wave function.

in the previous paragraph, the integral will be dominated by energies close to the corresponding on-shell energies. This sets the scale for  $k_0$  — especially we can safely assume  $k_0 \ll p$ . This is all that is needed to neglect  $k_0$  in the nucleon propagator of the pion loop integrals. On the other hand in these loops  $\vec{k}$  only enters as  $\vec{p} - \vec{k}$ . Thus, the terms that enter in the convolution integrals with the final state interaction to the order we are working are simply given by replacing  $\vec{p}$  by  $\vec{p} - \vec{k}$  in Eqs. (2.8), (2.11), and (2.13). This will obviously not change the relative strength of the individual diagrams — the cancellation survives the convolution with the wave functions. We therefore conclude that up to next-to-leading order all irreducible pion loops in the transition operator cancel with the only effect that the WT vertex in the rescattering diagram is to be put on-shell.

## 2.4 Effect of Delta isobar

Let us now turn to the contribution of Delta isobar to the  $s$ -wave pion production. As was argued in Ref. [70], the inclusion of Delta isobar leads to an overestimate of the cross-section for  $NN \rightarrow d\pi$ . Specifically, it was stated in this work that a very significant contribution comes from processes where Delta in the intermediate state emits a  $p$ -wave pion which is then rescattered on the nucleon in an  $s$ -wave. Such a process would correspond, for instance, to diagram (H) of Fig. 2.4. However, as was already mentioned in Section 2.2, it was shown in Ref. [30] that if one takes into account all the relevant loops (which is done in a consistent counting scheme), their total contribution cancels at this chiral order. Therefore up to NLO there is only one diagram that contains the Delta isobar, namely diagram (c) of Fig. 2.2. The contribution of this diagram, however, was shown to be small compared to that of diagram (a) of this figure [29, 60, 70]. In particular, in Ref. [29] an approximation of the  $NN \rightarrow N\Delta$  transition potential by one pion exchange was used. The contribution of the Delta to  $pp \rightarrow d\pi^+$  was found to be negligible compared to the rescattering one and to be model dependent. The latter result came due to the use of a static Delta propagator in the calculation of Ref. [29]

Figure 2.7:  $NN \rightarrow N\Delta$  transition potential.

— the matrix element appears in this case to be proportional to the wave function at origin. However, the static approximation for the Delta appears not to be justified in this case (see also the discussion concerning recoils in nucleon propagators in Section 5.4). In addition, we found that there is an error in Ref. [29], namely the formulae (35–40) that describe the Delta contribution are wrong. We performed calculations under the same assumptions as in the work of Ref. [29], both in coordinate and momentum spaces. The results of our two computations for Delta coincided with high precision, and were different to those of Ref. [29]. We obtained a very large Delta contribution, which was at the same time extremely model dependent. From the other hand, retaining the Delta recoil in the corresponding propagator reduces the role of the Delta a lot, however the Delta contribution is overestimated in this case by a factor about two compared to full model  $NN \rightarrow N\Delta$  potentials. Use of full Delta propagator also suppresses the model dependence since it leads to a better convergence of the integrals.

In what follows we calculate the Delta contribution to  $s$ -wave pion production using model  $NN \rightarrow N\Delta$  transition potentials (see Section 2.5). These phenomenological potentials include along with the one-pion exchange the  $\rho$ -meson exchange, which is known to cut the pion contribution [5]. This suppresses somewhat the effect of Delta isobar compared to the case when  $NN \rightarrow N\Delta$  transition matrix is given solely by the one-pion exchange. However, for a consistent NLO calculation one needs as input the  $NN \rightarrow N\Delta$  transition potential consistent with chiral symmetry, that is, along with the one-pion exchange the corresponding contact term (which is modeled by  $\rho$ -meson exchange in phenomenological potentials) at this order has to be included, as shown on Fig. 2.7. The corresponding parameters are to be fixed from a fit to  $NN$  data. Such a fit has not yet been performed. However, the model calculations (and also our hybrid calculation) show that the contribution of the Delta isobar to the  $s$ -wave pion production is only about 10 % in the amplitude [60].

## 2.5 Results

Since the NLO loop diagrams discussed in this work contribute only to  $A_{10}$ , we will now discuss their impact on the reaction  $pp \rightarrow d\pi^+$  that is fully determined by that amplitude. The cross section data for this reaction near threshold is traditionally parameterized as

$$\sigma = \alpha\eta + \beta\eta^3, \quad (2.15)$$

where Coulomb effects were neglected. To the reaction  $pn \rightarrow d\pi^0$  both  $\alpha$  and  $\beta$  contribute with only half their strength [86] due to isospin Clebsch-Gordan factor. Here  $\eta$  denotes the outgoing pion momentum in units of its mass. The first term gives the  $s$ -wave strength, whereas the second one denotes the  $p$ -wave contribution (as well as some possible energy dependencies of the  $s$ -wave [31]).

Before comparison with experiment is possible, the transition operators are to be convoluted with appropriate  $NN$  wave functions. The details of the formalism used here can be found in Appendices B, E. To calculate the leading order (LO) rescattering process (diagram (a) of Fig. 2.2) we use the standard expression for the WT term in threshold kinematics — thus we put  $3/2 m_\pi$  at the vertex [56, 69]. In addition we also evaluate the direct contribution (diagram (b) of Fig. 2.2) which also contributes to LO according to our counting. We performed two different calculations — namely neglecting the Delta contribution (which is NLO) given by diagram (c) on Fig. 2.2 and retaining it. For the  $NN$  distortions we use CD-Bonn potential [87] and Argonne AV18 potential [88] in the calculation without Delta and the CCF model [89], which treats  $NN$ ,  $N\Delta$ , and  $\Delta\Delta$  channels consistently, in the calculation with Delta. We also performed the calculation with Delta using somewhat more simplistic Hannover model [90, 91]. The obtained values of  $\alpha$  are listed in Table 2.1. It is also instructive to define for each diagram and the corresponding transition operator  $\hat{T}$  the quantity  $I_T$  as follows:

$$I_T = A_T e^{-i\delta_{pp}} \quad (2.16)$$

where  $A_T$  is the convolution of  $\hat{T}$  with initial and final  $NN$  wave functions (see Appendix E.3), and  $\delta_{pp}$  is the proton-proton scattering phase shift in the  ${}^3P_1$  partial wave at the pion production threshold. The quantity  $I_T$  is real and characterizes the magnitude of each diagram's contribution. The values of  $I_T$  we obtained are listed in Table 2.2.

Model	$\alpha^{LO}$ ( $3/2 m_\pi$ )	$\alpha^{NLO}$ (w/o Delta)	$\alpha^{NLO}$ (w. Delta)
CD Bonn	131	220	—
AV18	115	195	—
CCF	95	168	217
Hannover	105	187	248

Table 2.1: The values of  $\alpha$  obtained in calculations with different parameters,  $\mu b$ .

We obtain for various models values of  $\alpha^{LO}$  ranged between 95 and 131  $\mu b$ . These values are consistent with those given in Ref. [69]. They are dominated by the rescattering contribution. Note that the values of the rescattering contribution depend on

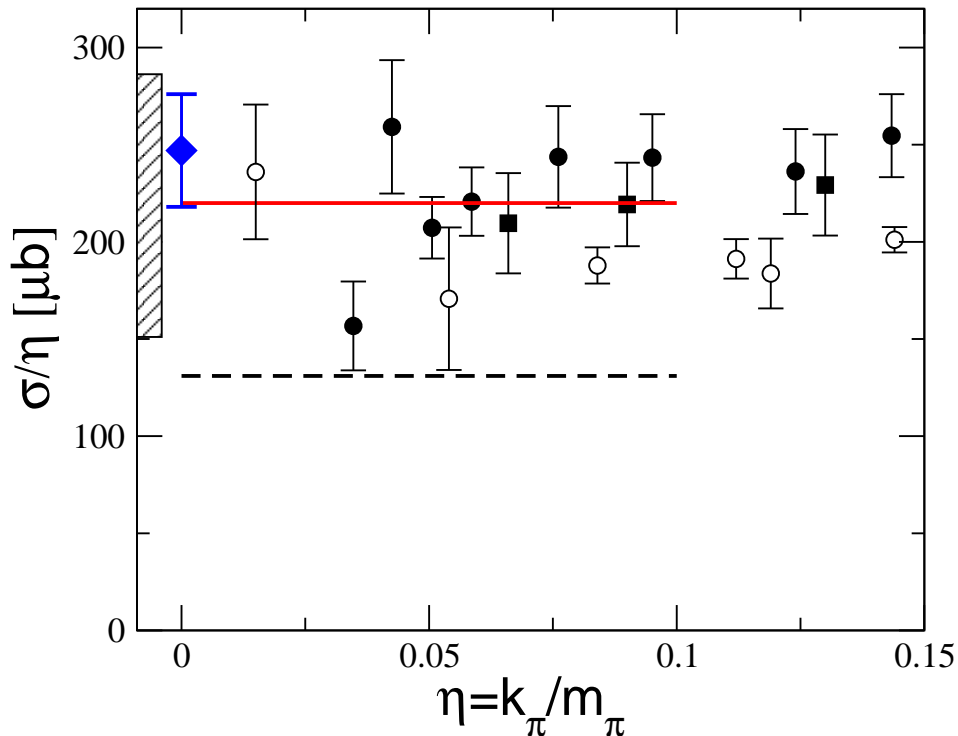


Figure 2.8: Comparison of our results to experimental data for  $pp \rightarrow d\pi^+$ . The dashed curve shows the LO results. The solid line shows the results at NLO. Both values correspond to the calculations with the CD Bonn model. The data are from Refs. [86] (open circles), [92] (filled circles) and [93] (filled squares). Blue diamond corresponds to the value obtained from the width of pionic deuterium [94]. The hatched bar shows the theoretical uncertainty as in the text.

the model only marginally, whereas the direct term is known to be quite model dependent [69] as one directly sees from Table 2.2 and is small because of a cancellation of individually sizable terms. Clearly such a cancellation can not be captured by the counting scheme. Still, we point out that in an EFT scheme as used here all terms at a given order have to be retained. Note that the direct term for the CD Bonn potential is rather large comparing to the other ones; we could not elucidate the reason for this.

As outlined above, in order to include the NLO contributions all we need to do is to replace the  $(3/2) m_\pi$  in the WT vertex by  $2 m_\pi$  — or, stated differently, to scale the given results for  $\alpha^{WT, LO}$  by a factor  $(4/3)^2$ . The corresponding values for the rescattering piece that we get at NLO —  $\alpha^{WT, NLO}$  — range from 166 to 191  $\mu\text{b}$ , whereas the full result including the direct term (without the Delta contribution) ranges from 168 to 220  $\mu\text{b}$ . The contribution of the Delta isobar to the  $s$ -wave pion production appears to be at the level of 10–15 % of the WT contribution in agreement with previous works [60], and acts constructively, which improves the description of experimental data in case of the Hannover and CCF models. The resulting values of  $\alpha^{NLO}$  with the Delta contribution included are between 217 and 248  $\mu\text{b}$ .



Model	Rescattering	Direct	Delta
CD Bonn	-22.11	-2.35	-
AV18	-21.60	-1.47	-
CCF	-21.12	-0.26	-2.95
Hannover	-22.67	+0.12	-3.45

Table 2.2: The values of  $I_T$  obtained in calculations with different parameters.

In Fig. 2.8 we compare the results of our calculation for  $\alpha$  to the experimental data<sup>#4</sup>. One clearly sees that going from LO to NLO improves the description of the data. Note also that even a change by about a factor of 2 in the cross section is in line with what is expected from the counting: after all the expansion parameter for the amplitude is  $\chi_\pi = 0.4$ . At the same time the relatively large expansion parameter implies a sizable theoretical uncertainty in  $\alpha^{NLO}$  that we estimate to be of order of  $2\chi_\pi^2 \sim 30\%$ . Thus, a calculation to N<sup>2</sup>LO is clearly called for.

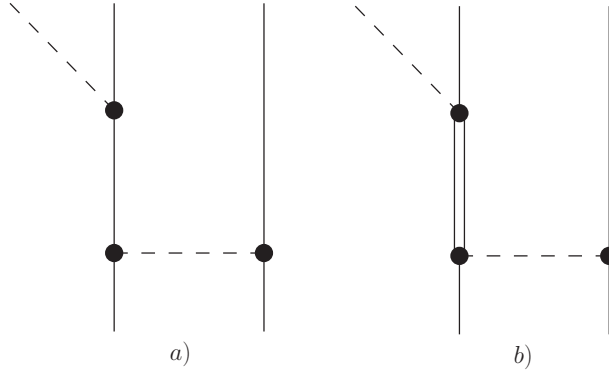


Figure 2.9: Tree level diagrams that contribute at leading (a) and next-to-leading order (b) to  $p$ -wave  $NN \rightarrow NN\pi$ . The double line denotes a  $\Delta$ -isobar. Again, in both diagrams with the one-pion exchange only one part of the  $NN$  and  $NN \rightarrow N\Delta$  potential is shown.

We also performed a calculation for  $p$ -wave pion production close to threshold up to NLO. The diagrams that enter the  $p$ -wave production amplitude near threshold are shown on Fig. 2.9. We calculated the parameter  $\beta$  in Eq. (2.15), to be precise—its part stemming from the  $p$ -wave diagrams on Fig. 2.9 (the parts that correspond to the energy dependence of  $\alpha$  are of higher orders). Note that loop diagrams start to contribute to  $p$ -wave pion production only at N<sup>3</sup>LO [22]. Calculations are performed for CCF model. Taking only nucleons into account results in  $\beta^N = 297 \mu\text{b}$ , which largely underestimates the value of  $\beta$  — the experimental values are  $\beta = 790 \mu\text{b}$  [93] and  $\beta = 1220 \mu\text{b}$  [92]. Taking one pion exchange as an approximate  $NN \rightarrow N\Delta$  transition matrix, one gets

<sup>#4</sup>Note that the data from  $pn \rightarrow d\pi^0$  [86] are considerably lower than those for  $pp \rightarrow d\pi^+$  [92, 93]. It appears unclear whether this discrepancy is due to systematic uncertainties (not shown in the figure) or due to other sources [95].

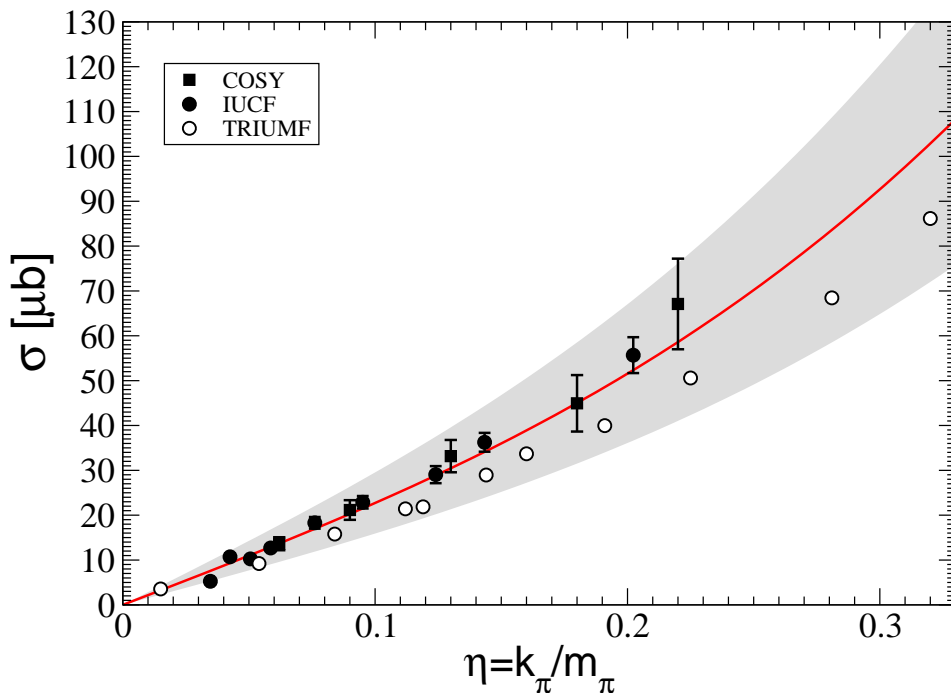


Figure 2.10: Comparison of our results to experimental data for  $pp \rightarrow d\pi^+$ , including  $s$ - and  $p$ -wave pion production as described in the text. The solid line shows the results at NLO, calculated with  $NN$  and  $N\Delta$  wave functions from CCF model. The data are as on Fig. 2.8 besides the pionic deuterium datum absent here. Theoretical uncertainty is shown as the filled stripe.

$\beta^{1\pi} = 1780 \mu\text{b}$ , which is far too large. The total result, calculated taking Delta into account and using full model wave functions, is

$$\beta^{NLO} = 1020 \mu\text{b}. \quad (2.17)$$

This number agrees with both experimental numbers within the uncertainty of 30% that we assign also to this result. The results for the total cross-section for  $pp \rightarrow d\pi^+$  are shown in Fig. 2.10. Note that we assign the theoretical uncertainty of  $2\chi_\pi^2 \sim 30\%$  also to  $\beta^{NLO}$ . The observed agreement with experimental data is quite good.

In the case of  $p$ -wave production Delta gives a very important contribution, which corresponds to the  ${}^1D_2(NN) \rightarrow {}^5S_2(N\Delta)$  transition. Two things should be mentioned concerning this contribution of Delta which is of the same size as the nucleon contribution. Firstly, comparing to the case of the  $s$ -wave production, we see that at threshold allowed  $NN \rightarrow N\Delta$  transitions that contribute are  ${}^3P_1 \rightarrow {}^3P_1$ ,  ${}^5P_1$ ,  ${}^5F_1$  for  $s$ -wave pions and  ${}^1S_0 \rightarrow {}^5D_0$ ,  ${}^1D_2 \rightarrow {}^5S_2$ ,  ${}^5D_2$ ,  ${}^3D_2$  for  $p$ -wave pions. The  $N\Delta$  intermediate state can be in an  $S$ -wave in the latter case.  $S$ -wave is not suppressed by the centrifugal barrier, and the energy of  $N\Delta$  system is under threshold, which means that low momenta in the convolution are the most important. Therefore the  ${}^1D_2 \rightarrow {}^5S_2$  contribution will be large compared to other Delta contributions, which is indeed the case. Secondly, the Delta contribution is of NLO in our counting, since we assign  $M_\Delta - M \sim p$ .

Therefore the Delta propagator gives us an additional factor of  $m_\pi/p = \chi_\pi$  compared to nucleon. However the numerical result for the Delta contribution to  $p$ -wave pion production is large. In fact, the quantity which enters the Delta propagator in this case is  $M_\Delta - M - m_\pi \sim m_\pi$ . Clearly, the counting can not account for such cancellations in general.

## 2.6 Summary of Chapter 2

We have shown that the proper set of diagrams that contributes to the transition operator for the reaction  $NN \rightarrow NN\pi$  at NLO in chiral perturbation theory is given by the diagrams of Fig. 2.2, however, with the  $\bar{N}N\pi\pi$  vertex in diagram (a) put on-shell. To get to realistic results these operators are to be convoluted with proper  $NN$  wave functions. The irreducible chiral loops that arise at this order exactly cancel those terms that arise from the off-shell parts of the WT vertex. This cancellation is required for formal consistency of the whole scheme, since the mentioned diagrams show a linear growth with respect to the outgoing  $NN$  momentum. Such a growth would have led to a large sensitivity to the  $NN$  wave function, when the convolution with the final state interaction is calculated. This, however, would have been in conflict with general arguments.

This at the same time also explains, why the sum of all loops has to vanish at next-to-leading order for the reaction  $pp \rightarrow pp\pi^0$ : in this channel there is no leading rescattering contribution. Thus, there is also nothing that could cancel the linear divergence discussed above. The consistency of the formalism therefore demands the sum of all loops to vanish.

As a result of our findings we can conjecture a general recipe on how to deal with pion reactions in a nuclear environment in the presence of time derivatives in vertices: one has to calculate all diagrams up to a given order, including those that are formally reducible. Then the energy dependence in the vertices is used to cancel one of the nucleon propagators. This produces an irreducible piece that is to be part of the transition operator as well as a reducible piece, where, however, the energy dependence of the vertices is replaced by the corresponding on-shell value<sup>#5</sup>.

This new rule has significant impact on the role of isoscalar rescattering in  $NN \rightarrow NN\pi$  (diagram (a) of Fig. 2.2, but with the leading isoscalar interaction used for  $\pi N \rightarrow \pi N$ ). Empirically the isoscalar  $\pi N$  scattering length is known to be very small. Theoretically it turned out that this smallness is a consequence of an efficient cancellation amongst individually large terms [97]. Due to the energy dependence of the  $\pi N \rightarrow \pi N$  operators, however, when evaluated in the kinematics relevant for pion production in  $NN$  collision this cancellation is much less efficient leading to a significant contribution from isoscalar rescattering [28, 71]. If, on the other hand, the above rule is used, isoscalar rescattering enters with the strength of the very small isoscalar  $\pi N$  scattering length and thus would give a negligible contribution.

We have demonstrated that the net effect of the inclusion of the NLO loops, shown in Fig. 2.3, is to enhance the leading rescattering amplitude by a factor of 4/3, bringing

---

<sup>#5</sup>Note that in the presence of quadratic time derivatives at individual vertices or the simultaneous appearance of several time derivatives in one diagram, additional vertices are to be included [96].

its contribution to the cross section for  $pp \rightarrow d\pi^+$  close to the experimental value.

The next steps will be to evaluate the  $NN \rightarrow NN\pi$  amplitudes to N<sup>2</sup>LO for both  $s$ - and  $p$ -wave pions for all possible amplitudes. At this order two counterterms enter for the pion  $s$ -waves and one for the pion  $p$ -waves both accompanied by  $S$ -wave nucleons in the final state. To this order  $p$ -wave pions together with  $P$ -wave nucleons are parameter free predictions. On the other hand there are in total more than 40 observables<sup>#6</sup> measured for the reaction channels  $pp \rightarrow pp\pi^0$  [98],  $pp \rightarrow pn\pi^+$  [99],  $pp \rightarrow d\pi^+$  [100] and  $pn \rightarrow pp\pi^-$  [101, 102]. Up to now only one phenomenological calculation was compared to this large amount of data [22, 66] and it was found that all charged channels are well described, whereas there are significant discrepancies for the neutral pions. It will therefore be of strong interest to see if the new structures that emerge from the chiral Lagrangian are able to cure these discrepancies.

Once the described channels are analyzed within ChPT one should move ahead to consistently investigate the isospin violating observables measured recently, namely the forward–backward asymmetry in  $pn \rightarrow d\pi^0$  [21] as well as the total cross section for  $dd \rightarrow \alpha\pi^0$  [53]. First steps in this direction were taken in Refs. [54, 55].

Another application of the developed counting scheme is the calculation of dispersive and absorptive corrections to the pion–deuteron scattering length. These corrections are directly related to the reaction  $NN \rightarrow d\pi$ , and we can directly apply the developed formalism to the calculation of these corrections. We address this issue in Chapter 5.

---

<sup>#6</sup>This large number is achieved by fully exploiting the five–dimensional phase space [98].

# Chapter 3

## Pion Photoproduction off the Deuteron: $\gamma d \rightarrow \pi^+ nn$

In this chapter we present a complete calculation within ChPT up to order  $\chi^{5/2}$  for the reaction  $\gamma d \rightarrow \pi^+ nn$ , where the expansion parameter for the chiral expansion is denoted by  $\chi = m_\pi/M$ .

### 3.1 Introduction

The calculation of the reaction  $\gamma d \rightarrow \pi^+ nn$  is of high theoretical interest, because it provides an important test for our understanding of those aspects of  $\pi NN$  dynamics that are relevant for pion production reactions on the deuteron. That understanding is a prerequisite for the reliable extraction of the pion photoproduction amplitude on the neutron, commonly done from corresponding deuteron data, but also for the determination of the  $nn$  scattering length from  $\pi^+$  production data discussed below. Data for the total cross-section on the channel  $\gamma d \rightarrow \pi^+ nn$  exist for excess energies  $Q = \sqrt{s} - (2M + m_\pi) \leq 20$  MeV [103], which allows us to verify our results.

In view of the high accuracy of the data and also because of the high reliability required for the extraction of the above mentioned quantities involving neutrons it is now time to critically investigate (and avoid whenever possible) the approximations traditionally used in pion reactions on few-nucleon systems. Here we will focus on approximations to the pion rescattering contribution as they are commonly used in both effective field theory calculations (see Ref. [104] and references therein) as well as phenomenological calculations (see Ref. [105] and references therein). Especially for the effective field theory calculations one might wonder how recoil corrections could be an issue, for the formalism allows for a rigorous expansion in  $m_\pi/M$  that should build up the recoil corrections perturbatively. However, it was stressed recently [32] that the  $\pi NN$  threshold introduces non-analyticities in the transition operators that call for special care: instead of being suppressed by one power in  $m_\pi/M$  compared to the formally leading rescattering contributions (static term), as one might expect naively, the nucleon recoil terms turn out to scale as  $\sqrt{m_\pi/M}$  relative to the static term. The only publication we are aware of, where the recoil corrections were treated properly for the near threshold region, is a phenomenological calculation for  $\gamma d \rightarrow \pi^0 d$  presented

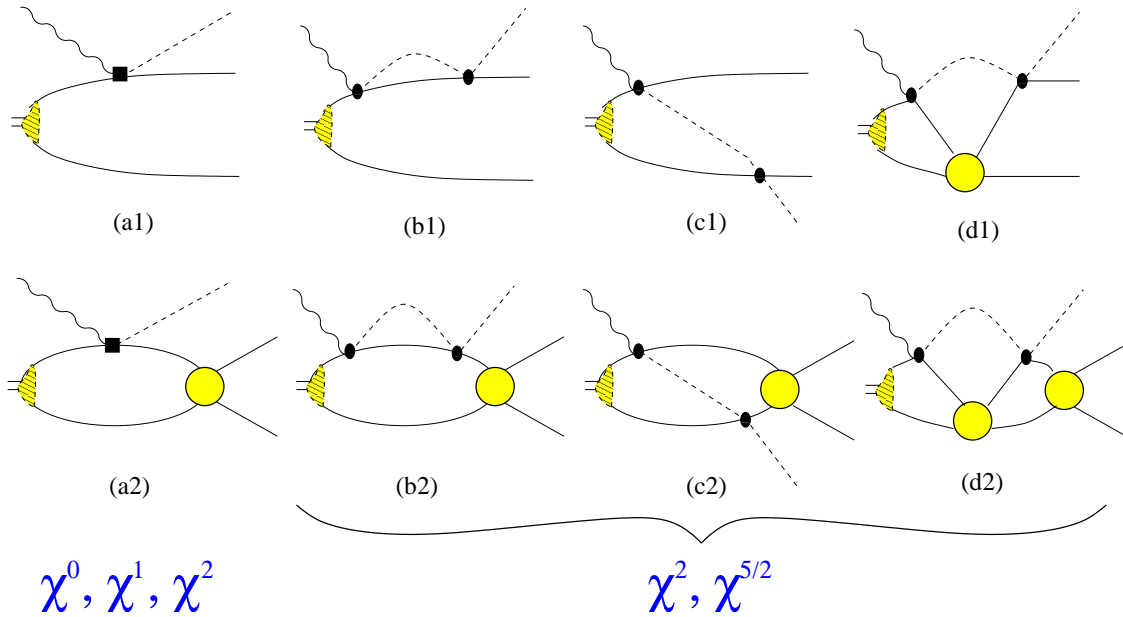


Figure 3.1: Diagrams for  $\gamma d \rightarrow \pi^+ nn$ . Shown are one-body terms (diagrams (a) and (b)), as well as the corresponding rescattering contribution (c)—all without and with final state interaction. The need to include the  $NN$  interaction non-perturbatively implies also the inclusion of diagrams with the two nucleon pair interacting, while a pion is in flight—this class is shown in diagrams (d). Solid straight, wiggly and dashed lines denote nucleons, photons and pions, in order. Filled squares and ellipses stand for the various vertices, the hatched area shows the deuteron wave function and the filled circle denotes the  $nn$  scattering amplitude. Crossed terms (where the external lines are interchanged) are not shown explicitly. The tree level  $\gamma p \rightarrow \pi^+ n$  vertex, as it appears in diagrams (a1) and (a2), contributes at leading order (order  $\chi^0$ ), and order  $\chi^1$  and  $\chi^2$ , depending on the one-body operator used. Loops start to contribute at order  $\chi^2$ , the corresponding recoil corrections enter at order  $\chi^{5/2}$ .

in Ref. [106] (so far most phenomenological studies concentrated on the  $\Delta$ -region, cf. Ref. [24] and references therein).

Recently the effect of the nucleon recoil on rescattering processes of pions in  $\pi d$  scattering was studied [32, 107, 108] (for previous investigations on the role of the nucleon recoil see Refs. [109–111]). In particular, in Ref. [32] it was demonstrated that, at least for the  $\pi d$  system, the nucleon recoil can be neglected as long as the two-nucleon intermediate state is Pauli forbidden, while the pion is in flight. Thus, in this case the static approximation for the pion exchange is justified. However, as soon as the two-nucleon state is Pauli allowed, the nucleon recoil has to be included. In this case it turned out that the whole rescattering contribution (i.e. static term + recoil corrections) practically canceled completely. It should be stressed that for  $\pi d$  elastic scattering the Pauli allowed two-nucleon intermediate states are suppressed by chiral symmetry. We will study the reaction  $\gamma d \rightarrow \pi^+ nn$  with special emphasis on the abovementioned recoil corrections. In this system the selection rules are such that the

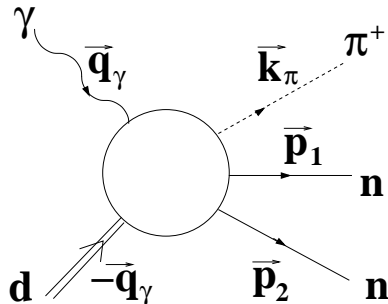


Figure 3.2: Kinematical variables for  $\gamma d \rightarrow \pi^+ nn$ . The relative neutron–neutron momentum is defined as  $\vec{p}_r = \frac{1}{2}(\vec{p}_1 - \vec{p}_2)$ .

S-wave two–nucleon intermediate state during the pion rescattering process is allowed by the Pauli principle. In addition, once the strength of the one–body operator is fixed to the reaction  $\gamma p \rightarrow \pi^+ n$ , no free parameters occur in the calculation for  $\gamma d \rightarrow \pi^+ nn$  to the order where the leading recoil corrections enter and thus we can compare our results to experimental data directly. At the same time we get a better understanding of the few–body corrections to  $\gamma d \rightarrow \pi^0 pn$ . This reaction will eventually allow one to extract the amplitude of  $\gamma n \rightarrow \pi^0 n$  complementary to using  $\gamma d \rightarrow \pi^0 d$  discussed in Ref. [112]. Note that up to now no calculation for  $\gamma d \rightarrow \pi^+ nn$  exists where the nucleon recoil was properly included.

Before going into the details some comments are necessary regarding the relevant scales of the problem. In the near threshold regime of interest here (excess energies of at most 20 MeV above pion production threshold) the outgoing pion momenta are small compared even to the pion mass. Thus, in addition to the conventional expansion parameters of ChPT  $m_\pi/\Lambda_\chi$  and  $q_\gamma/\Lambda_\chi$ , where  $\Lambda_\chi$  denotes the chiral symmetry breaking scale of order of the nucleon mass (in what follows we assign  $\Lambda_\chi = M$ ), and  $q_\gamma$  denotes the photon momentum in the center–of–mass system which is of order of the pion mass, we can also regard  $k_\pi/m_\pi$  as small, where  $k_\pi$  denotes the outgoing pion momentum (see Fig. 3.2 for the definition of kinematical variables). In what follows we will perform an expansion in two parameters, namely

$$\chi_m = m_\pi/M \text{ and } \chi_Q = k_\pi/m_\pi .$$

Obviously, the value of the second parameter depends on the excess energy. The energy regime of interest to us are excess energies up to 20 MeV. The maximum value of  $\chi_Q$ ,  $\chi_Q^{max} = \sqrt{2Q/m_\pi}$ , possible at maximum energy is thus about 1/2. Since this is numerically close to  $\sqrt{\chi_m}$  we use the following assignment for the expansion parameter

$$\chi \sim \chi_m \sim \chi_Q^2 . \quad (3.1)$$

In this chapter we will concentrate on total cross sections only and thus—up to one important exception— $\chi_Q$  appears with even powers only. In table 3.1 we show the powers of  $\chi_m$  and  $\chi_Q$  that appear in the amplitude as well as the corresponding order  $\chi$  for the total cross section. The pertinent diagrams will be discussed in detail below. Note that the diagrams with  $\pi N$  rescattering (see diagrams (b), (c) and (d) in Fig. 3.1)

order	$s$ -wave	$p$ -wave	$d$ -wave
1	$\chi_m^0$		
$\chi^1$	$\chi_m^1, \chi_Q^2$	$\chi_Q$	
$\chi^2$	$\chi_m^2, \chi_Q^2 \chi_m, \chi_Q^4$	$\chi_Q \chi_m$	$\chi_Q^2$
$\chi^{5/2}$	$\chi_m^2 \chi_Q, \chi_m^{5/2}, \chi_m^{1/2} \chi_Q^4$		

Table 3.1: Pattern of appearance of the expansion parameters  $\chi_m = m_\pi/M$  and  $\chi_Q = k_\pi/m_\pi$  on the amplitude level for a given order in  $\chi$  for the total cross section. The first column shows the order parameter  $\chi$ , whereas the other three columns show the order assignments for the amplitudes of the various pion partial waves of relevance. Note, as we here consider the total cross section only, different partial waves do not interfere—this was used in the order assignment.

contribute at order  $\chi_m^2$  as well as at  $\chi_m^2 \chi_Q, \chi_m^{5/2}$  and at  $\chi_m^{1/2} \chi_Q^4$ . The origin of the non-integer power of  $\chi$  are the two-body  $\pi N$  and three-body  $\pi NN$  singularities. This issue is discussed in detail in section 3.3.

The small pion momentum in the exit channel leads to a suppression of higher pion partial waves. As can be seen from table 3.1 we need to consider at most pion  $d$ -waves (here and in what follows we denote pion partial waves by small letters and  $NN$  partial waves by capital letters). On the other hand, at excess energies of 20 MeV the maximum two nucleon momentum in units of the pion mass is of order 1 and thus there is a priori no suppression of higher  $NN$  partial waves. However, since the  $NN$  phase shifts are only sizable for  $S$ - and  $P$ -waves at the small energies of relevance, we only include the  $NN$  final state interaction of those partial waves.

To summarize the scope of this work, it aims to improve the existing calculations for the reaction  $\gamma d \rightarrow \pi^+ nn$  in the following important aspects:

- A first complete ChPT calculation for the reaction  $\gamma d \rightarrow \pi^+ nn$  up to order  $\chi^{5/2}$  is presented. At this order loops contribute and the non-perturbative character of the  $NN$  interaction calls for the use of interacting two nucleon Green's functions (leading to up to 3 loop diagrams as shown in diagram (d2) of Fig. 3.1).
- The leading nucleon recoil is included without approximation. It enters at order  $\chi^{5/2}$ .
- As always in effective field theory studies an estimation of the accuracy of the calculation can be given. A conservative estimate points at an accuracy of 2 % for the few-body corrections to the amplitude near threshold which is of the same order as the uncertainty of the input quantity  $E_{0+}$ —the invariant electric dipole amplitude for  $\gamma p \rightarrow \pi^+ n$  at threshold. Adding the two uncertainties in quadrature we arrive at a total uncertainty of 3 % for the full transition operator. In this



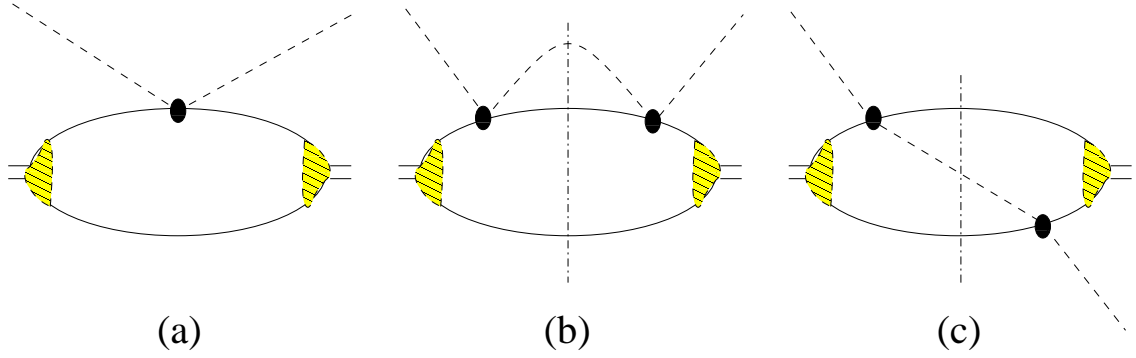


Figure 3.3: Typical diagrams for  $\pi d$  scattering. Shown are one-body terms (diagram (a) and (b)), as well as the corresponding rescattering contribution (c). Crossed terms (where the external pion lines are interchanged) are not shown explicitly.

chapter we use phenomenological  $NN$  wave functions and thus we are not in the position to estimate the uncertainty of the complete matrix elements (see the corresponding discussion in Section 3.6). We postpone the discussion of this issue until Chapter 4.

- For the first time pion  $p$ - and  $d$ -waves as well as the final state interaction in the  $NN$   $P$ -waves are included in a calculation for the near threshold regime. Note that the significance of  $NN$   $P$ -waves even at photon energies below 20 MeV was established long ago [23], however, so far they were only considered as plane waves in the impulse term (thus only through diagram (a1) of Fig. 3.1).

This chapter is structured as follows: in Section 3.2 we briefly review the central findings of Ref. [32]. The three-body dynamics is discussed in detail in Section 3.3. The same formalism as described for  $\pi d$  scattering in Section 3.2 is applied to the reaction  $\gamma d \rightarrow \pi^+ nn$  in Section 3.4. In Section 3.5 we present the results. We summarize in Section 3.6. The details of the calculation for the various diagrams are given in Appendix E.

## 3.2 Remarks on the $\pi d$ system

In this section we briefly review the findings of Ref. [32]. The relevant diagrams for  $\pi d$  scattering are shown in Fig. 3.3. Diagram (a) denotes the tree level one-body contribution, diagram (b) the loop correction to the one-body piece and diagram (c) the rescattering term. It should be clear that the Pauli principle calls for a consistent simultaneous treatment of (b) and (c), for an interchange of the two nucleons while the pion is in flight (this intermediate state is marked by the perpendicular line in Fig. 3.3) transforms one diagram into the other.

The calculations of Ref. [32] were based on the effective  $\pi N$  vertex,

$$\hat{V}_{\pi N}^{ba} = \delta^{ba} g_+ + \frac{i}{\sqrt{2}} \epsilon^{abc} \tau^c g_- , \quad (3.2)$$

where  $a, b$ , and  $c$  are the Cartesian pion indices. We note that this vertex leads, up to corrections of  $\mathcal{O}(m_\pi/M)$ , to identical results for the  $\pi d$  scattering length as the leading order chirally symmetric  $\pi N$  interaction (the Weinberg–Tomozawa term) if we choose  $g_- = -2\sqrt{2}m_\pi M/(2f_\pi^2)$  and  $g_+ = 0$ .

The main issue of Ref. [32] was to properly isolate the single nucleon contribution (the one that would be measured in  $\pi N$  scattering) from the few body corrections. It is clear that part of diagram (b) contributes to the former and part to the latter. As outlined in Ref. [32] the proper prescription to separate these two pieces is to add to the tree level scattering (diagram (a)) the single nucleon one-loop contribution on the free nucleon at rest—this sum is the expression for the  $\pi N$  scattering length,  $a^{(1\text{-body})}$ . The same loop needs to be subtracted from the full contribution depicted in diagram (b). This procedure at the same time renders the expression for the loop finite. This difference is a true two-nucleon operator. To obtain more symmetric, easier to interpret results we subtracted from the rescattering piece the expression for the static exchange, i.e. the contribution from diagram (c) of Fig. 3.3 calculated in the static limit. In order to leave the final result unchanged, this contribution needs to be added as  $a_{\text{LO}}^{(\text{st})}$  (and  $a_{\text{NLO}}^{(\text{st})}$ ) to the expression for the  $\pi d$  scattering length. Thus, the full result for the  $\pi d$  scattering length reads

$$a = a^{(1\text{-body})} + a_{\text{LO}}^{(\text{st})} + a^{(\text{rec})} + a_{\text{NLO}}^{(\text{st})} , \quad (3.3)$$

where the individual contributions for the static (st), the recoil (rec) and the NLO corrections to the static term are given by

$$a_{\text{LO}}^{(\text{st})} = (g_+^2 - g_-^2) I_0 ; \quad a^{(\text{rec})} = g_+^2 I_+ + g_-^2 I_- ; \quad a_{\text{NLO}}^{(\text{st})} \simeq -\frac{m_\pi}{M} (g_+^2 - g_-^2) I_0 . \quad (3.4)$$

Here the terms proportional to  $g_+^2$  ( $g_-^2$ ) correspond to isoscalar (isovector) rescattering and thus to Pauli allowed (Pauli blocked) intermediate  $NN$  state. The integrals denoted by  $I_0$  and  $I_\pm$  are [32]:

$$I_0 = \xi \int d^3p d^3q \Psi(\vec{p} - \vec{q})^\dagger \frac{1}{\vec{q}^2} \Psi(\vec{p}) , \quad (3.5)$$

$$I_\pm = \frac{\xi}{2} \int d^3p d^3q |\Psi(\vec{p}) \pm \Psi(\vec{p} - \vec{q})|^2 \left( \frac{1}{\vec{q}^2 + \rho} - \frac{1}{\vec{q}^2 + \tilde{\rho}} \right) , \quad (3.6)$$

where  $\xi = [64\pi^4 M^2 (1 + m_\pi/(2M))]^{-1}$ ,  $\rho = \omega(2\epsilon + (\vec{p}^2 + (\vec{p} - \vec{q})^2)/M)$ , and  $\tilde{\rho} = \omega\vec{q}^2/M$ , with  $\epsilon$  and  $\omega$  for the deuteron binding energy and the pion energy, respectively, and  $\Psi$  for the deuteron wave function. The integrals  $I_0$ ,  $I_\pm$  were evaluated numerically using the deuteron wave functions from the CD Bonn potential [87]:

$$I_+ = -0.88 I_0 , \quad I_- = -0.19 I_0 .$$

These numbers clearly reflect the claim made above: for the  $\pi d$  system the isovector  $\pi N$  interaction, proportional to  $g_-$ , leads to a Pauli blocked intermediate state and numerically we find that the recoil corrections lead only to a 20% correction (Integral  $I_-$  is numerically small,  $I_- \ll I_0$ ). When the NLO pieces mentioned above are added, the correction resulting from recoil and NLO terms together is only 4% and thus the static pion exchange is a good approximation for the total rescattering contribution. On

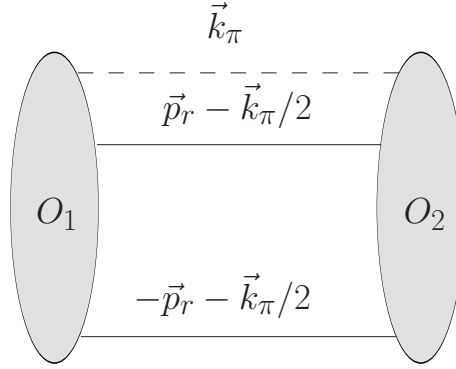


Figure 3.4: Notation used in the discussion of the  $\pi NN$  intermediate state. The ellipses labeled  $O_1$  and  $O_2$  denote the transition operators for the various possible reactions; e.g. for  $\gamma d \rightarrow \pi^+ nn$  the operators  $O_1$  and  $O_2$  refer to  $\gamma d \rightarrow \pi^+ nn$  and  $\pi^+ nn \rightarrow \pi^+ nn$ , respectively.

the other hand, the isoscalar  $\pi N$  interaction leads to a Pauli allowed intermediate state and in this case the recoil corrections cancel 90% of the static exchange ( $I_+$  is large and negative,  $(I_0 + I_+) \ll I_0$ ). The inclusion of the NLO piece in this case further reduces the total rescattering contribution down to 3 % of the static term. Therefore, in this case estimating the total rescattering contribution by the static exchange only is a very poor approximation. In addition, in this case one has to include the  $NN$  interaction in the intermediate state, which might change the picture [110].

### 3.3 The role of the $\pi NN$ cuts

In this section we discuss the role of the three–nucleon cuts in more general terms. All arguments presented for the three–body dynamics apply to pion–nuclear reactions in general (as, e.g.,  $\pi d$  scattering), however, in this section we will use only the reaction  $\gamma d \rightarrow \pi^+ nn$  as illustrative example.

Typical diagrams that contain a  $\pi NN$  intermediate state (e.g., diagram (c2) of Fig. 3.1 — cf. the corresponding Eq. (E.18) in Appendix E), can be cast into the following form by a proper choice of variables (and dropping terms of higher order in  $m_\pi/M$ )

$$I_{\pi NN}(Q) = \int \frac{dk_\pi k_\pi^2 dp_r p_r^2}{(2\pi)^6} \frac{f(k_\pi^2, p_r^2)}{Q - k_\pi^2/(2m_\pi) - p_r^2/M + i\gamma}, \quad (3.7)$$

where  $k_\pi$  denotes the pion momentum and  $p_r$  denotes the relative momentum of the two nucleons while the pion is in flight (cf. Fig. 3.4), and  $f(k_\pi^2, p_r^2)$  is a function that is supposed to fall off at momenta of order of  $m_\pi$ . Using the static approximation means to expand the denominator of the integral in Eq. (3.7) in powers of  $m_\pi/M$  before evaluation

of the integral. Thus, we get in the static approximation<sup>#1</sup>

$$I_{\pi NN}^{(\text{static})}(Q) = \int \frac{dk_\pi k_\pi^2 dp_r p_r^2}{(2\pi)^6} \frac{f(k_\pi^2, p_r^2)}{Q - k_\pi^2/(2m_\pi) + i\gamma} + \mathcal{O}\left(\frac{m_\pi}{M}\right). \quad (3.8)$$

We will demonstrate now analytically (and in Section 3.5 numerically) that this procedure misses an important contribution to  $I_{\pi NN}$ .

Above the pion production threshold the denominator in Eq. (3.7) has a three-body singularity that leads to an imaginary part. This imaginary part of  $I_{\pi NN}$  can be calculated by the replacement

$$(Q - k_\pi^2/(2m_\pi) - p_r^2/M + i\gamma)^{-1} \rightarrow -i\pi\delta(Q - k_\pi^2/(2m_\pi) - p_r^2/M).$$

Thus we find

$$I_{\pi NN}^{(\text{cut})}(Q) = -i\pi m_\pi \int \frac{dp_r p_r^2}{(2\pi)^6} f(2m_\pi(Q - p_r^2/M), p_r^2) \sqrt{2m_\pi(Q - p_r^2/M)}. \quad (3.9)$$

From this formula we see that the imaginary parts of the pion loops in diagrams (b2) and (c2) of Fig. 3.1 are finite and lead to a strongly energy-dependent contribution. As long as the momentum dependence of the function  $f$  can be neglected, this part of the amplitude grows like  $Q^2$ , i.e. like the three-body phase space. These are the contributions at order  $\chi_m^{1/2} \chi_Q^4$  given in Table 3.1. Note that the corresponding amplitudes without final state interaction ((b1) and (c1) of Fig. 3.1) do not have a three-body cut but only a two-body singularity. Thus their imaginary parts scale as  $\chi_m^2 \chi_Q$ .

On the other hand, the unitarity cut contribution of  $I_{\pi NN}^{(\text{static})}$  reads

$$I_{\pi NN}^{(\text{cut, static})}(Q) = -i\pi m_\pi \sqrt{2m_\pi Q} \int \frac{dp_r p_r^2}{(2\pi)^6} f(2m_\pi Q, p_r^2).$$

The most remarkable difference between  $I_{\pi NN}^{(\text{cut})}$  and  $I_{\pi NN}^{(\text{cut, static})}$  is that in contrast to the former the latter scales as  $\sqrt{Q}$ , i.e. like the two body phase space for all diagrams (even for those with final state interaction) and therefore shows an energy dependence that is completely wrong—and at variance even with perturbative three-body unitarity.

For values of  $p_r$  with  $Q > p_r^2/M$  the integral  $I_{\pi NN}^{(\text{cut})}(Q)$  (cf. Eq. (3.9)) contributes to the imaginary part of  $I_{\pi NN}(Q)$  (cf. Eq. (3.7)). To evaluate the contribution of the cut to the real part, the square root needs to be analytically continued to negative values of its argument through

$$\sqrt{2m_\pi(Q - p_r^2/M)} \rightarrow i\sqrt{2m_\pi(p_r^2/M - Q)}.$$

To demonstrate explicitly the impact of this, let us consider the case  $Q = 0$ . Then we get

$$I_{\pi NN}^{(\text{cut})}(0) = \pi m_\pi \sqrt{\frac{2m_\pi}{M}} \int \frac{dp_r p_r^2}{(2\pi)^6} f(-2m_\pi p_r^2/M, p_r^2) p_r. \quad (3.10)$$

<sup>#1</sup>Note, we here use the phrase 'static approximation' in a quite broad sense in that we also allow for the inclusion of correction terms analytic in  $\chi$ . In phenomenological studies those corrections are normally dropped.

The corresponding expression for  $I_{\pi NN}^{(\text{cut}, \text{static})}(0)$  vanishes. On the other hand, the expression for the leading static approximation (cf. Eq. (3.8)) gives at threshold

$$I_{\pi NN}^{(\text{static})}(0) = -2m_\pi \int \frac{dp_r p_r^2 dk_\pi}{(2\pi)^6} f(k_\pi^2, p_r^2). \quad (3.11)$$

The static approximation Eq. (3.11) only acquires corrections analytic in  $(m_\pi/M)$  and thus misses the contribution of Eq. (3.10). In fact, Eq. (3.10) corresponds to the threshold value of the mentioned non-analytic contribution from the three-body intermediate state that is dropped in the static approximation—the extension to arbitrary values of  $Q$  is straightforward. However, the contribution from  $I_{\pi NN}^{(\text{cut})}$  is significant as one can see from a naive dimensional analysis where all momenta—even those in the integral measure—are replaced by their typical values:

$$I_{\pi NN}^{(\text{cut})} \sim -\sqrt{\frac{m_\pi}{M}} I_{\pi NN}^{(\text{static})}, \quad (3.12)$$

as claimed in the introduction to this chapter. Therefore, in general the static approximation is to be avoided! As one can see, the contributions from the nucleon recoil through the three-body singularities to both the real and the imaginary part of the amplitude appear to be down by  $\sqrt{\chi}$  compared to the leading loop contribution (the static piece). To be more explicit they contribute at orders  $\chi_m^{5/2}$  and  $\chi_m^{1/2} \chi_Q^4$  (cf. table 3.1). On the other hand, if we expand the propagator in Eq. (3.7) before the integration, we only get terms analytic in the pion mass (order  $\chi$  corrections to the static piece) and miss the most prominent correction.

Now we are in the position to discuss in more detail the conjecture presented in Ref. [32] as well as in the previous section, namely that in general for all those diagrams, where the  $S$ -wave two-nucleon intermediate state that appears while the pion is in flight is forbidden by the Pauli principle, the various recoil corrections largely cancel, while in case of Pauli allowed  $S$ -wave intermediate states they add coherently. In the latter case the net effect of the rescattering diagrams was claimed to be small due to a destructive interference between the recoil corrections and the leading rescattering contribution (the static term—cf. Eq. (3.8)). We will now discuss the two cases in the light of the discussion above. The essential observation is that the recoil corrections are the analytic continuation of the imaginary parts related to on-shell  $\pi NN$  intermediate states.

*Pauli forbidden intermediate states:* in this case the imaginary contributions stemming from the three-body unitarity cut in diagrams of the type of (b2) and those from the type of (c2) of Fig. 3.1 need to cancel exactly, for the corresponding  $\pi NN$  state is forbidden. As a consequence, there will also be a cancellation for the analytic continuations (see Eq. (3.9)), *i.e.* for the corresponding principal value integrals, and thus the recoil corrections necessarily cancel to a large degree. Since this statement is based solely on the Pauli principle it must hold for all reactions.

*Pauli allowed intermediate states:* contrary to the first option in this case the corresponding unitarity cut parts of the diagrams (b2) and (c2) of Fig. 3.1 add coherently and, as above, the same is to be true for their analytic continuation. It is not possible to claim in general that the recoil contribution from the principal value integrals completely cancels the whole static term. However, as illustrated by the estimate of Eq. (3.12), the

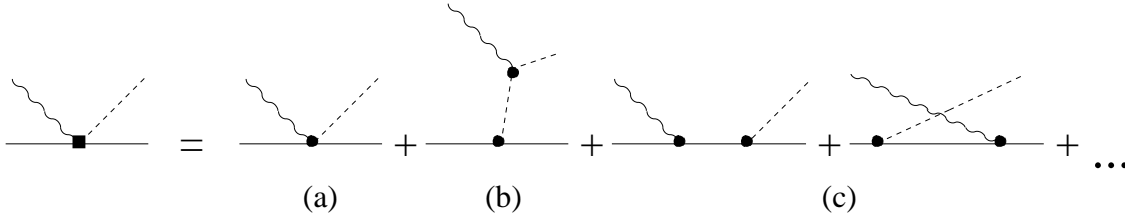


Figure 3.5: Diagrams that contribute to the one-body production operator in diagrams (a1) and (a2) of Fig. 3.1. Only tree level diagrams that contribute to  $\gamma p \rightarrow \pi^+ n$  up to order  $\chi^2$  are shown. The dots denote loops that contribute to the  $s$ -wave amplitude at order  $\chi^2$  as those shown in Fig. 3.6 (b) and (c).

recoil corrections tend to be of the order of magnitude of the static term and tend to interfere destructively with it. In addition, there might be significant contributions from intermediate  $NN$  interaction [110]. Here we refer to the discussion in Section 3.5 and to Fig. 3.11.

As we discussed in the previous section, the leading operator for  $\pi N$  scattering acting on a deuteron leads to a  $\pi NN$  state, where the  $S$ -wave is forbidden for the  $NN$ -pair by the Pauli principle. On the other hand, as will be outlined below, the leading operator for  $\gamma N \rightarrow \pi N$ , when acting on a deuteron field, leads to a  $\pi NN$  state, where the  $NN$ -pair is allowed to be in an  $S$ -wave. Thus, in the reactions  $\pi d \rightarrow \pi d$ ,  $\pi d \rightarrow \gamma NN$ , and  $\gamma d \rightarrow \pi^0 d$  the static approximation indeed accounts for a significant fraction of the few-body corrections, whereas in  $\gamma d \rightarrow \pi^+ nn$  and  $\gamma d \rightarrow \gamma d$ , when evaluated near the pion threshold, the static approximation is expected to work quite poorly. References for the corresponding calculations are given in the introduction to this chapter.

### 3.4 The reaction $\gamma d \rightarrow \pi^+ nn$

We will start with a discussion of the one-body contributions to be used in the diagrams of type (a1) and (a2) of Fig. 3.1.

At threshold the  $\pi\gamma NN$  vertex at leading order ( $\chi_m^0$ ) and at next-to-leading order ( $\chi_m^1$ ) is given by the so-called Kroll-Ruderman (KR) term [113] and its recoil correction<sup>#2</sup>,

$$\hat{V}_{\pi\gamma NN}^{\text{KR}} = ieg_{\pi N} \left( 1 - \frac{\omega_\pi}{2M} \right) (\vec{\epsilon}_\gamma \cdot \vec{\sigma}) \epsilon^{3ab} \tau^b, \quad (3.13)$$

where  $\vec{\epsilon}_\gamma$  denotes the photon polarization and  $\omega_\pi$  is the energy of the outgoing pion. The corresponding diagram is shown as diagram (a) in Fig. 3.5. Note that we use  $g_{\pi N} = 13.4$  in the calculation and the charge  $e$  is normalized such that the fine structure constant is given as  $e^2/(4\pi) = \alpha = 1/137$ . This vertex contributes to the one-nucleon operator (impulse term) as shown in diagram (a1) and (a2) of Fig. 3.1 and also provides

<sup>#2</sup>A list of the vertices relevant for chiral perturbation theory calculations can be found in Ref. [11]; however, in contrast to that reference we use the spinor normalization  $\bar{u}u = 2M$ , and this factor  $2M$  is attributed to vertices and propagators (see Appendix A). In addition we used the Goldberger-Treiman relation to replace  $g_A/f_\pi$  by  $g_{\pi N}/M$ .

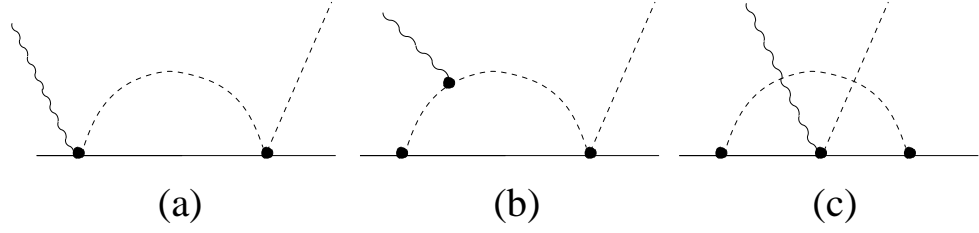


Figure 3.6: Typical pion loops that contribute to  $\gamma p \rightarrow \pi^+ n$ . Crossed terms for diagrams (a) and (b) are not shown explicitly.

the production vertex for the virtual pion to be rescattered. As the  $\pi\gamma NN$  vertex is both spin and isospin dependent, now, in contrast to  $\pi d$  scattering, for the rescattering contributions the two-nucleon intermediate state that occurs while the pion is in flight is allowed by the Pauli principle to be in an  $S$ -wave.

According to Table 3.1 at order  $\chi$  we also need to consider the leading correction in  $\chi_Q^2$  to the  $s$ -wave as well as the leading  $p$ -wave contribution which is of order of  $\chi_Q$ . Both are provided by the diagram where the photon couples to the pion in flight corresponding to diagram (b) of Fig. 3.5. The corresponding expression for the effective  $\pi\gamma NN$  vertex reads

$$\hat{V}_{\pi\gamma NN}^{(b)} = -ie g_{\pi N} \vec{\sigma} \cdot \left( \vec{k}_\pi - \vec{q}_\gamma \right) \frac{\vec{\epsilon}_\gamma \cdot \vec{k}_\pi}{\omega_\pi |\vec{q}_\gamma| - \vec{k}_\pi \cdot \vec{q}_\gamma} \epsilon^{3ab} \tau^b, \quad (3.14)$$

where  $\omega_\pi$  denotes the energy of the outgoing pion. This vertex contributes to the leading  $p$ -waves (order  $\chi_Q$  for the amplitude — order  $\chi_Q^2 = \chi$  for the total cross section), the leading energy dependence of the  $s$ -wave (order  $\chi_Q^2$  for the amplitude as well as the cross section, for this term can interfere with the contribution of order  $\chi^0$ ), and to the leading  $d$ -waves (order  $\chi_Q^2$  for the amplitude and thus order  $\chi_Q^4 = \chi^2$  for the cross section).

At order  $\chi_m^2$  pion loops start to contribute to the  $s$ -wave part of the  $\gamma p \rightarrow \pi^+ n$  amplitude (see Fig. 3.6) and thus to the reaction  $\gamma d \rightarrow \pi^+ nn$ . The only additional vertex needed for the evaluation of these loops is given in Eq. (3.2) with  $g_- = -2\sqrt{2}m_\pi M/(2f_\pi^2)$  and  $g_+ = 0$ . The imaginary part of diagram (a) in Fig. 3.6 contributes at  $\chi_m^2 \chi_Q$  whereas the imaginary part of diagram (b) starts to contribute only at higher order ( $\chi_m^2 \chi_Q^3$ ) and is thus not explicitly included in the calculation. In contrast to the imaginary parts the real parts of some of those pion loops on a single nucleon are divergent and need to be regularized (e.g. diagram (c) of Fig. 3.6) <sup>#3</sup>. In the calculation of the reaction  $\gamma d \rightarrow \pi^+ nn$  we use a prescription similar to that used for  $\pi d$  scattering, as described in the previous section. In practice this means to replace the expression of Eq. (3.13) by

$$\hat{V}_{\text{eff}} = i\kappa E_{0+} (\vec{\epsilon}_\gamma \cdot \vec{\sigma}) \epsilon^{3ab} \tau^b, \quad (3.15)$$

where  $\kappa = 4\pi\sqrt{2}(m_\pi + M)$ , and  $E_{0+}$  is the electric dipole amplitude. The experimental value of  $E_{0+}$  from the reaction  $\gamma p \rightarrow \pi^+ n$  is [116]:

$$E_{0+} = (28.06 \pm 0.27 \pm 0.45) \times 10^{-3} m_\pi^{-1}.$$

<sup>#3</sup>For a complete discussion of all relevant loops we refer to Refs. [114, 115].

This value coincides within errors with the result of ChPT up to order  $\chi_m^3$  [33]:

$$E_{0+} = (28.2 \pm 0.6) \times 10^{-3} m_\pi^{-1}. \quad (3.16)$$

Although this calculation was performed to higher order than what we aim at here, we will use the latter value as input quantity for the threshold value of  $E_{0+}$  since the contributions of order  $\chi_m^3$  are of the order of the assigned uncertainty.

It is straightforward to show that the  $s$ -wave contribution derived from Eq. (3.14) has the same operator structure as Eq. (3.15) and we may simply include its effect by replacing  $E_{0+}$  in Eq. (3.15) by  $E_{0+}(k_\pi^2)$  defined up to order  $\chi_Q^4$  through

$$E_{0+}(k_\pi^2) = E_{0+} + E'_{0+} \frac{k_\pi^2}{m_\pi^2} + E''_{0+} \frac{k_\pi^4}{m_\pi^4}. \quad (3.17)$$

The leading contribution to both coefficients  $E'_{0+}$  and  $E''_{0+}$  can be calculated directly from Eq. (3.14). At next-to-leading order the energy dependence of the  $\gamma\pi NN$  vertex enters as well (cf. Eq. (3.13)). Especially, we find

$$E'_{0+} = -\frac{eg_{\pi N}}{3\kappa} \left(1 + \frac{m_\pi}{M}\right) = -11.3 \times 10^{-3} m_\pi^{-1},$$

where  $|\vec{q}_\gamma|$  that enters Eq. (3.14) was evaluated in the center of mass system of the reaction  $\gamma d \rightarrow \pi^+ nn$  at threshold, and its value is  $|\vec{q}_\gamma| = m_\pi(1 - m_\pi/(8M) + \mathcal{O}(\chi^2))$ . The slope parameter  $E'_{0+}$  is calculated up to its leading and next-to-leading order. However, we assign an uncertainty of 10 % to this quantity, for higher order corrections are known to be enhanced by the  $\Delta$  resonance [117]. The given value for  $E'_{0+}$  compares well to that from the dispersive analysis of the Mainz group [118] and is consistent with that used as input in Ref. [116] to extract  $E_{0+}$  from the data.

At order  $\chi^2$  for our reaction, additional diagrams contribute to the transition  $\gamma p \rightarrow \pi^+ n$  where the photon gets absorbed on the nucleon, *e.g.* through the magnetic moment, followed by pion emission (diagrams (c) in Fig. 3.5). Thus, they are accompanied by a one-nucleon intermediate state. These diagrams, when used as the one-body operator in diagram (a2) of Fig. 3.1, acquire a two-nucleon cut that leads to an imaginary amplitude even at threshold due to the kinematically allowed transition  $\gamma d \rightarrow pn$  followed by  $pn \rightarrow \pi^+ nn$ . However, this two-nucleon cut introduces a new (large) momentum scale  $p \simeq \sqrt{m_\pi M}$  into the problem that calls for special care. According to the counting rules for pion production in  $NN$  collisions [22, 30, 79] (see also Section 2.2), the contribution of this two-nucleon cut is therefore suppressed by  $\chi_m^{3/2}$  compared to the rescattering diagram (c2) of Fig. 3.1 (cf. also Section 2.3). It is therefore justified within the ordering scheme used to replace the two-nucleon propagator by its static limit. The resulting contribution from the magnetic couplings to the  $s$ -wave pion production on the nucleon is already included in the effective operator of Eq. (3.15). For the pion  $p$ -waves we get the following expression for the sum of the  $s$ - and  $u$ -channel contributions of Fig. 3.5(c)

$$\hat{V}_{\pi\gamma NN}^{(c)} = -\frac{ieg_{\pi N}}{\sqrt{2}M_n m_\pi} \left( A + \vec{\sigma} \cdot \vec{B} \right), \quad (3.18)$$

where

$$A = i(\mu_p - \mu_n) \vec{k}_\pi \cdot [\vec{\epsilon}_\gamma \times \vec{q}_\gamma], \quad (3.19)$$

$$\vec{B} = -2(\vec{\epsilon}_\gamma \cdot \vec{p}) \vec{k}_\pi + (\mu_p + \mu_n) \left( (\vec{\epsilon}_\gamma \cdot \vec{k}_\pi) \vec{q}_\gamma - (\vec{q}_\gamma \cdot \vec{k}_\pi) \vec{\epsilon}_\gamma \right). \quad (3.20)$$



Here  $\vec{p}$  denotes the momentum of the incoming nucleon and  $\mu_p = 2.79$  and  $\mu_n = -1.91$  denote the magnetic moments of the proton and the neutron, respectively. The operator  $\hat{V}_{\pi\gamma NN}^{(c)}$  given by Eq. (3.18) was evaluated directly for the channel  $\gamma p \rightarrow \pi^+ n$ . As a consequence the expression does not show any explicit isospin dependence and an isospin factor of  $\sqrt{2}$  appears.

In Ref. [117] it is shown that the pion  $p$ -waves converge quite slowly: the next-to-leading order correction to the dominant  $p$ -wave multipoles  $M_{1+}$  and  $M_{1-}$  change the leading result by a factor of 2. The reason for this sizable correction is the large numerical value of  $(\mu_p - \mu_n) = 4.7$ . On the other hand, the contribution of the  $A$ -term to  $\gamma d \rightarrow \pi^+ nn$  is suppressed. One reason can be read off from Eq. (3.18) almost directly: since the  $A$ -term is a scalar in spin space, it will not change the total spin of the two nucleon system, when used as the one-body operator in diagram (a) of Fig. 3.1. Thus the final  $nn$  state is in a spin-triplet state. However, in the near threshold regime of interest here, the simultaneous appearance of an  $nn$   $P$ -wave ( $nn$  spin-triplet states are to have odd angular momenta as a consequence of the Pauli principle) and a pion  $p$ -wave is suppressed. In addition, it turns out that for the total cross section the  $A$ -term does not interfere with the leading pion  $p$ -wave contributions (the term proportional to  $\vec{q}_\gamma$  in Eq. (3.14)) which leads to an additional suppression. For details on the latter point we refer to the explicit expressions given in Appendix E.2. Thus, we expect a better behaviour of the contributions from the pion  $p$ -waves. One should also note that like for the slope of the  $s$ -wave amplitude, the  $\Delta$ -isobar gives potentially large corrections to the  $p$ -wave amplitudes [117]. Thus we assign an uncertainty of 10% also to those.

At order  $\chi^2$ , pion rescattering diagrams (see diagrams (b), (c) and (d) in Fig. 3.1) start to contribute. Here the same diagrams contribute as previously discussed for  $\pi d$  scattering, but with the first  $\pi N$  interaction being replaced by the  $\gamma N \rightarrow \pi N$  transition vertex. These diagrams are depicted in Fig. 3.1 (b2) and (c2). However, there is in addition a whole new class of diagrams, namely those without final state interaction (depicted as (b1) and (c1)). Another important difference to  $\pi d$  scattering is that, as already mentioned above, the S-wave two-nucleon state—while the pion is in flight—is now allowed by the Pauli principle. This has two consequences: first of all we expect that the static approximation will not work for the rescattering contribution and, as a second consequence, now nothing prevents the two-nucleon system to interact while the pion is in flight. As the  $NN$  interaction is to be taken into account to all orders, these diagrams are also potentially important. The latter statement becomes especially clear when observing that the scattering length in the  $nn$  channel is quite large; note that in the limit of an infinite scattering length the diagrams (d1) and (d2) acquire a logarithmic infrared divergence. In fact, then the two-nucleon propagator behaves as if it would describe the propagation of a massless particle<sup>#4</sup>.

Starting from the vertices given in this section it is straightforward to write down the corresponding matrix elements for the diagrams shown in Fig. 3.1. Note that all diagrams are evaluated in Coulomb gauge. This is a standard choice in ChPT calculations, for many diagrams with single photons are relegated to higher orders, such as those where the photon couples to the charge of the nucleon and of the deuteron.

Diagrams, where the photon couples to a rescattered pion in flight turn out to be

<sup>#4</sup>In a different scheme and for a different reaction this behavior was studied in Ref. [119].

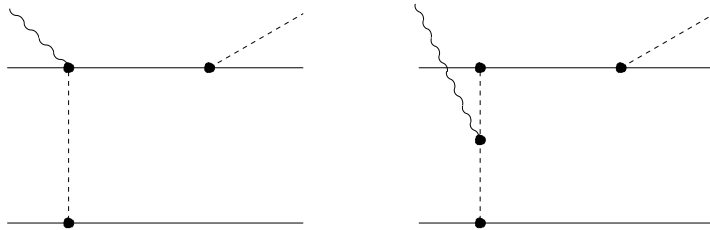


Figure 3.7: Diagrams where the photon couples to the structure of the deuteron. These diagrams start to contribute only at order  $\chi^3$  and are therefore not considered here.

strongly suppressed numerically compared to those shown in Fig. 3.1. The reason for this is twofold: their imaginary part is suppressed as a consequence of gauge invariance that forces the photon–pion coupling to be of the order of the (small) pion momentum in the loop and the appearance of a second pion propagator leads to an additional suppression. This is in complete analogy to  $\pi d$  scattering as discussed in detail in Ref. [120]. In addition gauge invariance in principle also calls for the inclusion of diagrams, where the photon couples to the internal structure of the deuteron. Typical representatives of this class are shown in Fig. 3.7. However, it is easy to show that these diagrams are suppressed by at least one power of  $\chi$  compared to the leading rescattering contribution and therefore start to contribute at most at order  $\chi^3$  to  $\gamma d \rightarrow \pi^+ nn$ <sup>#5</sup>. Therefore these diagrams are not included in the calculation. As a consequence, the diagrams given in Fig. 3.1 (together with Figs. 3.5 and 3.6) are all that contribute to the given order.

Details on how the various diagrams are evaluated are given in Appendix E.2. Especially, there it is explained how we dealt with the three–body singularities that occur in diagrams (c2), (b2), (d1), and (d2). We want to mention that we evaluated the loop diagrams for non–relativistic pions (see Appendix E.2) for that largely simplified the numerics. We checked by direct evaluation of diagrams (c1) and (c2) for threshold kinematics that switching to relativistic pions changes the individual contributions to the amplitude by less than 4 % (the contribution of these diagrams does not exceed 5 % on the amplitude level).

## 3.5 Results and discussion

In our calculations we use the standard values for the various constants, namely  $f_\pi = 92.4$  MeV,  $m_\pi = 139.57$  MeV (only the charged pions contribute to the order we are working) and  $M = 938.27$  MeV. The deuteron wave function and also the scattering wave functions needed for the  $nn$  scattering amplitudes (in the  $^1S_0$ ,  $^3P_0$ ,  $^3P_1$ , and  $^3P_2$  partial waves) are generated from the (charge–dependent) CD-Bonn potential [87]. Specifically, for the former we employ the analytical representation of the deuteron wave function provided in that reference because it allows us to perform some integrations analytically—see Appendix E.2.3. For the same reason the scattering wave functions

<sup>#5</sup>For this estimate we used  $m_\pi$  as typical momentum in the deuteron. A more accurate estimate of this quantity would be  $\gamma = \sqrt{E_B M}$ . If we were to use this for the power counting it would yield a suppression of the order of  $\gamma/M \sim 0.3\chi$ .

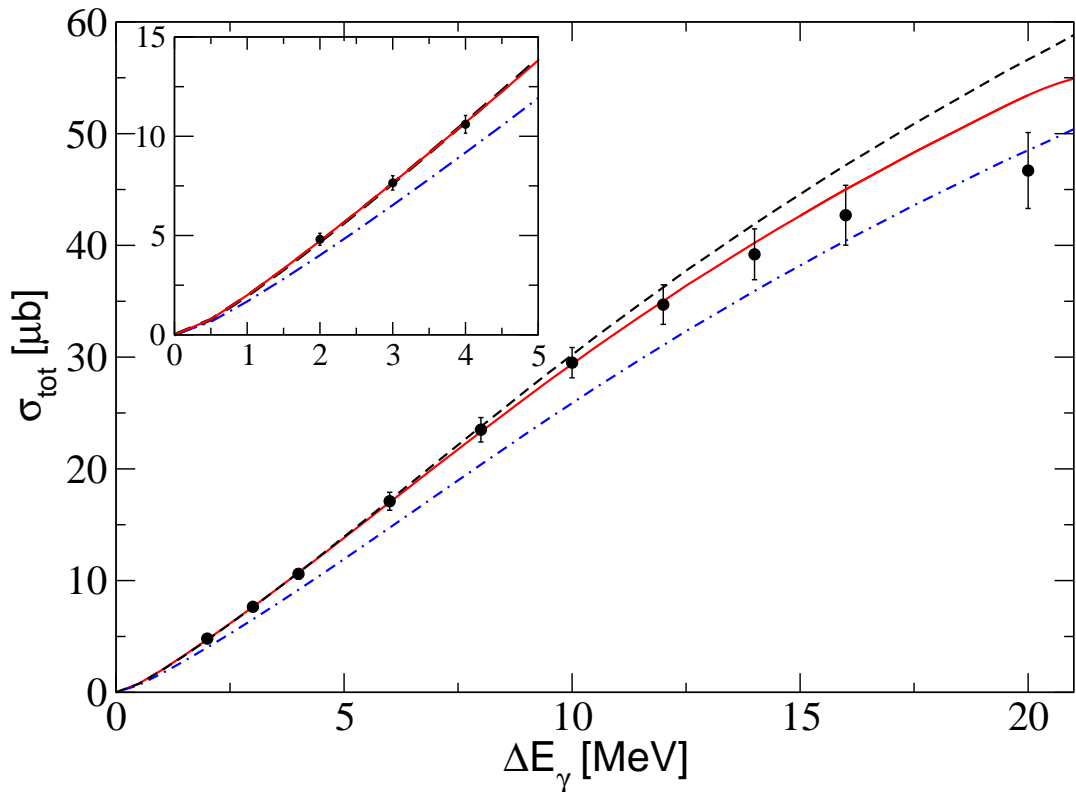


Figure 3.8: Total cross section of the reaction  $\gamma d \rightarrow \pi^+ nn$  at LO (dashed line), NLO (dash-dotted line) and  $\chi^{5/2}$  order (solid line) together with experimental data from Ref. [103].

are computed from rank 1 separable representations of the CD-Bonn model, constructed along the lines of Ref. [121] utilizing the so-called Ernst–Shakin–Thaler method [122], cf. also Appendix E.2.3. Note that the scattering length predicted by the CD-Bonn potential for the  $^1S_0$  partial wave in the  $nn$  system is  $a_{nn} = -18.97$  fm [87], which is in line with most of the recent experimental information [123, 124] (note, the analysis of Ref. [125] gave a significantly lower value). We want to point out that in our calculation the contribution of the deuteron D-wave is included. This contribution to the leading diagrams is rather important, because it guarantees the correct normalization of the S-wave component for the potential used.

The reaction  $\gamma d \rightarrow \pi^+ nn$  was calculated in DWBA by many authors in the middle of the seventies (cf., *e.g.*, the review paper by Laget [23] and references therein). The approach used in those investigations corresponds to the evaluation of diagrams (a1) and (a2) of Fig. 3.1 using the  $\gamma p \rightarrow \pi^+ n$  vertex of Eq. (3.13); thus, in our language those were incomplete calculations up to next-to-leading order ( $\chi$ ), because the energy dependence of the  $\gamma\pi NN$  vertex and higher pion partial waves were neglected. Since the most important contribution to the  $\gamma p \rightarrow \pi^+ n$  operator in the near threshold region originates from the Kroll-Rudermann operator and its first correction (see Eq. (3.13)), which is known, and the convergence of diagram (a2) of Fig. 3.1 is provided by the universal fall-off of the deuteron wave function for small momenta (fixed by the deuteron

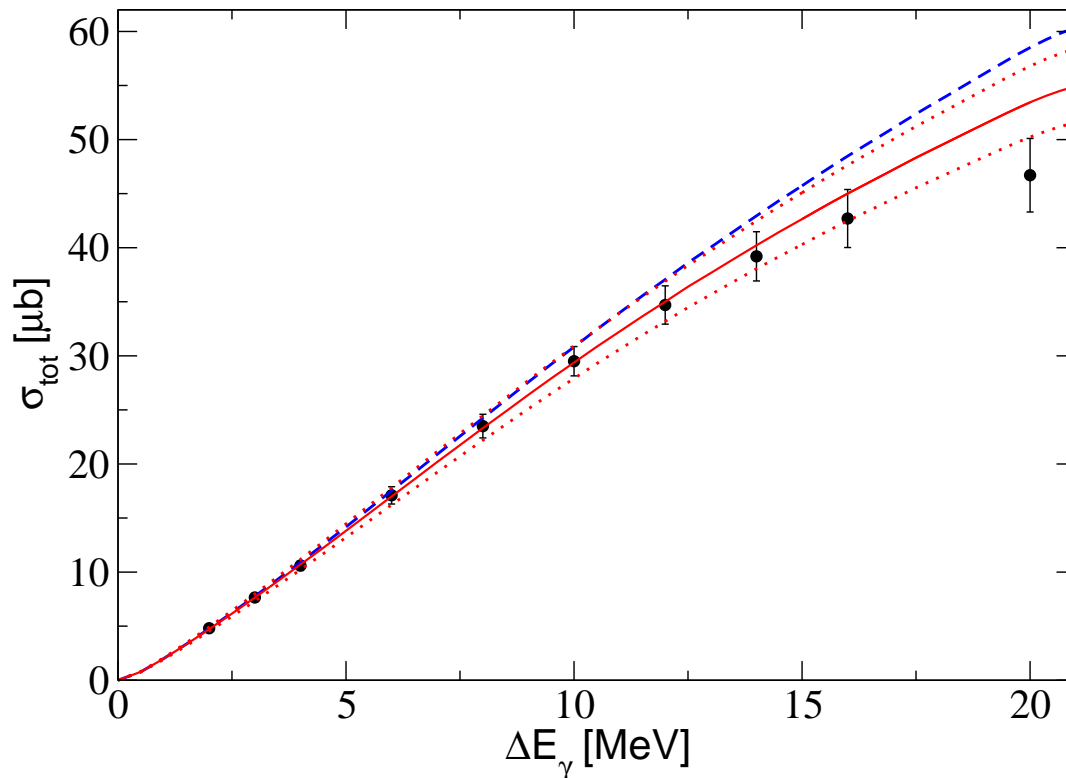


Figure 3.9: Importance of the slope parameter  $E'_{0+}$  defined in Eq. (3.17): The solid line shows the full result, whereas the long dashed line is produced with  $E'_{0+} = 0$ . The two dotted lines show the estimated uncertainty of full result as described in the text. The data are from Ref. [103].

binding energy), all those calculations led to very similar results (that we reproduce). To improve the calculations, some authors used instead of the prefactors of Eq. (3.13) the experimental input for  $E_{0+}(k_\pi^2)$  at threshold as the strength parameter for the one-body term (see, e.g., Ref. [103]). This, however, corresponds to an incomplete next-to-next-to-leading order calculation, as discussed above. In addition, none of the works reported in Ref. [23] considered the  $D$ -wave of the deuteron consistently. The slope of  $E_{0+}(k_\pi^2)$ , pion  $p$ -waves, or the  $NN$  final state interaction in the  $P$ -waves were also not considered. The only attempt to improve the mentioned calculations via inclusion of a pion rescattering contribution was made in Ref. [126], where diagram (c2) of Fig. 3.1 was evaluated in the static limit, i.e. without nucleon recoil. This contribution was found to be large, amounting to an increase of around 10 % of the total cross section (see the discussion of this question in Ref. [23]). However, as we stressed above, the static approximation is expected to work very poorly in this reaction.

Our results at order  $\chi^0$ ,  $\chi$ , and combined order  $\chi^2$  and  $\chi^{5/2}$  are shown in Fig. 3.8 by the dashed, dash-dotted and solid lines, respectively. The data are taken from Ref. [103] and the energy is measured in terms of  $\Delta E_\gamma = (1+m_\pi/(2M))Q$ —the photon lab energy subtracted by its threshold value. Up to order  $\chi^1$  the result is parameter free, *i.e.* it is determined by the value of  $g_{\pi N}$  only. For the value of  $E_{0+}(k_\pi^2)$  at threshold that is

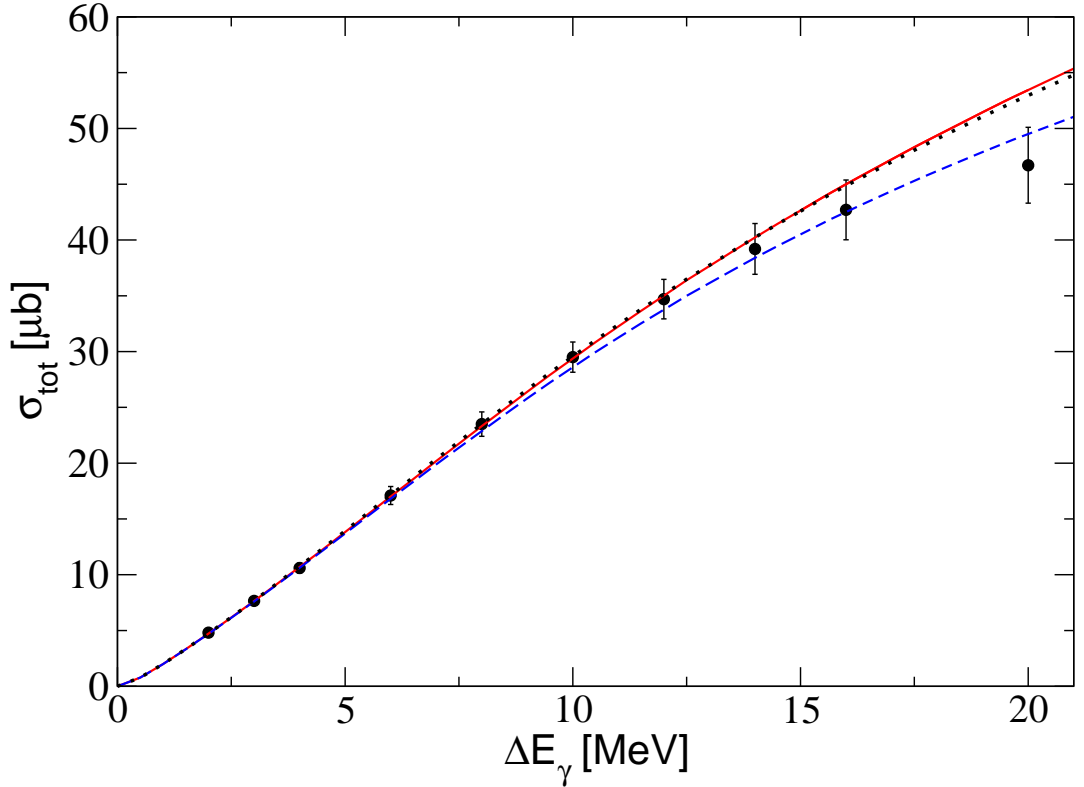


Figure 3.10: The role of the higher pion partial waves and effect of the  $NN$  interaction in the  $P$ -wave. The dashed line shows the calculation where only the  $S$ -wave interactions are taken into account, the dotted line includes also the higher pion partial waves and the solid line includes in addition the contribution of the  $NN$  final state interaction in the three possible  $P$ -waves included in diagram (a2) of Fig. 3.1.

needed as the only input quantity at order  $\chi^2$ , we use the central values of the ChPT calculation of Ref. [33] (that agrees with the experimental number, as mentioned in the previous section).

To illustrate the importance of the slope  $E'_{0+}$  we show in Fig. 3.9 both the full result as well as the one we get for a vanishing slope. For  $\Delta E_\gamma$  larger than 10 MeV we observe a quite large sensitivity to the energy dependence of  $E_{0+}(k_\pi^2)$ .

The counting scheme of Eq. (3.1) calls for an inclusion of  $p$ - and  $d$ -waves for the pion. The explicit expressions for the vertices are given in Eqs. (3.14) and (3.18). These vertices are to be considered embedded in diagrams (a1) and (a2) of Fig. 3.1 only. The contribution of the higher pion partial waves can be read off the difference of the dashed and the dotted line in Fig. 3.10.

The significance of  $NN$   $P$ -waves, even for  $\Delta E_\gamma \leq 20$  MeV, was established long ago [23], however, so far they were only included as plane waves (through diagram (a1) of Fig. 3.1). In this work for the first time the final state interaction in the  $NN$   $P$ -waves is considered as well: we include the  $NN$  interaction in the three possible  $P$ -waves ( $^3P_0$ ,  $^3P_1$  and  $^3P_2$ ) in diagram (a2). The effect of the nucleon  $P$ -wave interactions on the total cross section is shown in Fig. 3.10. We found the contribution of each  $NN$

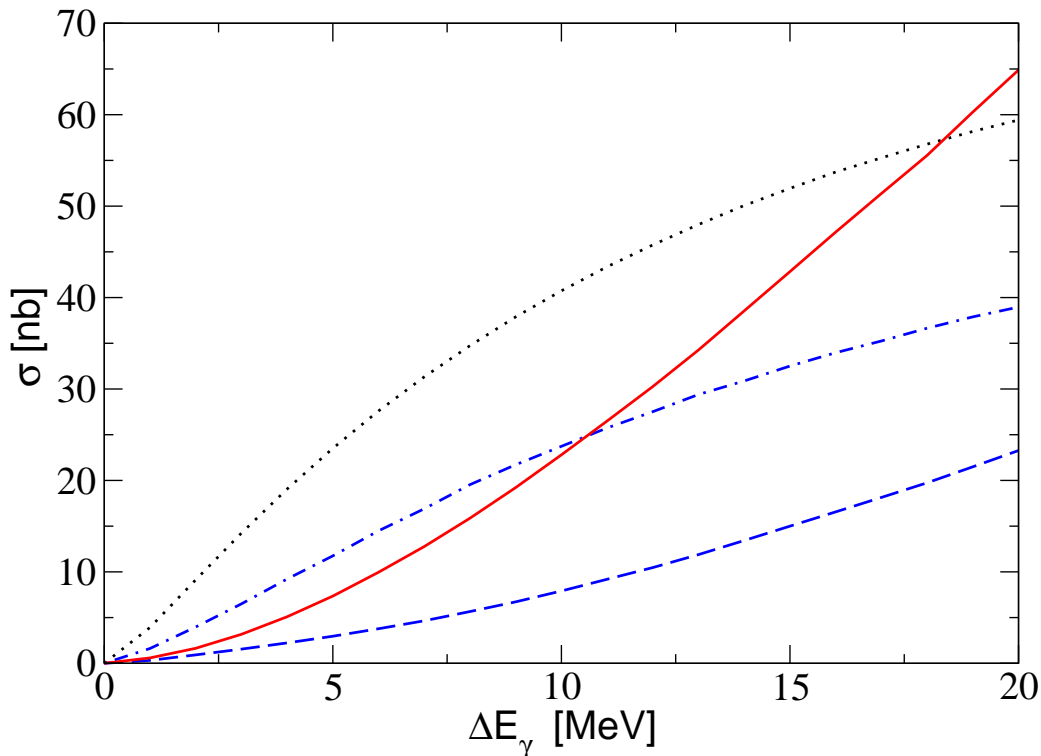


Figure 3.11: Quality of the static approximation for diagram (c2) of Fig. 3.1: The dash–dotted line shows the full calculation for diagram (c2), the dashed one that for diagram (b2), and the solid line the sum of the two. On the other hand, the result for diagram (c2) evaluated in the static approximation is given by the dotted line.

$P$ -wave interaction to be small and, in addition, there exists a significant cancellation amongst the  $P$ -wave contributions: it turns out that the contribution of the  ${}^3P_1$  partial wave, which is enhanced due to constructive interference of the diagram (a1) and (a2) of Fig. 3.1 for this particular  $NN$  partial wave, cancels to a large extent the contributions of the  ${}^3P_0$  and  ${}^3P_2$  partial waves. Note that the interference pattern of the various  $NN$   $P$ -waves can be traced to the fact that  ${}^3P_1$  is repulsive, whereas  ${}^3P_0$  and  ${}^3P_2$  are attractive for small relative momenta. The net effect of the  $NN$   $P$ -wave interactions in the final state on the total cross-section is negligible.

To summarize the results, we have calculated higher order chiral corrections to the impulse term used, *e.g.*, in Ref. [23]. We found that the effect of the  $NN$   $P$ -wave final state interaction on the total cross section is negligible. Moreover, the effects of the energy dependence of the pion  $s$ -wave production (parameterized by the slope  $E'_{0+}$ ) and of the pion  $p$ -waves are rather sizable, but they contribute with opposite signs and finally compensate each other largely, as one can read from Figs. 3.9, 3.10. In view of this finding, the good agreement of the results of, *e.g.*, Ref. [23] for the total cross section for photon energies above 10 MeV with the data should be considered accidental. However, for differential observables and especially for polarization observables we expect sizable effects from the chiral corrections calculated here.

Let us now discuss some of the results in detail. We found that all rescattering

contributions of order  $\chi^2$  and of order  $\chi^{5/2}$  contribute with similar strength. This is true also for those diagrams where the  $NN$  interaction appears inside the loop (diagrams (d1) and (d2) of Fig. 3.1). This clearly demonstrates the need to take into account the  $NN$   $S$ -wave interaction non-perturbatively also in intermediate states (as it is done routinely in three-nucleon calculations anyway).

Let us now compare in detail the results of different diagrams at the threshold. Here contributions from higher partial waves as well as those from the slope parameter  $E'_{0+}$  vanish. Therefore the uncertainty of the calculation in this regime can be estimated much more accurately than at higher energies. The results of the calculation of all possible contributions to the reaction amplitude at threshold are given in Table 3.2. Evidently, the total contribution from few-body (rescattering) corrections to the full amplitude at threshold is about 5 % of the contribution from the distorted wave impulse approximation. One can also see from this table that the net contribution of the orders  $\chi_m^2$  and  $\chi_m^{5/2}$  cancels largely the NLO contribution (see also the corresponding results in Fig. 3.8 at low energies). Due to this one might speculate that corrections to this result from higher orders, especially from  $\chi_m^3$ , may influence the results stronger than suggested by the power counting. However we think that the uncertainty of the calculation at low energies is indeed within the uncertainty for  $E_{0+}$  given by Eq. (3.16). Actually, no additional diagrams to those shown in Fig. 3.1 appear at order  $\chi_m^3$ . Thus, the contributions to the amplitude at this order originate basically from three sources:

1. NLO correction to the Kroll-Rudermann vertex when being used as a one-body operator in diagrams (b),(c) and (d) of Fig. 3.1 and the recoil corrections to the Weinberg-Tomozawa term. These corrections are of order  $(m_\pi/2M) \cdot 5\% = 0.4\%$ .
2. Relativistic corrections to the diagrams with pion rescattering. For diagram (c2) the relativistic correction gives only about 4% (to the 3 % contribution to the amplitude from diagram (c2)). Since there are no reasons a priori which could enhance the corresponding corrections to the other rescattering diagrams, we assign an uncertainty of order of 0.5 % to this effect.
3. The contributions from the coupling to the deuteron structure and the  $nn$  scattering  $T$ -matrix. These are the hardest to estimate. However, as argued above, they are expected to be numerically quite small (see footnote #5).

To summarize, we assign an uncertainty of 2 % to the few-body corrections of the amplitude. On the other hand the contribution at order  $\chi_m^3$  to  $E_{0+}$  at threshold is also about 2 % [33]. Adding these two uncertainties in quadrature we end up with a total uncertainty of 3 % for the transition operator near threshold.

In Fig. 3.9 the resulting uncertainty for the full calculation is shown by the two dotted lines. This range of uncertainties contains besides the 3 % just discussed also the 10 % uncertainties on both the pion  $p$ -waves as well as the slope parameter.

To show that the static exchange is indeed a poor approximation to the exact result for diagram (c2) of Fig. 3.1, as conjectured above, we compare in Fig. 3.11 the results for the static approximation with those from the exact calculation as well as with those for the one-body term (b2). As can be clearly seen, the static approximation fails to describe the full result in both strength as well as energy dependence. Evidently, for

operator	order	diagrams	contribution
one-body	$\chi_m^0$	(a1)+(a2)	1
	$\chi_m^1$	(a1)+(a2)	-0.07
	$\chi_m^2$	(a1)+(a2)	+0.028
few-body	$\chi_m^{5/2}$	(b2)	-0.016
	$\chi_m^2, \chi_m^{5/2}$	(c1)+(c2)	+0.039
	$\chi_m^2, \chi_m^{5/2}$	(d1)	+0.008
	$\chi_m^2, \chi_m^{5/2}$	(d2)	+0.024

Table 3.2: Contributions of different diagrams and operators to the reaction amplitude at threshold are given at different orders. The results in table are normalized to that of the calculation of diagrams (a1) + (a2) with the leading order Kroll-Rudermann vertex. Note that diagram (b1) does not contribute at threshold.

the exact calculation the total contribution of the sum of the results for (b2) and (c2) is extremely small near threshold, *i.e.* in the region where the real parts of both diagrams dominate. With increasing energy the contribution from the sum of these two diagrams increases rapidly. The reason for this effect is that at higher energies the role of the imaginary parts of both diagrams, which contribute coherently for the Pauli allowed  $NN$  states, is growing rapidly. The resulting contribution for the sum of both diagrams of Figs. 2 (b2) and 2 (c2) to the total cross section does not exceed 4 %.

### 3.6 Summary of Chapter 3

We presented a ChPT calculation for the reaction  $\gamma d \rightarrow \pi^+ nn$ . We calculated the diagrams displayed in Fig. 3.1, keeping explicitly the nucleon recoil for the intermediate states. This corresponds to a complete calculation up to order  $\chi^{5/2}$ , where  $\chi = m_\pi/M$ .

The results of the full calculation are shown in Fig. 3.8 by the solid line. A good agreement between theory and experiment at low energies is obtained without any free parameter. The only input parameter was the threshold value for  $E_{0+}$ , taken from an N<sup>3</sup>LO calculation for  $\gamma p \rightarrow \pi^+ n$  [33]. Estimated conservatively, the uncertainty for the transition operator of our calculation is about 3 % in the amplitude for photon energies  $\Delta E_\gamma$  below 5 MeV.

We found a strong suppression of the pionic rescattering contributions in comparison to the calculation in the frozen-nucleon approximation, *i.e.* in the static limit. This confirms the suggestion made in Ref. [23] and is in line with the general remark of the recent work of Ref. [32] where it was conjectured that the static limit is not adequate for pion rescattering processes with Pauli-allowed S-wave intermediate  $NN$  states.



As a next step a fully consistent chiral perturbation theory calculation for the given reaction should be performed. Such a calculation allows one to reliably assign a theoretical uncertainty to the full calculation and address questions raised in Ref. [127] for the consistency of the counting scheme and the scaling of four-nucleon operators. Although we do not expect the latter effects to be numerically significant for the reaction considered here, they are potentially important for  $\gamma d \rightarrow \pi^0 pn$ , where the leading contribution vanishes.

Once a fully consistent ChPT calculation and better data are available for the reaction  $\gamma d \rightarrow \pi^+ nn$  one can consider to extract the energy dependence of  $E_{0+}$  from this reaction, for the total cross section is very sensitive to the slope of  $E_{0+}$ , as illustrated in Fig. 3.9. However, before more definite conclusions can be drawn on this issue, better data on the total cross section as well as the differential cross section in the energy regime of 15–25 MeV is needed.

The work presented here allows one, amongst other things, to address the theoretical uncertainty of the  $nn$  scattering length extracted from  $\gamma d \rightarrow \pi^+ nn$  analogously to the studies of Ref. [104] for  $\pi^- d \rightarrow \gamma nn$ . These studies are of high interest in the light of the significant differences in the values for  $a_{nn}$  extracted from different groups in different reactions—cf., *e.g.*, Refs. [123, 124] and Ref. [125]. We discuss the extraction of the  $nn$  scattering length from  $\gamma d \rightarrow \pi^+ nn$  in Chapter 4.

# Chapter 4

## Neutron–Neutron Scattering Length from $\gamma d \rightarrow \pi^+ nn$

In this chapter we discuss the possibility to extract the neutron-neutron scattering length  $a_{nn}$  from experimental spectra on the reaction  $\gamma d \rightarrow \pi^+ nn$ . We argue that for properly chosen kinematics, the theoretical uncertainty of the method can be as low as 0.1 fm.

### 4.1 Introduction

A precise determination of the neutron-neutron scattering length  $a_{nn}$  is important, *e.g.*, for an understanding of the effects of charge symmetry breaking in nucleon–nucleon forces [128]. The scattering length  $a_{nn}$  characterizes scattering at low energies. It is related to the on-shell  $^1S_0$  scattering amplitude  $f^{\text{on}}$  as

$$f^{\text{on}}(p_r) = \frac{1}{p_r \cot \delta(p_r) - ip_r} = \frac{1}{-a_{nn}^{-1} + \frac{1}{2} r_{nn} p_r^2 + \mathcal{O}(p_r^4) - ip_r}, \quad (4.1)$$

where  $p_r$  is the relative momentum between the two neutrons,  $\delta(p_r)$  is the scattering phase shift in the  $^1S_0$  partial wave and  $r_{nn}$  is the effective range. At low energies the terms of order  $p_r^4$  can be neglected to very high accuracy. However, a direct measurement of  $a_{nn}$  in a scattering experiment is practically impossible due to the absence of a free neutron target. For this reason, the value for  $a_{nn}$  is to be obtained from analyses of reactions where there are three particles in the final state, *e.g.*  $\pi^- d \rightarrow \gamma nn$  [123, 129, 130] or  $nd \rightarrow pnn$  [124, 125, 131, 132]. There is some spread in the results for  $a_{nn}$  obtained by the various groups. In particular, two independent analyses of the reaction  $nd \rightarrow pnn$  give significantly different values for  $a_{nn}$ , namely  $a_{nn} = -16.1 \pm 0.4$  fm [125, 131] and  $a_{nn} = -18.7 \pm 0.6$  fm [132], whereas the latest value obtained from the reaction  $\pi^- d \rightarrow \gamma nn$  is  $a_{nn} = -18.5 \pm 0.3$  fm [123]. At the same time, for the proton-proton scattering length, which is directly accessible, a very recent analysis reports  $a_{pp} = -17.3 \pm 0.4$  fm [88] after correcting for electromagnetic effects. This means that even the sign of  $\Delta_a = a_{pp} - a_{nn}$  is not fixed. Note, that the value for  $a_{nn}$  given is not corrected for electromagnetic effects. However, since those are only of the order of 0.3 fm [128] they are not relevant for the sign of  $\Delta_a$ , although they ought to be taken into account for determining charge symmetry breaking effects quantitatively. It

should be also mentioned here that state-of-the-art calculations for the binding energy difference of  ${}^3\text{H}$  and  ${}^3\text{He}$  suggest that  $\Delta_a$  is positive [133, 134].

Here we discuss the possibility to determine  $a_{nn}$  from differential cross sections in the reaction  $\gamma d \rightarrow \pi^+ nn$ . Specifically, we show that one can extract the value of  $a_{nn}$  reliably by fitting the shape of a properly chosen momentum spectrum. In this case the main source of inaccuracies, caused by uncertainties in the single-nucleon photoproduction multipole  $E_0^+$ , is largely suppressed. Furthermore there is a suppression of the quasi-free pion production at specific angles. We show that at these angular configurations the extraction of  $a_{nn}$  can be done with minimal theoretical uncertainty.

This investigation is based on the developments that were presented in Chapter 3. We calculated there the transition operator for the reaction  $\gamma d \rightarrow \pi^+ nn$  up to order  $\chi^{5/2}$  in ChPT with  $\chi = m_\pi/M$ . Half-integer powers of  $\chi$  in the expansion arise from the unitarity (two- and three-body) cuts (see also Ref. [32]). The results presented in Chapter 3 for the total cross section are in very good agreement with the experimental data. The only input parameter that entered the calculation was the leading single-nucleon photoproduction multipole  $E_0^+$ , which was fixed from a N<sup>3</sup>LO calculation of Bernard et al. [33]. The uncertainty in  $E_0^+$  is the main theoretical error in that calculation. Besides this transition operator, in this study we use  $NN$  wave functions constructed likewise in the framework of ChPT, namely those of the NNLO interaction of Ref. [19]. This allows us to estimate the theoretical uncertainty which arises from variations in the wave functions. In fact, as soon as we include consistently all terms up to order  $\chi^{5/2}$ , we expect the ambiguities due to different wave functions not to be larger than a  $\chi^3$  correction, for only at this order the leading counter term which absorbs these effects enters. This expectation is indeed quantitatively confirmed in the concrete calculations.

Since we work within chiral perturbation theory we can estimate the effect of higher orders in terms of established expansion parameters together with the standard assumption that additional short ranged operators, that enter at higher orders, behave in accordance with the power counting (the so-called naturalness assumption). This method was also applied in Refs. [104, 135], where the reaction  $\pi^- d \rightarrow \gamma nn$  was investigated as a tool to extract  $a_{nn}$ . However, to know the effect of higher orders for sure, one has to calculate them. Therefore, to derive a reliable uncertainty estimate for the extraction of  $a_{nn}$  from the  $\gamma d \rightarrow \pi^+ nn$  reaction, we use our leading order calculation as baseline result and estimate the theoretical uncertainty from the effects of the higher orders that we calculated completely. Based on this, we find a theoretical uncertainty  $\delta a_{nn} \lesssim 0.1$  fm. We therefore argue that the reaction  $\gamma d \rightarrow \pi^+ nn$  appears to be a good tool for the extraction of  $a_{nn}$ .<sup>#1</sup>

## 4.2 ChPT calculation for $\gamma d \rightarrow \pi^+ nn$

The formalism that was used for calculation of the transition operator is given in Chapter 3. The diagrams that contribute to the reaction  $\gamma d \rightarrow \pi^+ nn$  are shown on Fig. 3.1. The kinematical variables are defined in Fig. 3.2.

---

<sup>#1</sup>In Ref. [136] a method was proposed to extract scattering lengths from  $\gamma d$ . However, this method can not be used here, since the momentum transfer is not sufficiently large. In addition, with our explicit calculation we can reach a significantly higher accuracy.

We remind that we expand the transition operators in the conventional ChPT parameter  $\chi = m_\pi/\Lambda_\chi \sim \chi_m = m_\pi/M$  as well as in the small parameter  $k_\pi/m_\pi$ , where  $k_\pi$  denotes the momentum of the outgoing pion. This latter expansion is justified since in the near threshold regime of interest here (excess energies of at most 20 MeV above the pion production threshold) the outgoing pion momenta are small compared even to the pion mass. Thus, we perform an expansion in two parameters

$$\chi = m_\pi/M \text{ and } \chi_Q = k_\pi/m_\pi .$$

The maximum value of  $\chi_Q$ ,  $\chi_Q^{\max} = \sqrt{2Q/m_\pi}$ , at the highest energy considered, which is 20 MeV above threshold, is about 1/2. Since this is numerically close to  $\sqrt{\chi}$  we use the following assignment for the expansion parameter:

$$\chi \sim \chi_Q^2 . \quad (4.2)$$

The tree level  $\gamma p \rightarrow \pi^+ n$  vertex, as it appears in diagrams (a1) and (a2) in Fig 3.1 (the vertex is labeled as filled square), contributes at leading order (order  $\chi^0$ ), and orders  $\chi^1$  and  $\chi^2$ , depending on the one–body operator used. Note that the loop diagrams with  $\pi N$  rescattering (see diagrams (b), (c) and (d) in Fig. 3.1) contribute at order  $\chi_m^2$  as well as at  $\chi_m^2 \chi_Q$ ,  $\chi_m^{5/2}$  and at  $\chi_m^{1/2} \chi_Q^4$ . The origin of the non–integer power of  $\chi$  are the two–body ( $\pi N$ ) and three–body ( $\pi NN$ ) singularities. Thus, all terms up to  $\chi^{5/2}$  are explicitly taken into account in our calculation of the transition operator.

As already emphasized, we employ wave functions evaluated in the same framework in order to have a fully consistent calculation. We use the N<sup>2</sup>LO wave functions corresponding to the chiral  $NN$  forces introduced in Ref. [18] and based on the spectral function regularization (SFR) scheme [34]. At this order, the  $NN$  force receives the contributions from one-pion exchange, two-pion exchange at the subleading order as well as from all possible short-range contact interactions with up to two derivatives. In addition, the dominant isospin-breaking correction due to the charged-to-neutral pion mass difference in the one-pion exchange potential together with the two leading isospin-breaking S-wave contact interactions were taken into account [18]. The two corresponding low-energy constants were adjusted to reproduce the scattering lengths  $a_{nn}$  and  $a_{pp}$ . The SFR cutoff  $\tilde{\Lambda}$  is varied in the range 500 . . . 700 MeV. It was argued in Ref. [34] that such a choice for  $\tilde{\Lambda}$  provides a natural separation of the long- and short-range parts of the nuclear force and allows to improve the convergence of the chiral expansion [34]. The cutoff  $\Lambda$  in the Lippmann-Schwinger equation is varied in the range 450 . . . 600 MeV. For an extensive discussion on the choice of  $\Lambda$  and  $\tilde{\Lambda}$  the reader is referred to [18, 19].

### 4.3 Differential cross sections: relevant features

In this section we outline the features of the differential cross section for unpolarized particles that are important for our considerations. For later convenience let us consider the function  $F$  proportional to the square of the matrix element as well as the five–fold differential cross section

$$F(p_r, \theta_r, \varphi_r, \theta_\pi, \varphi_\pi) = C p_r k_\pi(p_r) |\overline{\mathcal{M}(p_r, \theta_r, \varphi_r, \theta_\pi, \varphi_\pi)}|^2 \propto \frac{d^5\sigma(p_r, \theta_r, \varphi_r, \theta_\pi, \varphi_\pi)}{d\Omega_{\vec{p}_r} d\Omega_{\vec{k}_\pi} dp_r^2} , \quad (4.3)$$

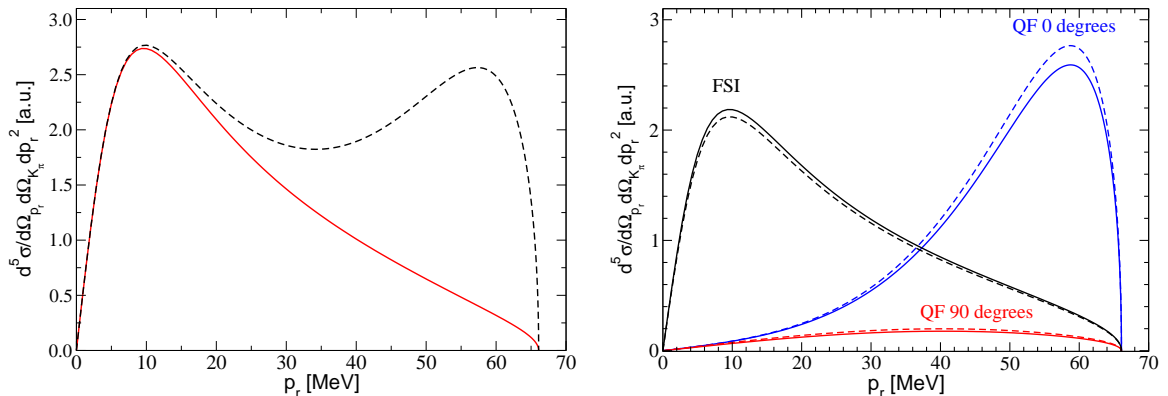


Figure 4.1: Left panel: Differential cross section. The solid line corresponds to the configuration when the quasi-free peak is suppressed ( $\theta_r = 90^\circ$ ), whereas the dashed line corresponds to one of the configurations when the quasi-free production amplitude is maximal ( $\theta_r = 0^\circ$ ). The values of the remaining angles are  $\theta_\pi = 135^\circ$ ,  $\varphi_r = \varphi_\pi = 0^\circ$ ; they are the same for both curves.

Right panel: Differential cross section — relative strength of QF and FSI peaks. Here the dashed curves correspond to the calculation at LO, the solid ones to the calculation at  $\chi^{5/2}$ . Curves denoted by "FSI" ("QF") are obtained by retaining only those diagrams of Fig. 3.1 that contain (do not contain) the final or the intermediate nucleon–nucleon interaction. The labels "0 degrees" and "90 degrees" denote the corresponding values of  $\theta_r$  for the "QF" curves whereas the "FSI" curves are almost insensitive to this angle. The values of the remaining angles are as on the left panel of this figure. The overall scale is arbitrary in both panels but the relative normalization is the same for all curves.

where  $\vec{p}_r$  ( $\vec{k}_\pi$ ) stands for the relative momentum of the two final neutrons (momentum of the final pion) in the center-of-mass frame,  $\theta_r$ ,  $\varphi_r$  ( $\theta_\pi$ ,  $\varphi_\pi$ ) for the corresponding polar and azimuthal angles, respectively, and  $|\mathcal{M}|^2$  for the squared and averaged amplitude. In Eq. (4.3)  $C$  is an irrelevant dimensionful constant. In what follows we will consider only shapes of cross sections and therefore the value of  $C$  is not important for our consideration. The value of  $k_\pi$  at given  $p_r$  and  $Q$  is fixed by energy conservation:

$$Q = \frac{p_r^2}{M} + \frac{k_\pi^2}{4M} + \frac{k_\pi^2}{2m_\pi}, \quad (4.4)$$

hence we write  $k_\pi(p_r)$  in Eq. (4.3). In the following we choose the momentum  $\vec{q}_\gamma$  of the initial photon to be along the  $z$ -axis. Then the cross sections at a certain excess energy  $Q$  depend on four variables, namely the magnitude of the relative momentum of the two final neutrons  $p_r$ , the polar angles of the vectors  $\vec{p}_r$  and  $\vec{k}_\pi$ , and the difference between the azimuthal angles of those two momenta. Unpolarized cross sections are invariant under rotations around the beam axis, which makes the dependence on the missing angle trivial.

Typical differential cross sections  $F$  are shown in Fig. 4.1 as a function of  $p_r$  at some fixed set of angles  $\{\varphi_r, \theta_\pi, \varphi_\pi\}$  and  $Q = 5$  MeV for two different values of  $\theta_r$ . One can see from this figure that for the differential cross section  $F$  of Eq. (4.3) there are two

characteristic regions:

1. The region of quasi-free production (QF) at large  $p_r$ , which corresponds to the dominance of those diagrams of Fig. 3.1 that do not contain the  $NN$  interaction in the final or intermediate states. In Appendix E.2.4 (see also Appendix E.2.3) we give explicit expressions for the diagram  $a1$ —the most significant diagram of this type. At large  $p_r$  the pion momentum  $k_\pi$  is small (see Eq. (4.4)) and the arguments of the deuteron wave function in Eqs. (E.34) and (E.35) may become small for particular combinations of  $\pm \vec{p}_r$  and  $\vec{q}_\gamma/2$ . This feature gives rise to a peak in the differential cross section at large  $p_r$ .
2. The region with prominence of the strong  $nn$  final–state interaction (FSI) at small  $p_r$  (in fact, we would have the strongest final state interaction at zero relative momentum, however the cross section goes to zero at  $p_r = 0$  due to the phase space, therefore we see a peak shape).

One can see from Fig. 4.1 that the FSI peak depends on the value of  $\theta_r$  only marginally, whereas the quasi-free peak shows significant dependence on this angle. In particular, the quasi-free production is largely suppressed at  $\theta_r = 90^\circ$  — at this angle the arguments of the wave functions in both terms in the r.h.s. of Eqs. (E.34) and (E.35) are large. It can also be seen from Fig. 4.1 (right panel) that the effect of higher orders is more important for the quasi-free production amplitude — the influence of higher-order effects on the FSI production is quite small. Another interesting observation is that the contributions of higher orders change the relative height of the two peaks – the FSI peak goes up whereas the QF peak goes down when we proceed from the LO calculation to the order  $\chi^{5/2}$ . In order to suppress the distortions of the spectrum due to higher orders in the chiral expansion, which is the condition for an extraction of  $a_{nn}$  with small theoretical uncertainty, configurations should be chosen where  $\theta_r = 90^\circ$ .

We now briefly discuss the dependence of the cross section on the remaining angles  $\theta_\pi, \varphi_\pi$  (we always may choose  $\varphi_r$  to be zero). The dependence on  $\theta_\pi$  is illustrated in Fig. 4.2. One can see from this figure that the dependence on  $\theta_\pi$  is significant for both the quasi-free as well as the FSI peak. This can be easily understood from the explicit expressions for the matrix elements given in Appendix E.2.4 keeping in mind that already at  $Q = 5$  MeV the maximal value of  $k_\pi$  is about  $m_\pi/3$  while  $q_\gamma \approx m_\pi$ . Thus, the momentum transfer to the nucleon pair,  $|\vec{q}_\gamma - \vec{k}_\pi|$ , varies in the range  $\frac{2}{3}m_\pi$  to  $\frac{4}{3}m_\pi$  depending on  $\theta_\pi$ . Since the  $S$ -wave deuteron wave function is large only for very small arguments, the influence of the direction of  $\vec{k}_\pi$  is significant. In addition, from Fig. 4.2 it follows that a variation of  $\theta_\pi$  not only changes the magnitude but also the shape of the cross section, even in the FSI region. This has to be taken into account in the analysis of any experiment.

In contrast to the polar angles, the dependence of  $F$  on  $\varphi_\pi$  is negligible for all configurations (there is no dependence at all for  $\theta_r = 0^\circ$ , and at  $\theta_r = 90^\circ$  only the anyway small QF contribution changes by just 5 %).

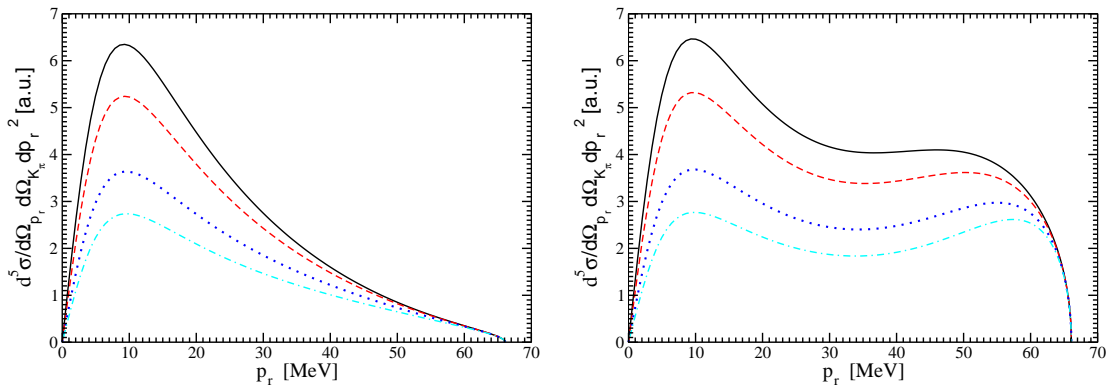


Figure 4.2: Dependence of the differential cross section on  $\theta_\pi$ . The left panel corresponds to the suppressed quasi-free amplitude ( $\theta_r = 90^\circ$ ), the right panel to the maximal quasi-free amplitude ( $\theta_r = 0^\circ$ ). Solid, dashed, dotted, and dash-dotted lines correspond to  $\theta_\pi = 0^\circ, 45^\circ, 90^\circ, 135^\circ$  respectively. The values of the remaining angles are  $\varphi_r = \varphi_\pi = 0^\circ$ . The overall scale is arbitrary in both panels but the relative normalization is the same for all curves.

## 4.4 Extraction of $a_{nn}$ and estimate of the theoretical uncertainty

In this section we discuss how to extract the scattering length from future data on  $\gamma d \rightarrow \pi^+ nn$  as well as the resulting theoretical uncertainty. Our focus is especially the latter point. As in the previous section we will only discuss results at excess energy  $Q = 5$  MeV. However, the analysis can be repeated analogously at any excess energy within the range of applicability of the formalism, i.e.  $Q \leq 20$  MeV.

We are interested in extracting the value of  $a_{nn}$ , which, in turn, is a low-energy characteristic of neutron-neutron scattering and manifests itself in the momentum dependence of the cross section at small values of the momentum  $p_r$ . The influence of the value of  $a_{nn}$  on the cross section is illustrated in Fig. 4.3, where the cross sections are shown for three different values of  $a_{nn}$ , namely  $-18, -19, -20$  fm. For each value there are two curves, the dashed one corresponds to  $\theta_r = 0^\circ$ , and the solid one to  $\theta_r = 90^\circ$ . One can see from Fig. 4.3 that the influence of different values of  $a_{nn}$  is significant in the FSI peak and marginal in the quasi-free peak, as one would have expected.

In the previous section we have shown (see right panel in Fig. 4.1) that the relative height of the quasi-free and the FSI peak changes if the effects of higher orders are included in the cross sections. Therefore those angular configurations are to be preferred, where the quasi-free production is suppressed.

The central point of this study is to demonstrate that there is a large sensitivity of the momentum spectra to the scattering length and that this scattering length can be extracted with a small and controlled theoretical uncertainty. As outlined in the introduction to this chapter, we can estimate this uncertainty reliably, because the effect of the higher orders up to  $\chi^{5/2}$  are calculated completely. In order to demonstrate the effect of those higher orders on the shape of the momentum distribution, in Fig. 4.4

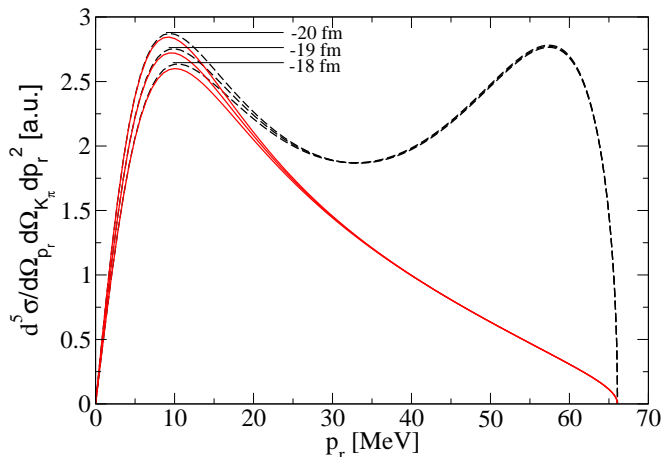


Figure 4.3: The effect of varying the value of  $a_{nn}$  on the differential cross section. The solid and dashed lines correspond to the same angular configurations as in Fig. 4.1, left panel. The different values of  $a_{nn}$  are shown on the figure. The overall scale is arbitrary but the relative normalization is the same for all curves.

we show as the light band the spread in the results for the calculation from LO to  $\chi^{5/2}$ . The results also include higher partial waves for the pion as well as the final  $nn$  system.

There is some sensitivity to the behavior of the deuteron wave function at short distances. For the reaction  $\pi^-d \rightarrow \gamma nn$  this sensitivity was identified as the largest effect at N<sup>3</sup>LO [104] #2. Guided by this we include in the uncertainty estimate also the spread in the results due to the use of different wave functions. In order to remove the effect of the change in normalization when, *e.g.*, changing the chiral order, all curves are normalized at  $p_{\text{norm}} = 30$  MeV in Fig. 4.4. In the same figure (with the same normalization) we also show the change in the shape that comes from different values of the scattering length: the dark band is generated by a variation of  $a_{nn}$  by  $\pm 1$  fm around the central value of  $-18.9$  fm. Clearly, the theoretical uncertainty is negligibly small compared to the signal of interest.

One way to quantify the theoretical uncertainty is through the use of the function  $\mathcal{S}$ , defined as

$$\mathcal{S}(a_{nn}, \Phi) = \int_0^{p_{\text{max}}} dp_r \left( F(p_r | a_{nn}^{(0)}, \Phi^{(0)}) - N(a_{nn}, \Phi) F(p_r | a_{nn}, \Phi) \right)^2 w(p_r), \quad (4.5)$$

where  $p_{\text{max}} = \sqrt{MQ}$  is the maximum value of  $p_r$ ,  $F(p_r | a_{nn}, \Phi)$  is proportional to the five-fold differential cross section as defined in Eq. (4.3). In the latter we refrained from showing the angular dependence in favor of the parametric dependence of the cross section on the  $nn$  scattering length  $a_{nn}$  as well as on the multi-index  $\Phi$ , which symbolizes the dependence of the cross section on the chosen chiral order and the wave

#2 Within the framework of ChPT with a consistent power counting scheme, the quantitative impact of the wave-function dependence is governed by the order at which a counter term appears that can absorb this model dependence. The corresponding counter term for the  $\gamma d$  as well as the  $\pi d$  reaction arises at N<sup>3</sup>LO.



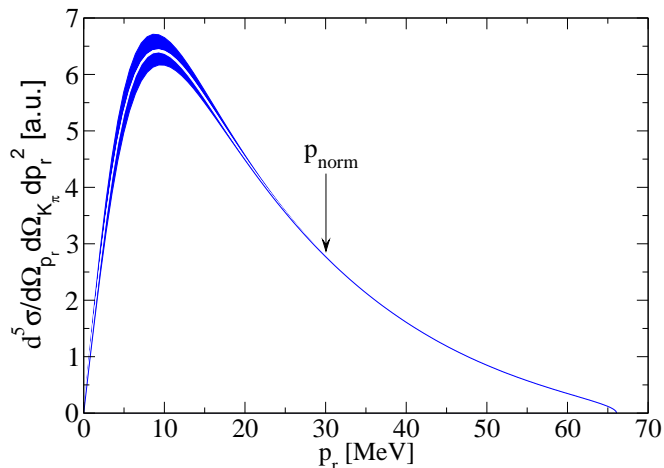


Figure 4.4: The light (white) band is the error band, and dark (blue) band correspond to  $\pm 1$  fm shift in the scattering length from the central value  $-18.9$  fm.

functions used, as outlined above. The weight function  $w(p_r)$  was introduced to allow us to suppress particular regions of momenta in the analysis—the role of  $w(p_r)$  will be discussed in detail below. For simplicity we may assume that  $\mathcal{S}$  is dimensionless; all dimensions can be absorbed into the constant  $C$  defined in Eq. (4.3).

The value  $a_{nn}^{(0)}$  denotes the central value of the scattering length ( $-18.9$  fm) for which we perform the estimate of the theoretical uncertainty<sup>#3</sup> whereas  $\Phi^{(0)}$  corresponds to the baseline type of calculation, namely leading order with chiral wave functions as specified in Appendix E.2.4. The relative normalization  $N(a_{nn}, \Phi)$  is fixed by demanding that  $\mathcal{S}$  gets minimized for any given pair of parameters  $a_{nn}, \Phi$  ( $\partial\mathcal{S}/\partial N = 0$ ). This gives

$$N(a_{nn}, \Phi) = \frac{\int_0^{p_{\max}} dp_r F(p_r | a_{nn}^{(0)}, \Phi^{(0)}) F(p_r | a_{nn}, \Phi) w(p_r)}{\int_0^{p_{\max}} dp_r F^2(p_r | a_{nn}, \Phi) w(p_r)} . \quad (4.6)$$

Thus,  $\mathcal{S}$  characterizes the mean-square deviation of the shape from the baseline cross section  $F(p_r | a_{nn}^{(0)}, \Phi^{(0)})$ . In this way we determine the theoretical uncertainty in full analogy to the standard method of data analysis.

In order to quantify the theoretical uncertainty we may define  $\Phi_{\max}$  as that chiral order and choice of wave function, where  $\mathcal{S}(a_{nn}^{(0)}, \Phi_{\max})$  gets maximal:

$$\mathcal{S}(a_{nn}^{(0)}, \Phi_{\max}) = \max_{\Phi} \{ \mathcal{S}(a_{nn}^{(0)}, \Phi) \} . \quad (4.7)$$

Therefore  $\mathcal{S}(a_{nn}^{(0)}, \Phi_{\max})$  provides an integral measure of the theoretical uncertainty of the differential cross section. Demanding that the effect of a change in the scattering length by the amount  $\Delta a_{nn}$  matches that by the inclusion of higher orders *etc.* we can

<sup>#3</sup>Note that the theoretical uncertainty practically does not change when the central value of the scattering length varies in the relevant interval  $\pm 1$  fm.

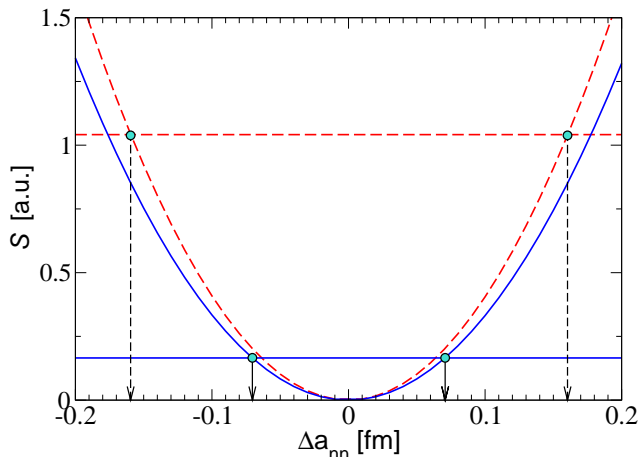


Figure 4.5: The functions  $\mathcal{S}(a_{nn}^{(0)}, \Phi_{\max})$  and  $\mathcal{S}(a_{nn}^{(0)} + \Delta a_{nn}, \Phi^{(0)})$  are shown by the horizontal and parabolic curves, respectively. The solid curves are obtained by adding the weight factor in Eq. (4.5) that cuts all momenta above 30 MeV in distinction from the dashed ones. The calculation is performed for the scattering length  $a_{nn}^{(0)} = -18.9$  fm,  $\theta_r = 90^\circ$ , and  $\theta_\pi = 0^\circ$ . The value of  $\Delta a_{nn}$  corresponding to the crossing point of the horizontal and parabolic curves determines the theoretical uncertainty of the calculation.

identify  $\Delta a_{nn}$  as an uncertainty in the scattering length. Expressed in terms of  $\mathcal{S}$ , we may define  $\Delta a_{nn}$  via

$$\mathcal{S}(a_{nn}^{(0)} + \Delta a_{nn}, \Phi^{(0)}) = \mathcal{S}(a_{nn}^{(0)}, \Phi_{\max}) . \quad (4.8)$$

This relation is illustrated in Fig. 4.5. The dashed horizontal line corresponds to  $\mathcal{S}(a_{nn}^{(0)}, \Phi_{\max})$ , where we use  $w(p_r) = 1$ . The dashed parabolic line shows the corresponding  $\mathcal{S}(a_{nn}^{(0)} + \Delta a_{nn}, \Phi^{(0)})$  as a function of  $\Delta a_{nn}$ . The calculation is performed for  $\theta_r = 90^\circ$ , and  $\theta_\pi = 0^\circ$ . The crossing point of the curves corresponds to  $\Delta a_{nn} = 0.16$  fm, which can be identified as the theoretical uncertainty for the extraction of the scattering length.

In the previous section we showed that the signal region is located at momenta lower than 30 MeV. On the other hand, the theoretical uncertainty of the differential cross section is largest for large values of  $p_r$  due to the onset of the quasi-free contribution. In view of these two facts it seems reasonable to use such weight functions  $w(p_r)$  that suppress the contribution of large momenta. For instance, we may use  $w(p_r) = \Theta(p^{\text{cut}} - p_r)$  for the weight function. If we choose, *e.g.*,  $p^{\text{cut}} = 30$  MeV, the theoretical uncertainty of the extraction of the scattering length reduces to 0.07 fm, as is demonstrated by the solid lines in Fig. 4.5. This figure nicely illustrates that the parabolic curve that represents the signal changes only very little when a restriction to small values of  $p_r$  is applied. At the same time this procedure significantly reduces the value of the uncertainty  $\mathcal{S}(a_{nn}^{(0)}, \Phi_{\max})$ .

The observation that the dependence of  $\mathcal{S}(a_{nn}^{(0)} + \Delta a_{nn}, \Phi^{(0)})$  on  $\Delta a_{nn}$  is very well approximated by a parabola allows for a more systematic study of the  $p^{\text{cut}}$  dependence

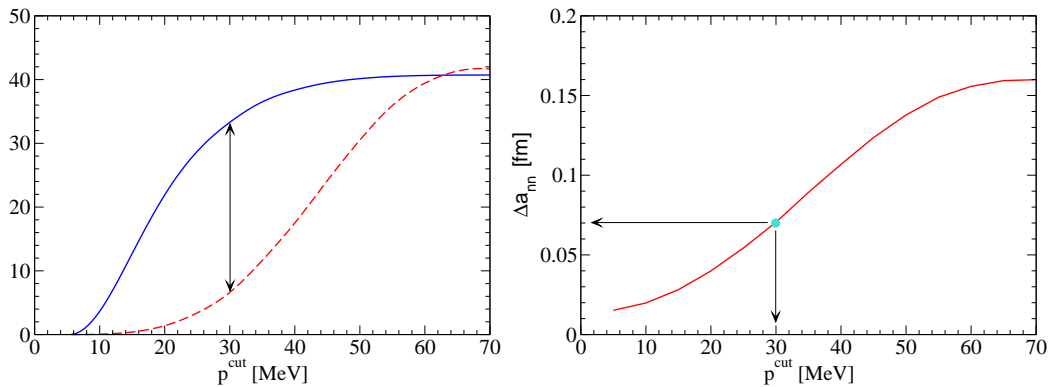


Figure 4.6: Left panel: Comparison of the  $p^{\text{cut}}$  dependence of functions  $\mathcal{S}(a_{nn}^{(0)}, \Phi_{\text{max}}|p^{\text{cut}})$  (dashed curve) and  $\alpha(p^{\text{cut}})$  (solid curve). The calculation is performed for the scattering length  $a_{nn}^{(0)} = -18.9$  fm,  $\theta_r = 90^\circ$ , and  $\theta_\pi = 0^\circ$ . Right panel: The corresponding theoretical uncertainty  $\Delta a_{nn}$  as a function of  $p^{\text{cut}}$ .

of the theoretical uncertainty. We therefore define

$$\alpha(p^{\text{cut}}) = \frac{\mathcal{S}(a_{nn}^{(0)} + \Delta a_{nn}, \Phi^{(0)}|p^{\text{cut}})}{(\Delta a_{nn})^2}, \quad (4.9)$$

where the explicit  $p^{\text{cut}}$  dependence is introduced into the function  $\mathcal{S}$  through the weight function  $w$  as explained above. The dashed and the solid parabola in Fig. 4.5 can then be written as  $\alpha(p^{\text{cut}})(\Delta a_{nn})^2$ , with  $\alpha(p_{\text{max}}) = 41 \text{ fm}^{-2}$  and  $\alpha(30 \text{ MeV}) = 33 \text{ fm}^{-2}$ . In the left panel of Fig. 4.6 we show  $\alpha(p^{\text{cut}})$  as the solid line. In the same panel the dashed line represents the measure of the theoretical uncertainty given by  $\mathcal{S}(a_{nn}^{(0)}, \Phi_{\text{max}}|p^{\text{cut}})$ , multiplied by a factor of 40. This figure makes more quantitative the statement made above: for very small values of  $p^{\text{cut}}$  we cut into the signal region and therefore  $\alpha$  shows a very rapid variation. However, as soon as  $p^{\text{cut}}$  is larger than 30 MeV it goes to a plateau (in the figure indicated by the arrow). On the other hand, the theoretical uncertainty is monotonously growing once  $p^{\text{cut}}$  is larger than 30 MeV. From this figure we deduce that the ideal value for  $p^{\text{cut}}$  is between 25 and 40 MeV. This translates into a theoretical uncertainty between 0.05 and 0.1 fm, as illustrated in the right panel of the same figure. The value of  $\theta_\pi$  also has some impact on the theoretical uncertainty, however, in its whole parameter range the estimated uncertainty stays below 0.1 fm for  $p^{\text{cut}} = 30$  MeV.

Clearly, also the experimental data, once they exist, should be analyzed using a procedure analogous to the one given above. This means that the scattering length is to be extracted from a  $\chi^2$  fit of the theoretical curves to the data. In this work we used the calculation at LO as baseline result and the results at higher orders to estimate the theoretical uncertainty. Consequently, we propose to use the momentum spectrum calculated at LO in the fitting procedure of the experiment. The corresponding analytical expressions are given in Appendix E.2.4. The only parameter to be adjusted besides the scattering length is the overall normalization. In this fitting procedure only those data points should be included that are below a given  $p^{\text{cut}}$ , in order to keep the theoretical uncertainty small.

## 4.5 Summary of Chapter 4

We showed that for the angular configurations that suppress the quasi-free production the inclusion of higher order effects (NLO, N<sup>2</sup>LO, and  $\chi^{5/2}$ ) as well as the use of different wave functions leads only to a minor change in the momentum dependence of the five-fold differential cross sections.

Based on this observation we propose to use the momentum spectrum calculated at LO for the extraction of the neutron–neutron scattering length from the data. This procedure has the advantage that the corresponding matrix elements can be given in an analytic form (see Appendix E.2.4) that could be used directly in the Monte Carlo simulation for the experiment analysis. In this way the non-trivial dependence of the spectra on  $\theta_\pi$ , discussed above, can be easily controlled. The scattering length can then be extracted by a two parameter fit to the data where, simultaneous to a variation in  $a_{nn}$ , the normalization constant needs to be adjusted.

Note that the leading order calculation basically agrees to the expression given in Ref. [23] long ago. However, a systematic and reliable study of the theoretical uncertainties of the extraction was possible only within our full calculation up to order  $\chi^{5/2}$  in ChPT. In this way we could show that the reaction  $\gamma d \rightarrow \pi^+ nn$  is very well suited for a determination of the  $nn$  scattering length. The theoretical uncertainty of order 0.1 fm for the extracted scattering length, estimated in this paper, is of the same order as that claimed for  $\pi^- d \rightarrow \gamma nn$  [135] and  $nd \rightarrow pnn$  [123, 132].

We discussed in detail the theoretical uncertainty for a fixed excess energy of  $Q = 5$  MeV only, however, it should be clear that the procedure can be easily repeated for any energy within the range of applicability of our approach ( $Q < 20$  MeV). For example, we checked that the theoretical uncertainty stays below 0.1 fm also at  $Q = 10$  MeV. Note that the number of events in the signal region scales roughly with  $\sqrt{Q}$ , the phase space available for the pion. It remains to be seen what energy is the best for the corresponding experiment.

We showed that for a proper choice of both kinematics and weight function  $w$ , the theoretical uncertainty for the extraction of the neutron–neutron scattering length from  $\gamma d \rightarrow \pi^+ nn$  can be as low as 0.1 fm. It should be stressed, however, that this error was evaluated most conservatively—we use our LO calculation as baseline result and estimate the theoretical uncertainty from the effects of the higher orders that we calculated completely. This error can be significantly reduced by further studies. For example, if we include in the uncertainty estimate only the spread in the results due to the use of different wave functions, which is identified as the largest effect at N<sup>3</sup>LO for the reaction  $\pi^- d \rightarrow \gamma nn$  [104], the theoretical uncertainty of the extracted scattering length reduces by one order of magnitude. This indicates that the theoretical uncertainty is indeed under control. However to put this N<sup>3</sup>LO estimation on more solid ground a complete calculation should be performed to this order. Most of the operators that are relevant at this order are the same as those of  $\pi^- d \rightarrow \gamma nn$ , given explicitly in Ref. [137]. One counter term enters, which can be fixed *e.g.* from  $nd$  scattering [20], the reaction  $NN \rightarrow NN\pi$  [79], or from weak decays [135]. Once this is done we may use our calculation to order  $\chi^{5/2}$  as baseline result and estimate the theoretical uncertainty from the then available N<sup>3</sup>LO calculation.

Although we have identified the angles  $\theta_r = 90^\circ$  as the preferred kinematics, also

other configurations could be studied in order to control the systematics. However, then the spectra calculated at  $\chi^{5/2}$  should be used in the analysis.

# Chapter 5

## Dispersive and Absorptive Corrections to the $\pi d$ Scattering Length

In this chapter we consider dispersive and absorptive corrections to the pion-deuteron scattering length  $a_{\pi d}$ . These corrections are closely related to the process  $NN \rightarrow NN\pi$ . We apply the formalism developed in Chapter 2 to calculation of these corrections.

### 5.1 Introduction

The pion-nucleon ( $\pi N$ ) scattering lengths are fundamental quantities of low-energy hadron physics since they test the QCD symmetries and the pattern of chiral symmetry breaking. As stressed by Weinberg and Tomozawa long time ago, chiral symmetry suppresses the isoscalar  $\pi N$  scattering length  $a_+$  substantially compared to its isovector counterpart  $a_-$ . Thus, a precise determination of  $a_+$  demands in general high accuracy experiments.

Here pion-deuteron ( $\pi d$ ) scattering near threshold plays an exceptional role for  $\text{Re}(a_{\pi d}) = 2a_+ + (\text{few-body corrections})$ . The first term  $\sim a_+$  is simply generated from the impulse approximation (scattering off the proton and off the neutron) and is independent of the deuteron structure. Thus, if one is able to calculate the few-body corrections in a controlled way,  $\pi d$  scattering is a prime reaction to extract  $a_+$  (most effectively in combination with pionic hydrogen measurements). In addition, already at threshold the  $\pi d$  scattering length is a complex-valued quantity. It is therefore also important to gain a precise understanding of its imaginary part—this is one of the issues addressed in this chapter.

Recently the  $\pi d$  scattering length was measured to be [94, 138]

$$a_{\pi d}^{\text{exp}} = (-26.1 \pm 0.5 + i(6.3 \pm 0.7)) \times 10^{-3} m_{\pi}^{-1}, \quad (5.1)$$

where  $m_{\pi}$  denotes the mass of the charged pion. In the near future a new measurement with a projected total uncertainty of 0.5% for the real part and 4% for the imaginary part of the scattering length will be performed at PSI [139]. Clearly, performing calculations up to this accuracy poses a challenge to theory that several groups recently took up

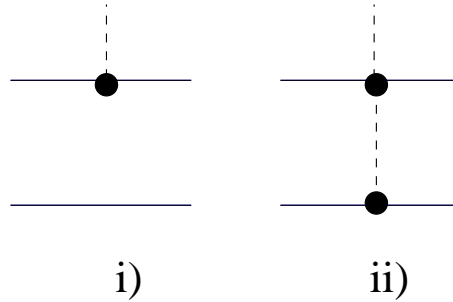


Figure 5.1: Diagrams contributing to the  $\pi NN \rightarrow NN$  transition up to the order considered: *i)* direct contribution and *ii)* rescattering.

[83, 120, 127, 140–143]. In addition, an interesting isospin violating effect in pionic deuterium was found, see [144]. For a review on older work we refer to Ref. [145].

The imaginary part for the  $\pi d$  scattering length can be expressed by unitarity in terms of the  $\pi d$  total cross section through the optical theorem. One gets

$$4\pi\text{Im}(a_{\pi d}) = \lim_{q \rightarrow 0} q \{ \sigma(\pi d \rightarrow NN) + \sigma(\pi d \rightarrow \gamma NN) \} , \quad (5.2)$$

where  $q$  denotes the relative momentum of the initial  $\pi d$  pair. The so-called Panofsky ratio

$$R = \lim_{q \rightarrow 0} (\sigma(\pi d \rightarrow NN) / \sigma(\pi d \rightarrow \gamma NN)) \quad (5.3)$$

was measured to be  $2.83 \pm 0.04$  [146]. At low energies diagrams that lead to a sizable imaginary part of some amplitude are expected to also contribute significantly to its real part. Those contributions are called dispersive corrections. As a first estimate Brückner speculated that the real and imaginary part of these contributions should be of the same order of magnitude [147]. This expectation was confirmed within Faddeev calculations in Refs. [148, 149]. Given the high accuracy of the measurement and the size of the imaginary part of the scattering length, another critical look at this result is called for as already stressed in Refs. [150, 151]. A consistent calculation is only possible within a well defined effective field theory.

What is needed a priori for such an endeavor is a controlled power counting for  $NN \rightarrow NN\pi$  using chiral perturbation theory (ChPT) that is consistent with the one used for  $\pi d$  scattering. We showed in Chapter 2 that using of such a counting scheme leads to a good description of the total cross-section for the reaction  $NN \rightarrow d\pi$ .

In addition to the hadronic part of the dispersive and absorptive corrections to the  $\pi d$  scattering length, we estimate the corresponding contribution from the transition  $\pi d \rightarrow \gamma NN \rightarrow \pi d$  using the full structure of the one-photon exchange. Note that the inelastic channel  $\pi d \rightarrow \gamma NN$  accounts for 1/4 of the imaginary part of  $a_{\pi d}$  and therefore one can expect a sizable contribution also to its real part.

This chapter is organized as follows: in Section 5.2 we will present the power counting for the  $\pi d$  system including the dispersive part. In Section 5.3 we give our results, while a comparison to previous works is done in Section 5.4. We again close this chapter with a brief summary.

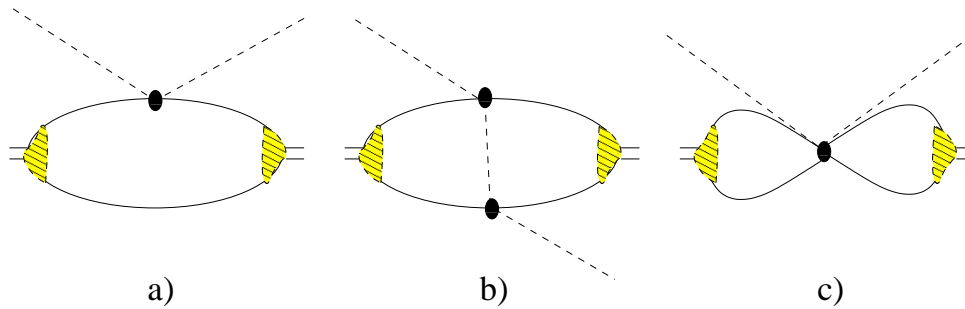


Figure 5.2: Typical Feynman diagrams for  $\pi d$  scattering; shown are the one-body term (a), the double-scattering contribution (b) and a four-nucleon-contact term (c). Solid black dots stand for the  $\pi N$  interaction, whereas the hatched area shows the deuteron wave function.

## 5.2 Power counting

The basis of any effective field theory calculation is a proper power counting that allows one to organize the diagrams according to some a priori known hierarchy. The important thing is to identify the relevant expansion parameter in the transition operators. For  $\pi d$  scattering in Ref. [52] the series is organized in powers of momenta and pion masses in units of the chiral symmetry breaking scale  $\Lambda_\chi \sim 1$  GeV. The typical one- and two-body diagrams are shown in Fig 5.2 (a) and (b), respectively. The small binding energy of the deuteron introduces a new small scale that can be accounted for systematically [120]. In Refs. [32, 82] it was demonstrated how the scheme is to be modified in the presence of three-body ( $\pi NN$ ) cuts — see also the discussion in Sections 3.2, 3.3. Based on calculations with deuteron wave functions obtained solely from contact  $NN$  interactions, in Refs. [152, 153] it was argued that field theoretical consistency calls for a counter term at leading order. However, in Refs. [83, 141–143] it was shown that this is no longer necessary as soon as the finite range of the one-pion exchange is included in the  $NN$  potential.

So far no attempt was made to also include consistently — within ChPT — the so called dispersive corrections that emerge from the hadronic  $\pi d \rightarrow NN \rightarrow \pi d$  and photonic  $\pi d \rightarrow \gamma NN \rightarrow \pi d$  reaction chains. We define dispersive corrections as contributions from diagrams with an intermediate state that contains only nucleons, photons and at most real pions. Thus, all other potentially important corrections to the  $\pi d$  scattering length that come from, e.g., the  $\Delta$  resonance will not be discussed here (although we outline some issues concerning the Delta contributions). The diagrams contributing to the hadronic and photonic parts of the dispersive corrections in accordance to our definition are shown schematically in Figs. 5.3 and 5.4, respectively.

Before we present the results of the calculation we first need to establish the power counting. The fact that the hadronic reaction chain  $\pi d \rightarrow NN \rightarrow \pi d$  is a process with large momentum transfer introduces a new scale into the problem that needs to be accounted for by a modified power counting, in full analogy with our considerations for the reaction  $NN \rightarrow NN\pi$  in Chapter 2.

To establish the counting scheme we focus on two-body currents only — how to



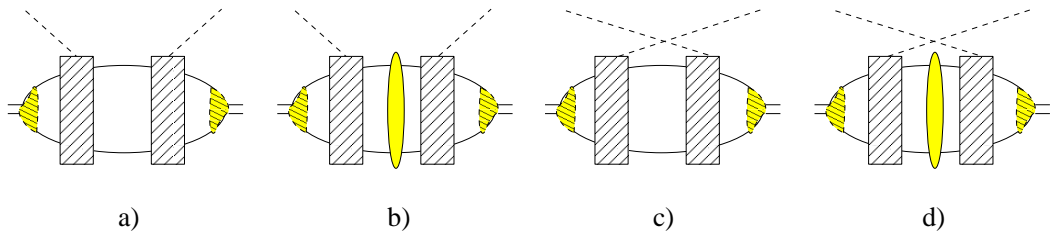


Figure 5.3: The classes of the hadronic contributions to the dispersive corrections. Diagram (a) and (b) denote the direct and (c) and (d) the crossed terms. The filled ellipse denotes the  $NN$  interaction in the intermediate state. The diagrams contributing to the  $\pi NN \rightarrow NN$  transition to the given order are shown in Fig. 5.1. The diagrams with emission of pion on the second nucleon are not shown explicitly but taken into account in the calculation.

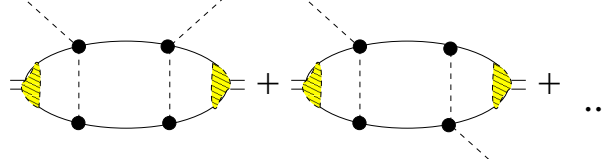
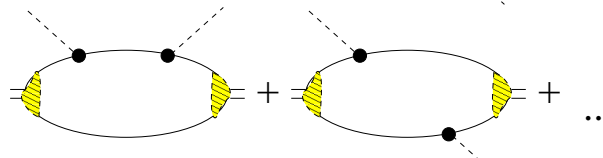
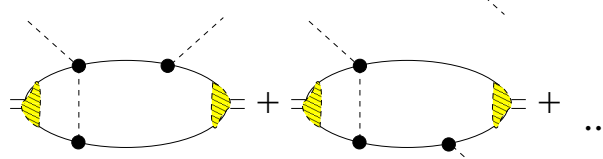
include one-body currents into the standard scheme is described in Ref. [52]<sup>#1</sup>. Thus, in what follows we will compare our two body  $\pi NN \rightarrow NN \rightarrow \pi NN$  operators with the leading two body operator shown in Fig. 5.2(b). Then it is sufficient to read off the vertex factors for the  $\pi NN \rightarrow \pi NN$  transitions to identify the order of any given diagram. We therefore estimate  $m_\pi^2/(f_\pi^4 q^2)$  for the diagram (b) of Fig. 5.2 where  $q$  here defines the momentum of intermediate pion. Utilizing Weinberg's counting scheme where all internal momenta are assumed to be of order  $m_\pi$  we find diagram (b) to be  $\mathcal{O}(1)$  — here and in what follows we drop a factor  $1/f_\pi^4$  common to all diagrams to get the order estimate. Power counting gives that the  $4N2\pi$  contact term shown in Fig.5.2 (c) contributes at  $\mathcal{O}(\chi^2)$ , where  $\chi = m_\pi/M$  is the standard expansion parameter of ChPT with  $M$  for the nucleon mass. This last contribution comes with a yet unknown coefficient. As such, an estimate for its size provides the theoretical accuracy that a calculation for the  $\pi d$  scattering length can have at most. Therefore, assuming naturalness for the strength of the contact term, the theoretical limit of accuracy is of order  $\chi^2$  which translates into a few percent. Reverting this statement, in order to reach a theoretical accuracy that is comparable to that expected for the experimental value of the  $\pi d$  scattering length, all contributions of lower order than  $\chi^2$  should be evaluated. We will now show that the dispersive corrections contribute to  $\mathcal{O}(\chi^{3/2})$ .

Transitions of the type  $\pi NN \rightarrow NN \rightarrow \pi NN$  — sketched in Fig. 5.3 (a) — get contributions from small values of the  $NN$  intermediate momentum  $q$  ( $q \sim m_\pi$  or smaller) as well as from large values of  $q$  ( $q \sim p_{\text{thr}} = \sqrt{m_\pi M}$ ). The latter value refers to the on-shell momentum of the intermediate  $NN$  state (or, equivalently, to the threshold initial momentum of the reaction  $NN \rightarrow NN\pi$ ). The power counting as given for  $NN \rightarrow NN\pi$  relates to the latter part of the contribution. It is based on the assignment  $p_{\text{thr}}/M = \chi_\pi \sim \mathcal{O}(\chi^{1/2})$  (see Chapter 2). To derive the order of the dispersive corrections let us start with diagram  $d1$  of Table 5.1. (See footnote #1 for how to include diagrams of the type  $d2$ ). For this one we find in units of the amplitude

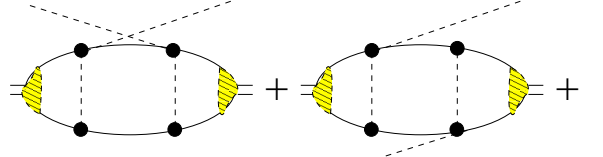
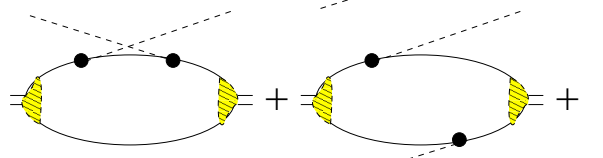
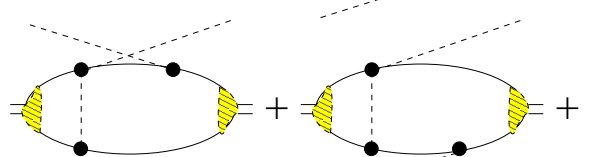
<sup>#1</sup> In Ref. [28] the corresponding recipe is given that needs to be applied to  $NN \rightarrow NN\pi$  and therefore also to the dispersive corrections. It implies that the diagrams shown in Fig. 5.1(a) and (b) contribute at the same order for  $s$ -wave pion production.

Table 5.1: Hadronic contribution to the real and imaginary part of  $a_{\pi d}$  in units of  $m_{\pi}^{-1} \times 10^{-3}$ . We only show the typical topologies — all permutations are included as indicated by the ellipses.

*direct contributions*

$d1$		$= 0.49 + i 6.68$
$d2$		$= -0.8 + i 0.1$
$d3$		$= -6.02 - i 1.65$
$d4-d6$	sum of this group	$= -6.33 + i 5.13$
	corresp. terms with intermediate $NN$ interaction	$= 1.96 - i 0.88$
	sum of all direct terms	$= -4.37 + i 4.25$

*crossed contributions*

$c1$		$= 1.83$
$c2$		$= 1.37$
$c3$		$= -0.09$
$c4-c6$	sum of this group	$= 3.11$
	corresp. terms with intermediate $NN$ interaction	$= -0.37$
	sum of all crossed terms	$= 2.74$

*direct + crossed*

	total sum	$= -1.63 + i 4.25$
--	-----------	--------------------

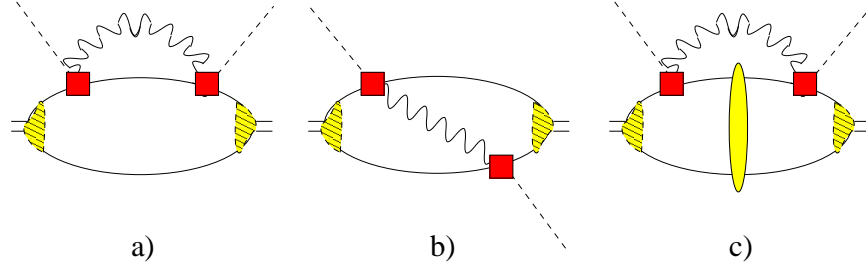


Figure 5.4: Diagrams contributing to the dispersive corrections from photon-exchange interactions: one-body term (a) and double scattering (b). The filled ellipse denotes the  $NN$  interaction in the intermediate state. The solid squares denote the full  $\pi N \rightarrow \gamma N$  transition amplitude as depicted in Fig. 5.5.

for diagram (b) of Fig. 5.2 (estimated to be  $\mathcal{O}(1)$ ) <sup>#2</sup>

$$\left[ \left( \frac{m_\pi}{f_\pi^3 q} \right)^2 \frac{1}{m_\pi - q^2/M + i\gamma} \left( \frac{q^3}{(4\pi)^2} \right) \right] / \left( \frac{1}{f_\pi^4} \right) \sim \begin{cases} \mathcal{O}(\chi^2) & \text{for } q \sim m_\pi \\ \mathcal{O}(\chi^{\frac{3}{2}}) & \text{for } q \sim p_{\text{thr}} \end{cases} \quad (5.4)$$

where the first term in the square brackets comes from the  $\pi NN \rightarrow NN$  transition operator, the second one from the  $NN$  propagator in the intermediate state and the last one from the integral measure. To arrive at the estimate for  $q \sim p_{\text{thr}}$ , where the l.h.s of Eq. (5.4) involves a singularity, we replaced the two-nucleon propagator by the corresponding  $\delta$ -function term for this estimate should apply to both the real part as well as the imaginary part that emerges from  $\pi NN \rightarrow NN \rightarrow \pi NN$ . Furthermore we used  $4\pi f_\pi \simeq M$ . The small momentum part of the integral is thus of order  $\chi^2$  and not relevant for this study. That is why dispersive corrections were not considered in the studies of Refs. [120, 127]. However, the part of the integral where  $q$  is of the order of  $p_{\text{thr}}$  is indeed of lower order than  $\chi^2$  and thus should be considered. It is important to stress that as we saw in Chapter 2 for a consistent understanding of  $NN \rightarrow NN\pi$  within ChPT it was also necessary to include the large scale  $p_{\text{thr}}$  explicitly in the power counting [22, 28].

For the imaginary part of the amplitude  $\pi NN \rightarrow NN \rightarrow \pi NN$  we have an experimental value —  $(3/4)\text{Im}(a_{\pi d})/\text{Re}(a_{\pi d}) \simeq 1/6$ , where the factor of  $3/4$  was introduced since this fraction of the width comes from  $\pi d \rightarrow NN$  (see Eqs. 5.2, 5.3). To check the power counting we need some estimate for the real part of the scattering length, which is known to be dominated by the double rescattering term (Fig. 5.2(b)) and was shown above to be  $\mathcal{O}(1)$ . Therefore we expect from the above considerations a relative suppression of the imaginary part to the real part of the order of  $(m_\pi/M)^{3/2} = 1/17$ . Thus, the hadronic contribution to the imaginary part of the  $\pi d$  scattering length is about a factor of 3 larger than predicted by the power counting — a deviation that is tolerable.

Since the  $NN$  interaction is non-perturbative in diagrams, where a two-nucleon state contributes near on-shell, the full  $NN$  interaction in intermediate states should be

<sup>#2</sup>For a brief description on how to identify the order of a particular diagram we refer to Appendix E of Ref. [22].

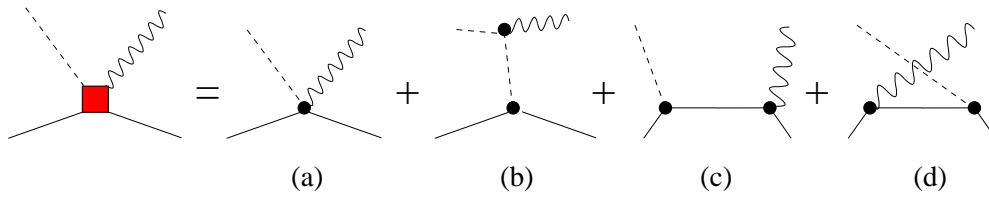


Figure 5.5: Diagrams contributing to the  $\pi N \rightarrow \gamma N$  transition operator: Kroll-Rudermann term (a), pion in flight (b) and nucleon s- (c) and u- (d) channel.

taken into account — the corresponding diagram is depicted in Fig. 5.3(b). These are also included in our calculation using the techniques outlined in Appendix B. At the same chiral order there is an additional class of contributions — these are the crossed terms shown as diagrams (c) and (d) in Fig. 5.3. Already in Ref. [154] an evaluation of those diagrams was called for, however, a consistent calculation of the terms that emerge from diagram *ii*) of Fig. 5.1 has not been possible so far [145]. Since we work within a consistent field theory no such problem exists. The numerical importance of some crossed diagrams for  $\pi d$  scattering was already observed before and referred to as the so-called Jennings mechanism [155]: to understand data measured with tensor polarized deuterons for elastic  $\pi d$  scattering at backward angles, a particular crossed pion contribution needs to be included — see also the discussion in Ref. [156]. The order assignment for the crossed diagrams is obvious once one applies the same procedure that leads to the estimate given in Eq. (5.4) — the only necessary change is to switch the sign of  $m_\pi$  in the  $NN$  propagator. Note, in these diagrams the two-nucleon intermediate state is always off-shell in contrast to the  $NN$  state in the direct contributions that are expected to receive the dominant contributions from (near) on-shell nucleons. It is therefore surprising that direct and crossed terms appear at the same order. However, one should recall that the chiral expansion is an expansion around the chiral limit. When approaching the chiral limit the intermediate two-nucleon states of both direct and crossed diagrams approach the same kinematical point. Therefore it is natural that they also contribute to the same chiral order for physical pion masses.

A priori there is no rule how to include the electromagnetic contribution to both the real and the imaginary part of the  $\pi d$  scattering length (see Fig. 5.4) into the power counting — the fine structure constant  $\alpha$  is clearly an independent parameter. Based on the observation that the electromagnetic and the hadronic contribution to the imaginary part are of the same order of magnitude, we assign the same chiral order to both — as it is often done in chiral perturbation theory studies.

### 5.3 Results

In this section we present the results of our investigations. We first focus on the hadronic contribution to the dispersive corrections. The results are given in Table 5.1. Note, for the contributions that involve the  $NN$  interaction in the intermediate state we do not give the individual results explicitly. All calculations are done with the CD-Bonn NN potential [87].

First of all we observe that with a value of  $4.25 \times 10^{-3} m_\pi^{-1}$  the imaginary part of the scattering length turns out to be very close to the experimental number of  $(3/4)\text{Im}(a_{\pi d}^{\text{exp}}) = (4.7 \pm 0.5) \times 10^{-3} m_\pi^{-1}$  (c.f. Eqs. (5.1) and (5.2) and discussion below the latter). This is not too surprising given the good description for the near threshold cross section of  $NN \rightarrow d\pi$  as we showed in Chapter 2. For the real part on the other hand we observe a striking pattern: although the individual contributions can be quite large, the total sum turns out to be rather small. About 1/3 of the contribution from the direct diagrams of Table 5.1 gets canceled by the corresponding ones with  $NN$  interactions in the intermediate state. This is the same pattern as for the imaginary part — the fact that the latter reduction in the magnitude is natural for processes of the type  $NN \rightarrow NNx$  was discussed in Ref. [157]. However, about 60 % of the contribution of the direct diagrams of Table 5.1 is canceled by the corresponding crossed diagrams. As we will see, part of this cancellation is quite natural. When comparing the direct and the crossed diagrams we observe that the two-nucleon propagator in the intermediate state of the former reads  $1/(m_\pi - q^2/M)$  (c.f. Eq. (5.4)), where  $q$  denotes the relevant loop momentum. The corresponding expression for the latter reads  $1/(-m_\pi - q^2/M)$ . Thus, for small values of  $q$ , where the two-nucleon propagator becomes static, one obtains  $1/m_\pi$  and  $-1/m_\pi$  respectively, and some contributions of direct and crossed diagrams, specifically d2 and c2, will largely cancel. Note, this cancellation does not mean that the full contribution of each pair of diagrams cancels. The numbers given in the table also contain the contributions from large values of  $q$ , where such a cancellation does not necessarily occur. Note also that it is the structure of the two-nucleon propagator that is responsible for the smallness of diagram d1 as compared to its crossed partner c1. In contrast to diagram c1, the two-nucleon propagator in d1 changes its sign when passing through the point  $q^2 = m_\pi M$  whereas all other terms such as vertex functions, pion propagators, etc., have the same sign throughout the region of integration. Thus, a strong cancellation takes place for the latter and as a result the real part of diagram d1 is much smaller than that of c1. The situation for diagram d3 is different to d1, since also the S-wave deuteron wave function changes sign at  $q \sim \sqrt{m_\pi M}$ . This leads to a constructive interference of contributions from small and large momenta.

In Fig. 5.4 we show the diagrams that contribute to the electromagnetic piece of the dispersive contributions. To evaluate the real part of the one-body contribution (diagram (a)) we use the same prescription as used in Chapter 3 (see also Ref. [32]), namely we subtract the term corresponding to the one-body operator at zero momentum. This removes the leading divergence that in a full calculation needs to be absorbed into the electromagnetic corrections of the  $\pi N$  scattering lengths (note, this quantity was recently estimated in Ref. [158])<sup>#3</sup>. To ensure gauge invariance the  $\pi N \rightarrow \gamma N$  amplitude needs to contain all diagrams shown in Fig. 5.5. However, since for the calculation of the photonic part of the dispersive correction the  $\pi N \rightarrow \gamma N$  amplitude contributes at threshold, diagrams (c) and (d) are suppressed by one power of  $\chi$  as compared to diagrams (a) and (b). Thus, we did not take them into account in this leading order calculation. Because of the same reasoning we neglect also the contributions to the  $\pi N \rightarrow \gamma N$  amplitude from the  $\Delta$  resonance [117]. We calculated the full  $\pi d \rightarrow \gamma NN \rightarrow \pi d$  amplitude in

<sup>#3</sup>A more precise calculation within QCD+QED requires a much more sophisticated framework, see e.g. [159] — this is beyond the scope of this work.

Coulomb gauge. The corresponding propagator is given, e.g., in Ref. [160]. The final result is  $(-0.1 + i1.4) \times 10^{-3} m_\pi^{-1}$ . Again, the imaginary part of the photonic part of the absorption correction, which is dominated by the imaginary part of the  $\pi^- p$  scattering length due to the process  $\pi^- p \rightarrow \gamma n \rightarrow \pi^- p$ , is sufficiently close to the corresponding experimental value of  $(1/4)\text{Im}(a_{\pi d}^{\text{exp}}) = (1.6 \pm 0.2) \times 10^{-3} m_\pi^{-1}$ , whereas the real part is negligible. This conclusion is consistent with that of Ref. [150], where the real part was found to be  $-0.2 \times 10^{-3} m_\pi^{-1}$  within a less complete calculation<sup>#4</sup>.

## 5.4 Discussion

We now compare our results for the hadronic contributions to other works. The dispersive corrections to  $\pi d$  scattering were investigated using Faddeev calculations in Refs. [148, 149]. Since these works considered only those intermediate states that contain at most one pion at a time, all direct diagrams were included. The authors found  $-5.6(1.4) \times 10^{-3} m_\pi^{-1}$  as contribution to the real part — this number was also used in the reanalysis of  $\pi d$  scattering in Ref. [150]. This is to be compared with  $-4.37 \times 10^{-3} m_\pi^{-1}$  from our work, which agrees to the above result within the uncertainty. Note, the Faddeev equations produce amplitudes that are non-perturbative in the  $\pi N$  and the  $NN$  interaction simultaneously. Thus, in addition to the direct terms as shown in Table 5.1 there are many more diagrams included like contributions where the  $NN$ -pair interacts while there is a pion in flight. However, all those are of higher order in the chiral expansion. The closeness of our result for the direct terms and the corresponding result of Ref. [148, 149] is thus an indication for the convergence of the chiral expansion. Recall that our final result to the real part of  $a_{\pi d}$  is smaller because of a cancellation of the mentioned contribution with the crossed diagrams that were not included in Refs. [148, 149].

In Ref. [140] the diagrams  $d1$  of Table 5.1 were evaluated explicitly, besides many others that are difficult to match to our amplitudes. In this work they contribute with  $(0.24 + i6.0) \times 10^{-3} m_\pi^{-1}$  to the  $\pi d$  scattering length. This number is to be compared to our  $(0.49 + i6.68) \times 10^{-3} m_\pi^{-1}$ . In Ref. [140] a value of  $3/2m_\pi$  was used at the  $\pi N \rightarrow \pi N$  vertex in contrast to the proper  $2m_\pi$  as derived recently [81]. On the other hand, Ref. [140] includes a (small) isoscalar piece into this vertex — chiral power counting assigns a subleading order to this piece. However, the pattern of the result is the same: a small real part is accompanied by a sizable imaginary part.

Our results for diagrams  $d2$  and  $c2$  agree to those of Ref. [108], once the same  $\pi NN$  coupling constant is used.

Some of the diagrams in Table 1 were included in the phenomenological studies of Refs. [140, 151]. In particular, the second diagrams of  $d3$  and  $c3$  contribute to the so-called SP-interference term (a double scattering diagram, where the first  $\pi N \rightarrow \pi N$  transition is in an  $s$ -wave, whereas the second is  $p$ -wave). In those studies the  $p$ -wave amplitude was taken from fits to  $\pi N$  data and parameterized as a strength parameter times the square of the  $\pi N$  relative momentum. Indeed, what appears at

---

<sup>#4</sup>In Ref. [161] the corresponding integral was evaluated to be one order of magnitude larger; however, the author assumes the photon energy  $q_0$  in the exchange to vanish instead of using the correct value of  $q_0 \simeq m_\pi$ .

the lower nucleon can be regarded as the  $\pi N$  scattering in  $p$ -wave but in the boosted frame. However, this treatment misses an important momentum dependence, since in the boosted frame the nucleon propagator in the intermediate state contains a term  $q^2/M$  in the denominator. As a consequence the  $p$ -wave subamplitude in the phenomenological studies grows quadratically with momentum, even for momenta  $q^2 \sim m_\pi M$  and the full matrix element scales with the wave function at the origin [140], which is theoretically not controlled. On the other hand, in our case this subamplitude goes to a constant leading to a controlled behaviour of the matrix element [83]. This is why those parts of Refs. [140, 151] can not be matched to our results. Based on the arguments given, we call for microscopic calculations, now possible within ChPT, instead of applying the phenomenological techniques.

## 5.5 Summary of Chapter 5

In this chapter we presented a calculation of the absorptive and dispersive corrections to the  $\pi d$  scattering length using ChPT. To our knowledge, the calculation provided here is the first calculation of such kind within effective field theory. Especially we found for the absorptive part

$$\text{Im}(a_{\pi d}) = ((4.25 \pm 1.2) + (1.4 \pm 0.4)) \times 10^{-3} m_\pi^{-1} \quad (5.5)$$

to be compared with the experimental value of

$$\text{Im}(a_{\pi d}^{\text{exp}}) = ((4.7 \pm 0.5) + (1.6 \pm 0.2)) \times 10^{-3} m_\pi^{-1} . \quad (5.6)$$

In both Eq. (5.5) as well as Eq. (5.6) we give the hadronic and electromagnetic contribution separately. We thus find good agreement between theory and experiment for each of the contributions. The theoretical uncertainty is estimated to be of order  $2 m_\pi/M$  in both cases<sup>#5</sup>.

For the corresponding dispersive part we get

$$a_{\pi d}^{\text{disp}} = -1.7 \times 10^{-3} m_\pi^{-1} \implies a_{\pi d}^{\text{disp}}/\text{Re}(a_{\pi d}^{\text{exp}}) \sim 6.5\% . \quad (5.7)$$

The number given for  $a_{\pi d}^{\text{disp}}$  now contains both the hadronic as well as the electromagnetic contribution and for  $\text{Re}(a_{\pi d}^{\text{exp}})$  we used Eq. (5.1). This result is quite small given that the imaginary part of the  $\pi d$  scattering length is about 1/4 of the real part. It is difficult to provide a proper estimate for the uncertainty of  $a_{\pi d}^{\text{disp}}$ , since it emerged from a cancellation of individually sizable terms. The most naive method would be to use the uncertainty of order  $2 m_\pi/M$  one has for, e.g., the sum of all direct diagrams to derive a  $\Delta a_{\pi d}^{\text{disp}}$  of around  $1.4 \times 10^{-3} m_\pi^{-1}$ , which corresponds to about 6 % of  $\text{Re}(a_{\pi d}^{\text{exp}})$ . However, given that the operators that contribute to both direct and crossed diagrams are almost the same (see Appendix E.4) and that part of the mentioned cancellations is a direct consequence of kinematics, this number for  $\Delta a_{\pi d}^{\text{disp}}$  is probably too large. A reliable error estimate for  $a_{\pi d}^{\text{disp}}$  requires an explicit evaluation of the next order contributions.

---

<sup>#5</sup>The factor of 2 appears, because the  $\pi NN \rightarrow NN$  and  $\pi NN \rightarrow \gamma NN$  transition operators — both evaluated with an uncertainty of order  $m_\pi/M$  — appear twice in each amplitude.

We showed that the smallness of the dispersive contribution to the real part of the  $\pi d$  scattering length is a consequence of efficient cancellations amongst various, individually sizable terms. To gain a better understanding of the real part of the pion-deuteron scattering length, a complete calculation of all isospin-breaking corrections at N(N)LO in the EFT with virtual photons is called for (as also stressed in [144]).



# Summary and Outlook

We performed investigations of some reactions in few-nucleon systems involving pions using techniques of effective field theory. We conclude with a summary of our achievements and an outlook.

1. In Chapter 2 we considered pion production in nucleon-nucleon collisions close to threshold within the framework of ChPT. We survey the current situation with theoretical predictions of  $NN \rightarrow NN\pi$ . In particular, we review the most recent developments of Hanhart and Kaiser [30], who applied in  $s$ -wave pion production the modified counting that accounts for large transfer momenta of order of  $\sqrt{Mm_\pi}$  typical for this reaction (in this case the expansion parameter is  $\chi_\pi = \sqrt{m_\pi/M}$ ), and showed that there are some cancellations between loops that start to enter the transition operator at NLO ( $\mathcal{O}(\chi_\pi)$ )—see Section 2.2.

Within the modified expansion in powers of  $\chi_\pi$  and the corresponding counting scheme we solved several problems concerning  $NN \rightarrow NN\pi$  risen recently in the literature, namely:

- We showed that the proper treatment of reducible and irreducible pieces for the  $s$ -wave pion production in  $NN \rightarrow NN\pi$  leads to complete cancellation of all loop diagrams at NLO. This solves the problem pointed out recently by Gårdestig, Elster, and Phillips [31], who found the loop diagram contribution to cause huge off-shell dependence in the channel  $pp \rightarrow d\pi^+$  when convoluted with deuteron wave functions. We showed in our work that there are genuinely irreducible contributions arising from diagrams that seem naively reducible, and that these induced contributions cancel completely the badly behaving loop contributions, thus solving the problem. We argue that this cancellation is necessary for the consistency of the whole counting scheme since there are no counterterm at this order that would have cured the situation otherwise;
- We showed that along with this cancellation of NLO loop contributions the proper treatment of reducible and irreducible diagrams brings the leading isovector rescattering vertex—the Weinberg–Tomozawa vertex—on-shell, which results in the enhancement of the corresponding contribution to the reaction amplitude by a factor  $4/3$  compared to what was used in the literature before. This enhancement leads to a ChPT prediction of the total cross-section for  $pp \rightarrow d\pi^+$  in agreement with experimental data—for the first time in the literature. The results of our calculation are shown in Fig. 2.8. We should notice that this result was obtained owing to mechanisms completely different from those commonly used in phenomenology,

*e.g.* from heavy meson exchanges. This difference could reveal itself in polarization observables in the reaction  $pp \rightarrow pn\pi^+$ .

- We also calculated the  $p$ -wave pion production total cross-section for  $pp \rightarrow d\pi^+$  up to NLO, thus providing complete calculation of  $pp \rightarrow d\pi^+$  up to NLO in expansion in powers  $\chi_\pi$ . The results agree with the experimental data in a broad range of energies—see Fig. 2.10;
- We conjecture that in order to deal with pion reactions in a nuclear environment in the presence of time derivatives in vertices in general one has to calculate all diagrams up to a given order, including those that are formally reducible. Then the energy dependence in the vertices is used to cancel one of the nucleon propagators. This produces an irreducible piece that is to be part of the transition operator as well as a reducible piece, where, however, the energy dependence of the vertices is replaced by the corresponding on-shell value. This conjecture, however, remains to be made more accurate.

**2.** In Chapter 3 we calculated transition operator for the reaction  $\gamma d \rightarrow \pi^+ nn$  up to  $\chi^{5/2}$ , where  $\chi = m_\pi/M$  is the natural expansion parameter for processes, in which typical momentum transfer is of order of  $m_\pi$ . We considered this reaction in following aspects:

- One of the main goals of this work was to critically investigate various approximations that are commonly used in few-body calculations. In particular, we wanted to better understand the role of the recoil corrections that are commonly taken into account by expanding three-body  $\pi NN$  propagator in powers of  $\chi$  (or neglected—the so-called static approximation). However, it was recently shown by Baru et al. [32] that the recoil corrections give non-analytic contribution in  $\chi$ —they scale as  $\sqrt{\chi}$ , therefore they are missed if the propagator is expanded. The recoil contribution was also shown to be dependent on whether the intermediate nucleon-nucleon  $S$ -wave state is Pauli blocked or allowed. Our numerical results confirm the suggestion that for Pauli allowed intermediate states the static approximation is not justified. In addition, in the case of Pauli allowed intermediate states one has also to take into account the complete  $NN$  intermediate state interaction, which gives significant contribution—cf. Table 3.2;
- We also aimed at high-accuracy calculation for  $\gamma d \rightarrow \pi^+ nn$  in view of possible extraction of the neutron-neutron scattering length and the pion photoproduction multipole strength. Therefore we considered all corrections to the transition operator up to order  $\chi^{5/2}$ —the fractional powers of  $\chi$  came from the recoil corrections that we took explicitly into account;
- We calculated the total cross-section for  $\gamma d \rightarrow \pi^+ nn$  for excess energies up to 20 MeV. We found the contribution of higher chiral orders as well as the contribution of higher nucleon-nucleon and pion-nucleon partial waves to be small due to eventual cancellations of individually rather sizable contributions. The only parameter that enters our calculation is  $E_{0+}$ —the leading production multipole.

We took the value of  $E_{0+}$  from a ChPT calculation up to  $\chi^3$  of Ref [33] (their value agrees with recent experimental data [116]). The results of our calculation shown in Fig. 3.8 demonstrate excellent agreement with the experimental data. We should mention that the previous phenomenological calculations in the literature (see, *e.g.* Ref. [23] and references therein) correspond to our calculation up to NLO. One can see from Fig. 3.8 that the NLO curve systematically underestimates the data.

**3.** In Chapter 4 we give arguments in favor of the reaction  $\gamma d \rightarrow \pi^+ nn$  as a good tool to extract the neutron-neutron scattering length  $a_{nn}$  from experimental data. The data on the reaction  $\gamma d \rightarrow \pi^+ nn$  that would allow for the extraction of  $a_{nn}$  do not exist at present; however, experiments of such kind are being actively discussed, for instance, the free-electron laser-based High Intensity Gamma ray Source (HI $\gamma$ S) [162] at TUNL is planned to be able to reach necessary energies after upgrade. We used the results of Chapter 3 to calculate the transition operator for  $\gamma d \rightarrow \pi^+ nn$ . In addition, we employed the  $NN$  wave functions evaluated in the ChPT framework in order to have a fully consistent calculation and allow for a reliable uncertainty estimate. The wave functions we used correspond to the N<sup>2</sup>LO (*i.e.* up to terms  $\mathcal{O}(\chi^2)$ ) calculations developed in Refs. [18, 34]. The object of our analysis was the five-fold differential cross-section for the reaction  $\gamma d \rightarrow \pi^+ nn$ . The results of our investigation were:

- We showed that at certain angles, at which the quasi-free pion production is suppressed, the effect of high chiral orders (NLO ( $\chi$ ), N<sup>2</sup>LO ( $\chi^2$ ),  $\chi^{5/2}$ ) on the shape of the momentum distribution of the cross-section is very marginal. At the same time a large sensitivity of the momentum spectra to the value of  $a_{nn}$  was observed;
- We showed that taking into account only the low momenta region (up to momenta about 30 MeV, cf. Fig. 4.4) when extracting the value of  $a_{nn}$  which corresponds to the region of dominating final-state neutron-neutron interaction, allows for significant reduction of the theoretical uncertainty of  $a_{nn}$ ;
- We showed that for a proper choice of kinematics and momenta region to be considered, the theoretical uncertainty  $\Delta a_{nn}$  for the extraction of  $a_{nn}$  does not exceed 0.1 fm. The estimate of uncertainty was performed very conservatively by evaluating the effect of calculated NLO and N<sup>2</sup>LO+ $\chi^{5/2}$  on the momentum spectra in the five-fold differential cross-section. This estimate, however, can be significantly improved when a consistent calculation for  $\gamma d \rightarrow \pi^+ nn$  up to N<sup>3</sup>LO is done. For instance, if we estimate the uncertainty as due only to the different wave functions due to variation of cutoffs—which should be an N<sup>3</sup>LO effect—the resulting number for  $\Delta a_{nn}$  decreases by an order of magnitude. We should stress that the systematic and reliable study of the theoretical uncertainty was possible only within our full calculation up to order  $\chi^{5/2}$  in ChPT;
- In Appendix E.2.4 we provided a simple analytic expression for the shape of the differential cross-section we consider. This expression can be used in the Monte-Carlo simulations for the analysis of possible experimental setup.

4. In Chapter 5 we presented for the first time a calculation of dispersive and absorptive corrections to the pion-deuteron scattering length  $a_{\pi d}$  using ChPT. Since  $a_{\pi d}$  is a sum of doubled isoscalar pion-nucleon scattering length  $a_+$  and few-body corrections, a precise knowledge of these latter would allow to extract  $a_+$ , which is a fundamental quantity of low-energy hadron physics, from experimental data on pion-deuteron scattering.

The dispersive and absorptive corrections to  $a_{\pi d}$  are closely related to the reactions  $NN \rightarrow NN\pi$  and  $\gamma d \rightarrow \pi NN$ . In fact, the absorptive correction, which is nothing else as imaginary part of  $a_{\pi d}$ , is related to total cross-section of these reactions via optical theorem. This means, in particular, that the modified power counting that is used in  $NN \rightarrow NN\pi$  in order to account for large momentum transfer should be used here as well. Therefore we applied the developments of Chapter 2 to calculate the hadronic corrections to  $a_{\pi d}$ , which resulted in the following:

- We showed that the power counting for dispersive and absorptive corrections based on the counting for the reaction  $NN \rightarrow NN\pi$  gives for these corrections a result of order  $\chi^{3/2}$ . Note that at order  $\chi^2$  a  $4N2\pi$  counterterm starts to contribute, therefore the limit of theoretical accuracy for  $a_{\pi d}$  is of order of  $\chi^2$ . Since the dispersive and absorptive corrections being considered contribute at order  $\chi^{3/2}$ , they have to be taken into account;
- We showed that crossed diagrams have to be taken into account along with direct ones, as explained in Section 5.2, which is necessary for consistent treatment. In particular, power counting gives the same estimate both for crossed and direct diagrams. In addition, there is a cancellation of low-momenta (lower or of order of  $m_\pi$ ) contributions between direct and crossed diagrams, which makes the momenta of order of  $\sqrt{Mm_\pi}$  to play the most prominent role—in agreement to what we have found for  $NN \rightarrow NN\pi$ ;
- We also calculated the electromagnetic part of the dispersive and absorptive corrections to  $a_{\pi d}$  stemming from the process  $\pi d \rightarrow \gamma NN \rightarrow \pi d$ —it enters at the same order as the hadronic part. Approximately 1/4 of the absorptive correction to  $a_{\pi d}$  is known to be due to the electromagnetic process;
- The numerical results we obtained for the corrections to  $a_{\pi d}$  show up the following properties (see Table 5.1 and Section 5.3):

The result for absorptive correction, *i.e.* for the imaginary part of  $a_{\pi d}$ , is in agreement with the experimental results (it is not surprising since we achieved theoretical cross-section for  $pp \rightarrow d\pi^+$  in agreement with experimental data—see Chapter 2);

Due to cancellation of individually sizable terms, the dispersive correction to  $a_{\pi d}$  is significantly smaller than it was obtained in previous works—in fact, the corresponding value is compatible with zero within our uncertainty (although this uncertainty is probably too large as explained in Section 5.5).

It should be mentioned here that our calculation differs from earlier phenomenological calculations in two very important aspects. First, along with the direct diagram that were usually included say, in Faddeev type calculations, we included

crossed diagrams. The total answer appeared to be smaller than in previous works that did not include the crossed diagrams due to the cancellation, whereas our answer for the direct contributions only agrees nicely with the results of Faddeev-type calculations. This at the same time is an indication for the convergence of the chiral expansion, since there are many more diagrams of higher chiral orders that are included in the Faddeev calculations. Second, there are double-scattering diagrams of a particular kind (the so-called *SP*-interference), where one of the  $\pi N$  rescatterings is in an *s*-wave, and the second is in a *p*-wave, as well as the so-called boost correction diagrams. We showed that the proper treatment of such diagrams should include the full momentum-dependent (non-static) nucleon propagator. At large values of momenta the momentum dependence in the propagator suppresses the quadratic growth of *p*-wave  $\pi N$  rescattering amplitude. In this case the result is well-behaved in the sense its wave function dependence is small contrary to the usual phenomenology calculations where the propagators are considered static whereas the quadratically growing *p*-wave amplitude is retained. This growth makes the full result to be proportional to the wave function at origin for the *SP*-interference terms and to the expectation value of the kinetic energy for the boost correction terms—both of which are off-shell quantities.

**5.** We developed a diagram technique for calculations of various processes in a two-baryon system based on expansion of spin operators in a series of spherical tensors. This technique incorporates in a very natural way the baryon-baryon interaction, and drastically simplifies algebraic manipulations needed in order to calculate matrix elements. The formal developments of this technique are contained in Appendices B, C. In this our work we applied this technique for  $NN$  and  $N\Delta$  systems, however, it can be straightforwardly generalized to various other two-baryon systems.

**6.** Further developments of our achievements presented in this work should include the following aspects:

- The calculation for the reaction  $NN \rightarrow NN\pi$  up to N<sup>2</sup>LO in the expansion in powers of  $\chi_\pi$  is definitely called for. There are many accurate data on various channels of this reaction, unpolarized as well as polarized. Therefore this calculation would deepen our understanding of low-energy pion and nucleon dynamics. In particular, it would be interesting to see whether all these data can be well described within ChPT framework. It should be mentioned that the number of counterterms that contribute to  $NN \rightarrow NN\pi$  at N<sup>2</sup>LO is quite low (two counterterms for *s*-wave and one for *p*-wave pion production). This calculation would be also a good starting point for studying isospin violation in  $pn \rightarrow d\pi^+$  and  $dd \rightarrow \alpha\pi^0$ ;
- A calculation for the reaction  $\gamma d \rightarrow \pi^+ nn$  up to N<sup>3</sup>LO could provide better estimate for the uncertainty of  $a_{nn}$ , if needed;
- On the basis of our calculation, a possibility to determine the value of  $E_{0+}$  from  $\gamma d \rightarrow \pi^+ nn$  could be discussed;

- Concerning the pion–deuteron scattering length issue, one should calculate contributions to  $a_{\pi d}$  that come from  $\Delta(1232)$ , taking the isobar explicitly into account. The treatment of Delta as an explicit degree of freedom is necessary since there are contributions from Delta to the  $SP$  interference and to the boost corrections that have the same properties as those stemming solely from nucleons—see Section 5.4. Hence the momentum dependence of the Delta propagator should not be neglected—in full analogy to our result for nucleons. These diagrams containing Delta together with the purely nucleonic dispersive and absorptive corrections exhaust the set of diagrams that contribute at order  $\chi^{3/2}$ . Thus, the calculation of these corrections would complete the calculation of  $a_{\pi d}$  up to  $\chi^{3/2}$ .

# Acknowledgements

Finally, I would like to say words of sincere gratitude to my colleagues and friends.

I thank Dr. Christoph Hanhart for his continuous enthusiasm for my work, and also for his support and help in various ways. I also thank Prof. Dr. Ulf-G. Meißner for the opportunity to perform this research at the Institut für Kernphysik in Jülich, for providing financial support in various travels, and also for his interest in this work. I also would like to thank them both for numerous useful comments given to this manuscript.

I am grateful to Prof. Dr. Alexander Kudryavtsev and Dr. Vadim Baru for our fruitful work and research carried out together, for their encouragement, and also for their kind hospitality at ITEP, Moscow. We are a great team and we have spent a very pleasant time working together.

I thank Dr. Johann Haidenbauer and Dr. Evgeny Epelbaum for numerous discussions that deepened my understanding of various topics in nuclear physics.

So, I deeply appreciate all my collaborators from IKP, Jülich, and ITEP, Moscow, for a very fruitful team-work that led to the results presented here, and I would like to express my desire for this work to continue.

I would like to thank Prof. Dr. Siegfried Krewald, Dr. Adreas Nogga, Dr. Alexander Sibirtsev, Prof. Dr. Nikolay Nikolaev, and other members of IKP, Jülich, for creating a very pleasant and friendly atmosphere.

I thank the participants and the lecturers of the Marie Curie Doctoral Training Programme in 2005 for the invaluable time in Trento.

I express my gratitude to Prof. Jean-Paul Blaizot and the members of ECT\*, Trento, for their hospitality during this Programme.

I thank organizers and participants of the WE-Heraeus seminars, ECT\* workshop, MESON and HadronTH workshops, and ECT\* seminar, for the opportunities to actively participate in the life of physicists' community and for fruitful and interesting discussions.

I would like to thank Ashot, Fedor, Ilya, Alexander, Nikita, Ivan, ... all my numerous friends in different parts of the world for their friendship and support.

Finally, I thank my family for their patience, help and encouragement during this work.

I say "thank you" to Svetlana.

# Appendix A

## Lagrangian Densities

In this appendix we present the Lagrangian densities that are relevant for our calculations, as well as the corresponding vertices and propagators.

### The reaction $NN \rightarrow NN\pi$ and corrections to $a_{\pi d}$

The appropriate Lagrangian density, constructed to be consistent with the symmetries of the underlying more fundamental theory (in this case QCD) and ordered according to a particular counting scheme, is the starting point for our research. Omitting terms that do not contribute to the order we consider here, we therefore have for the relevant terms of the leading and next-to-leading order Lagrangian in sigma gauge for the pion field [14, 15]

$$\begin{aligned} \mathcal{L} = & \frac{1}{2}(\partial_\mu \boldsymbol{\pi})^2 - \frac{1}{2}m_\pi^2 \boldsymbol{\pi}^2 + \frac{1}{6f_\pi^2} [(\boldsymbol{\pi} \cdot \partial_\mu \boldsymbol{\pi})^2 - \boldsymbol{\pi}^2 (\partial^\mu \boldsymbol{\pi})^2] \\ & + N^\dagger [i\partial_0 - \frac{1}{4f_\pi^2} \boldsymbol{\tau} \cdot (\boldsymbol{\pi} \times \dot{\boldsymbol{\pi}})] N + \frac{g_A}{2f_\pi} N^\dagger \boldsymbol{\tau} \cdot \vec{\sigma} \cdot \left( \vec{\nabla} \boldsymbol{\pi} + \frac{1}{2f_\pi^2} \boldsymbol{\pi} (\boldsymbol{\pi} \cdot \vec{\nabla} \boldsymbol{\pi}) \right) N \\ & + \Psi_\Delta^\dagger [i\partial_0 - \delta] \Psi_\Delta + \frac{h_A}{2f_\pi} [N^\dagger (\mathbf{T} \cdot \vec{S} \cdot \vec{\nabla} \boldsymbol{\pi}) \Psi_\Delta + \text{h.c.}] + \dots \end{aligned} \quad (\text{A.1})$$

$$\begin{aligned} & + \frac{1}{2M} N^\dagger \vec{\nabla}^2 N + \frac{1}{2M_\Delta} \Psi_\Delta^\dagger \vec{\nabla}^2 \Psi_\Delta + \frac{1}{8Mf_\pi^2} (iN^\dagger \boldsymbol{\tau} \cdot (\boldsymbol{\pi} \times \vec{\nabla} \boldsymbol{\pi}) \cdot \vec{\nabla} N + \text{h.c.}) \\ & - \frac{g_A}{4Mf_\pi} [iN^\dagger \boldsymbol{\tau} \cdot \dot{\boldsymbol{\pi}} \vec{\sigma} \cdot \vec{\nabla} N + \text{h.c.}] - \frac{h_A}{2M_\Delta f_\pi} [iN^\dagger \mathbf{T} \cdot \dot{\boldsymbol{\pi}} \vec{S} \cdot \vec{\nabla} \Psi_\Delta + \text{h.c.}] , \end{aligned} \quad (\text{A.2})$$

where  $f_\pi$  denotes the pion decay constant in the chiral limit,  $g_A$  is the axial-vector coupling of the nucleon,  $h_A$  is the  $\Delta N\pi$  coupling,  $\delta = M_\Delta - M$  is the Delta-nucleon mass difference, and  $\vec{S}$  and  $\mathbf{T}$  are the transition spin and isospin matrices; explicit form of this matrices is given below in this appendix. The dots symbolize that what is shown are only those terms that are relevant for the calculations of the reactions  $NN \rightarrow NN\pi$  and dispersive and absorptive corrections to  $a_{\pi d}$ . As demanded by the heavy baryon formalism, the baryon fields  $N$  and  $\Psi_\Delta$  are the velocity-projected pieces of the corresponding relativistic fields, *e.g.*  $N = 1/2(1+\not{v})\psi$ , where  $v^\mu = (1, 0, 0, 0)$  denotes the nucleon 4-velocity. The corresponding vertex functions that do not contain Deltas can be read off directly from Appendix A of Ref. [11]. Note, however, that we



use different normalizations of spinors, namely  $\chi^\dagger\chi = 1$ , which results in additional factors of  $2M$  ( $2\sqrt{MM_\Delta}$ ) in each nucleon vertex and  $1/2M$  in the nucleon propagators, compared to Ref. [11]. Note also that we keep the baryon kinetic term in the propagator if the diagram we are considering is reducible—see the corresponding discussions in Chapter 2. For the sake of completeness we give below explicit expressions for the vertex functions that contain Delta and Delta propagators. The notations are:  $\varepsilon$  ( $\vec{p}$ ) is the energy (momentum) of Delta, and  $\omega$  ( $\vec{q}$ ) is the energy (momentum) of the outgoing pion.

$\Delta$  propagator

$$\frac{i}{2M(\varepsilon - \delta) - p^2 + i\gamma}.$$

$N\Delta\pi$  vertex

$$-\frac{h_A\sqrt{MM_\Delta}}{F}\mathbf{T}^a(\vec{S} \cdot \vec{q}) + \frac{h_A\omega}{F}\sqrt{\frac{M}{M_\Delta}}\mathbf{T}^a(\vec{S} \cdot \vec{p}).$$

The matrices  $S_i$  have the following form:

$$S_1 = \begin{pmatrix} -\frac{1}{\sqrt{2}} & 0 & \frac{1}{\sqrt{6}} & 0 \\ 0 & -\frac{1}{\sqrt{6}} & 0 & \frac{1}{\sqrt{2}} \end{pmatrix}, \quad S_2 = \begin{pmatrix} -\frac{i}{\sqrt{2}} & 0 & -\frac{i}{\sqrt{6}} & 0 \\ 0 & -\frac{i}{\sqrt{6}} & 0 & -\frac{i}{\sqrt{2}} \end{pmatrix}, \quad S_3 = \begin{pmatrix} 0 & \sqrt{\frac{2}{3}} & 0 & 0 \\ 0 & 0 & \sqrt{\frac{2}{3}} & 0 \end{pmatrix}, \quad (\text{A.3})$$

and the same form for  $T_i$ . The matrices  $\vec{S}$  and  $\mathbf{T}$  are normalized such that

$$S_i S_j^\dagger = \frac{1}{3}(2\delta_{ij} - i\epsilon_{ijk}\sigma_k), \quad T_i T_j^\dagger = \frac{1}{3}(2\delta_{ij} - i\epsilon_{ijk}\tau_k). \quad (\text{A.4})$$

They have the following properties:

$$\epsilon_{ijk}\sigma_i S_j = -i S_k; \quad \epsilon_{ijk} S_j^\dagger \sigma_i = -i S_k^\dagger; \quad (\text{A.5})$$

$$\sigma_i S_i = 0; \quad S_i^\dagger \sigma_i = 0. \quad (\text{A.6})$$

### The reaction $\gamma d \rightarrow \pi^+ nn$ and electromagnetic correction to $a_{\pi d}$

The Lagrangian density relevant for the reaction  $\gamma d \rightarrow \pi^+ nn$  is obtained by gauging the pion gradient term, nucleon gradient term and pion-nucleon axial coupling, and adding the interaction of electromagnetic field strength with anomalous magnetic moment of the nucleon. The expression for the resulting Lagrangian density reads:

$$\begin{aligned} \mathcal{L}_{\gamma\pi N} = & -\frac{eg_A}{2f_\pi}\epsilon_{ab3}\pi_a N^\dagger(\vec{\sigma} \cdot \vec{A})\tau_b N \\ & -\frac{e}{4M}\left(i N^\dagger(\vec{\sigma} \cdot \vec{A})(\vec{\sigma} \cdot \vec{\nabla})(1 + \tau_3)N + \text{h.c.}\right) - \frac{e}{2}(1 + \tau_3)A_0 \\ & + \frac{e}{4M}N^\dagger[\vec{\nabla} \times \vec{A}] \cdot \vec{\sigma} [\kappa_p(1 + \tau_3) + \kappa_n(1 - \tau_3)]N \\ & + \frac{1}{2}e\epsilon_{ab3}A^\mu(\pi_a\partial_\mu\pi_b - \pi_b\partial_\mu\pi_a), \end{aligned} \quad (\text{A.7})$$

where  $A^\mu = (A_0, \vec{A})$  is the vector potential of electromagnetic field,  $e$  is the electric charge of proton,  $\kappa_p = 1.79$  and  $\kappa_n = -1.93$  are proton and neutron anomalous magnetic moments, respectively. The first line of this equation—the so-called Kroll-Ruderman term [113]—corresponds to the  $\gamma\pi NN$  vertex, and the third line describes the electromagnetic interaction of nucleon's anomalous magnetic momenta. We neglected the terms of higher orders in  $1/M$  as well as in  $e$ . These expressions for  $\mathcal{L}_{\gamma\pi N}$  are written in the Coulomb gauge  $\vec{\nabla} \cdot \vec{A} = 0$ . The corresponding vertices are also given in Appendix A of Ref. [11]. Notice that we do not consider analogous interactions of pions and photons with Delta since they are of higher orders in our expansion—cf. Chapter 3.

The terms relevant for the calculation of the photonic part of the dispersive and absorptive corrections to  $a_{\pi d}$  are given by the first and the last lines of this equation.

# Appendix B

## Diagram Technique

In this appendix we provide the rules of diagram technique we use for evaluation of amplitudes. The technique we use is based on ideas formulated in Refs. [82, 108]. This technique appeared to be very useful in calculations of different reactions in two-baryon system where the initial or final pair of nucleons is in a state with certain values of total angular momentum, orbital angular momentum, and total spin, *i.e.* in a certain *JLS* state. The main feature of this technique is that it embeds the natural description of the *NN* interaction in terms of *JLS* matrix elements of the *NN* *T*-matrix.

### B.1 Application of projectors to *NN* system

#### B.1.1 Projector expansion of the *NN* *T*-matrix

To derive the diagram technique, we will assume that the nucleons are treated non-relativistically—this assumption is natural when describing low-energy *NN* interactions. The matrix elements of the *NN* *T* matrix between the states with given momenta  $\vec{p}, \vec{p}'$  and projections of spins of initial and final nucleons  $\lambda_{1,2}, \lambda_{1',2'}$  (we suppress the energy dependence of *T* for shortness) can be written in the following form:

$$\langle \vec{p}' \lambda_{1'} \lambda_{2'} | T | \lambda_1 \lambda_2 \vec{p} \rangle = \sum_{ij} \chi_{1'}^\dagger \hat{O}_i \chi_1 T_{ij}(\vec{p}, \vec{p}') \chi_{2'}^\dagger \hat{O}_j \chi_2, \quad (\text{B.1})$$

where  $\chi$  with corresponding indices stand for nucleon spinors,  $\hat{O}_i$ ,  $i = 0, 1, 2, 3$  are four  $2 \times 2$  matrices that make the basis in the linear space of  $2 \times 2$  matrices, and  $T_{ij}(\vec{p}, \vec{p}')$  are functions of initial and final momenta. We choose  $\hat{O}_0 = 1/\sqrt{2}$ ,  $\hat{O}_i = \sigma_i/\sqrt{2}$ ,  $i = 1, 2, 3$ , where 1 stands for  $2 \times 2$  unit matrix and  $\sigma_i$  for Pauli matrices. The form of matrix elements as in Eq. (B.1) is automatically obtained from (time-ordered) expansion of *S*-matrix and subsequent solution of the Lippmann-Schwinger equation (which is needed to sum up all reducible graphs). The expansion for the matrix element given by Eq. (B.1) is schematically shown in Fig. B.1.1. The expressions like  $\chi_{\lambda'}^\dagger \hat{O} \chi_\lambda$  correspond to nucleonic lines going through the diagram. In order to proceed let us apply to the matrix elements in Eq. (B.1) the Fierz transformation as follows:

$$\chi_{1'}^\dagger \hat{O}_i \chi_1 \chi_{2'}^\dagger \hat{O}_j \chi_2 = \sum_{kl} C_{ijkl} \chi_{1'}^\dagger \hat{O}_k \chi_{2'}^c \chi_2^{c\dagger} \hat{O}_l \chi_1, \quad (\text{B.2})$$

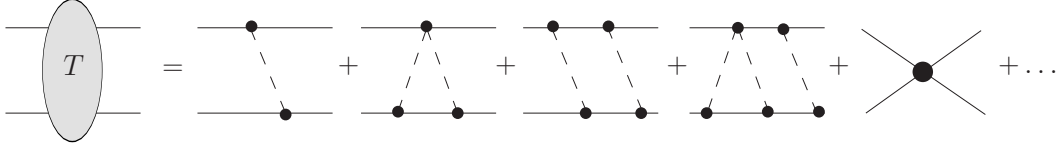


Figure B.1: Series of the diagrams corresponding to the  $NN$   $T$  matrix. Solid lined denote nucleons, dashed lines denote mesons (pions *etc.*), black circles stand for various vertices.

with  $\chi^c = \sigma_2 \chi^*$  being the charge conjugated spinors. The transformation coefficients  $C_{ijkl}$  are given by

$$C_{ijkl} = -\text{Tr} \left( \hat{O}_i \hat{O}_l \hat{O}_j^c \hat{O}_k \right), \quad (\text{B.3})$$

where  $\hat{O}_j^c = -\sigma_2 \hat{O}_j^t \sigma_2$  is a charge conjugated matrix ( $\hat{O}_j^t$  stands for transposed matrix). Using Eq. (B.2) we can rewrite the expression for matrix elements of the  $NN$   $T$  matrix as

$$\begin{aligned} \langle \vec{p}' \lambda'_1 \lambda'_2 | T | \lambda_1 \lambda_2 \vec{p} \rangle &= \sum_{kl} \chi_{1'}^\dagger \hat{O}_k \chi_{2'}^c \tilde{T}_{kl}(\vec{p}, \vec{p}') \chi_2^{c\dagger} \hat{O}_l \chi_1, \\ \tilde{T}_{kl}(\vec{p}, \vec{p}') &= \sum_{ij} C_{ijkl} T_{ij}(\vec{p}, \vec{p}'). \end{aligned} \quad (\text{B.4})$$

Using the technique of projectors developed in Appendix C, we can write down the following expansion of  $\langle \vec{p}' \lambda'_1 \lambda'_2 | T | \lambda_1 \lambda_2 \vec{p} \rangle$ :

$$\langle \vec{p}' \lambda'_1 \lambda'_2 | T | \lambda_1 \lambda_2 \vec{p} \rangle = \sum_{JLSL'S'} \frac{1}{4\pi} \chi_2^{c\dagger} \mathcal{P}_{ij\dots m}^{JLS}(\vec{n}) \chi_1 T_{L'S'}^{JLS}(p, p') \chi_{1'}^\dagger \mathcal{P}_{ij\dots m}^{JL'S'}(\vec{n}')^\dagger \chi_{2'}^c, \quad (\text{B.5})$$

where  $\vec{n} = \vec{p}/p$ ,  $\vec{n}' = \vec{p}'/p'$ , and  $T_{L'S'}^{JLS}(p, p')$  are defined by

$$T_{L'S'}^{JLS}(p, p') = \frac{4\pi}{2J+1} \sum_{kl} \int \frac{d\Omega_{\vec{n}}}{4\pi} \frac{d\Omega_{\vec{n}'}}{4\pi} \tilde{T}_{kl}(\vec{p}, \vec{p}') \text{Tr} \left( \mathcal{P}_{ij\dots m}^{JLS}(\vec{n})^\dagger \hat{O}_l \right) \text{Tr} \left( \mathcal{P}_{ij\dots m}^{JL'S'}(\vec{n}') \hat{O}_k \right). \quad (\text{B.6})$$

We will now justify the expansion of Eq. (B.5) and show that

$$T_{L'S'}^{JLS}(p, p') = \langle JLS' | T | JLS \rangle, \quad (\text{B.7})$$

*i.e.*  $T_{L'S'}^{JLS}(p, p')$  is nothing else but the matrix element of the  $NN$   $T$  matrix in the  $JLS$  basis, the relation of which to the on-shell phase shifts is given in Ref. [5]. We will give here this relation only for the uncoupled partial waves, for which it reads

$$T_{LS}^{JLS}(p, p) = -\frac{2}{\pi p M} \sin \delta_{JLS} e^{i\delta_{JLS}}. \quad (\text{B.8})$$

Let us establish the expansion. Consider a single term that enters the sum in the first line of Eq. (B.4). We can rewrite it, using Eq. (C.30), in the following form:

$$\begin{aligned} \chi_{1'}^\dagger \hat{O}_k \chi_{2'}^c \tilde{T}_{kl}(\vec{p}, \vec{p}') \chi_2^{c\dagger} \hat{O}_l \chi_1 &= \\ &= \chi_{1'}^\dagger \hat{O}_k \chi_{2'}^c \sum_{JLS} \chi_2^{c\dagger} \mathcal{P}_{ij\dots m}^{JLS}(\vec{n}) \chi_1 \int \frac{d\Omega_{\vec{n}}}{4\pi} \text{Tr} \left( \mathcal{P}_{ij\dots m}^{JLS}(\vec{n})^\dagger \hat{O}_l \right) \tilde{T}_{kl}(\vec{p}, \vec{p}'), \end{aligned}$$

where we applied projector expansion separately to the matrix  $F(\vec{n}) = \hat{O}_l \tilde{T}_{kl}(\vec{p}, \vec{p}')$ . Applying the expansion in hermitian conjugate projectors (which means to replace in Eq. (C.30)  $\mathcal{P}^{JLS}$  by  $\mathcal{P}^{JLS^\dagger}$  and vice versa) to the matrix  $\tilde{F}(\vec{n}') = \hat{O}_k \int d\Omega_{\vec{n}} \tilde{T}_{kl}(\vec{p}, \vec{p}')/(4\pi)$ , we get

$$\begin{aligned} & \chi_{1'}^\dagger \hat{O}_k \chi_{2'}^c \tilde{T}_{kl}(\vec{p}, \vec{p}') \chi_{2'}^{c\dagger} \hat{O}_l \chi_1 = \\ & = \sum_{J'L'S'} \sum_{JLS} \chi_{2'}^{c\dagger} \mathcal{P}_{ij\dots m}^{JLS}(\vec{n}) \chi_1 \chi_{1'}^\dagger \mathcal{P}_{i'j'\dots m'}^{J'L'S'}(\vec{n}') \chi_{2'}^c \\ & \quad \times \int \frac{d\Omega_{\vec{n}}}{4\pi} \frac{d\Omega_{\vec{n}'}}{4\pi} \text{Tr} \left( \mathcal{P}_{ij\dots m}^{JLS}(\vec{n})^\dagger \hat{O}_l \right) \tilde{T}_{kl}(\vec{p}, \vec{p}') \text{Tr} \left( \mathcal{P}_{i'j'\dots m'}^{J'L'S'}(\vec{n}') \hat{O}_k \right). \end{aligned}$$

The expansion of the remainder in the hermitian conjugate projectors is dictated by convenience as will be discussed below in this appendix—see the section on inclusion of the Delta isobar. Since the matrix elements should be scalars with respect to  $SO(3)$ , all tensor indices have to be contracted after the integration over the angles is performed. From the other hand, the integral over the two solid angles in this equation can have the only possible tensor structure that is compatible with symmetries of projectors and that leads to a scalar expression, namely

$$\frac{2\delta_{JJ'}}{J^2 - J + 2} (\delta_{ii'} \delta_{jj'} \dots \delta_{mm'} + \delta_{ji'} \delta_{ij'} \dots \delta_{mm'} + \text{further permutations} - \text{trace}),$$

where permutations are needed to symmetrize the expression with respect to all non-hatched and hatched indices and trace has to be subtracted since the tensors  $\mathcal{P}^{JLS}$  are traceless. This structure arises due to the facts that the integrand depends only on vectors  $\vec{n}$  and  $\vec{n}'$ , and the projectors are symmetric with respect to their indices and give zero when any two indices of a projector are contracted with each other. The factor  $2/(J^2 - J + 2)$  accounts for the number of permutations. We also see that the total angular momentum is conserved.

Inserting this tensor structure into the expansion we consider and summing the result over  $k$  and  $l$ , we finally get the expansion for matrix elements of the  $NN$   $T$  matrix given by Eqs. (B.5), (B.6).

We will now turn to Equation (B.7). Let us prove this equation for  $S = S' = 1$ ; the proof for all other values of  $S$  and  $S'$  is completely analogous. Firstly we rewrite Eq. (B.6) in the following form:

$$\begin{aligned} T_{L'1}^{JL1}(p, p') &= \frac{4\pi}{2J+1} \sum_{\lambda_1 \lambda_2 \lambda_{1'} \lambda_{2'}} \sum_{kl} \int \frac{d\Omega_{\vec{n}}}{4\pi} \frac{d\Omega_{\vec{n}'}}{4\pi} \tilde{T}_{kl}(\vec{p}, \vec{p}') \left( \chi_{1'}^\dagger \mathcal{P}_{ij\dots m}^{JL1}(\vec{n})^\dagger \chi_{2'}^c \chi_{2'}^{c\dagger} \hat{O}_l \chi_1 \right) \\ & \quad \times \left( \chi_{2'}^{c\dagger} \mathcal{P}_{ij\dots m}^{JL'1}(\vec{n}') \chi_{1'} \chi_{1'}^\dagger \hat{O}_k \chi_{2'}^c \right). \end{aligned}$$

Making use of Eqs. (C.10), (C.26), we get

$$\begin{aligned} T_{L'1}^{JL1}(p, p') &= \frac{4\pi}{2J+1} \sum_{\lambda_1 \lambda_2 \lambda_{1'} \lambda_{2'}} \sum_{kl} \sum_{J_z} \int \frac{d\Omega_{\vec{n}}}{\sqrt{4\pi}} \frac{d\Omega_{\vec{n}'}}{\sqrt{4\pi}} \tilde{T}_{kl}(\vec{p}, \vec{p}') \left( \chi_{1'}^\dagger \Psi_{JL1J_z}^\dagger(\vec{n}) \chi_{2'}^c \chi_{2'}^{c\dagger} \hat{O}_l \chi_1 \right) \\ & \quad \times \left( \chi_{2'}^{c\dagger} \Psi_{JL'1J_z}(\vec{n}') \chi_{1'} \chi_{1'}^\dagger \hat{O}_k \chi_{2'}^c \right), \end{aligned}$$

where

$$\Psi_{JL_1J_z}(\vec{n}) = \sum_{Mm} C_{LM_1m}^{JJ_z} Y_{LM}(\vec{n}) \mathcal{S}_m$$

with  $\mathcal{S}_{\pm 1} = (\sigma_1 \mp i\sigma_2)/2$ ,  $\mathcal{S}_0 = \sigma_3/\sqrt{2}$  being the linear combinations of the basis spin operators  $\sigma_i/\sqrt{2}$ , and analogously for  $\Psi_{JL'_1J_z}(\vec{n}')$ . These linear combinations  $\mathcal{S}_m$  transform as vectors having certain polarizations  $m$  along  $z$  axis (cf. Eq. (C.22)). Here  $C_{LM_1m}^{JJ_z}$  are the Clebsch-Gordan coefficients. Using now the fact that

$$\chi_1^\dagger \mathcal{S}_m^\dagger \chi_2^c = i C_{\frac{1}{2}\lambda_1 \frac{1}{2}\lambda_2}^{1m}, \quad (\text{B.9})$$

we obtain for  $T_{L'_1}^{JL_1}(p, p')$ , recalling the definition of Eq. (B.4):

$$\begin{aligned} T_{L'_1}^{JL_1}(p, p') &= \frac{4\pi}{2J+1} \sum_{\lambda_1\lambda_2\lambda_1'\lambda_2'} \sum_{kl} \sum_{MmM'm'} \sum_{J_z} \int \frac{d\Omega_{\vec{n}}}{\sqrt{4\pi}} \frac{d\Omega_{\vec{n}'}}{\sqrt{4\pi}} \tilde{T}_{kl}(\vec{p}, \vec{p}') \chi_1^\dagger \hat{O}_k \chi_2^c \chi_2^{c\dagger} \hat{O}_l \chi_1 \\ &\quad \times C_{\frac{1}{2}\lambda_1 \frac{1}{2}\lambda_2}^{1m} C_{\frac{1}{2}\lambda_1' \frac{1}{2}\lambda_2'}^{1m'} C_{LM_1m}^{JJ_z} C_{L'M'_1m'}^{JJ_z} Y_{LM}^*(\vec{n}) Y_{L'M'}(\vec{n}') \\ &= \frac{4\pi}{2J+1} \sum_{\lambda_1\lambda_2\lambda_1'\lambda_2'} \sum_{J_z} \sum_{MmM'm'} C_{\frac{1}{2}\lambda_1 \frac{1}{2}\lambda_2}^{1m} C_{\frac{1}{2}\lambda_1' \frac{1}{2}\lambda_2'}^{1m'} C_{LM_1m}^{JJ_z} C_{L'M'_1m'}^{JJ_z} \\ &\quad \times \int \frac{d\Omega_{\vec{n}}}{\sqrt{4\pi}} \frac{d\Omega_{\vec{n}'}}{\sqrt{4\pi}} \langle L'M' | \vec{n}' \rangle \langle \vec{p}' \lambda_1' \lambda_2' | T | \vec{p} \lambda_1 \lambda_2 \rangle \langle \vec{n} | LM \rangle; \end{aligned}$$

since  $\int d\Omega_{\vec{n}} |\vec{p}\rangle \langle \vec{n} | LM \rangle = |p, LM\rangle$ , we have after summation of Clebsch-Gordan coefficients:

$$T_{L'_1}^{JL_1}(p, p') = \frac{1}{(2J+1)} \sum_{J_z} \langle JL'_1 J_z p' | T | JL_1 J_z p \rangle = \langle JL'_1 | T | JL_1 \rangle,$$

where we used the fact that the matrix elements do not depend on  $J_z$ . The proof is thus completed. As we mentioned before, the proof for other possible values of  $S$  and  $S'$  is completely analogous. The only thing that is remaining to be shown is that the normalization of  $T_{L'_1}^{JL_1}(p, p')$  corresponds to that of Ref. [5]. In order to do this, one has to perform Fierz transformation of the Lippmann-Schwinger equation for  $T$  which reads

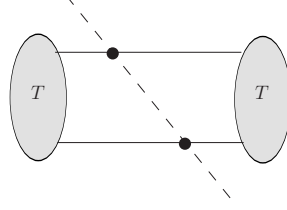
$$\langle \vec{p} \lambda_1 \lambda_2 | T | \vec{p}' \lambda_1' \lambda_2' \rangle = \langle \vec{p} \lambda_1 \lambda_2 | V | \vec{p}' \lambda_1' \lambda_2' \rangle + \sum_{\lambda_3, \lambda_4} \int d^3q \frac{\langle \vec{p} \lambda_1 \lambda_2 | V | \vec{q} \lambda_3 \lambda_4 \rangle \langle \vec{q} \lambda_3 \lambda_4 | T | \vec{p}' \lambda_1' \lambda_2' \rangle}{E - q^2/M + i\gamma},$$

and show that the projected equation coincides with the corresponding equation used in Ref. [5].

Note that all formalism applied in this section to spin-angular matrix elements of  $NN$   $T$  matrix is applied to its isospin part without significant changes. In particular, one has to apply Fierz transformation analogous to Eq. (B.2) also to isospinors.

### B.1.2 Projector expansion of matrix elements

Now we are going to proceed and write an expansion for matrix elements for various processes in the  $NN$  system. In doing so we will use the hybrid approach, that is

Figure B.2: Typical diagram for  $\pi NN$  rescattering.

the matrix elements are obtained as a result of convolution of the transition operator with  $NN$   $T$  matrix. We suppose the transition operator to be obtained from some appropriate Lagrangian density. A typical diagram representing pion rescattering is shown in Fig. B.2. The matrix element corresponding to this diagram can be written as

$$M_{fi} = \sum_{\lambda_3 \lambda_4} \sum_{\lambda_5 \lambda_6} \int \frac{d^3 q}{(2\pi)^3} \frac{d^3 \ell}{(2\pi)^3} \frac{\langle \vec{p} \lambda_1 \lambda_2 | T | \lambda_3 \lambda_4 \vec{q} \rangle \langle \vec{q} \lambda_3 \lambda_4 | A | \lambda_5 \lambda_6 \vec{\ell} \rangle \langle \vec{\ell} \lambda_5 \lambda_6 | T | \lambda_1' \lambda_2' \vec{p}' \rangle}{q^2 - k^2 - i\gamma}, \quad (\text{B.10})$$

where  $A$  is the transition operator. The overall normalization of this matrix element is not important for us now—we will establish all normalizations later.

Expanding the matrix elements of  $T$  as given by Eq. (B.5) and recalling that the matrix elements of  $A$  obtained from the Lagrangian have the form

$$\langle \vec{q} \lambda_3 \lambda_4 | A | \lambda_5 \lambda_6 \vec{\ell} \rangle = \chi_5^\dagger \hat{A}_1(\vec{q}, \vec{\ell}) \chi_3 \chi_6^\dagger \hat{A}_2(\vec{q}, \vec{\ell}) \chi_4,$$

where  $A_{1,2}$  are elementary vertices that describe the meson-nucleon interaction, we get the following expression for the matrix element  $M_{fi}$ :

$$\begin{aligned} M_{fi} = & \sum_{\{JLS\}} \sum_{\lambda_3 \lambda_4} \sum_{\lambda_5 \lambda_6} \int \frac{d^3 q}{(2\pi)^3} \frac{d^3 \ell}{(2\pi)^3} \frac{\chi_5^\dagger \hat{A}_1(\vec{q}, \vec{\ell}) \chi_3 \chi_6^\dagger \hat{A}_2(\vec{q}, \vec{\ell}) \chi_4}{q^2 - k^2 - i\gamma} \\ & \times \chi_2^{c\dagger} \mathcal{P}_{ij\dots m}^{JLS}(\vec{n}) \chi_1 T_{L'S'}^{JLS}(p, q) \chi_3^\dagger \mathcal{P}_{ij\dots m}^{JL'S'}(\vec{n}_q)^\dagger \chi_4^c \\ & \times \chi_6^{c\dagger} \mathcal{P}_{i'j'\dots m'}^{J'L''S''}(\vec{n}_\ell) \chi_5 T_{L''S''}^{J'L''S''}(\ell, p') \chi_{1'}^\dagger \mathcal{P}_{i'j'\dots m'}^{J'L''S''}(\vec{n}')^\dagger \chi_{2'}^c, \end{aligned} \quad (\text{B.11})$$

where  $\{JLS\}$  denotes the whole set of spins and angular momenta, and  $\vec{n}$ 's stand for the corresponding unit vectors. Notice the appearance of  $\chi$ 's in this equation. Recalling now the definition for charged conjugate spinors and summing over polarizations, we obtain

$$\begin{aligned} M_{fi} = & - \sum_{\{JLS\}} \chi_2^{c\dagger} \mathcal{P}_{ij\dots m}^{JLS}(\vec{n}) \chi_1 \chi_{1'}^\dagger \mathcal{P}_{i'j'\dots m'}^{J'L''S''}(\vec{n}')^\dagger \chi_{2'}^c \\ & \times \int \frac{d^3 q}{(2\pi)^3} \frac{d^3 \ell}{(2\pi)^3} \text{Tr} \left( \mathcal{P}_{i'j'\dots m'}^{J'L''S''}(\vec{n}_\ell) \hat{A}_1(\vec{q}, \vec{\ell}) \mathcal{P}_{ij\dots m}^{JL'S'}(\vec{n}_q)^\dagger \hat{A}_2^c(\vec{q}, \vec{\ell}) \right) \\ & \times \frac{T_{L'S'}^{JLS}(p, q) T_{L''S''}^{J'L''S''}(\ell, p')}{q^2 - k^2 - i\gamma}, \end{aligned} \quad (\text{B.12})$$

where  $\hat{A}^c$  stands for charge conjugated operator. Analogous expression holds for isospin part of this matrix elements.

Using the developments presented in this appendix, this formula is straightforwardly generalized in the form of the following set of rules:

1. When there is a convolution with  $NN$  interaction vertices, we expand the  $NN$   $T$  matrix in series of spin-angular and isospin projectors;
2. Due to the Fierz transformation that makes use of charge conjugated spinors, one of the two nucleon lines becomes charge conjugated, *i.e.* the product of one-nucleon operators that describe interaction of one of the nucleons with other particles should be charge conjugated;
3. The sum over polarizations of intermediate nucleons turns into a trace over the product of all one-nucleon operators from usual nucleon line times one projector times the charge conjugated product of one-nucleon operators of charge conjugated nucleon line times second projector hermitian conjugated—the spin-isospin loop;
4. The external nucleon spinors and isospinors are contracted with external projectors, spinors and isospinors of one nucleon in each pair of either incoming or outgoing nucleons become charge conjugated;
5. If there is only one  $NN$  interaction vertex corresponding either to the initial or to the final state interaction, the statements given above should be changed: in this case there is no trace over the spin and isospin loop. All other statements hold without changes.

The inclusion of Delta isobar into these rules is straightforward. We restrict ourselves to  $N\Delta$  system, since we do not consider  $\Delta\Delta$  states. The matrix elements of  $N\Delta$   $T$  matrix are expanded in series of  $N\Delta$  projectors defined in Appendix C. The development of the analog of Eqs.(B.5)–(B.7) for the  $N\Delta$  system proceeds just as for the  $NN$  system. The corresponding Fierz transformation is also completely analogous to that for the  $NN$  system, however is more tedious because of more complicated spin structure of  $N\Delta$  system. In this case it is convenient to apply Fierz transformation to the corresponding matrix elements in such a way that only nucleon spinors and isospinors get charge conjugated. This saves from dealing with charge conjugated matrices  $S_i$  that couple  $N$  and  $\Delta$ . In other words, this means that if we have  $N\Delta$  interaction vertices being convoluted with some transition operator, we always choose the Delta fermion line to be not conjugated.

This choice corresponds to the expansion of the  $T$  matrix partially in hermitian conjugate projectors. These hermitian conjugate projectors contain information about the spin-angular properties of the final two-baryon system. The projectors defined in Appendix C are constructed in such a way that after expansion the projectors that correspond to final Delta have to be multiplied by hermitian conjugated Delta spinors  $\chi_\Delta^\dagger$  rather than by charge conjugated  $\chi_\Delta^c$ .

## B.2 Rules of the diagram technique

Now we are at the position to formulate the rules of diagram technique. We start from usual Feynman rules and perform non-relativistic expansion of nucleon and Delta



vertices and propagators. These rules are supplemented by the projector expansion of  $NN$  and  $N\Delta$  interaction as discussed above in this appendix.

We work with  $NN$  and  $N\Delta$  matrices  $\mathcal{M}$  which are related to  $T$  via

$$\mathcal{M} = -8\pi^2 \sqrt{\varepsilon_1 \varepsilon_2 \varepsilon_3 \varepsilon_4} T,$$

rather than directly with  $T$  matrix. Here,  $\varepsilon_i$  is the energy of  $i$ -th particle. In the non-relativistic case which we are considering the energies equal to masses and this relation transforms into

$$\mathcal{M} = -8\pi^2 \sqrt{M_1 M_2 M_3 M_4} T. \quad (\text{B.13})$$

However, this relation between  $\mathcal{M}$  and  $T$  is valid only for on-shell particles. The relation between these two operators off-shell is not fixed, although one could extrapolate the energies by the usual formula  $\varepsilon = \sqrt{p^2 + M^2}$ , or use the fourth component of the four-momentum, and so on. The only requirement for the recipe how to connect  $\mathcal{M}$  and  $T$  off-shell is that the on-shell relation should remain. In this respect this relation between  $\mathcal{M}$  and  $T$  is something formalism-dependent. We will use for our non-relativistic treatment of baryons the non-relativistic relation between  $\mathcal{M}$  and  $T$  given by Eq. (B.13).

We modify the usual Feynman rules only in their part that deals with nucleons (and Deltas). The rules that account for pions, photons *etc.* remain unchanged. Therefore we provide here only the changed rules for nucleons, Deltas, and their interactions amongst themselves and with bosons:

1. *a)* One of the nucleon lines (free or containing  $N$  interaction with bosons) incoming into and one going out from a diagram should be made charge-conjugated (CC). The choice of charge conjugated lines should be the same for all diagrams contributing to a given process. This rule originates from Fierz transformation of the full transition amplitude. This amplitude is the sum of all diagrams with identical external nucleon legs. Therefore Fierz transformation makes one of the incoming and one of the outgoing nucleon lines charge conjugated and also fixes the choice of the charge conjugated external nucleon lines simultaneously for all diagrams that contribute to this particular process;
- b)* One in the each pair of internal nucleon lines, *i.e.* of the pair of nucleon lines that connect two neighbouring  $NN$  interaction vertices, should be made charge-conjugated. In this case the choice is arbitrary since we sum over all internal spin and isospin states;
- c)* In case there are  $N\Delta$  states, only nucleon lines should be chosen as charge conjugated. This is always possible since we consider only  $NN$  and  $N\Delta$  states;
2. *a)* An external incoming nucleon leg (CC nucleon leg) corresponds to spinor  $\chi$  (hermitian conjugate CC spinor  $(\chi^c)^\dagger$ ) and isospinor  $\varphi$  (hermitian conjugate CC isospinor  $(\varphi^c)^\dagger$ );
- b)* An external outgoing nucleon leg (CC nucleon leg) corresponds to hermitian conjugated nucleon spinor  $\chi^\dagger$  (CC spinor  $\chi^c$ ) and hermitian conjugated isospinor  $\varphi^\dagger$  (CC isospinor  $\varphi^c$ );

c) An external incoming (outgoing) Delta leg corresponds to Delta spinor  $\chi_\Delta$  (hermitian conjugate Delta spinor  $\chi_\Delta^\dagger$ ) and isospinor  $\varphi_\Delta$  (hermitian conjugate isospinor  $\varphi_\Delta^\dagger$ );

3. An  $NN \rightarrow NN$  vertex corresponds to a factor

$$i\mathcal{M}_{NN}(\vec{p}, \vec{p}', E) = \sum_{TT'} \mathcal{I}_\alpha^T \mathcal{I}_\alpha^{T'\dagger} \sum_{JLSL'S'} \mathcal{P}_{ij\dots k}^{JLS}(\hat{p}) \frac{i}{2} \mathcal{M}_{L'S'}^{JLS}(p, p', E) \mathcal{P}_{ij\dots k}^{JL'S'}(\hat{p}')^\dagger,$$

where  $\mathcal{P}^{JLS}$  ( $\mathcal{I}^T$ ) are spin-angular (isospin) projectors defined in Appendix C, and  $\mathcal{M}_{L'S'}^{JLS}(p, p', E)$  are matrix elements of  $NN$   $\mathcal{M}$  matrix in  $JLS$  basis:

$$\mathcal{M}_{L'S'}^{JLS}(p, p', E) = \langle JL'S' | \mathcal{M} | JLS \rangle.$$

In this equation the formal sum is over all values of total isospin  $T$ , total angular momentum  $J$  and initial (final) spin  $S$  and angular momentum  $L$  ( $S'$  and  $L'$ ). However in practice most often only a few partial waves are relevant. The vectors  $\hat{p}$  ( $\hat{p}'$ ) are unit vectors of the initial (final) relative momenta, whereas  $E$  is the center-of-mass frame energy of two nucleons. The choice of the sign of the relative momenta should be identical for initial and final two-nucleon systems, *i.e.* we use either  $(\vec{p}_1 - \vec{p}_2)/2$  and  $(\vec{p}'_1 - \vec{p}'_2)/2$  or these with both opposite signs. Different choices would lead to change of the signs of the projectors with odd angular momenta and simultaneous change of the signs of the corresponding  $\mathcal{M}_{L'S'}^{JLS}$ , therefore the total result would not change. However, it is more convenient to adopt same conventions for all  $NN$  states. The factor  $1/2$  in the front of  $\mathcal{M}_{L'S'}^{JLS}$  comes from taking into account identical particles [163];

4. An  $NN \rightarrow d$  vertex corresponds to a factor

$$i\mathcal{M}_{NNd}(\vec{p}, E) = \mathcal{I}^0 \sum_{L=0,2} \mathcal{P}_i^{1L1}(\hat{p}) \frac{i}{\sqrt{2}} \psi_L(p) \epsilon_i^{d*} 4\sqrt{M}(p^2 + \alpha^2),$$

where  $\vec{\epsilon}^d$  is the deuteron polarization vector, and  $\psi_L(p)$  are the components of the deuteron wave function corresponding to angular momentum  $L$ . The factor  $1/\sqrt{2}$  is again a consequence of presence of identical particles. The factor  $4\sqrt{M}(p^2 + \alpha^2)$ , where  $\alpha = ME_D$  with  $E_D$  being the deuteron binding energy, is needed for the correct normalization as will be discussed below. The vertex corresponding to the process  $d \rightarrow NN$  is the hermitian conjugate of the one for  $NN \rightarrow d$ ;

5. An  $NN \rightarrow N\Delta$  vertex corresponds to the following factor:

$$i\mathcal{M}_{N\Delta}(\vec{p}, \vec{p}', E) = \sum_{TT'} \mathcal{I}_\alpha^T \mathcal{I}_{N\Delta\alpha}^{T'\dagger} \sum_{JLSL'S'} \mathcal{P}_{ij\dots k}^{JLS}(\hat{p}) \frac{i}{\sqrt{2}} \mathcal{M}_{L'S'}^{JLS}(p, p', E) \mathcal{P}_{N\Delta ij\dots k}^{JL'S'}(\hat{p}')^\dagger$$

where  $\mathcal{P}_{N\Delta}^{JL'S'}$  ( $\mathcal{I}_{N\Delta}$ ) are spin-angular (isospin) projectors for  $N\Delta$  system defined in Appendix C, and  $\mathcal{M}_{L'S'}^{JLS}(p, p', E)$  are matrix elements of  $NN \rightarrow N\Delta$   $\mathcal{M}$  matrix in  $JLS$  basis:

$$\mathcal{M}_{L'S'}^{JLS}(p, p', E) = \langle JL'S' (N\Delta) | \mathcal{M} | (NN) JLS \rangle.$$

The factor  $1/\sqrt{2}$  accounts for two identical nucleons in the initial state. The expressions for the processes  $N\Delta \rightarrow NN$ ,  $N\Delta \rightarrow N\Delta$  are analogous: we only need to put in appropriate projectors and matrix elements for these processes;

6. An elementary interaction vertex for baryon-meson interaction on a normal baryon line corresponds to usual expression obtained from Lagrangian in the form

$$iV_{\text{int}} = iA_S B_T \quad (\text{B.14})$$

with  $A_S$  ( $B_T$ ) being spin (isospin) operators;

7. An elementary interaction vertex for nucleon-meson interaction on a CC nucleon line corresponds to charge conjugated expression

$$iV_{\text{int}}^c = iA_S^c B_T^c, \quad (\text{B.15})$$

where  $A_S^c = -\sigma_2 A_S^t \sigma_2$ ,  $B_T^c = -\tau_2 B_T^t \tau_2$  with  $A_S^t$ ,  $B_T^t$  being transposed operators;

8. A loop between any two  $NN$  or  $N\Delta$  interaction vertices corresponds to an integral over loop four-momenta (besides eventual integrations over four-momenta between these two vertices, *i.e.* in the transition operator), and to a trace of product of all spin matrices—projectors and matrices accounting for fermion-boson elementary interactions—that enter this loop, and analogously for isospin matrices. The order of the product is given by the direction against the normal fermionic line and along the CC fermionic line;

9. The choice of normalizations given above corresponds to  $N$  and  $\Delta$  non-relativistic propagators in the following form:

$$i\mathcal{G}_N^0(\varepsilon, \vec{p}) = \frac{i}{2M\varepsilon - p^2 + i\gamma},$$

$$i\mathcal{G}_\Delta^0(\varepsilon, \vec{p}) = \frac{i}{2M_\Delta(\varepsilon - \delta) - p^2 + i\gamma},$$

where  $\delta = M_\Delta - M$  is the Delta-nucleon mass difference. The  $NN$  and  $N\Delta$  interaction amplitudes  $\mathcal{M}_{L'S'}^{JLS}$  should be considered as having no singularities as functions of energy. This is naturally true for we are working at energies below pion threshold where the first hadronic inelasticity occurs. This assumption leads to the situation when the pole structure of the integrand in the integrals over zeroth components of four-momenta is fixed by the propagators of interacting particles.

The only missing thing is to show that the normalization of  $NN$  and  $N\Delta$  vertices is correct. In order to show this, it is useful to consider the Lippmann-Schwinger equation for the  $T$  matrix. Of course, the diagram technique should reproduce the Lippmann-Schwinger equation correctly. Using the rules given above and the properties of projectors given in Appendix C, it is straightforward to show that the Lippmann-Schwinger equation for amplitudes  $\mathcal{M}_{L'S'}^{JLS}(p, p', E)$  obtained from the diagram technique has the form

$$\mathcal{M}_{L'S'}^{JLS}(p, p', E) = \mathcal{V}_{L'S'}^{JLS}(p, p', E) + \frac{1}{4M} \sum_{L''S''} \int \frac{d^3q}{(2\pi)^2} \frac{\mathcal{V}_{L''S''}^{JLS}(p, q, E) \mathcal{M}_{L'S'}^{JL''S''}(q, p', E)}{q^2 - ME - i\gamma}$$

where  $\mathcal{V}_{L'S'}^{JLS}(p, p', E) = -8\pi^2 \sqrt{M_1 M_2 M_3 M_4} V_{L'S'}^{JLS}(p, p', E)$  are the matrix elements of the  $NN$  potential scaled with the same factor that connects  $T$  and  $\mathcal{M}$ . Using the relations between  $\mathcal{M}$  and  $T$  and between  $\mathcal{V}$  and  $V$ , we get the following Lippmann-Schwinger equation for  $T_{L'S'}^{JLS}(p, p', E)$ :

$$T_{L'S'}^{JLS}(p, p', E) = V_{L'S'}^{JLS}(p, p', E) + \sum_{L''S''} \int_0^\infty q^2 dq \frac{V_{L''S''}^{JLS}(p, q, E) T_{L'S'}^{JL''S''}(q, p', E)}{E - \frac{q^2}{M} + i\gamma},$$

which coincides with the corresponding equation used in Ref. [5]. This means that we should use in our technique exactly this definition of  $T_{L'S'}^{JLS}(p, p', E)$ , in particular, the relation between  $T_{L'S'}^{JLS}(p, p, p^2/M)$  and the scattering phase shifts should be the same as in Ref. [5].

The correctness of the normalizations for  $NN \rightarrow d$  and  $NN \rightarrow N\Delta$  vertices is proved in full analogy with  $NN \rightarrow NN$  vertices. Note, however, that since the  $NN \rightarrow N\Delta$  transitions are off-diagonal, the phase of the corresponding vertices can not be fixed from the Lippmann-Schwinger equation. In order to obtain the correct phase, one can, for instance, calculate matrix elements corresponding to a diagram that contributes to the  $NN \rightarrow N\Delta$  transition potential—say, for one-pion exchange—directly from the Lagrangian. Then one has to compare phases of the so obtained matrix elements with the phases that correspond to a concrete solution of Lippmann-Schwinger equation, and fix the missing phases if necessary. For the calculations of matrix elements for one-pion  $NN \rightarrow N\Delta$  transition potential see Appendix D. We note here that in our calculations with the phases of projectors as in Appendix C and  $NN \rightarrow N\Delta T$  matrices taken from the CCF model [89] there are additional phase factors of  $(-1)$  in the front of  $\mathcal{M}_{L'S'}^{JLS}$  for  $N\Delta$  partial waves  ${}^5F_1$ ,  ${}^5S_2$ ,  ${}^5D_2$ , and  ${}^5G_2$ .

# Appendix C

## Projectors

In this appendix we describe basic ideas that underlie the technique of spin–angular projectors and provide the relevant expressions.

### C.1 Spin–angular projectors

#### C.1.1 Irreducible tensors *vs* spherical harmonics

Let us firstly discuss the angular part of the wave function of two particles having relative momentum  $\vec{p} = (\vec{p}_1 - \vec{p}_2)/2$ . The usual description of the transformation properties of two particles having zero spins proceeds in terms of spherical harmonics  $Y_{LM}(\vec{n})$ , where  $\vec{n} = \vec{p}/p$ ,  $L = 0, 1, 2, \dots$ , and  $M = -L, -L+1, \dots, L$ . The spherical harmonics have the following properties of orthonormality and completeness:

$$\begin{aligned} \int d\Omega_{\vec{n}} Y_{LM}(\vec{n}) Y_{L'M'}^*(\vec{n}) &= \delta_{LL'} \delta_{MM'}; \\ \sum_{L=0}^{\infty} \sum_{M=-L}^L Y_{LM}(\vec{n}) Y_{LM}^*(\vec{n}') &= \delta(\vec{n} - \vec{n}'). \end{aligned} \quad (\text{C.1})$$

These properties of spherical harmonics allow one to expand an arbitrary function of vector  $\vec{n}$ ,  $f(\vec{n})$ , in Fourier series of spherical harmonics:

$$\begin{aligned} f(\vec{n}) &= \sum_{L=0}^{\infty} \sum_{M=-L}^L f_{LM} Y_{LM}(\vec{n}), \\ f_{LM} &= \int d\Omega_{\vec{n}} f(\vec{n}) Y_{LM}^*(\vec{n}). \end{aligned} \quad (\text{C.2})$$

From the point of view of theory of group representations (we refer to books [164–166] for further information on this theory), the functions  $Y_{LM}$  with fixed value of  $L$  consist a basis of an irreducible representation of the three-dimensional rotation group  $SO(3)$ . The rank of these representation is  $L$ , which is identified with the angular momentum of the corresponding state. It is known that these representations of  $SO(3)$

are finite-dimensional, namely the dimension of the rank  $L$  representation is  $2L + 1$  — this is the number of different values of  $M$  at given  $L$ .

Instead of using the conventional description in terms of spherical harmonics, one can describe the angular part of the wave function in terms of any other complete set of functions, which are in general linear combinations of the conventional spherical harmonics. For instance, it appears that the choice of the Cartesian irreducible tensors as the basis states appears to be very convenient when dealing with systems of two nonrelativistic particles (*e.g.*  $NN$ ,  $N\Delta$ ). In what follows we describe this formalism. First of all, we note that a (reducible) representation of  $SO(3)$  can be constructed as a direct product of components of vector  $\vec{n}$ :

$$v_{ijk\dots m}^L = n_i n_j n_k \dots n_m, \quad i, j, k, \dots m = 1, 2, 3 \text{ (there are } L \text{ indices)}. \quad (\text{C.3})$$

For instance, we have

$$v^0 = 1 \quad \text{— scalar}, \quad (\text{C.4})$$

$$v_i^1 = n_i \quad \text{— vector}, \quad (\text{C.5})$$

$$v_{ij}^2 = n_i n_j \quad \text{— tensor of rank two}, \quad (\text{C.6})$$

... *etc.*

These representations are in general not irreducible — for  $L \geq 2$  they contain all irreducible representations of the same parity  $(-1)^L$ , that is  $v_{ijk\dots m}^L$  contains in fact components that transform under representations with ranks  $L - 2$ ,  $L - 4$ , and so on. To ensure irreducibility, one has to subtract from  $v_{ijk\dots m}^L$  all irreducible representations of lower ranks analogously to what is done by conventional Clebsch-Gordan expansion. A straightforward way to construct an irreducible tensor of rank  $L$  is to write it in the form

$$\begin{aligned} V_{ijk\dots pqrs}^L = & v_{ijk\dots pqrs}^L + \alpha(\delta_{ij}v_{km\dots pqrs}^{L-2} + \delta_{ik}v_{jm\dots pqrs}^{L-2} + \dots) \\ & + \beta(\delta_{ij}\delta_{pq}v_{km\dots rs}^{L-4} + \delta_{ik}\delta_{ps}v_{jm\dots qr}^{L-4} + \dots) + \dots, \end{aligned} \quad (\text{C.7})$$

where  $\alpha, \beta$  and so on are unknown constants, and sums in brackets are properly symmetrized — one has to ensure that the resulting tensor remains symmetric with respect to interchange of any two of its indices. The values of  $\alpha, \beta, \dots$  are obtained from the equation

$$V_{ijk\dots pqrs}^L \delta_{ij} = 0. \quad (\text{C.8})$$

The quantity in the l.h.s. of Eq. (C.8), regarded as function of  $n_i$ 's, is a polynomial of power  $L - 2$  containing only even (odd) powers of  $n_i$ 's if  $L$  is even (odd). The requirement that this function is zero gives  $\text{int}(L/2)$  (where  $\text{int}$  stands for integer part) conditions on coefficients of this polynomial. Thus, we have a system of linear equations from which we find the values of the coefficients  $\alpha, \beta$ , and so on — note that we have exactly  $\text{int}(L/2)$  coefficients to determine.

It is easy to show that totally symmetric tensor  $V^L$  of rank  $L$  with zero trace contains exactly  $2L + 1$  independent components. Indeed, an element of this tensor is identified by two numbers  $m_1$  and  $m_2$ , which in order denote how many Cartesian indices of this

element are 1's and how many are 2's (the number of 3's is then  $m_3 = L - m_1 - m_2$ , and the values of  $m_i$  are between 0 and  $L$ ). The number of different choices of  $m_1$  and  $m_2$  is then

$$N_{\text{sym}} = (L + 1) + L + (L - 1) + \cdots + 1 = \frac{1}{2}(L + 1)(L + 2),$$

where  $L + 1$  is the number of different possible choices of  $m_2$  at  $m_1 = 0$ ,  $L$  — the number of different possible choices of  $m_2$  at  $m_1 = 1$ , and so on. From the other hand, the requirement that the trace over any two indices is zero gives additional  $L(L - 1)/2$  constraints on the components — this is the number of different traces. Thus, we get in total

$$N_L = \frac{1}{2}(L + 2)(L + 1) - \frac{1}{2}L(L - 1) = 2L + 1.$$

Therefore the components of a totally symmetric tensor of rank  $L$  which is constructed as explained above make up an irreducible representation of  $SO(3)$  with the rank  $L$ . Since all irreducible representations of  $SO(3)$  with the same rank are linearly dependent, there exists a matrix  $A$  that connects the conventional spherical harmonics  $Y_{LM}$  with given momentum  $L$  and projection on the  $z$  axis  $M$  to the components of the tensor  $V^L$ :

$$\begin{aligned} V_{ijk\dots prs}^L &= \sum_M A_{ijk\dots prs}^{LM} Y_{LM}, \\ Y_{LM} &= A_{ijk\dots prs}^{*LM} V_{ijk\dots prs}^L. \end{aligned} \quad (\text{C.9})$$

We assume here, as usual, that over all repeated Cartesian indices a summation is to be performed. The matrix  $A$  can be chosen to be unitary by an appropriate choice of the normalization of  $V^L$ :

$$\begin{aligned} A_{ijk\dots prs}^{LM} A_{ijk\dots prs}^{*LM'} &= \delta_{MM'}, \\ \sum_M A_{ijk\dots prs}^{LM} A_{i'j'k'\dots p'r's'}^{*LM} &= \frac{2}{L^2 - L + 2} (\delta_{ii'} \delta_{jj'} \delta_{kk'} \dots \delta_{pp'} \delta_{rr'} \delta_{ss'} \\ &\quad + \text{permutations} - \text{trace}). \end{aligned} \quad (\text{C.10})$$

Here permutations are performed so as to symmetrize the resulting tensor with respect to its indices. Note there are exactly  $(L^2 - L + 2)/2$  different permutations. Trace has to be subtracted since  $V^L$  should be traceless.

The expressions for the tensors  $V_{ijk\dots m}^L$  for  $L \leq 4$  are:

$$V^0(\vec{n}) = 1, \quad (\text{C.11})$$

$$V_i^1(\vec{n}) = n_i, \quad (\text{C.12})$$

$$V_{ij}^2(\vec{n}) = n_i n_j - \frac{1}{3} \delta_{ij}, \quad (\text{C.13})$$

$$V_{ijk}^3(\vec{n}) = n_i n_j n_k - \frac{1}{5} (n_i \delta_{jk} + n_j \delta_{ik} + n_k \delta_{ij}), \quad (\text{C.14})$$

$$\begin{aligned} V_{ijkl}^4(\vec{n}) &= n_i n_j n_k n_l \\ &\quad - \frac{1}{7} (n_i n_j \delta_{kl} + n_i n_k \delta_{jl} + n_i n_l \delta_{jk} + n_j n_k \delta_{il} + n_j n_l \delta_{ik} + n_k n_l \delta_{ij}) \\ &\quad + \frac{1}{35} (\delta_{ij} \delta_{kl} + \delta_{ik} \delta_{jl} + \delta_{il} \delta_{jk}). \end{aligned} \quad (\text{C.15})$$

Note that the tensors given by Eqs. (C.15) are not normalized. The normalization condition can be derived directly from the first equation of Eqs. (C.1), and Eqs. (C.9), (C.10). It reads

$$V_{ij\dots m}^L(\vec{n}) \left[ \int d\Omega_{\vec{n}'} V_{ij\dots m}^L(\vec{n}') V_{i'j'\dots m'}^{L'}(\vec{n}') \right] V_{i'j'\dots m'}^{L'}(\vec{n}'') = V_{ij\dots m}^L(\vec{n}) V_{ij\dots m}^L(\vec{n}'') \delta_{LL'}. \quad (\text{C.16})$$

However, we choose to normalize the complete spin-angular projectors rather than normalize their spin and angular parts separately — see below in this appendix.<sup>#1</sup>

### C.1.2 Expansion of spin operators

Consider now the spin part of the wave function. A particle having spin  $\frac{1}{2}$  is characterized by a two-component spinor  $\chi$ . The transformation properties of  $\chi$  under infinitesimal transformation from  $SO(3)$  is given by

$$\chi' = \left[ 1 - i \frac{\theta}{2} \vec{e}_i \sigma_i \right] \chi, \quad (\text{C.17})$$

where  $\theta$  is the infinitesimal rotation angle,  $\vec{e}$  is the unit vector along the rotation axis (we assume a right-handed coordinate system), and  $\sigma_i$ ,  $i = 1, 2, 3$  are the usual  $2 \times 2$  Pauli matrices having the following properties:

$$\sigma_i^\dagger = \sigma_i, \quad \sigma_i \sigma_j = \delta_{ij} + i \epsilon_{ijk} \sigma_k, \quad \sigma_2 \sigma_i^t \sigma_2 = \sigma_2 \sigma_i^* \sigma_2 = -\sigma_i; \quad (\text{C.18})$$

here and below we assume the Kronecker delta to be multiplied by the unit matrix of an appropriate rank — which we do not write out explicitly, and  $\sigma_i^t$  stands for transposed matrix.

Consider the linear space of the linear operators  $A$  that act on 2-component spinors  $\chi$ , realized as the linear space of  $2 \times 2$  matrices. The number of dimensions of this space equals four. It is known that four operators  $s = 1/\sqrt{2}$ ,  $t_i = \sigma_i/\sqrt{2}$ ,  $i = 1, 2, 3$  form an orthonormal basis in this linear space (with the scalar product of two operators introduced as  $(A, B) = \text{Tr } A^\dagger B$ ). This allows us to conclude that any operator  $A$  that acts on 2-component spinors can be expanded as

$$A = A^0 s + \sum_i A_i^1 t_i, \quad (\text{C.19})$$

where  $A^0 = (A, s)$ ,  $A_i^1 = (A, t_i)$ . The matrices of linear operators  $A$  transform under (infinitesimal) rotations from  $SO(3)$  as

$$A' = T A T^\dagger, \quad (\text{C.20})$$

---

<sup>#1</sup>Note that there exists a simpler normalization condition for angular irreducible tensors based on the standard addition formula for spherical harmonics (see. *e.g.*, Ref. [167]):  $\sum_{M=-L}^L Y_{LM}(\vec{n}) Y_{LM}^*(\vec{n}') = \frac{2L+1}{4\pi} P_L(\cos \theta)$ , where  $P_L$  is the  $L$ -th Legendre polynomial and  $\theta$  is the angle between  $\vec{n}$  and  $\vec{n}'$ . For the tensors  $V^L$  this translates to  $V_{ij\dots m}^L(\vec{n}) V_{ij\dots m}^L(\vec{n}') = \frac{2L+1}{4\pi} P_L(\cos \theta)$ .



where  $T = 1 - i \frac{\theta}{2} e_i \sigma_i$  is the matrix that transforms the spinors—see Eq. (C.17). Using Eqs. (C.18) it is straightforward to show that the transformation laws are different for the basis operators  $s$  and  $t_i$  and read as follows:

$$s' = s \quad (C.21)$$

$$t'_i = [\delta_{ij} - i\theta I_{ij}^k e_k] t_j, \quad i = 1, 2, 3, \quad (C.22)$$

where  $I_{ij}^k = -i \epsilon_{ijk}$  are the matrix elements of the generators that correspond to the  $SO(3)$  representation with rank 1.

Thus, the linear space of operators that act on two-component spinors splits into two subspaces. Each of these subspaces transforms independently under rotations from  $SO(3)$ :  $s$  transforms as a scalar and  $t_i$  transform as components of a vector. This means, in particular, that the corresponding matrix elements of  $s$  and  $t_i$  between any two spinors  $\chi_\alpha$  and  $\chi_\beta$  transform under rotations from  $SO(3)$  as

$$(\chi_\alpha^\dagger s \chi_\beta)' = \chi'^\dagger_\alpha s \chi'_\beta \quad (C.23)$$

$$(\chi_\alpha^\dagger t_i \chi_\beta)' = [\delta_{ij} - i\theta I_{ij}^k e_k] \chi'^\dagger_\alpha t_j \chi'_\beta, \quad i = 1, 2, 3, \quad (C.24)$$

where  $\chi'$  stand for transformed spinors.

### C.1.3 Construction of spin-angular projectors

Now one can proceed to the construction of projector operators. We define projector operator  $\mathcal{P}_{ijk\dots m}^{JLS}$  for given values of total angular momentum  $J$ , orbital angular momentum  $L$ , and total spin  $S$ , as

$$\mathcal{P}_{ijk\dots m}^{JLS}(\vec{n}) = \begin{cases} C^{JLS} s V_{ijk\dots m}^L(\vec{n}), & S = 0, J = L; \\ C^{JLS} t_p V_{pijk\dots m}^L(\vec{n}), & S = 1, J = L - 1; \\ C^{JLS} t_i V_{ijk\dots m}^L(\vec{n}) + \text{symm.} - \text{trace}, & S = 1, J = L + 1; \\ C^{JLS} \epsilon_{ipr} t_p V_{rjk\dots m}^L(\vec{n}) + \text{symm.}, & S = 1, J = L, \end{cases} \quad (C.25)$$

where  $C^{JLS}$  are normalization constants. Here "symm." and "trace" mean that one should properly symmetrize the projector and ensure that it gives zero when trace over any two tensor indices is performed. Note that  $\mathcal{P}_{ijk\dots m}^{JLS}$  is a totally symmetric traceless tensor of rank  $J$ , by construction. Therefore the components of this tensor transform under a rank  $J$  representation of  $SO(3)$ . Hence they are related to the usual states  $\Psi_{JJ_z}$  with certain  $J$ ,  $J_z$  through the matrix  $A$  from Eq. (C.9), in full analogy with angular momentum tensors:

$$\begin{aligned} \mathcal{P}_{ijk\dots prs}^{JLS} &= \sqrt{4\pi} \sum_{J_z} A_{ijk\dots prs}^{JJ_z} \Psi_{JJ_z}, \\ \Psi_{JJ_z} &= A_{ijk\dots prs}^{*JJ_z} \frac{1}{\sqrt{4\pi}} \mathcal{P}_{ijk\dots prs}^{JLS}. \end{aligned} \quad (C.26)$$

The factors of  $\sqrt{4\pi}$  are purely conventional. The normalization is given by the following condition

$$\begin{aligned} \int \frac{d\Omega_{\vec{n}'}}{4\pi} \mathcal{P}_{ij\dots m}^{JLS}(\vec{n}) \text{Tr} \left( \mathcal{P}_{ij\dots m}^{JLS}(\vec{n}')^\dagger \mathcal{P}_{i'j'\dots m'}^{JL'S'}(\vec{n}') \right) \mathcal{P}_{i'j'\dots m'}^{JL'S'}(\vec{n}'')^\dagger &= \\ &= \mathcal{P}_{ij\dots m}^{JLS}(\vec{n}) \mathcal{P}_{ij\dots m}^{JLS}(\vec{n}'')^\dagger \delta_{LL'} \delta_{SS'}, \end{aligned} \quad (\text{C.27})$$

where  $\text{Tr}$  stands for the trace of spin matrices (*i.e.* for the scalar product in the corresponding hilbert space). From this equation the values of  $C^{JLS}$  are known up to an arbitrary phase coefficient. Our choice of  $C^{JLS}$  is dictated by convenience — see below in this appendix.

The projectors defined by Eq. (C.25) are constructed as linear combinations of products of quantities  $V^L$ ,  $s$ , and  $t$ , which transform under representations of  $SO(3)$  with different ranks. It is obvious that there exists a matrix  $\mathcal{O}$ , which is a tensor analog of the Clebsch-Gordan coefficients, such that

$$\mathcal{P}_{ijk\dots prs}^{JLS}(\vec{n}) = \sqrt{4\pi} \mathcal{O}_{ijk\dots prs \ i'j'k'\dots m' \ a'b'\dots c'}^{JLS} V_{i'j'k'\dots m'}^L(\vec{n}) T_{a'b'\dots c'}^S, \quad (\text{C.28})$$

where  $T^S$  stands for the corresponding irreducible spin operator structure— $s$ ,  $t$ , or further structures if we consider spins different from one half—see below for  $N\Delta$  case. We assume that spins should be half-integer and therefore the linear space of spin operators again splits in subspaces each of which transform under an integer-rank representation of  $SO(3)$ .

Consider the states  $\Psi_{JJ_z}$  as constructed from states with angular momentum  $L$  and spin  $S$ , *i.e.*

$$\Psi_{JJ_z} \equiv \Psi_{JJ_z LS} = \sum_{MS_z} \mathcal{C}_{LMSS_z}^{JJ_z} Y_{LM}(\vec{n}) \Psi_{SS_z},$$

where  $\mathcal{C}_{LMSS_z}^{JJ_z}$  are the Clebsch-Gordan coefficients, and  $\Psi_{SS_z}$  are the corresponding spin states. This equality allows us to deduce the expression for matrix  $\mathcal{O}$  through  $\mathcal{C}_{LMSS_z}^{JJ_z}$  and transformation matrix  $A$  defined in Eq. (C.9). This expression reads

$$\mathcal{O}_{ijk\dots prs \ i'j'k'\dots m' \ a'b'\dots c'}^{JLS} = \sum_{J_z MS_z} \mathcal{C}_{LMSS_z}^{JJ_z} A_{ijk\dots prs}^{JJ_z} A_{i'j'k'\dots m'}^{*LM} A_{a'b'\dots c'}^{*SS_z} \quad (\text{C.29})$$

This equation will help us to formulate the properties of the projectors defined by Eq. (C.25), especially the completeness of the set of projectors.

This property of completeness means that any matrix operator  $F(\vec{n})$  that acts on (two-component) spinors and is a well-behaving<sup>#2</sup> function of vector  $\vec{n}$  can be expanded in Fourier series as

$$\begin{aligned} F(\vec{n}) &= \sum_{JLS} \mathcal{P}_{ij\dots k}^{JLS}(\vec{n}) F_{ij\dots k}^{JLS}, \\ F_{ij\dots k}^{JLS} &= \int \frac{d\Omega_{\vec{n}'}}{4\pi} \text{Tr} \left( \mathcal{P}_{ij\dots k}^{JLS}(\vec{n}')^\dagger F(\vec{n}') \right), \end{aligned} \quad (\text{C.30})$$

<sup>#2</sup>In the sense that each of four components of this operator is a function that can be expanded in a series of spherical harmonics.

in full analogy with Eq. (C.2). Indeed, let us write Eqs. (C.30) in the following way:

$$F(\vec{n}) = \sum_{JLS} \mathcal{P}_{i\dots k}^{JLS}(\vec{n}) \int \frac{d\Omega_{\vec{n}'}}{4\pi} \text{Tr} \left( \mathcal{P}_{i\dots k}^{JLS}(\vec{n}')^\dagger F(\vec{n}') \right).$$

Changing the order of integration and summation and using Eq. (C.28), we get

$$\begin{aligned} F(\vec{n}) &= \int \frac{d\Omega_{\vec{n}'}}{4\pi} \sum_{JLS} \mathcal{P}_{ij\dots k}^{JLS}(\vec{n}) \text{Tr} \left( \mathcal{P}_{i\dots k}^{JLS}(\vec{n}')^\dagger F(\vec{n}') \right) \\ &= \int d\Omega_{\vec{n}'} \sum_{JLS} \mathcal{O}_{ij\dots k}^{JLS}{}_{i'j'\dots m' a'b'\dots c'} \mathcal{O}_{ij\dots k}^{*JLS}{}_{i''j''\dots m'' a''b''\dots c''} \\ &\quad \times V_{i'j'\dots m'}^L(\vec{n}) T_{a'b'\dots c'}^S V_{i''j''\dots m''}^{*L}(\vec{n}') \text{Tr} \left( T_{a''b''\dots c''}^{S\dagger} F(\vec{n}') \right). \end{aligned} \quad (\text{C.31})$$

Using now Eqs. (C.29), (C.10), and the properties of the Clebsch-Gordan coefficients, we can write the following:

$$\begin{aligned} &\sum_J \mathcal{O}_{ij\dots k}^{JLS}{}_{i'j'\dots m' a'b'\dots c'} \mathcal{O}_{ij\dots k}^{*JLS}{}_{i''j''\dots m'' a''b''\dots c''} = \\ &= \sum_J \sum_{J_z M S_z} \sum_{J'_z M' S'_z} \mathcal{C}_{LMSS_z}^{JJ_z} \mathcal{C}_{LM'SS'_z}^{JJ'_z} \underbrace{A_{ij\dots m}^{JJ_z} A_{ij\dots m}^{*JJ'_z}}_{\delta_{J_z J'_z}} A_{i'j'\dots m'}^{*LM} A_{i''j''\dots m''}^{LM'} A_{a'b'\dots c'}^{*SS_z} A_{a''b''\dots c''}^{SS'_z} \\ &= \sum_{MS_z M' S'_z} \sum_{JJ_z} \underbrace{\mathcal{C}_{LMSS_z}^{JJ_z} \mathcal{C}_{LM'SS'_z}^{JJ'_z}}_{\delta_{MM'} \delta_{S_z S'_z}} A_{i'j'\dots m'}^{*LM} A_{i''j''\dots m''}^{LM'} A_{a'b'\dots c'}^{*SS_z} A_{a''b''\dots c''}^{SS'_z} \\ &= \sum_{MS_z} A_{i'j'\dots m'}^{*LM} A_{i''j''\dots m''}^{LM} A_{a'b'\dots c'}^{*SS_z} A_{a''b''\dots c''}^{SS_z} \\ &= \frac{2}{L^2 - L + 2} (\delta_{i'i''} \delta_{j'j''} \dots \delta_{m'm''} + \dots) \frac{2}{S^2 - S + 2} (\delta_{a'a''} \delta_{b'b''} \dots \delta_{c'c''} + \dots), \end{aligned} \quad (\text{C.32})$$

where ellipses in the last line stand for various permutations—cf. Eq. (C.10). Inserting this result<sup>#3</sup> into the expression for  $F(\vec{n})$ , we get

$$F(\vec{n}) = \int d\Omega_{\vec{n}'} \sum_{LS} V_{i'j'\dots m'}^L(\vec{n}) T_{a'b'\dots c'}^S V_{i'j'\dots m'}^{*L}(\vec{n}') \text{Tr} \left( T_{a'b'\dots c'}^{S\dagger} F(\vec{n}') \right).$$

Since the spin operators  $T_{a'b'\dots c'}^S$  form a basis in the linear space of matrices (note that we do not assume the corresponding matrices be  $2 \times 2$  matrices; the only assumption is that the corresponding space splits into subspaces that transform under different irreducible representations of  $SO(3)$ ), the equality

$$F(\vec{n}') = \sum_S T_{a'b'\dots c'}^S \text{Tr} \left( T_{a'b'\dots c'}^{S\dagger} F(\vec{n}') \right)$$

<sup>#3</sup>Note that traces that are to be subtracted from these expressions according to Eq. (C.10) give anyway zero contribution.

holds for arbitrary matrix that belongs to the linear space under consideration. Since  $\sum_L V_{i'j'...m'}^L(\vec{n}) V_{i'j'...m'}^{*L}(\vec{n}') = \delta(\vec{n} - \vec{n}')$ , we finally get identity, thus proving the expansion for  $F(\vec{n})$  given by Eq. (C.30).

The projectors for states where one particle has spin  $\frac{1}{2}$  and the other—spin  $\frac{3}{2}$  ( $N\Delta$  states) are defined analogously. The angular part of the projectors for  $N\Delta$  system is the same as for  $NN$  system. The substantial difference is that along with Pauli matrices  $\sigma_i$  there are matrices  $S_i$  (see Eq. (A.3)) that couple spins  $\frac{1}{2}$  and  $\frac{3}{2}$  into spin 1, and total spin for  $N\Delta$  system may have values 1 and 2. There are two sets of quantities that can be constructed for  $N\Delta$ -system analogously to  $s$  and  $t_i$ , namely

$$d_i = \sqrt{\frac{3}{4}} S_i, \quad i = 1, 2, 3, \quad (\text{C.33})$$

$$q_{ij} = \sqrt{\frac{1}{8}} (\sigma_i S_j + \sigma_j S_i), \quad i, j = 1, 2, 3; \quad (\text{C.34})$$

it is easy to show that they form the bases of subspaces that transform under representations with rank one and two, respectively. Thus, there are in total  $8 = 3 + 5$  linearly independent vectors that form a complete basis in the linear space of all  $2 \times 4$  matrices. Note that the general expression for an irreducible tensor of second rank build up from  $\sigma_i$  and  $S_j$  has structure  $(\sigma_i S_j + \sigma_j S_i - \frac{2}{3} \delta_{ij} \sigma_k S_k)$ , however the latter term is zero due to Eq. (A.6), which corresponds to the fact that total spin 0 is not possible in this case. Note also that the third possible structure is  $\epsilon_{ijk} \sigma_j S_k$ , which reduces to  $-i S_i$  (cf. Eq. (A.5)) in full accordance with the fact that different irreducible representations of  $SO(3)$  that have the same rank are linearly dependent.

The projectors for  $N\Delta$  system are defined as

$$\mathcal{P}_{ijk...m}^{JLS}(\vec{n}) = \begin{cases} C^{JLS} d_p V_{pijk...m}^L(\vec{n}), & S = 1, J = L - 1; \\ C^{JLS} d_i V_{jk...m}^L(\vec{n}) + \text{symm.} - \text{trace}, & S = 1, J = L + 1; \\ C^{JLS} \epsilon_{ipr} d_p V_{rjk...m}^L(\vec{n}) + \text{symm.}, & S = 1, J = L; \\ \\ C^{JLS} q_{pr} V_{prijk...m}^L(\vec{n}), & S = 2, J = L - 2; \\ C^{JLS} \epsilon_{pri} q_{ps} V_{rsjk...m}^L(\vec{n}) + \text{symm.}, & S = 2, J = L - 1; \\ C^{JLS} q_{ip} V_{pj k...m}^L(\vec{n}) + \text{symm.} - \text{trace}, & S = 2, J = L; \\ C^{JLS} \epsilon_{prj} q_{ip} V_{rk...m}^L(\vec{n}) + \text{symm.} - \text{trace}, & S = 2, J = L + 1; \\ C^{JLS} q_{ij} V_{k...m}^L(\vec{n}) + \text{symm.} - \text{trace}, & S = 2, J = L + 2. \end{cases} \quad (\text{C.35})$$

The normalization condition for the projectors for  $N\Delta$  system is the same as for  $NN$  system—see Eq. (C.27). Again, the projectors defined by Eqs. (C.35) have properties analogous to the projectors defined for  $NN$  system with appropriate changes due to different spin structure, and all arguments concerning the completeness, orthogonality *etc* are extended to the  $N\Delta$  projectors with minimal changes. Particularly, the  $N\Delta$  projectors form a complete set of functions such that any  $2 \times 4$  matrix function of vector  $\vec{n}$  can be expanded in Fourier series given by Eq. (C.30).

The explicit expressions for projectors relevant for this our work are given below. For reference we also provide notations in the form  ${}^{2S+1}L_J$  for the spin-angular states.

Note that we choose the constants  $C^{JLS}$  to be imaginary for  ${}^5P_1$  and  ${}^5F_1$   $N\Delta$  projectors. This makes the corresponding partial wave amplitudes from one-pion exchange between  $N$  and  $\Delta$  to be real (see discussion in Appendix D).

$NN$  states

$${}^1S_0 \quad \mathcal{P}^{000} = s \quad (\text{C.36})$$

$${}^3P_0 \quad \mathcal{P}^{011} = \sqrt{3} t_i V_i^1(\vec{n}) \quad (\text{C.37})$$

$${}^3S_1 \quad \mathcal{P}_i^{101} = t_i \quad (\text{C.38})$$

$${}^3P_1 \quad \mathcal{P}_i^{111} = \sqrt{\frac{3}{2}} \epsilon_{ijk} t_j V_k^1(\vec{n}) \quad (\text{C.39})$$

$${}^3D_1 \quad \mathcal{P}_i^{121} = \frac{3}{\sqrt{2}} t_j V_{ij}^2(\vec{n}) \quad (\text{C.40})$$

$${}^3P_2 \quad \mathcal{P}_{ij}^{211} = \sqrt{\frac{3}{4}} \left( t_i V_j^1(\vec{n}) + t_j V_i^1(\vec{n}) - \frac{2}{3} \delta_{ij} t_k V_k^1(\vec{n}) \right) \quad (\text{C.41})$$

$${}^1D_2 \quad \mathcal{P}_{ij}^{220} = \sqrt{\frac{15}{2}} s V_{ij}^2(\vec{n}) \quad (\text{C.42})$$

$N\Delta$  states

$${}^3P_1 \quad \mathcal{P}_i^{111} = \sqrt{9} \epsilon_{ijk} d_j V_k^1(\vec{n}) \quad (\text{C.43})$$

$${}^5P_1 \quad \mathcal{P}_i^{112} = -i \sqrt{\frac{18}{5}} q_{ik} V_k^1(\vec{n}) \quad (\text{C.44})$$

$${}^5F_1 \quad \mathcal{P}_i^{132} = i \sqrt{\frac{15}{2}} q_{jk} V_{ijk}^3(\vec{n}) \quad (\text{C.45})$$

$${}^5D_0 \quad \mathcal{P}^{022} = \sqrt{\frac{3}{4}} q_{ij} V_{ij}^2(\vec{n}) \quad (\text{C.46})$$

$${}^5S_2 \quad \mathcal{P}_{ij}^{202} = q_{ij} \quad (\text{C.47})$$

$${}^3D_2 \quad \mathcal{P}_{ij}^{221} = \sqrt{\frac{135}{2}} (\epsilon_{ipr} d_p V_{pj}^2(\vec{n}) + \epsilon_{jpr} d_p V_{pi}^2(\vec{n})) \quad (\text{C.48})$$

$${}^5D_2 \quad \mathcal{P}_{ij}^{222} = \sqrt{\frac{45}{14}} \left( q_{ik} V_{kj}^2(\vec{n}) + q_{jk} V_{ki}^2(\vec{n}) - \frac{2}{3} \delta_{ij} q_{kl} V_{kl}^2(\vec{n}) \right) \quad (\text{C.49})$$

$${}^5G_2 \quad \mathcal{P}_{ij}^{242} = \sqrt{\frac{175}{8}} q_{kl} V_{ijkl}^4(\vec{n}). \quad (\text{C.50})$$

## C.2 Isospin projectors

Analogous considerations apply to the isospin operators. There is no analogy to angular part in the case of isospin, and the projectors are pure (iso)spin projectors. Again, we

can construct quantities  $\mathcal{J}^0$  and  $\mathcal{J}_i^1$  for  $NN$  system as

$$\mathcal{J}^0 = \frac{1}{\sqrt{2}} \quad (\text{C.51})$$

$$\mathcal{J}_i^1 = \frac{\tau_i}{\sqrt{2}}, \quad i = 1, 2, 3, \quad (\text{C.52})$$

where  $\tau_i$  are isospin Pauli matrices. The quantities  $\mathcal{J}^0$  and  $\mathcal{J}_i^1$  transform under isospin rotations as isoscalar and components of isovector, and correspond to total isospin 0 and 1, respectively. For the  $N\Delta$  system we can construct quantities  $\mathcal{F}_i^1$  and  $\mathcal{F}_{ij}^2$ , which correspond to total isospin of  $N\Delta$  system 1 and 2 in order, analogously:

$$\mathcal{F}_i^1 = \sqrt{\frac{3}{4}} T_i, \quad i = 1, 2, 3, \quad (\text{C.53})$$

$$\mathcal{F}_{ij}^2 = \sqrt{\frac{1}{8}} (\tau_i T_j + \tau_j T_i), \quad i, j = 1, 2, 3, \quad (\text{C.54})$$

where  $T^i$  are matrices that couple isospins  $\frac{1}{2}$  and  $\frac{3}{2}$  into isospin 1 (they are equal to  $S_i$ —see Eq. (A.3)).

The normalization condition for isospin projectors  $\mathcal{I}_{ij\dots m}^{\mathcal{T}}$  with given isospin  $\mathcal{T}$  reads

$$\mathcal{I}_{ij\dots m}^{\mathcal{T}} \text{Tr} \left( \mathcal{I}_{ij\dots m}^{\mathcal{T} \dagger} \mathcal{I}_{i'j'\dots m'}^{\mathcal{T}} \right) \mathcal{I}_{i'j'\dots m'}^{\mathcal{T} \dagger} = \mathcal{I}_{ij\dots m}^{\mathcal{T}} \mathcal{I}_{ij\dots m}^{\mathcal{T} \dagger}. \quad (\text{C.55})$$

The resulting expressions for isospin projectors after the normalization is performed are:

$NN$  states

$$\text{isospin 0} \quad \mathcal{I}^0 = \mathcal{J}^0 \quad (\text{C.56})$$

$$\text{isospin 1} \quad \mathcal{I}_i^1 = \mathcal{J}_i^1 \quad (\text{C.57})$$

$N\Delta$  states

$$\text{isospin 1} \quad \mathcal{I}_i^1 = \mathcal{F}_i^1 \quad (\text{C.58})$$

$$\text{isospin 2} \quad \mathcal{I}_{ij}^2 = \mathcal{F}_{ij}^2. \quad (\text{C.59})$$

# Appendix D

## One-pion exchange $NN \rightarrow N\Delta$

In this Appendix we present expressions for amplitude of  $NN \rightarrow N\Delta$  transition via one pion exchange projected onto  ${}^3P_1$ ,  ${}^1S_0$ , and  ${}^1D_2$  spin-angular states of initial nucleons. These expressions are needed when one wants to incorporate the full  $NN \rightarrow N\Delta$  transition amplitude obtained from a (model) potential into the diagram technique described in Appendix B. The correct phase of the  $NN \rightarrow N\Delta$  vertex is not defined from the Lippmann–Schwinger equation since this is a non-diagonal transition—see the discussion in Appendix B. Therefore one has to match phases. A straightforward way to do it is to calculate the corresponding partial amplitudes from the one-pion exchange with the vertices taken from the Lagrangian and using projectors with some fixed choice of phase, and compare with the corresponding amplitudes from the model which the full amplitudes are taken from.

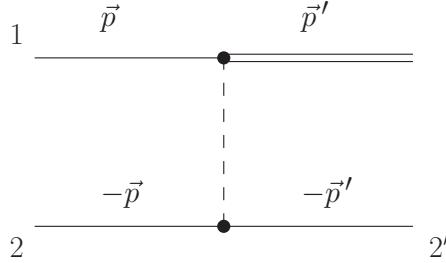


Figure D.1: One pion exchange diagram for transition  $NN \rightarrow N\Delta$ .

The diagram that corresponds to the one-pion exchange transition  $NN \rightarrow N\Delta$  is shown in Fig. D.1. The corresponding amplitude reads

$$\mathcal{M} = \frac{g_A h_A}{F^2} M \sqrt{MM_\Delta} \left[ \zeta^\dagger T_b^\dagger \varphi_1 \varphi_2^\dagger \tau_b \varphi_2 \right] \left[ \xi^\dagger \left( \vec{S}^\dagger \cdot (\vec{p}' - \vec{p}) \right) \chi_1 \cdot \chi_{2'}^\dagger (\vec{\sigma} \cdot (\vec{p}' - \vec{p})) \chi_2 \right] \frac{1}{(\vec{p}' - \vec{p})^2 + m_\pi^2}. \quad (\text{D.1})$$

Here  $\chi, \xi$  ( $\varphi, \zeta$ ) stand in order for nucleon and Delta spinors (isospinors). This expression was obtained neglecting pion energies.

In order to get the expressions for partial amplitudes, one has to project amplitude given by Eq. (D.1) onto corresponding spin-angular states with given total angular

momentum  $J$  and orbital momenta and total spins  $L, S, L', S'$ , and isospin states with given isospin  $T$ , using projectors defined in Appendix C:

$$\mathcal{M}_{JLSL'S'} = \sum_{\text{isospin}} \sum_{\text{spin}} \int \frac{d\Omega_{\vec{p}}}{4\pi} \frac{d\Omega_{\vec{p}'}}{4\pi} \varphi_2^{c\dagger} \mathcal{I}_a^{T\dagger} \varphi_1 \chi_2^{c\dagger} \mathcal{P}_{i\dots m}^{JLS}(\hat{p})^\dagger \chi_1 \mathcal{M} \xi^\dagger \mathcal{P}_{i\dots m}^{JL'S'}(\hat{p}') \chi_{2'}^c \zeta^\dagger \mathcal{I}_a^{T'} \chi_{2'}^c, \quad (\text{D.2})$$

where sum is performed over spin and isospin projections of all four particles, and  $\hat{p}$  ( $\hat{p}'$ ) denotes unit vector of initial (final) momentum. Resulting expressions for partial amplitudes are given below for initial states  ${}^3P_1$  ( $s$ -wave pion production) and  ${}^1S_0, {}^1D_2$  ( $p$ -wave pion production) Note, we give the notations for the initial and partial waves in the form  ${}^{2S+1}L_J$  rather than  $JLS$ .

### Initial $NN$ state ${}^3P_1$

Final  $N\Delta$  state

$${}^5F_1 \quad \mathcal{M} = \alpha_s \sqrt{\frac{4}{15}} A(p, p') \quad (\text{D.3})$$

$${}^5P_1 \quad \mathcal{M} = \alpha_s \sqrt{\frac{4}{10}} B(p, p') \quad (\text{D.4})$$

$${}^3P_1 \quad \mathcal{M} = \alpha_s \sqrt{\frac{2}{9}} (4C(p, p') + B(p, p')), \quad (\text{D.5})$$

### Initial $NN$ state ${}^1S_0$

Final  $N\Delta$  state

$${}^5D_0 \quad \mathcal{M} = \alpha_p \sqrt{\frac{4}{15}} D(p, p') \quad (\text{D.6})$$

### Initial $NN$ state ${}^1D_2$

Final  $N\Delta$  state

$${}^5G_2 \quad \mathcal{M} = \frac{4}{3} \alpha_p \sqrt{\frac{2}{35}} E(p, p') \quad (\text{D.7})$$

$${}^5D_2 \quad \mathcal{M} = \frac{8}{3} \alpha_p \sqrt{\frac{7}{2}} F(p, p') \quad (\text{D.8})$$

$${}^3D_2 \quad \mathcal{M} = 0 \quad (\text{D.9})$$

$${}^5S_2 \quad \mathcal{M} = -\alpha_p \sqrt{\frac{16}{5}} G(p, p'), \quad (\text{D.10})$$



where  $\alpha_s = -\sqrt{2}\frac{g_A h_A}{4F^2}M\sqrt{MM_\Delta}$ ,  $\alpha_p = \sqrt{2}\alpha_s$ , and

$$A(p, p') = \frac{p}{2p'} (5f_3(\nu) - 3f_1(\nu)) + \frac{p'}{p} f_1(\nu) + 3f_2(\nu) - f_0(\nu) \quad (\text{D.11})$$

$$B(p, p') = \frac{1}{2}f_2(\nu) + \left(\frac{p'}{p} + \frac{p}{p'}\right) f_1(\nu) + \frac{3}{2}f_0(\nu) \quad (\text{D.12})$$

$$C(p, p') = \frac{1}{2} [f_2(\nu) - f_0(\nu)] \quad (\text{D.13})$$

$$D(p, p') = \frac{1}{12} \left[ 3\frac{p}{p'}f_2(\nu) + 4f_1(\nu) + \left(2\frac{p'}{p} - \frac{p}{p'}\right) f_0(\nu) \right] \quad (\text{D.14})$$

$$E(p, p') = \frac{3}{16} \left[ 35\frac{p}{p'}f_4(\nu) + 40f_3(\nu) - \left(30\frac{p}{p'} - 12\frac{p'}{p}\right) f_2(\nu) - 24f_1(\nu) + \left(3\frac{p}{p'} - 4\frac{p'}{p}\right) f_0(\nu) \right] \quad (\text{D.15})$$

$$F(p, p') = \frac{1}{28} \left[ 3f_3(\nu) + 3\left(\frac{p}{p'} + \frac{p'}{p}\right) f_2(\nu) + f_1(\nu) - \left(\frac{p}{p'} + \frac{p'}{p}\right) f_0(\nu) \right] \quad (\text{D.16})$$

$$G(p, p') = -\frac{1}{12} \left[ 3\frac{p'}{p}f_2(\nu) + 4f_1(\nu) + \left(2\frac{p}{p'} - \frac{p'}{p}\right) f_0(\nu) \right] \quad (\text{D.17})$$

with

$$\nu = \frac{p^2 + p'^2 + m_\pi^2}{2pp'}, \quad (\text{D.18})$$

$$f_j(\eta) = \int_{-1}^1 \frac{x^j dx}{x + \eta}. \quad (\text{D.19})$$

One sees from Eq. (D.9) that partial amplitude in the  ${}^3D_2$  state appears to be zero in this approximation. In order to match the phase of the amplitude corresponding to this transition, one has to include nucleon and Delta recoil into the vertices on Fig. D.1, which are effects of higher orders. In this case the corresponding amplitude will not be zero. However, since the  ${}^3D_2$  partial amplitude appears to give a negligible contribution to  $p$ -wave pion production (it changes the value of the corresponding  $p$ -wave reduced cross-section by  $\pm 5\%$  which is far less than our error estimate), we neglect the contribution coming from the transition  ${}^1D_2(NN) \rightarrow {}^3D_2(N\Delta)$ .

# Appendix E

## Matrix Elements and Observables

In this section we give expressions for observables and matrix elements for reactions that are subject of our study.

### E.1 General definitions

The differential cross section for a reaction  $2 \rightarrow N$ , when there are two particles in the initial state, is related to the reaction amplitude via [160]

$$d\sigma = (2\pi)^4 \delta^{(4)}(P_f - P_i) \frac{1}{4I} |\mathcal{M}_{fi}|^2 \prod_a \frac{d^3 p_a}{(2\pi)^3 2E_a}, \quad (\text{E.1})$$

where the product is taken over the phase volumes of all final particles labeled by  $a$ , and  $\mathcal{M}_{fi}$  stands for the sum of all amplitudes that are relevant for the calculation. The quantity  $I$  in Eq. (E.1) is the covariant flux factor given by

$$I = \sqrt{(p_1^\mu p_{2\mu})^2 - m_1^2 m_2^2}, \quad (\text{E.2})$$

where  $p_{1,2}^\mu$  and  $m_{1,2}$  stand in order for four-vectors and masses of the corresponding particles. In addition, if there are  $N_a$  identical particles of  $a$ -th kind in the final state, then a factor of  $1/N_a!$  should be introduced when integration over the phase space is performed.

When the initial particles are not polarized, and the polarizations of the final particles are not registered by the detector, which is true in all cases considered by us, the differential cross-section is given by Eq. (E.1) with the only difference that  $|\mathcal{M}_{fi}|^2$  should be substituted by the sum

$$\overline{|\mathcal{M}_{fi}|^2} = \frac{1}{2S_1 + 1} \frac{1}{2S_2 + 1} \sum |\mathcal{M}_{fi}|^2, \quad (\text{E.3})$$

where the sum is performed over the polarizations of initial and final particles, and  $S_{1,2}$  is the spin of the corresponding initial particle. Note that for the photon  $2S + 1$  should be substituted by 2 since only two photon polarisations are possible.

## E.2 Reaction $\gamma d \rightarrow \pi^+ nn$

### E.2.1 Observables

The differential cross-section is given by

$$d\sigma = (2\pi)^4 \delta^{(4)}(P_f - P_i) \frac{1}{2} \frac{1}{4q_\gamma \sqrt{s}} |M_{fi}|^2 \frac{d^3 p_1}{(2\pi)^3 2E_1} \frac{d^3 p_2}{(2\pi)^3 2E_2} \frac{d^3 k_\pi}{(2\pi)^3 2\omega_\pi}, \quad (\text{E.4})$$

where the indices 1 and 2 label momenta and energies of the final nucleons, and  $k_\pi$  ( $\omega_\pi$ ) denotes the pion three-momentum (energy). The photon momentum is denoted by  $q_\gamma$  and  $\sqrt{s} = 2M + m_\pi + Q$  where  $M$  ( $m_\pi$ ) and  $Q$  are the nucleon (pion) mass and the excess energy, respectively (we work in the center-of-mass frame of the reaction). The choice of variables is illustrated in Fig. 3.2. The factor of 1/2 accounts for the two identical nucleons in the final state.

We treat the nucleons as non-relativistic particles — it is certainly justified as soon as we consider excess energies not more than 25 MeV. In this case, the nucleon energies in Eq. (E.4) are replaced by  $M$ . It is also convenient to use instead of the momenta of the two neutrons,  $\vec{p}_1$  and  $\vec{p}_2$ , the relative and the total momenta which are defined as  $\vec{p}_r = (\vec{p}_1 - \vec{p}_2)/2$ ,  $\vec{P} = \vec{p}_1 + \vec{p}_2 = -\vec{k}_\pi$ . This allows to remove the delta function in a simple way and rewrite the cross-section in the form

$$d\sigma = \frac{1}{(4\pi)^5} \frac{p_r k_\pi^2 dk_\pi d\Omega_\pi d\Omega_r}{4M\omega_\pi q_\gamma (q_\gamma + 2M + q_\gamma^2/4M)} |M_{fi}|^2, \quad (\text{E.5})$$

where  $\Omega_\pi$  ( $\Omega_r$ ) are the solid angles of the vector  $\vec{k}_\pi$  ( $\vec{P}_R$ ). The values of  $p_r$  and  $k_\pi$  are connected by the energy conservation law:

$$Q = \frac{p_r^2}{M} + \frac{k_\pi^2}{4M} + \omega_\pi - m_\pi. \quad (\text{E.6})$$

In what follows we use nonrelativistic kinematics also for the pion. In this case one should change  $\omega_\pi$  to  $m_\pi + k_\pi^2/(2m_\pi)$  in these formulae.

### E.2.2 Matrix elements

Let us now present the explicit expressions for the amplitudes corresponding to the diagrams in Fig. 3.1. All calculations are done in the center-of-mass system of the reaction. Note that in the calculation of the leading diagrams (a1) and (a2) in Fig. 3.1 the D-wave component of the deuteron wave function was taken into account, whereas in all other diagrams which are already suppressed by  $\chi_m^2$  as compared to the leading ones, the inclusion of the D-wave is not necessary. This is also true for the diagrams with  $NN$   $P$ -wave final state interaction. The loops are evaluated using nonrelativistic kinematics even for the pion.

The calculation of the diagrams of Fig.3.1 were done using the rules of the diagram technique given in Appendix B. The explicit expressions for each individual term are:

**Diagram (a1)**

$$\mathcal{M}_{a1} = C_{N^2LO} \chi_1^\dagger (\sigma \cdot \vec{\epsilon}_\gamma) \sigma^j \epsilon_D^k \left[ u(q_2) \delta^{jk} - \frac{w(q_2)}{\sqrt{2}} (3 \hat{q}_2^j \hat{q}_2^k - \delta^{jk}) \right] \frac{\sigma_2}{\sqrt{2}} \chi_2^* - (1 \leftrightarrow 2), \quad (\text{E.7})$$

where  $C_{N^2LO} = 16\pi\sqrt{M}(M + m_\pi)E_{0+}$ ,  $\vec{q}_{1,2} = \vec{p}_{1,2} + \vec{q}_\gamma/2$ ,  $\hat{q}_{1,2} = \vec{q}_{1,2}/q_{1,2}$ , and  $\vec{\epsilon}_\gamma$  and  $\vec{\epsilon}_D$  are polarization vectors of the photon and the deuteron, respectively. The notation  $-(1 \leftrightarrow 2)$  points that one has to subtract the same term with spin and momentum variables of the two nucleons interchanged, in order to get properly anti-symmetrized amplitude.

Here  $u(p)$  and  $w(p)$  are the S-wave and D-wave components of the deuteron wave function defined in Appendix E.2.3. The expression  $\chi_1^\dagger \hat{O} \chi_2^*$  corresponds to the spin structure of the final  $NN$  pair:

$$\chi_1^\dagger (\sigma \cdot \epsilon_\gamma) (\sigma \cdot \epsilon_D) \frac{\sigma_2}{\sqrt{2}} \chi_2^* = (\epsilon_\gamma \cdot \epsilon_D) \left( \chi_1^\dagger \frac{\sigma_2}{\sqrt{2}} \chi_2^* \right) + i[\epsilon_\gamma \times \epsilon_D] \cdot \left( \chi_1^\dagger \vec{\sigma} \frac{\sigma_2}{\sqrt{2}} \chi_2^* \right) \quad (\text{E.8})$$

and analogously for the D-wave part. Here the first and second terms on the r.h.s. are the spin-singlet and spin-triplet contributions, respectively ( $\chi^\dagger \chi = 1$ ). Note that we do not write out explicitly the isospin part of the amplitude  $I = \varphi_1^\dagger \tau^- \tau^2 \varphi_2^*$ , which equals 1 in this case.

**Diagram (a2)**

$$\begin{aligned} \mathcal{M}_{a2} = C_{NNLO} \frac{1}{2M} \int \frac{d^3p}{(2\pi)^3} \left\{ \frac{\mathcal{M}_{NN}^0(\vec{p} + \vec{k}_\pi/2, \vec{p}_{12}, E_{12})}{(\vec{p} + \vec{k}_\pi/2)^2 - p_{12}^2 - i0} u(\vec{p} + \vec{q}_\gamma/2) (\vec{\epsilon}_\gamma \cdot \vec{\epsilon}_D) \left( \chi_1^\dagger \frac{\sigma_2}{\sqrt{2}} \chi_2^* \right) \right. \\ \left. + \frac{\mathcal{M}_{NN}^1(\vec{p} + \vec{k}_\pi/2, \vec{p}_{12}, E_{12})_{\alpha\beta}}{(\vec{p} + \vec{k}_\pi/2)^2 - p_{12}^2 - i0} u(\vec{p} + \vec{q}_\gamma/2) i[\epsilon_\gamma \times \epsilon_D]_\beta \left( \chi_1^\dagger \sigma_\alpha \frac{\sigma_2}{\sqrt{2}} \chi_2^* \right) \right\}, \quad (\text{E.9}) \end{aligned}$$

where  $\vec{p}_{12} = (\vec{p}_1 - \vec{p}_2)/2$  and the amplitudes  $\mathcal{M}_{NN}^L$  are related to the  $NN$  partial wave amplitudes with angular momentum  $L$  as given below in this subsection. The energy of the  $NN$  system is  $E_{12} = p_{12}^2/M$ . The formula for  $M_{a2}$  as given shows the contribution from the deuteron S-wave only. The inclusion of the D-wave in the convolution with  $^1S_0$   $NN$  final state interaction is done like in the expression for diagram (a1). Note that this diagram is antisymmetrized as well, but in this case the antisymmetrization reduces just to an additional factor of two, so we have written the resulting expression explicitly. The same is done for all diagrams with the half off-shell  $NN$  final state interaction, i.e. for the diagrams (b2), (c2), and (d2), and corresponding diagrams with pion higher partial waves.

The amplitudes  $\mathcal{M}_{NN}^L$  in this formula are related to the standard  $NN$  partial wave amplitudes  $f_S^{JL}$ , where  $J$  denotes the total angular momentum,  $L$  the angular momentum in the initial and final state (we do not consider couplings between partial waves with different angular momenta, e.g., the coupling of the  $^3P_2$  to the  $^3F_2$  partial wave), and  $S$

the total spin, through

$$\begin{aligned}\mathcal{M}_{NN}^0(\vec{p}, \vec{p}', E) &= 16\pi M f_0^{00}(p', p, E) \\ \mathcal{M}_{NN}^1(\vec{p}, \vec{p}', E)_{\alpha\beta} &= 16\pi M \sum_J \mathcal{R}_{\alpha\beta}^J f_1^{J1}(p', p, E).\end{aligned}\quad (\text{E.10})$$

The  $f_S^{JL}(p', p, E)$  are related on the mass shell to the partial phase shifts via

$$f_S^{JL}(p, p, p^2/M) = \frac{1}{2ip} \left( e^{2i\delta_S^{JL}} - 1 \right).$$

The products of the angular parts of the projectors for the various total angular momenta with  $L = L' = 1$  and for the  $S = 1$  read

$$\begin{aligned}\mathcal{R}_{\alpha\beta}^0 &= \hat{p}'_\alpha \hat{p}_\beta, \\ \mathcal{R}_{\alpha\beta}^1 &= \frac{3}{2} \epsilon^{\alpha\lambda\tau} \epsilon^{\beta\rho\tau} \hat{p}'_\lambda \hat{p}_\rho = \frac{3}{2} (\delta_{\alpha\beta}(\hat{p}, \hat{p}') - \hat{p}'_\beta \hat{p}_\alpha), \\ \mathcal{R}_{\alpha\beta}^2 &= \frac{3}{4} \left( \delta_{\lambda\alpha} \hat{p}'_\rho + \delta_{\rho\alpha} \hat{p}'_\lambda - \frac{2}{3} \delta_{\lambda\rho} \hat{p}'_\alpha \right) \left( \delta_{\lambda\beta} \hat{p}_\rho + \delta_{\rho\beta} \hat{p}_\lambda - \frac{2}{3} \delta_{\lambda\rho} \hat{p}_\beta \right) \\ &= \frac{3}{2} \left( \delta_{\alpha\beta}(\hat{p}, \hat{p}') + \hat{p}'_\beta \hat{p}_\alpha - \frac{2}{3} \hat{p}'_\alpha \hat{p}_\beta \right),\end{aligned}$$

where  $\hat{p} = \vec{p}/p$  and analogously for  $\hat{p}'$ .

### Diagram (b1)

The real part of the diagram (b1) renormalizes the bare vertex in the leading diagram (a1) resulting in the experimentally observed value  $E_0^+$  for  $\gamma p \rightarrow \pi^+ n$  process. Thus, the real part of this diagram is already included in the expression for diagram (a1). The imaginary part of (b1) is

$$\mathcal{M}_{b1} = iC_{LO} \frac{m_\pi}{8\pi(1 + m_\pi/M)f_\pi^2} u(\vec{p}_2 + \vec{q}_\gamma/2) k_{\pi N_1} \chi_1^\dagger(\vec{\sigma} \cdot \vec{\epsilon}_\gamma)(\vec{\sigma} \cdot \vec{\epsilon}_D) \frac{\sigma_2}{\sqrt{2}} \chi_2^* - (1 \leftrightarrow 2), \quad (\text{E.11})$$

where  $k_{\pi N_i} = |M\vec{k}_\pi - m_\pi \vec{p}_i|/(M + m_\pi)$  is the magnitude of the relative momentum of the final pion and the final nucleon with momentum  $p_i$  and  $C_{LO} = 4\sqrt{M}g_{\pi N e}/(\sqrt{2})$ .

### Diagram (c1)

$$\mathcal{M}_{c1} = -C_{LO} \frac{m_\pi}{2(1 + m_\pi/M)f_\pi^2} I_{c1} \chi_1^\dagger(\vec{\sigma} \cdot \vec{\epsilon}_\gamma)(\vec{\sigma} \cdot \vec{\epsilon}_D) \frac{\sigma_2}{\sqrt{2}} \chi_2^* - (1 \leftrightarrow 2), \quad (\text{E.12})$$

where the integral  $I_{c1}$  is

$$I_{c1} = \int \frac{d^3p}{(2\pi)^3} \frac{u(\vec{p} + \vec{q}_\gamma/2)}{k_{\pi N_1}^2 - (\vec{p} + \frac{M}{M+m_\pi} \vec{p}_1)^2 + i0}. \quad (\text{E.13})$$

**Diagram (b2)**

$$\mathcal{M}_{b_2} = C_{LO} \frac{1}{8Mf_\pi^2} I_{b_2}(\vec{\epsilon}_\gamma \cdot \vec{\epsilon}_D) \left( \chi_1^\dagger \frac{\sigma_2}{\sqrt{2}} \chi_2^* \right), \quad (\text{E.14})$$

with

$$I_{b_2} = \int \frac{d^3p d^3l}{(2\pi)^6} \frac{\mathcal{M}_{NN}^0(\vec{p} + \vec{k}_\pi/2, \vec{p}_{12}, E_{12})}{p_{12}^2 - (\vec{p} + \vec{k}_\pi/2)^2 + i0} \frac{u(\vec{p} + \vec{q}_\gamma/2)}{Q - \frac{p^2}{2M} - \frac{l^2}{2M} - \frac{(\vec{l} + \vec{p})^2}{2m_\pi} + i0} \quad (\text{E.15})$$

The integral with the  $\pi N$  loop, i.e. over  $d^3l$ , is divergent and has to be renormalized (cf. discussion of diagram (b1)). After renormalization it takes the form

$$I_{b_2} = \frac{-im_\pi}{2\pi(1+m_\pi/M)} \int \frac{d^3p}{(2\pi)^3} \frac{\mathcal{M}_{NN}^0(\vec{p} + \vec{k}_\pi/2, \vec{p}_{12}, E_{12})}{p_{12}^2 - (\vec{p} + \vec{k}_\pi/2)^2 + i0} u(\vec{p} + \vec{q}_\gamma/2) K(Q, p), \quad (\text{E.16})$$

where  $m_{\pi N} = m_\pi M / (M + m_\pi)$ ,  $\mu_N = M(M + m_\pi) / (2M + m_\pi)$ , and

$$K(Q, p) = \sqrt{2m_{\pi N}(Q - p^2/2\mu_N)}.$$

Note that the square root needs to be replaced by  $i\sqrt{2m_{\pi N}(p^2/2\mu_N - Q)}$  for negative arguments. Thus, we get a purely real, non-vanishing contribution from diagram (b2) even at production threshold.

**Diagram (c2)**

$$\mathcal{M}_{c_2} = C_{LO} \frac{1}{8Mf_\pi^2} I_{c_2}(\vec{\epsilon}_\gamma \cdot \vec{\epsilon}_D) \left( \chi_1^\dagger \frac{\sigma_2}{\sqrt{2}} \chi_2^* \right), \quad (\text{E.17})$$

with

$$I_{c_2} = \int \frac{d^3p d^3l}{(2\pi)^6} \frac{\mathcal{M}_{NN}^0(\vec{p} + \vec{k}_\pi/2, \vec{p}_{12}, E_{12})}{p_{12}^2 - (\vec{p} + \vec{k}_\pi/2)^2 + i0} \frac{u(\vec{l} + \vec{q}_\gamma/2)}{Q - \frac{p^2}{2M} - \frac{l^2}{2M} - \frac{(\vec{p} + \vec{l})^2}{2m_\pi} + i0}. \quad (\text{E.18})$$

The integral  $I_{c_2}$  develops an angle dependent three-body singularity as soon as we move away from the production threshold. Fortunately, for non-relativistic pions, it transformed into an angle independent one. Indeed, rewriting the denominator in  $I_{c_2}$  that creates the three-body singularity, as follows

$$Q - \frac{p^2}{2M} - \frac{l^2}{2M} - \frac{(\vec{p} + \vec{l})^2}{2m_\pi} = Q - \frac{p^2}{2\mu_N} - \frac{(\vec{l} + \frac{m_{\pi N}}{m_\pi} \vec{p})^2}{2m_{\pi N}},$$

and shifting the integration variable  $\vec{l}$  by  $\frac{m_{\pi N}}{m_\pi} \vec{p}$ , we get the integral over  $d^3l$  in Eq. (E.18) as

$$\int \frac{d^3l}{(2\pi)^3} \frac{u(\vec{l} + \vec{q}_\gamma/2)}{Q - \frac{l^2}{2M} - \frac{p^2}{2M} - \frac{(\vec{l} + \vec{p})^2}{2m_\pi} + i0} = 2m_{\pi N} \int \frac{d^3l}{(2\pi)^3} \frac{u(\vec{l} + \vec{q}_\gamma/2 - \frac{m_{\pi N}}{m_\pi} \vec{p})}{K^2(Q, p) - l^2 + i0},$$

from which one can immediately see that the moving three-body singularity turned to the frozen one – the pole position does not depend on  $\vec{l}$  angles. This is possible, because in our reaction the initial two nucleons are always off the mass shell – they form a bound state. Therefore, there is no additional propagator which can cause a singularity.

Furthermore, for non-relativistic pions and specific analytical parameterizations of the deuteron wave functions, the three body singularity can be integrated analytically. In particular, using the parameterization for the deuteron wave function (cf. Appendix E.2.3) we may write

$$\int \frac{d^3l}{(2\pi)^3} \frac{u(\vec{l} + \vec{q}_\gamma/2)}{Q - \frac{l^2}{2M} - \frac{p^2}{2M} - \frac{(\vec{l} + \vec{p})^2}{2m_\pi} + i0} = -\gamma_1 \sum_j \frac{C_j}{8\pi i r} \log \left( \frac{\beta_j - iK(Q, p) + ir}{\beta_j - iK(Q, p) - ir} \right) \quad (\text{E.19})$$

where  $\gamma_1 = \frac{2m_\pi}{1 + m_\pi/M}$  and  $\vec{r} = \frac{1}{1 + m_\pi/M} \vec{p} - \vec{q}_\gamma/2$ . The integration in Eq. (E.19) has been performed similarly to the case of diagram (a2): we applied an inverse Fourier transform separately to the deuteron wave function and to the Green's function. Then the integration over  $d^3l$  gives a delta-function, which kills one of the remaining three-dimensional integrations and the integral reduces to a sum of integrals of the type considered, e.g., in Ref.[108]. The three-body singularities of the diagrams (d1) and (d2) can be handled analogously. Also for the  $NN$  final state interaction the integration over one of the loops can be performed analytically after applying the procedure outlined in Refs. [121, 122] to the  $NN$  amplitudes, for they can then be represented in the same analytical form as the deuteron wave functions, cf. Appendix E.2.3 for details. Moreover, it turns out that in diagram (d2) one can perform analytically two of the three loop integrations, thus reducing the nine-dimensional integral to the three-dimensional one.

### Diagram (d1)

$$\mathcal{M}_{d_1} = C_{LO} \frac{1}{8M f_\pi^2} I_{d_1}(\vec{\epsilon}_\gamma \cdot \vec{\epsilon}_D) \left( \chi_1^\dagger \frac{\sigma_2}{\sqrt{2}} \chi_2^* \right) - (1 \leftrightarrow 2), \quad (\text{E.20})$$

with

$$I_{d_1} = \int \frac{d^3p d^3s}{(2\pi)^6} \frac{\mathcal{M}_{NN}^0(\vec{p} + \vec{s}/2, \vec{p}_2 + \vec{s}/2, E_{NN})}{M E_{NN} - (\vec{p}_2 + \vec{s}/2)^2 + i0} \frac{u(\vec{p} + \vec{q}/2)}{Q - \frac{p^2}{2M} - \frac{s^2}{2m_\pi} - \frac{(\vec{p} + \vec{s})^2}{2M} + i0}, \quad (\text{E.21})$$

where  $E_{NN} = Q - s^2/2\mu_\pi$  with  $\mu_\pi = 2Mm_\pi/(2M + m_\pi)$ .

### Diagram (d2)

$$\mathcal{M}_{d_2} = C_{LO} \frac{1}{16M f_\pi^2} I_{d_2}(\vec{\epsilon}_\gamma \cdot \vec{\epsilon}_D) \left( \chi_1^\dagger \frac{\sigma_2}{\sqrt{2}} \chi_2^* \right), \quad (\text{E.22})$$

with

$$\begin{aligned} I_{d_2} &= -\frac{1}{M} \int \frac{d^3l d^3s d^3p}{(2\pi)^9} \frac{\mathcal{M}_{NN}^0(\vec{p} + \vec{k}_\pi/2, \vec{p}_{12}, E_{12})}{p_{12}^2 - (\vec{p} + \vec{k}_\pi/2)^2 + i0} \\ &\times \frac{\mathcal{M}_{NN}^0(\vec{l} + \vec{s}/2, \vec{p} + \vec{s}/2, E_{NN})}{M E_{NN} - (\vec{p} + \vec{s}/2)^2 + i0} \frac{u(\vec{l} + \vec{q}/2)}{Q - \frac{l^2}{2M} - \frac{s^2}{2m_\pi} - \frac{(\vec{l} + \vec{s})^2}{2M} + i0}. \end{aligned} \quad (\text{E.23})$$

### Corrections to diagrams (a1) and (a2) from higher pion partial waves

We start from the explicit expression for the pion  $p$ -wave contribution (below labeled as  $(\pi-p)$ ) stemming from diagram (b) of Fig. 3.5. To implement this, the term  $(\vec{\sigma}\vec{\epsilon}_\gamma)$  in the expressions for diagram (a1) and (a2) of Fig. 3.1 (see above) needs to be replaced by  $(\vec{\sigma}\hat{q})(\vec{\epsilon}_\gamma\vec{k}_\pi)/m_\pi$ , where  $\hat{q} = \vec{q}_\gamma/q_\gamma$ . Thus we get

$$\mathcal{M}_{a1}^{(\pi-p)} = C_{LO} \frac{1}{m_\pi} (\vec{\epsilon}_\gamma \cdot \vec{k}_\pi) \chi_1^\dagger (\vec{\sigma} \cdot \hat{q}) (\vec{\sigma} \cdot \vec{\epsilon}_D) \frac{\sigma_2}{\sqrt{2}} \chi_2^* u(\vec{q}_2) - (1 \leftrightarrow 2)$$

for the diagram without final state interaction and

$$\begin{aligned} \mathcal{M}_{a2}^{(\pi-p)} &= -C_{LO} \frac{1}{m_\pi} (\vec{\epsilon}_\gamma \cdot \vec{k}_\pi) \frac{1}{2M} \left( \chi_1^\dagger \frac{\sigma_2}{\sqrt{2}} \chi_2^* \right) \\ &\times \int \frac{d^3p}{(2\pi)^3} \frac{\mathcal{M}_{NN}^0(\vec{p} + \vec{k}_\pi/2, \vec{p}_{12}, E_{12})}{p_{12}^2 - (\vec{p} + \vec{k}_\pi/2)^2 + i0} u(\vec{p} + \vec{q}_\gamma/2) (\hat{q} \cdot \vec{\epsilon}_D) \end{aligned} \quad (\text{E.24})$$

for the diagram with  $NN$  final state interaction.

Note, that when the pion is in a  $p$ -wave, only those terms where the  $NN$  final state is in an  $S$ -wave are to be considered. The simultaneous appearance of two  $p$ -waves in the final state is strongly suppressed by the centrifugal barrier. Our numerical calculations confirm this statement.

Using the vertex  $V_{\pi\gamma NN}^{(c)}$  given by Eq. (3.18) as input for the diagrams (a1) and (a2) of Fig. 3.1 one can get the corresponding contribution from the  $s$ - and  $u$ -channel nucleon pole diagrams (cf. diagrams (c) in Fig. 3.5) to our reaction as follows

$$\mathcal{M}^{\text{nuc-su}} = -\frac{C_{LO}}{2m_\pi M} \left\{ (A^{\text{nuc-su}} + F^{\text{nuc-su}}) \left( \chi_1^\dagger \frac{\sigma_2}{\sqrt{2}} \chi_2^* \right) + \vec{B}^{\text{nuc-su}} \cdot \left( \chi_1^\dagger \vec{\sigma} \frac{\sigma_2}{\sqrt{2}} \chi_2^* \right) \right\}, \quad (\text{E.25})$$

where

$$\begin{aligned} A^{\text{nuc-su}} &= u(\vec{q}_2) \left\{ 2(\vec{\epsilon}_\gamma \cdot \vec{p}_2)(\vec{k}_\pi \cdot \vec{\epsilon}_D) + (\mu_p + \mu_n) \left( (\vec{\epsilon}_\gamma \cdot \vec{k}_\pi)(\vec{q}_\gamma \cdot \vec{\epsilon}_D) - (\vec{q}_\gamma \cdot \vec{k}_\pi)(\vec{\epsilon}_\gamma \cdot \vec{\epsilon}_D) \right) \right\} \\ &+ (1 \leftrightarrow 2), \end{aligned} \quad (\text{E.26})$$

$$\begin{aligned} \vec{B}^{\text{nuc-su}} &= u(\vec{q}_2) \left\{ 2(\vec{\epsilon}_\gamma \cdot \vec{p}_2)[\vec{k}_\pi \times \vec{\epsilon}_D] + (\mu_p - \mu_n)(\vec{k}_\pi \cdot [\vec{\epsilon}_\gamma \times \vec{q}_\gamma]) \vec{\epsilon}_D \right. \\ &\left. + (\mu_p + \mu_n) \left( (\vec{\epsilon}_\gamma \cdot \vec{k}_\pi)[\vec{q}_\gamma \times \vec{\epsilon}_D] - (\vec{q}_\gamma \cdot \vec{k}_\pi)[\vec{\epsilon}_\gamma \times \vec{\epsilon}_D] \right) \right\} - (1 \leftrightarrow 2), \end{aligned} \quad (\text{E.27})$$

and  $F^{\text{nuc-su}}$  stands for the contributions from the diagrams with  $NN$  final state interaction:

$$F^{\text{nuc-su}} = (\mu_p + \mu_n) \left( (\vec{\epsilon}_\gamma \cdot \vec{k}_\pi)(\vec{q}_\gamma \cdot \vec{\epsilon}_D) - (\vec{q}_\gamma \cdot \vec{k}_\pi)(\vec{\epsilon}_\gamma \cdot \vec{\epsilon}_D) \right) F_1 - (\vec{k}_\pi \cdot \vec{\epsilon}_\gamma)(\vec{k}_\pi \cdot \vec{\epsilon}_D) F_2,$$



where

$$\begin{aligned}
F_1 &= -\frac{1}{2M} \int \frac{d^3p}{(2\pi)^3} \frac{\mathcal{M}_{NN}^0(\vec{p}+\vec{k}_\pi/2, \vec{p}_{12}, E_{12})}{p_{12}^2 - (\vec{p}+\vec{k}_\pi/2)^2 + i0} u(\vec{p}+\vec{q}_\gamma/2), \\
F_2 &= -\frac{1}{2M} \int \frac{d^3p}{(2\pi)^3} \frac{\mathcal{M}_{NN}^0(\vec{p}+\vec{k}_\pi/2, \vec{p}_{12}, E_{12})}{p_{12}^2 - (\vec{p}+\vec{k}_\pi/2)^2 + i0} u(\vec{p}+\vec{q}_\gamma/2) \\
&\quad \times \left( 1 - \frac{(\vec{p} + \vec{k}_\pi/2) \cdot (\vec{k}_\pi/2 - \vec{q}_\gamma/2)}{(\vec{k}_\pi/2 - \vec{q}_\gamma/2)^2} \right). \quad (\text{E.28})
\end{aligned}$$

### E.2.3 Parameterization of the $NN$ wave functions for CD-Bonn potential

Here we give the parameterization of the wave functions we used in the calculations of Chapter 3.

For the deuteron wave function, and for the  $nn$  scattering amplitudes that appear in the final-state interaction, we take those of the (charge dependent) CD-Bonn  $NN$  potential [87]. In particular, we utilize the analytic parameterization of the deuteron wave function provided in Ref. [87] which is given by

$$u(p) = \sqrt{4\pi} \sum_j C_j / (p^2 + m_j^2); \quad w(p) = \sqrt{4\pi} \sum_j D_j / (p^2 + m_j^2), \quad (\text{E.29})$$

with parameters listed in Table 20 of Ref [87]. The wave function is normalized according to

$$\int \frac{d^3p}{(2\pi)^3} (u^2(p) + w^2(p)) = 1. \quad (\text{E.30})$$

With this parameterization some of the diagrams can be evaluated analytically. In order to facilitate also an analytic evaluation of the diagrams involving the  $nn$  scattering amplitude, the CD-Bonn potential in the relevant partial waves ( $^1S_0$ ,  $^3P_0$ ,  $^3P_1$ ,  $^3P_2$ ) is cast into a separable representation by means of the so-called EST method [122]. The resulting rank 1 separable interactions exactly reproduce the on- and off-shell properties of the CD-Bonn potential at the chosen approximation energies ( $E_{Lab} = 0$  MeV for  $^1S_0$  and  $E_{Lab} = 30$  MeV for the  $P$  waves) [122] and they provide also an excellent approximation in a broad neighborhood of these energies. The form factors  $g(p)$  of these separable representations, that consist of the scattering solutions of the CD-Bonn potential at the specified approximation energies [122], are parameterized in analytical form,

$$g(p) = \sum_i c_i / (p^2 + \beta_i^2), \quad (\text{E.31})$$

for  $^1S_0$  and

$$g(p) = \sum_i c_i p / (p^2 + \beta_i^2)^2, \quad (\text{E.32})$$

for the  $P$  waves and the scattering amplitude is then given by

$$f(p, p'; k) = \frac{2\pi^2 M_N g(p)g(p')}{\pm 1 - M_N \int d^3q \frac{g^2(q)}{q^2 - k^2 - i0}}. \quad (\text{E.33})$$

Here the positive sign pertains to the  $^1S_0$ ,  $^3P_0$ , and  $^3P_2$  partial waves, and the negative sign to the  $^3P_1$  partial wave. The parameters  $c_i$  and  $\beta_i$  for each partial wave are listed in Table E.1.

	$^1S_0$		$^3P_0$	
	$c_i$ [MeV]	$\beta_i$ [MeV]	$c_i$ [MeV <sup>2</sup> ]	$\beta_i$ [MeV]
1	-1.6788489	105.64868	5.6091364	87.697924
2	38.388276	208.40749	-47.29225	196.68429
3	-204.19687	311.16630	-52680.52	305.67065
4	-265.30647	413.92511	25403.007	414.65702
5	604.93218	516.68392	140524.04	523.64338
	$^3P_1$		$^3P_2$	
	$c_i$ [MeV <sup>2</sup> ]	$\beta_i$ [MeV]	$c_i$ [MeV <sup>2</sup> ]	$\beta_i$ [MeV]
1	-26.122635	151.92170	-169.35853	139.80616
2	107984.65	329.53539	12651.165	243.67922
3	-1107050.3	507.14909	-149453.00	347.55228
4	3691951.8	684.76279	405215.24	451.42534
5	-3372798.2	862.37648	-389168.49	555.29840

Table E.1: Parameters of the form factors for the separable representation of the CD-Bonn potential.

## E.2.4 Parameterization of the ChPT $NN$ wave functions

In this section we provide parameterization of the ChPT  $NN$  wave functions that were used in the analysis of Chapter 4. For the sake of completeness we repeat here explicit expressions for the amplitudes that appear at leading order in the calculation for  $\gamma d \rightarrow \pi^+ nn$ . As outlined in Chapter 4 these expressions can be used directly in the analysis of the data for extraction of neutron-neutron scattering length  $a_{nn}$ , once available. In addition, they should also prove useful for the design of the corresponding experiment. Note, as outlined in Chapter 4, only near  $\theta_r = 90^\circ$  the leading order calculation gives a sufficiently accurate representation of the spectra. At all other angles one should use the complete calculation.

At leading order only diagrams  $a1$  and  $a2$  of Fig. 3.1 contribute. Since only the momentum dependence of the amplitudes is relevant for the experimental analysis we

drop an overall factor compared to Section E.2. The corresponding amplitudes read:

$$M_{a1}^s = \left( u(\vec{p}_r - \vec{k}_\pi/2 + \vec{q}_\gamma/2) + u(-\vec{p}_r - \vec{k}_\pi/2 + \vec{q}_\gamma/2) \right) \quad (\text{E.34})$$

$$M_{a1}^t = \left( u(\vec{p}_r - \vec{k}_\pi/2 + \vec{q}_\gamma/2) - u(-\vec{p}_r - \vec{k}_\pi/2 + \vec{q}_\gamma/2) \right) \quad (\text{E.35})$$

$$\begin{aligned} M_{a2} &= 8\pi \frac{f^{\text{on}}(p_r)}{g(p_r)} \int \frac{d^3 p}{(2\pi)^3} \frac{u(\vec{p} - \vec{k}_\pi/2 + \vec{q}_\gamma/2) g(p)}{p^2 - p_r^2 - i0} \\ &= \frac{f^{\text{on}}(p_r)}{iq_{\pi\gamma} g(p_r)} \sum_{ij} \frac{C_i D_j}{p_r^2 + \beta_j^2} \ln \left( \frac{\alpha_i - ip_r + iq_{\pi\gamma}}{\alpha_i - ip_r - iq_{\pi\gamma}} \cdot \frac{\alpha_i + \beta_j - iq_{\pi\gamma}}{\alpha_i + \beta_j + iq_{\pi\gamma}} \right) \end{aligned} \quad (\text{E.36})$$

with  $u(\vec{p})$  being the  $S$ -wave part of the deuteron wave function in momentum space. We checked by explicit calculations that the inclusion of the deuteron  $D$ -wave changes only the absolute scale of the differential cross sections but not its momentum dependence. Thus, the  $D$ -wave contribution is not taken into account in this parameterization. The quantity  $q_{\pi\gamma}$  is defined as  $q_{\pi\gamma} = |\vec{k}_\pi - \vec{q}_\gamma|/2$ . The labels  $s$  and  $t$  stand for spin singlet and triplet final two-nucleon state—we do not write out the corresponding spin structures. We take into account only the  $^1S_0$  partial wave in the final state interaction.

To derive the expression for  $M_{a2}$  we used the fact that the neutron–neutron scattering amplitude can be represented to high accuracy in separable form [82, 122]. The neutron–neutron scattering amplitude,  $f(p, k; E)$ , can be written in half off-shell kinematics as

$$f(p, k; k^2/M) = \frac{2\pi^2 M g(p) g(k)}{1 - M \int d^3 q \frac{g^2(q)}{q^2 - k^2 - i0}} = f^{\text{on}}(k) \frac{g(p)}{g(k)}, \quad (\text{E.37})$$

where the corresponding on-shell amplitude  $f^{\text{on}}(k)$  can then be expressed in terms of the scattering phase-shifts through

$$f^{\text{on}}(k) = f(k, k; k^2/M) = \frac{1}{k \cot \delta(k) - ik}.$$

For small momenta one can use the effective range expansion for  $k \cot \delta(k) = -1/a_{nn} + r_{nn}k^2/2 + O(k^4)$ , in agreement with Eq. (4.1). Here  $a_{nn}$  is the parameter to be fitted to the data and  $r_{nn} = 2.76$  fm. We checked that changing the value of  $r_{nn}$  within the bounds allowed ( $\pm 0.1$  fm [133]) leads to negligible effects on the extraction of the scattering length. In this way we expressed the matrix element explicitly in terms of the scattering length. We checked that the ratio  $g(p)/g(k)$  in Eq. (E.37) does not change when we vary the scattering length within acceptable range bounds.

In order to evaluate the convolution of the deuteron wave function with the  $nn$  final state interaction analytically, we needed to employ the following parameterizations for the  $^1S_0$   $nn$  form factor  $g(p)$  (see Eq. (E.37)) and the  $S$ -wave deuteron wave function

$$g(p) = \sum_i \frac{D_i}{p^2 + \beta_i^2}; \quad u(p) = \sum_i \frac{C_i}{p^2 + \alpha_i^2};$$

where the parameters corresponding to the ChPT calculation at N<sup>2</sup>LO with cut offs  $\{\Lambda, \tilde{\Lambda}\} = \{550 \text{ MeV}, 600 \text{ MeV}\}$  (see Ref [18] for details) are listed in Table E.2. Note,

the coefficients in the parameterization of the wave function have to fulfill the relation  $\sum C_i = 0$  in order to ensure the regularity of the deuteron wave function at the origin in coordinate space [168].

The squared and averaged amplitude to be used in the expression for the differential cross section, defined in Eq. (4.3) is

$$\overline{|\mathcal{M}(p_r, \theta_r, \varphi_r, \theta_\pi, \varphi_\pi)_{\text{fit}}|^2} = |M_{a1}^S + M_{a2}|^2 + 2|M_{a1}^T|^2. \quad (\text{E.38})$$

In a fit to data two parameters are to be adjusted, namely the overall normalization  $C$  of Eq. (4.3) and the object of desire,  $a_{nn}$ .

	$^1S_0$ form factor		S-wave deuteron w.f.	
	$\beta_i$ [MeV]	$D_i$ [MeV]	$\alpha_i$ [MeV]	$C_i$ [MeV $^{1/2}$ ]
1	164.53278	31.101228	45.334919	43.543212
2	246.85751	-1310.3056	242.66091	-35.643003
3	329.18224	9455.9603	439.98691	419.25214
4	411.50697	-9666.0268	637.31291	-1833.4708
5	493.83170	-55571.615	834.63891	-3710.8173
6	576.15643	64600.071	1031.9649	24903.150
7	658.48116	149128.85	1229.2909	-31673.576
8	740.80589	-84844.967	1426.6169	26476.636
9	823.13062	-295594.17	1623.9429	-118733.48
10	905.45536	-30332.710	1821.2689	259759.15
11	987.78009	560829.89	2018.5949	-223816.07
12	1070.1048	-307006.25	2215.9209	$C_{12}$

Table E.2: Parameters of the  $^1S_0$  form factor and the S-wave deuteron wave function for the separable representation of the N<sup>2</sup>LO chiral  $NN$  potential. Here  $C_{12} = -\sum_{i=1}^{11} C_i$ .

## E.3 Reaction $pp \rightarrow d\pi^+$

### E.3.1 Observables

The differential cross-section is given by

$$d\sigma = \frac{k_\pi}{64\pi^2 s p} |M_{fi}|^2 d\Omega_{\vec{k}_\pi}, \quad (\text{E.39})$$

where  $k_\pi$  is the momentum of final pion in the center-of-mass frame,  $s \approx 2M + m_\pi$  is the total center-of-mass frame energy of the system, and  $p$  is the momentum of one of initial protons. The relevant diagrams for  $s$ - and  $p$ -wave pion production near threshold are shown on Fig. E.1.

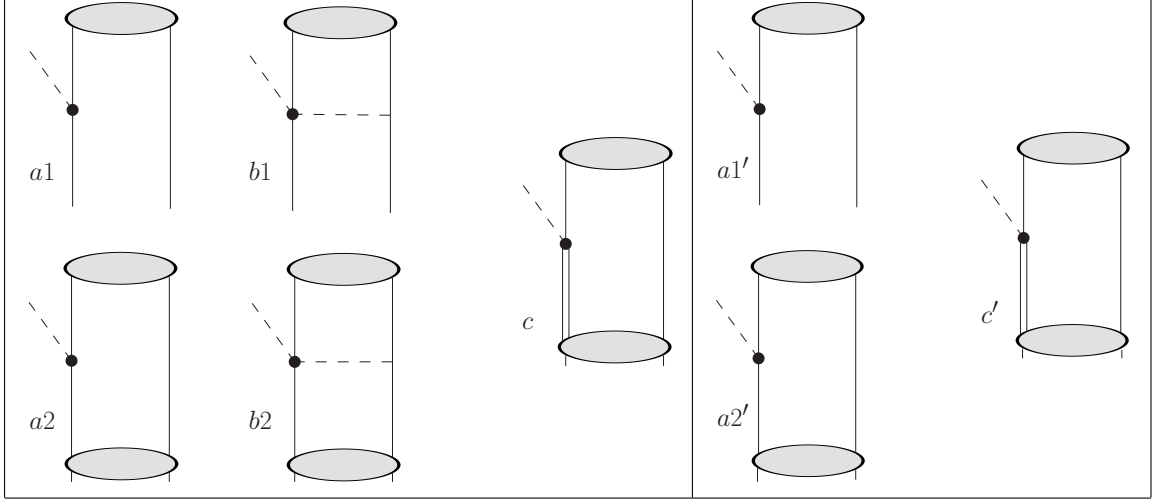


Figure E.1: Diagrams for reaction  $pp \rightarrow d\pi^+$ . Left panel corresponds to  $s$ -wave pion production, right panel — to  $p$ -wave pion production. Blobs denote the deuteron wave function and the initial state interaction amplitude.

### E.3.2 Matrix elements for $s$ -wave pion production

Here we present the explicit expressions for the amplitudes corresponding to the diagrams in Fig. E.1 for  $s$ -wave pion production. All calculations are done in the center-of-mass system of the reaction.

At threshold the  $s$ -wave pion production in the reaction  $pp \rightarrow d\pi^+$  corresponds to the  ${}^3P_1$  spin-angular state of initial protons. This corresponds to the following spin-angular dependence of the amplitude common for all diagrams  $a1$ ,  $a2$ ,  $b1$ ,  $b2$ ,  $c$  of Fig. E.1:

$$\mathcal{M}_{3P_1} = \chi_2^t \frac{\sigma^2}{\sqrt{2}} \vec{\sigma} \cdot [\hat{p} \times \vec{\epsilon}_d^*] \chi_1 A, \quad (\text{E.40})$$

where  $\vec{p}$  is the relative momentum between the two initial protons,  $\hat{p} = \vec{p}/p$ ,  $\chi_{1,2}$  ( $\chi_{1,2}^t$ ) are spinors (transposed spinors) of initial protons,  $\varphi_{1,2}$  ( $\varphi_{1,2}^t$ ) are their isospinors (transposed isospinors),  $\vec{\epsilon}_d^*$  is the polarization of the final deuteron. We provide below expressions for quantities  $A$  in which spin-angular part is factorized. In addition, we do not write out the isospin factor  $\varphi_2^t \tau^2 \tau^- \varphi_1 = 1$  for two initial protons.

#### Diagram a1

$$A_{a1} = -C_s \frac{p f_\pi^2}{M} \left( u(p) + w(p)/\sqrt{2} \right), \quad (\text{E.41})$$

where  $C_s = 4g_A m_\pi M \sqrt{2M}/f_\pi^3$ , The quantities  $u(p)$  and  $w(p)$  are the  $S$ - and  $D$ -wave components of the deuteron wave functions in order.

**Diagram a2**

$$A_{a2} = -C_s 4\pi \int \frac{d^3 s}{(2\pi)^3} \frac{u(s) + w(s)/\sqrt{2}}{s^2 - p^2 - i0} \frac{s f_\pi^2}{M} f^{3P_1}(p, s, E_p), \quad (\text{E.42})$$

where  $E_p = p^2/M$ , and  $f^{3P_1}(p, s, p^2/M)$  is the half-offshell  $NN$ -scattering amplitude which is related with the scattering phase  $\delta^{3P_1}$  as follows:

$$f^{3P_1}(p, p, E_p) = \frac{1}{2ip} \left( e^{2i\delta^{3P_1}} - 1 \right). \quad (\text{E.43})$$

**Diagram b1**

The calculation according the diagram technique rules gives for the amplitude of this diagram (including the spin-angular part):

$$\mathcal{M}_{b1} = C_s \chi_2^t \sigma^2 \int \frac{d^3 q}{(2\pi)^3} \frac{(\vec{\sigma} \cdot (\vec{q} + \vec{p})) (\vec{\Gamma}^*(\vec{q}) \cdot \vec{\sigma})}{(\vec{q} + \vec{p})^2 + \tilde{m}_\pi^2} \chi_1, \quad (\text{E.44})$$

where the fixed kinematics approximation was used, and therefore  $\tilde{m}_\pi^2 = m_\pi^2 - (p^2/2M)^2 = 3/4 m_\pi^2$ ;  $\vec{\Gamma}(\vec{q}) = \vec{\epsilon}_d u(q)/\sqrt{2} - (3(\vec{\epsilon}_d \cdot \hat{q})\hat{q} - \vec{\epsilon}_d) w(q)/2$  with  $\hat{q} = \vec{q}/q$  is the deuteron vertex. It appears then convenient to apply inverse Fourier transform to this expression according with

$$\begin{aligned} \int \frac{d^3 q}{(2\pi)^3} \frac{(\vec{q} + \vec{p})^j \Gamma^{k*}(\vec{q})}{(\vec{q} + \vec{p})^2 + \tilde{m}_\pi^2} &= \int \frac{d^3 q}{(2\pi)^3} d^3 r d^3 r' f^j(\vec{r}) \Gamma^{k*}(\vec{r}') e^{-i\vec{q}\cdot\vec{r}' - i(\vec{q}+\vec{p})\cdot\vec{r}} \\ &= \int d^3 r f^j(\vec{r}) \Gamma^{k*}(\vec{r}) e^{-i\vec{p}\cdot\vec{r}}, \end{aligned} \quad (\text{E.45})$$

where  $\Gamma^{k*}(\vec{r})$  is the deuteron vertex in coordinate space, and  $f^j(\vec{r})$  is given by

$$f^j(\vec{r}) = \int \frac{d^3 q}{(2\pi)^3} e^{i\vec{q}\cdot\vec{r}} \frac{q^j}{q^2 + \tilde{m}_\pi^2} = -i \frac{\partial}{\partial r^j} \frac{e^{-\tilde{m}_\pi r}}{4\pi r} = i \hat{r}^j \frac{e^{-\tilde{m}_\pi r}}{4\pi r} \left( \tilde{m}_\pi + \frac{1}{r} \right)$$

with  $\hat{r} = \vec{r}/r$ . Using this formula and performing the angular integration, after which the spin-angular part of the amplitude factorizes according with Eq. (E.40) we end up with the following expression for  $A_{b1}$ :

$$A_{b1} = C_s \int_0^\infty dr \left( \frac{\cos pr}{pr} - \frac{\sin pr}{p^2 r^2} \right) \left( \tilde{m}_\pi + \frac{1}{r} \right) e^{-\tilde{m}_\pi r} \left( u(r) + w(r)/\sqrt{2} \right). \quad (\text{E.46})$$

Note that here  $u(r)$  and  $w(r)$  are the  $S$  and  $D$  components of the deuteron wave function in coordinate space related with their momentum space counterparts according to

$$\int \frac{d^3 q}{(2\pi)^3} \vec{\Gamma}(\vec{q}) e^{i\vec{q}\cdot\vec{r}} = \vec{\Gamma}(\vec{r}) = \vec{\epsilon}_d u(r)/\sqrt{2} - (3(\vec{\epsilon}_d \cdot \hat{r})\hat{r} - \vec{\epsilon}_d) w(r)/2. \quad (\text{E.47})$$

**Diagram b2**

$$A_{b2} = C_s 4\pi \int \frac{d^3 s}{(2\pi)^3} \frac{f^{3P_1}(p, s, E_p)}{s^2 - p^2 - i0} I(s), \quad (\text{E.48})$$

where

$$I(s) = \int_0^\infty dr \left( \frac{\cos sr}{sr} - \frac{\sin sr}{s^2 r^2} \right) \left( \tilde{m}_\pi + \frac{1}{r} \right) e^{-\tilde{m}_\pi r} \left( u(r) + w(r)/\sqrt{2} \right)$$

is the integral corresponding to the diagram b1 ( $u(r)$  and  $w(r)$  are the  $S$  and  $D$  components of the deuteron wave function in coordinate space).

**Diagram c**

$$\begin{aligned} A_c = C_{s\Delta} 4\pi \int \frac{d^3 s}{(2\pi)^3} \frac{s}{s^2 - 2\mu_{N\Delta}(m_\pi - \delta)} & \left( \sqrt{\frac{3}{5}} w(s) f_{N\Delta}^{5F_1}(p, s, E_p) \right. \\ & + \frac{1}{3} \sqrt{\frac{1}{5}} \left( 5u(s) - w(s)/\sqrt{2} \right) f_{N\Delta}^{5P_1}(p, s, E_p) \\ & \left. + \frac{1}{3} \left( u(s) + w(s)/\sqrt{2} \right) f_{N\Delta}^{3P_1}(p, s, E_p) \right), \quad (\text{E.49}) \end{aligned}$$

where  $C_{s\Delta} = 4h_A M \sqrt{2MM_\Delta(M + M_\Delta)}/f_\pi$ ,  $\mu_{N\Delta}$  is the nucleon-Delta reduced mass,  $\delta = M_\Delta - M$ , and  $f_{N\Delta}(p, s, E_p)$  are  $NN \rightarrow N\Delta$  transition amplitudes in corresponding partial waves (see Appendix B for the details).

**E.3.3 Matrix elements for  $p$ -wave pion production**

Here we present the explicit expressions for the amplitudes corresponding to the diagrams in Fig. E.1 for  $s$ -wave pion production. Again, all calculations are done in the center-of-mass system of the reaction. For the case of the  $p$ -wave pion production near threshold in the reaction  $pp \rightarrow d\pi^+$  there are two possible spin-angular states of initial protons, namely  $^1S_0$  and  $^1D_2$ . This corresponds to the following spin-angular dependences of the amplitude for diagrams  $a1'$ ,  $a2'$ ,  $c'$  of Fig. E.1:

$$\mathcal{M}^{1S_0} = \chi_2^t \frac{\sigma^2}{\sqrt{2}} \chi_1 \left( \vec{k}_\pi \cdot \vec{\epsilon}_d^* \right) A^{1S_0} \quad (\text{E.50})$$

$$\mathcal{M}^{1D_2} = \chi_2^t \frac{\sigma^2}{\sqrt{2}} \chi_1 \left( 3(\vec{k}_\pi \cdot \hat{p})(\vec{\epsilon}_d^* \cdot \hat{p}) - (\vec{k}_\pi \cdot \vec{\epsilon}_d^*) \right) A^{1D_2}, \quad (\text{E.51})$$

where  $\vec{k}_\pi$  is the momentum of the final pion, and other notations are the same as for  $s$ -wave pion production. We give below expressions for quantities  $A$  in which spin-angular part is factorized. We again do not write out the isospin factor  $\varphi_2^t \tau^2 \tau^- \varphi_1 = 1$  for two initial protons.

**Diagram a1'**

$$\begin{aligned}
A_{a'_1}^{1S_0} &= C_p u(p) \\
A_{a'_1}^{1D_2} &= -C_p w(p)/\sqrt{2},
\end{aligned} \tag{E.52}$$

where  $C_p = 4i g_A M \sqrt{2M}/f_\pi$ .

**Diagram a2'**

$$\begin{aligned}
A_{a'_2}^{1S_0} &= C_p 4\pi \int \frac{d^3 s}{(2\pi)^3} \frac{u(s) f^{1S_0}(p, s, E_p)}{s^2 - p^2 - i0} \\
A_{a'_2}^{1D_2} &= -C_p 4\pi \int \frac{d^3 s}{(2\pi)^3} \frac{w(s) f^{1D_2}(p, s, E_p)}{s^2 - p^2 - i0},
\end{aligned} \tag{E.53}$$

where  $f(p, s, E_p)$  are the half-offshell scattering amplitudes in the corresponding partial waves.

**Diagram c'**

$$\begin{aligned}
A_{c'}^{1S_0} &= -\sqrt{\frac{2}{9}} C_{p\Delta} 4\pi \int \frac{d^3 s}{(2\pi)^3} \frac{w(s) f_{N\Delta}^{5D_0}(p, s, E_p)}{s^2 - 2\mu_{N\Delta}(m_\pi - \delta)} \\
A_{c'}^{1D_2} &= \frac{2}{3} \sqrt{5} C_{p\Delta} 4\pi \int \frac{d^3 s}{(2\pi)^3} \frac{1}{s^2 - 2\mu_{N\Delta}(m_\pi - \delta)} \left( \frac{1}{2} u(s) f_{N\Delta}^{5S_2}(p, s, E_p) \right. \\
&\quad \left. - \frac{1}{4} \sqrt{\frac{7}{5}} w(s) f_{N\Delta}^{5D_2}(p, s, E_p) \right),
\end{aligned} \tag{E.54}$$

where  $C_{p\Delta} = 4i h_A M \sqrt{2MM_\Delta(M + M_\Delta)}/f_\pi$ ,  $\mu_{N\Delta}$  is the nucleon-Delta reduced mass,  $\delta = M_\Delta - M$ , and  $f_{N\Delta}(p, s, E_p)$  are  $NN \rightarrow N\Delta$  transition amplitudes in corresponding partial waves (see Appendix B for the details).

**E.4 Corrections to  $a_{\pi d}$** 

In this appendix we present the explicit expressions for the amplitudes depicted in Table 5.1. Note, in accordance with the definition used for dispersive corrections as well as the power counting, we only keep those amplitudes that contain two-nucleon cuts in time-ordered perturbation theory (TOPT). Especially, we dropped the so-called stretched boxes.

Using the same labels as in the table, one finds for the corresponding corrections to the  $\pi d$  scattering length for sum of the diagrams without the  $NN$  interaction in the intermediate state:

$$a_{\pi d}^{disp} = \frac{g_A^2 m_\pi^2}{6\pi f_\pi^6 (1+m_\pi/2M)(1+q_0/2M)} \int \frac{d^3 q}{(2\pi)^3} \frac{q^2 (F_1(q) + F_2(q))^2}{q^2/M - q_0 - i\epsilon} \tag{E.55}$$



where

$$F_1(q) = \left( I_1(q) - \frac{3}{2\sqrt{2}} I_2(q) \right) \quad \text{and} \quad F_2(q) = \frac{f_\pi^2}{M} \left( u(q) + \frac{w(q)}{\sqrt{2}} \right). \quad (\text{E.56})$$

Here  $I_1$  and  $I_2$  are the integrals that correspond to the overlap of the deuteron wave function ( $u(q)$  and  $w(q)$  for the S- and D-waves, respectively) with the one pion exchange operator

$$\begin{aligned} I_1(q) &= - \int \frac{d^3p}{(2\pi)^3} \frac{(1 + (\vec{p} \cdot \vec{q})/q^2)}{2\omega_{\vec{p}+\vec{q}}} \left( u(p) + \frac{w(p)}{\sqrt{2}} \right) \left( \frac{1}{P_1} + \frac{1}{P_2} \right), \\ I_2(q) &= - \int \frac{d^3p}{(2\pi)^3} \frac{(1 - (\vec{p} \cdot \vec{q})^2/(p^2q^2))}{2\omega_{\vec{p}+\vec{q}}} w(p) \left( \frac{1}{P_1} + \frac{1}{P_2} \right) \end{aligned} \quad (\text{E.57})$$

where  $P_1$  and  $P_2$  correspond to the TOPT components of the pion propagator  $P_1 = q_0 - \omega_{\vec{p}+\vec{q}} - (p^2 + q^2)/2M$  and  $P_2 = -\omega_{\vec{p}+\vec{q}} - (p^2 + q^2)/2M$  with  $\omega_{\vec{q}} = \sqrt{\vec{q}^2 + m_\pi^2}$ .

The expressions for the amplitudes with the intermediate state interaction read

$$\begin{aligned} a_{\pi d}^{disp, NN} &= 4\pi \frac{g_A^2 m_\pi^2}{6\pi f_\pi^6 (1+m_\pi/2M)(1+q_0/2M)} \int \frac{d^3q}{(2\pi)^3} \frac{d^3l}{(2\pi)^3} \frac{q(F_1(q)+F_2(q))}{q^2/M - q_0 - i\epsilon} \\ &\quad \times f^{3P_1}(q, l, q_0) \frac{l(F_1(l)+F_2(l))}{l^2/M - q_0 - i\epsilon}. \end{aligned} \quad (\text{E.58})$$

The diagrams of Table 5.1 can be easily matched to the individual terms under the integrals in the r.h.s. of Eqs. (E.55) and (E.58): type 1 contains  $F_1^2$ , type 2 contains  $F_2^2$ , whereas the interference terms of type 3 contain  $2F_1F_2$ . For the direct terms, labeled as  $d$  in the table, one needs to take  $q_0 = m_\pi$  and for the crossed terms, labeled as  $c$  in the table,  $q_0 = -m_\pi$ .

All integrals are evaluated up to a sharp momentum cut-off of 1 GeV. All higher momentum components are to be absorbed in a counter term that is to be included at order  $\chi^2$  (c.f. discussion in section 2). By enlarging the cut-off by a factor of 20 we checked that the integrals change by less than 10 % — fully in line with the power counting.

# Appendix F

## Loops for $NN \rightarrow NN\pi$

In this appendix we provide details of evaluation of loop diagrams of Fig. 2.3.

In what follows we consider the spin-isospin matrix elements of the transition operator projected on the final state with spin 1 and isospin 0, which corresponds to the reaction  $pp \rightarrow d\pi^+$ . The spin matrix element of the transition operator for a general process is written in the following form:

$$\mathcal{T} = \chi_{1'}^\dagger \hat{O}_1(\vec{p}, \vec{p}') \chi_1 \chi_{2'}^\dagger \hat{O}_2(\vec{p}, \vec{p}') \chi_2 + \chi_{1'}^\dagger \hat{O}_2(-\vec{p}, -\vec{p}') \chi_1 \chi_{2'}^\dagger \hat{O}_1(-\vec{p}, -\vec{p}') \chi_2, \quad (\text{F.1})$$

where  $\chi_{1,2}$  ( $\chi_{1',2'}$ ) are the spinors of initial (final) nucleons, and  $\hat{O}_{1,2}(\vec{q})$  are spin operators ( $2 \times 2$  matrices), which depend on the relative momenta of the initial and final  $NN$  pairs —  $\vec{p}$  and  $\vec{p}'$ . The second term in the r.h.s. of Eq. (F.1) corresponds to the interchange of the two nucleon lines. The part of the spin matrix element that corresponds to the spin 1 final state is given by (see also Appendices C and B)

$$\mathcal{T}_1 = \sum \mathcal{T} \times \chi_{2'}^t \frac{\sigma^2}{\sqrt{2}} (\vec{\sigma} \cdot \vec{\epsilon}) \chi_{1'}, \quad (\text{F.2})$$

where the sum is performed over the polarizations of the final nucleons,  $\chi^t$  stands for the transposed spinor, and  $\vec{\epsilon}$  is the polarization vector that corresponds to the final  $S = 1$  state (for instance, the (complex conjugated) deuteron polarization vector in the case of deuteron final state). Eq. (F.2) gives a simple recipe how to calculate the spin projected matrix element. Analogous consideration are applied to projection of the isospin matrix element — the only difference is that the isospin of the channel that we are investigating is 0, therefore instead of an isospin analog of  $(\vec{\sigma} \cdot \vec{\epsilon})$  one should insert a unit matrix. The corresponding calculations for the reaction  $pp \rightarrow pp\pi^0$  are also done in full analogy.

Let us as an illustration calculate the spin and isospin projected matrix element corresponding to isovector rescattering pion production, *i.e.* to diagram (a) of Fig. 2.2. We show in Fig. F.1 the definition of relevant momenta and energies. The corresponding matrix element reads (note that we include the recoil correction to the WT term fully in line with arguments of Chapter 2):

$$\begin{aligned} \mathcal{T}^{\text{WT}} &= \chi_{1'}^\dagger \varphi_{1'}^\dagger \frac{M}{2f_\pi^2} \left( (q_0 + m_\pi) - \frac{1}{2M} [(-\vec{p} + \vec{p}') \cdot (\vec{p} + \vec{p}')] \right) \epsilon^{bac} \tau^c \chi_1 \varphi_1 \\ &\quad \times \chi_{2'}^\dagger \varphi_{2'}^\dagger \frac{g_A M}{f_\pi} [-\vec{\sigma} \cdot (-\vec{p} + \vec{p}')] \tau^b \chi_2 \varphi_2 \times \frac{1}{q_\mu^2 - m_\pi^2}, \end{aligned} \quad (\text{F.3})$$

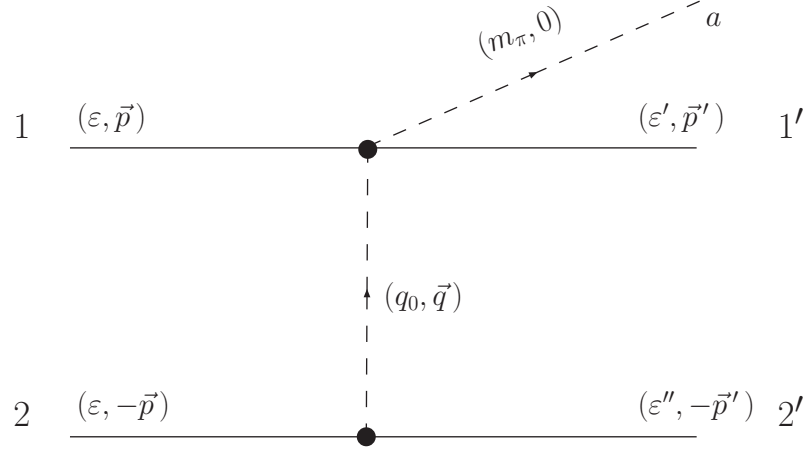


Figure F.1: Definition of momenta and energies for diagram (a) of Fig. 2.2. Labels 1 and 2 (1' and 2') denote the initial (final) nucleons. Label "a" corresponds to isospin of outgoing pion. Zeroth and spatial components of four-vectors are shown explicitly. The four-vector  $q$  is  $q = (\varepsilon - \varepsilon'', \vec{p}' - \vec{p})$ .

where  $\varphi$ 's stand for the corresponding isospinors, and  $q = (\varepsilon - \varepsilon'', \vec{p}' - \vec{p})$ . Simplifying this expression using  $\vec{p}^2/2M = m_\pi/2$  at threshold and neglecting the energies of final nucleons (which is justified as soon as we suppose the momenta of final nucleons to be small compared to  $p \sim \sqrt{m_\pi M}$ ), we get

$$\begin{aligned} \mathcal{T}^{\text{WT}} &= \chi_{1'}^\dagger \varphi_{1'}^\dagger \frac{M}{2f_\pi^2} (2m_\pi) \epsilon^{bac} \tau^c \chi_1 \varphi_1 \\ &\quad \times \chi_{2'}^\dagger \varphi_{2'}^\dagger \frac{g_A M}{f_\pi} \vec{\sigma} \cdot (\vec{p} - \vec{p}') \tau^b \chi_2 \varphi_2 \times \frac{-1}{(\vec{p} - \vec{p}')^2 + 3m_\pi^2/4}. \end{aligned} \quad (\text{F.4})$$

Adding the corresponding term with the interchanged nucleon lines (*i.e.* with interchanged spinor indices 1 and 2, 1' and 2' and changed signs of the momenta in Eq. (F.4)) and performing spin and isospin projection according to Eq. (F.2), we end up with the following result:

$$\begin{aligned} \mathcal{T}_1^{\text{WT}} &= \frac{g_A m_\pi M^2}{f_\pi^3} \frac{1}{(\vec{p} - \vec{p}')^2 + 3m_\pi^2/4} \\ &\quad \times \chi_2^t \frac{\sigma^2}{\sqrt{2}} ((\vec{\sigma} \cdot (\vec{p} - \vec{p}'))(\vec{\sigma} \cdot \vec{\epsilon}) - (\vec{\sigma} \cdot \vec{\epsilon})(\vec{\sigma} \cdot (\vec{p} - \vec{p}'))) \chi_1 \\ &\quad \times \varphi_2^t \frac{\tau^2}{\sqrt{2}} \tau^b \tau^c \varphi_1 \epsilon^{abc}, \end{aligned} \quad (\text{F.5})$$

which finally gives

$$\mathcal{T}_1^{\text{WT}} = -\frac{4g_A m_\pi M^2}{f_\pi^3} \frac{1}{(\vec{p} - \vec{p}')^2 + 3m_\pi^2/4} \chi_2^t \frac{\sigma^2}{\sqrt{2}} \vec{\sigma} \cdot [(\vec{p} - \vec{p}') \times \vec{\epsilon}] \chi_1 \varphi_2^t \frac{\tau^2}{\sqrt{2}} \tau^a \varphi_1 \quad (\text{F.6})$$

— cf. also Eqs. (2.5), (2.6); note that  $\varphi_2^t \tau^2 \tau^a \varphi_1 / \sqrt{2} = 1$  for the reaction  $pp \rightarrow d\pi^+$ . Note an additional factor of two in this equation compared with  $A_{10}^{2a}$  in Eq. (2.6), which

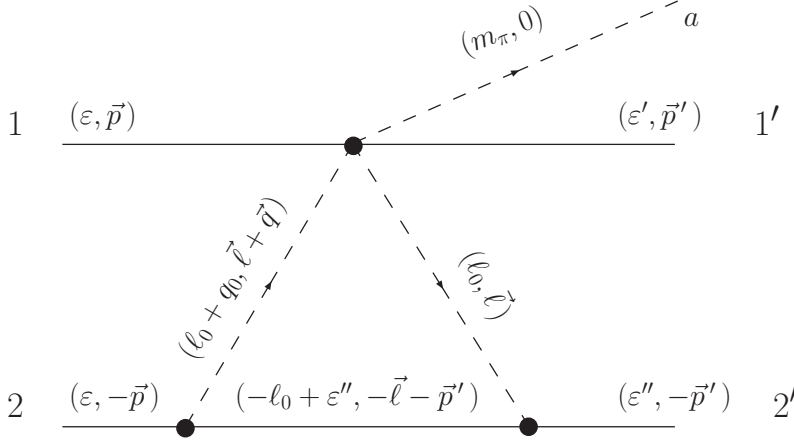


Figure F.2: Definition of momenta and energies for diagram (b) of Fig. 2.3. The notations are as in Fig. F.1.

comes due to the fact that here we calculated the sum of the production amplitudes on each nucleon — those are equal and give the factor of two.

We turn now to the evaluation of pion loops shown in Fig. 2.3. Let us start with diagram (b) of that figure. The definition of momenta is shown on Fig. F.2. The matrix element corresponding to this figure reads

$$\begin{aligned} \mathcal{T}^{3b} = & \frac{g_A^3 M^3}{2f_\pi^5} \int \frac{d^4\ell}{(2\pi)^4} \frac{1}{[\ell_\mu^2 - m_\pi^2 + i\gamma][(\ell + q)_\mu^2 - m_\pi^2 + i\gamma][2M(-\ell_0 + \varepsilon'') - (\vec{\ell} + \vec{p}')^2 + i\gamma]} \\ & \times \chi_1^\dagger \varphi_1^\dagger [\tau^a \delta^{bc} (\vec{\sigma} \cdot \vec{q}) + \tau^b \delta^{ac} (\vec{\sigma} \cdot (\vec{\ell} + \vec{q})) - \tau^c \delta^{ab} (\vec{\sigma} \cdot \vec{\ell})] \chi_1 \varphi_1 \\ & \times \chi_2^\dagger \varphi_2^\dagger (\vec{\sigma} \cdot \vec{\ell}) (\vec{\sigma} \cdot (\vec{\ell} + \vec{q})) \tau^b \tau^c \chi_2 \varphi_2. \end{aligned} \quad (\text{F.7})$$

Adding to this expression the result of interchange of the nucleon lines and using Eq. (F.2), after straightforward but somewhat tedious calculations one gets the projected on the final state with spin 1 and isospin 0 matrix element — in full analogy with the calculation for the isovector rescattering. Note that in doing so we neglected the energies of final nucleons and also momentum of the final nucleon in the nucleon propagator, since its magnitude is supposed to be much smaller than typical value of  $\ell \sim p$ . Notice that according to these prescriptions  $q_0 = p^2/2m$ . The resulting expression for  $\mathcal{T}_1^{3b}$  reads:

$$\begin{aligned} \mathcal{T}_1^{3b} = & -\frac{i g_A^3 M^2}{f_\pi^5} \int \frac{d^4\ell}{(2\pi)^4} \frac{1}{[\ell_\mu^2 - m_\pi^2 + i\gamma][(\ell + q)_\mu^2 - m_\pi^2 + i\gamma][-\ell_0 - \frac{\ell^2}{2M} + i\gamma]} \\ & \times \chi_2^t \frac{\sigma^2}{\sqrt{2}} \left\{ (\vec{\ell} \cdot (\vec{\ell} + \vec{q})) (\vec{\sigma} \cdot [(3\vec{q} + 2\vec{\ell}) \times \vec{\epsilon}]) + 2(\vec{\sigma} \cdot [\vec{q} \times \vec{\ell}]) (\vec{\epsilon} \cdot \vec{\ell}) + 2(\vec{\sigma} \cdot \vec{\ell}) (\vec{\ell} \cdot [\vec{\epsilon} \times \vec{q}]) \right. \\ & \left. + 3(\vec{\sigma} \cdot [\vec{q} \times \vec{\ell}]) (\vec{\epsilon} \cdot \vec{q}) + 3(\vec{\sigma} \cdot \vec{q}) (\vec{\ell} \cdot [\vec{\epsilon} \times \vec{q}]) \right\} \chi_1 \varphi_2^t \frac{\tau^2}{\sqrt{2}} \tau^a \varphi_1. \end{aligned} \quad (\text{F.8})$$

There are two different tensor structures formed by components of vector  $\vec{\ell}$  that appear in the four last terms in the curly brackets in Eq. (F.8), namely  $\ell^i \ell^j$  and  $\ell^k$ , contracted

with constant vectors that can be taken out of the integral sign. Since the only vector that enters the integral over  $d^3\ell$  is  $\vec{q}$ , we can substitute these structures according to the following:

$$\ell^k \rightarrow q^k \frac{\vec{\ell} \cdot \vec{q}}{q^2}, \quad \ell^i \ell^j \rightarrow \frac{1}{2} \left( 3 \frac{(\vec{\ell} \cdot \vec{q})^2}{q^4} - \frac{\ell^2}{q^2} \right) q^i q^j + \frac{1}{2} \left( \frac{\ell^2}{q^2} - \frac{(\vec{\ell} \cdot \vec{q})^2}{q^4} \right) q^2 \delta^{ij}$$

— this is a consequence of the rotational invariance. The last two terms in the curly brackets in Eq. (F.8) therefore appear to be proportional to  $\epsilon^{ijk} q^i q^j$  and thus give zero, whereas the second and the third terms cancel each other. The vector  $3\vec{q} + 2\vec{\ell}$  that enters the vector product in the first term in the curly brackets is also substituted as  $3\vec{q} + 2\vec{\ell} = \vec{q}(3 + 2\vec{\ell} \cdot \vec{q}/q^2)$ . The result of these operations is:

$$\begin{aligned} \mathcal{T}_1^{3b} &= -\frac{i g_A^3 M^2}{f_\pi^5} \int \frac{d^4\ell}{(2\pi)^4} \frac{(\vec{\ell} \cdot (\vec{\ell} + \vec{q}))(3 + 2\vec{\ell} \cdot \vec{q}/q^2)}{[\ell_\mu^2 - m_\pi^2 + i\gamma][(\ell + q)_\mu^2 - m_\pi^2 + i\gamma][-\ell_0 - \frac{\ell^2}{2M} + i\gamma]} \\ &\quad \times \chi_2^t \frac{\sigma^2}{\sqrt{2}} (\vec{\sigma} \cdot [\vec{q} \times \vec{\epsilon}]) \chi_1 \varphi_2^t \frac{\tau^2}{\sqrt{2}} \tau^a \varphi_1. \end{aligned} \quad (\text{F.9})$$

This expression can be further simplified. First, taking the integral over  $d\ell_0$  gives

$$\int \frac{d\ell_0}{2\pi} \frac{1}{[\ell_\mu^2 - m_\pi^2 + i\gamma][(\ell + q)_\mu^2 - m_\pi^2 + i\gamma][-\ell_0 - \frac{\ell^2}{2M} + i\gamma]} = \frac{-i}{2\omega_\ell^2 \omega_{\ell+\vec{q}}^2}, \quad (\text{F.10})$$

where  $\omega_\ell = \sqrt{\ell^2 + m_\pi^2}$  and analogously for  $\omega_{\ell+\vec{q}}$ , and we neglected  $q_0$  compared to  $\omega_{\ell+\vec{q}}$ . Then we note that

$$\vec{\ell} \cdot (\vec{\ell} + \vec{q}) = \frac{1}{2} \left( (\vec{\ell} + \vec{q})^2 + \ell^2 - q^2 \right), \quad (\text{F.11})$$

and therefore the following equality is justified:

$$\frac{\vec{\ell} \cdot (\vec{\ell} + \vec{q})}{2\omega_\ell^2 \omega_{\ell+\vec{q}}^2} = \frac{1}{2} \left( \frac{1}{2\omega_\ell^2} + \frac{1}{2\omega_{\ell+\vec{q}}^2} + \frac{-q^2 - 2m_\pi^2}{2\omega_\ell^2 \omega_{\ell+\vec{q}}^2} \right). \quad (\text{F.12})$$

Using this equation, the integral from Eq. (F.8) can be rewritten in the form

$$\begin{aligned} I &= \int \frac{d^4\ell}{(2\pi)^4} \frac{(\vec{\ell} \cdot (\vec{\ell} + \vec{q}))(3 + 2\vec{\ell} \cdot \vec{q}/q^2)}{[\ell_\mu^2 - m_\pi^2 + i\gamma][(\ell + q)_\mu^2 - m_\pi^2 + i\gamma][-\ell_0 - \frac{\ell^2}{2M} + i\gamma]} \\ &= -\frac{i}{2} \int \frac{d^3\ell}{(2\pi)^3} \left( 3 + 2 \frac{\vec{\ell} \cdot \vec{q}}{q^2} \right) \left[ \frac{1}{2\omega_\ell^2} + \frac{1}{2\omega_{\ell+\vec{q}}^2} + \frac{-q^2}{2\omega_\ell^2 \omega_{\ell+\vec{q}}^2} \right] \\ &\quad + \text{higher orders in } \chi_\pi, \end{aligned} \quad (\text{F.13})$$

where we also neglected the term  $2m_\pi^2$  compared to  $q^2$ . After an appropriate shift of the integration variable we obtain for the integral  $I$  the following expression:

$$I = -i \int \frac{d^3\ell}{(2\pi)^3} \left[ \frac{1 + \vec{\ell} \cdot \vec{q}/q^2}{\omega_\ell^2} - q^2 \frac{3 + 2\vec{\ell} \cdot \vec{q}/q^2}{4\omega_\ell^2 \omega_{\ell+\vec{q}}^2} \right]. \quad (\text{F.14})$$

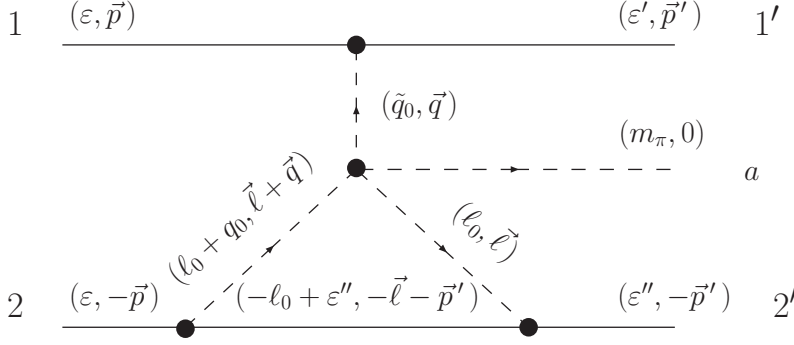


Figure F.3: Definition of momenta and energies for diagram (c) of Fig. 2.3. Here  $\tilde{q}_0 = \epsilon' - \epsilon$ . The remaining notations are as in Fig. F.1.

Since the first term in the integrand does not depend on large transfer momentum  $q$  for the integral over the angles from  $\vec{\ell} \cdot \vec{q}$  is zero, we state that typical momenta  $\ell$  in the corresponding part of the integral should be of order  $m_\pi$ , whereas the second part of the integral depends on  $q$  non-trivially (which can be seen after the integration over the angles), and typical values of  $\ell$  are of order  $q \sim \sqrt{m_\pi M}$  in this case, according to the general counting rules. Note also that the second integral converges. We then substitute all  $\ell$ 's by their typical values to obtain an estimate — as is usually done in counting — and get  $I \sim m_\pi$  for the first term in Eq. (F.14) and  $I \sim q$  for the second. Therefore up to higher orders in  $\chi_\pi$

$$I = i \int \frac{d^3 \ell}{(2\pi)^3} \left[ q^2 \frac{3 + 2 \vec{\ell} \cdot \vec{q} / q^2}{4\omega_\ell^2 \omega_{\ell+\vec{q}}^2} \right]. \quad (\text{F.15})$$

Eq. (F.15) means that we can substitute  $\vec{\ell} \cdot (\vec{\ell} + \vec{q}) = -q^2/2 + (\text{higher orders in } \chi_\pi)$  in the initial expression for  $\mathcal{T}_1^{3b}$  in Eq. (F.8). Furthermore, we can conclude on the same grounds that the substitution  $\vec{\ell} \cdot \vec{q} = -q^2/2 + (\text{higher orders in } \chi_\pi)$  is also justified.

Collecting all arguments given above, we are now able to rewrite Eq. (F.8) as

$$\begin{aligned} \mathcal{T}_1^{3b} &= \frac{2i q^2 g_A^3 M^2}{4f_\pi^5} \int \frac{d^4 \ell}{(2\pi)^4} \frac{1}{[\ell_\mu^2 - m_\pi^2 + i\gamma][(\ell + q)_\mu^2 - m_\pi^2 + i\gamma][-\ell_0 + i\gamma]} \\ &\quad \times 2 \chi_2^t \frac{\sigma^2}{\sqrt{2}} (\vec{\sigma} \cdot [\vec{q} \times \vec{\epsilon}]) \chi_1 \varphi_2^t \frac{\tau^2}{\sqrt{2}} \tau^a \varphi_1 \\ &= -2 \frac{g_A^3 M^2}{4f_\pi^5} (\vec{p} - \vec{p}')^2 I_0(|\vec{p} - \vec{p}'|^2) \times 2 \chi_2^t \frac{\sigma^2}{\sqrt{2}} (\vec{\sigma} \cdot [(\vec{p} - \vec{p}') \times \vec{\epsilon}]) \chi_1 \varphi_2^t \frac{\tau^2}{\sqrt{2}} \tau^a \varphi_1 \\ &\quad + \text{terms of higher orders in } \chi_\pi \end{aligned} \quad (\text{F.16})$$

— cf. Eqs. (2.5), (2.8); we again returned here to the integral over  $d^4 \ell$  in order to match it to the integral  $I_0$  defined in Eq. (2.7). Note again the extra factor of two compared to Eq. (2.8).

We turn now to the evaluation of diagram (c) of Fig. 2.3. The momenta and energies

are defined in Fig. F.3. The matrix element corresponding to this figure reads

$$\begin{aligned}
\mathcal{T}^{3c} = & -\frac{g_A^3 M^3}{f_\pi^5} \int \frac{d^4 \ell}{(2\pi)^4} \frac{1}{[\ell_\mu^2 - m_\pi^2 + i\gamma][(\ell + q)_\mu^2 - m_\pi^2 + i\gamma][2M(-\ell_0 + \varepsilon'') - (\vec{\ell} + \vec{p}')^2 + i\gamma]} \\
& \times \chi_1^\dagger \varphi_1^\dagger (\vec{\sigma} \cdot \vec{q}) \tau^d \chi_1 \varphi_1 \chi_2^\dagger \varphi_2^\dagger (\vec{\sigma} \cdot \vec{\ell}) (\vec{\sigma} \cdot (\vec{\ell} + \vec{q})) \tau^b \tau^c \chi_2 \varphi_2 \\
& \times [\delta^{ac} \delta^{bd} [(\ell + q)_\mu^2 - m_\pi^2 + 2m_\pi(\ell_0 + q_0)] + \delta^{ab} \delta^{cd} [\ell_\mu^2 - m_\pi^2 + 2m_\pi \ell_0] \\
& + \delta^{ad} \delta^{bc} [(m_\pi + \tilde{q}_0)^2 - \vec{q}^2 - m_\pi^2]] / (\tilde{q}_0^2 - \vec{q}^2 - m_\pi^2). \tag{F.17}
\end{aligned}$$

After adding to this expression the result of the interchange of the two nucleon lines and projection on final spin 1 and isospin 0, one gets (we again neglected the energies of final nucleons and the momentum of the final nucleon in the nucleon propagator):

$$\begin{aligned}
\mathcal{T}_1^{3c} = & -\frac{i g_A^3 M^2}{2 f_\pi^5} \int \frac{d^4 \ell}{(2\pi)^4} \frac{1}{[\ell_\mu^2 - m_\pi^2 + i\gamma][(\ell + q)_\mu^2 - m_\pi^2 + i\gamma][-\ell_0 - \frac{\ell^2}{2M} + i\gamma]} \\
& \times \frac{3[(\ell + q)_\mu^2 - m_\pi^2 + 2m_\pi(\ell_0 + q_0)] - [\ell_\mu^2 - m_\pi^2 + 2m_\pi \ell_0] + 3[(m_\pi + \tilde{q}_0)^2 - \vec{q}^2 - m_\pi^2]}{(\tilde{q}_0^2 - \vec{q}^2 - m_\pi^2)} \\
& \times \chi_2^t \frac{\sigma^2}{\sqrt{2}} \left\{ 2(\vec{\ell} \cdot (\vec{\ell} + \vec{q})) (\vec{\sigma} \cdot [\vec{\epsilon} \times \vec{q}]) + 2(\vec{\epsilon} \cdot \vec{q}) (\vec{\sigma} \cdot [\vec{q} \times \vec{\ell}]) + (\vec{\sigma} \cdot \vec{q}) (\vec{q} \cdot [\vec{\ell} \times \vec{\epsilon}]) \right\} \chi_1 \\
& \times \varphi_2^t \frac{\tau^2}{\sqrt{2}} \tau^a \varphi_1. \tag{F.18}
\end{aligned}$$

In full analogy to the calculation that we performed above for diagram (b) of Fig. 2.3, only the first term in the curly brackets in Eq. (F.18) gives a nonzero contribution. Replacing again  $\vec{\ell} \cdot (\vec{\ell} + \vec{q})$  by  $-q^2/2$  and neglecting all contributions of higher orders analogously to what was done for diagram (b) of Fig. 2.3, we arrive to the following result for  $\mathcal{T}_1^{3c}$ :

$$\begin{aligned}
\mathcal{T}_1^{3c} = & -\frac{3iq^2 g_A^3 M^2}{4f_\pi^5} \int \frac{d^4 \ell}{(2\pi)^4} \frac{1}{[\ell_\mu^2 - m_\pi^2 + i\gamma][(\ell + q)_\mu^2 - m_\pi^2 + i\gamma][-\ell_0 + i\gamma]} \\
& \times 2\chi_2^t \frac{\sigma^2}{\sqrt{2}} (\vec{\sigma} \cdot [\vec{\epsilon} \times \vec{q}]) \chi_1 \varphi_2^t \frac{\tau^2}{\sqrt{2}} \tau^a \varphi_1 \\
= & 3 \frac{g_A^3 M^2}{4f_\pi^5} (\vec{p} - \vec{p}')^2 I_0(|\vec{p} - \vec{p}'|^2) \times 2\chi_2^t \frac{\sigma^2}{\sqrt{2}} (\vec{\sigma} \cdot [(\vec{p} - \vec{p}') \times \vec{\epsilon}]) \chi_1 \varphi_2^t \frac{\tau^2}{\sqrt{2}} \tau^a \varphi_1 \\
& + \text{terms of higher orders in } \chi_\pi \tag{F.19}
\end{aligned}$$

— compare with Eqs. (2.5), (2.8). Note again the extra factor of two.

The calculation of diagrams (a) and (d) of Fig. 2.3 is performed analogously to the calculations presented in this appendix. The essential details on how to treat the WT vertex and nucleon propagators in diagrams (a) of that figure are given in Chapter 2.

# Bibliography

- [1] E. Gardner and C. M. G. Lattes. *Science*, **107**:270, 1948.
- [2] E. Gardner, C. M. G. Lattes, and W. Barkas. *Phys. Rev.*, **74**:1558, 1948.
- [3] H. Yukawa. Nobel Lecture, 1949.
- [4] H. Yukawa. *Proc. Phys. Math. Soc. (Japan)*, **17**:48, 1935.
- [5] R. Machleidt, K. Holinde, and C. Elster. The Bonn meson exchange model for the nucleon nucleon interaction. *Phys. Rept.*, **149**:1–89, 1987.
- [6] S. Weinberg. Phenomenological Lagrangians. *Physica A*, **96**:327, 1979.
- [7] J. Gasser and H. Leutwyler. Chiral perturbation theory to one loop. *Ann. Phys.*, **158**:142, 1984.
- [8] J. Gasser and H. Leutwyler. Chiral perturbation theory: Expansions in the mass of the strange quark. *Nucl. Phys. B*, **250**:465, 1985.
- [9] E. Jenkins and A. V. Manohar. Baryon chiral perturbation theory using a heavy fermion Lagrangian. *Phys. Lett. B*, **255**:558–562, 1991.
- [10] V. Bernard, N. Kaiser, J. Kambor, and U.-G. Meißner. Chiral structure of the nucleon. *Nucl. Phys. B*, **388**:315–345, 1992.
- [11] V. Bernard, N. Kaiser, and U.-G. Meißner. Chiral dynamics in nucleons and nuclei. *Int. J. Mod. Phys. E*, **4**:193–346, 1995.
- [12] G. Colangelo, J. Gasser, and H. Leutwyler.  $\pi\pi$  scattering. *Nucl. Phys. B*, **603**:125–179, 2001.
- [13] N. Fettes and U.-G. Meißner. Complete analysis of pion nucleon scattering in chiral perturbation theory to third order. *Nucl. Phys. A*, **693**:693–709, 2001.
- [14] C. Ordonez, L. Ray, and U. van Kolck. Nucleon-nucleon potential from an effective chiral lagrangian. *Phys. Rev. Lett.*, **72**:1982–1985, 1994.
- [15] C. Ordonez, L. Ray, and U. van Kolck. The two-nucleon potential from chiral lagrangians. *Phys. Rev. C*, **53**:2086–2105, 1996.
- [16] S. R. Beane, P. F. Bedaque, W. C. Haxton, D. R. Phillips, and M. J. Savage. From hadrons to nuclei: Crossing the border. 2000.



- [17] E. Epelbaum, W. Glöckle, and U.-G. Meißner. Nuclear forces from chiral Lagrangians using the method of unitary transformation. I: Formalism. *Nucl. Phys. A*, **637**:107–134, 1998.
- [18] E. Epelbaum, W. Glöckle, and U.-G. Meißner. The two-nucleon system at next-to-next-to-next-to-leading order. *Nucl. Phys. A*, **747**:362–424, 2005.
- [19] E. Epelbaum. Few-nucleon forces and systems in chiral effective field theory. *Prog. Part. Nucl. Phys.*, **57**:654–741, 2006.
- [20] E. Epelbaum et al. Three-nucleon forces from chiral effective field theory. *Phys. Rev. C*, **66**:064001, 2002.
- [21] A. K. Opper et al. Charge symmetry breaking in  $np \rightarrow d\pi^0$ . *Phys. Rev. Lett.*, **91**:212302, 2003.
- [22] C. Hanhart. Meson production in nucleon nucleon collisions close to the threshold. *Phys. Rept.*, **397**:155–256, 2004.
- [23] J. M. Laget. Pion photoproduction on few body systems. *Phys. Rept.*, **69**:1–84, 1981.
- [24] H. Arenhövel, E. M. Darwish, A. Fix, and M. Schwamb. Present status of electromagnetic reactions on the deuteron above pion threshold. *Mod. Phys. Lett. A*, **18**:190–199, 2003.
- [25] H. Krebs, V. Bernard, and U.-G. Meißner. Near threshold neutral pion electroproduction on deuterium in chiral perturbation theory. *Nucl. Phys. A*, **713**:405–437, 2003.
- [26] H. Krebs, V. Bernard, and U.-G. Meißner. Improved analysis of neutral pion electroproduction off deuterium in chiral perturbation theory. *Eur. Phys. J. A*, **22**:503–514, 2004.
- [27] A. Fix and H. Arenhovel. Incoherent pion photoproduction on the deuteron with polarization observables. ii. influence of final state rescattering. *Phys. Rev. C*, **72**:064005, 2005.
- [28] T. D. Cohen, J. L. Friar, G. A. Miller, and U. van Kolck. The  $pp \rightarrow pp\pi^0$  reaction near threshold: A chiral power counting approach. *Phys. Rev. C*, **53**:2661–2673, 1996.
- [29] C. da Rocha, G. Miller, and U. van Kolck. The  $NN \rightarrow NN\pi^+$  reaction near threshold in a chiral power counting approach. *Phys. Rev. C*, **61**:034613, 2000.
- [30] C. Hanhart and N. Kaiser. Complete next-to-leading order calculation for pion production in nucleon nucleon collisions at threshold. *Phys. Rev. C*, **66**:054005, 2002.
- [31] A. Gårdestig, D. R. Phillips, and Ch. Elster. The near threshold  $NN \rightarrow d\pi$  reaction in chiral perturbation theory. *Phys. Rev. C*, **73**:024002, 2006.

- [32] V. Baru, C. Hanhart, A. E. Kudryavtsev, and U.-G. Meißner. The role of the nucleon recoil in low-energy meson nucleus reactions. *Phys. Lett. B*, **589**:118–124, 2004.
- [33] V. Bernard, N. Kaiser, and U.-G. Meißner. Chiral corrections to the Kroll-Ruderman theorem. *Phys. Lett. B*, **383**:116–120, 1996.
- [34] E. Epelbaum, W. Glöckle, and U.-G. Meißner. Improving the convergence of the chiral expansion for nuclear forces. I: Peripheral phases. *Eur. Phys. J. A*, **19**:125–137, 2004.
- [35] H. Leutwyler. Chiral dynamics. In M. Shifman, editor, *At the Frontier of Particle Physics: Handbook of QCD. Boris Ioffe Festschrift*, volume 1, page 271. World Scientific, 2000. (hep-ph/0008124).
- [36] H. Leutwyler. Principles of Chiral Perturbation Theory. Bern University Preprint BUTP-94/13 (hep-ph/9406283).
- [37] E. Epelbaum. *The Nucleon–Nucleon Interaction in a Chiral Effective Field Theory*. PhD thesis, Ruhr–Universität Bochum, 2000.
- [38] S. L. Adler. Axial vector vertex in spinor electrodynamics. *Phys. Rev.*, **177**:2426–2438, 1969.
- [39] J. S. Bell and R. Jackiw. A PCAC puzzle:  $\pi^0 \rightarrow \gamma\gamma$  in the sigma model. *Nuovo Cim. A*, **60**:47–61, 1969.
- [40] W. M. Yao et al. Review of particle physics. *J. Phys. G*, **33**:1–1232, 2006.
- [41] J. Goldstone. Field theories with superconductor solutions. *Nuovo Cim.*, **19**:154–164, 1961.
- [42] J. Goldstone, A. Salam, and S. Weinberg. Broken symmetries. *Phys. Rev.*, **127**:965–970, 1962.
- [43] S. Weinberg. *The Quantum Theory of Fields*, volume 2. Cambridge University Press, 1996.
- [44] S. Weinberg. Nonlinear realizations of chiral symmetry. *Phys. Rev.*, **166**:1568–1577, 1968.
- [45] S. Coleman, J. Wess, and B. Zumino. Structure of phenomenological lagrangians. i. *Phys. Rev.*, **177**:2239–2247, 1969.
- [46] C. G. Callan, S. Coleman, J. Wess, and B. Zumino. Structure of phenomenological lagrangians. ii. *Phys. Rev.*, **177**:2247–2250, 1969.
- [47] M. Gell-Mann, R. J. Oakes, and B. Renner. Behavior of current divergences under  $SU(3) \times SU(3)$ . *Phys. Rev.*, **175**:2195–2199, 1968.

- [48] A. Manohar and H. Georgi. Chiral quarks and the nonrelativistic quark model. *Nucl. Phys. B*, **234**:189, 1984.
- [49] J. Gasser, M. E. Sainio, and A. Svarc. Nucleons with chiral loops. *Nucl. Phys. B*, **307**:779, 1988.
- [50] S. Weinberg. Nuclear forces from chiral lagrangians. *Phys. Lett. B*, **251**:288–292, 1990.
- [51] S. Weinberg. Effective chiral lagrangians for nucleon - pion interactions and nuclear forces. *Nucl. Phys. B*, **363**:3–18, 1991.
- [52] S. Weinberg. Three body interactions among nucleons and pions. *Phys. Lett. B*, **295**:114–121, 1992.
- [53] E. J. Stephenson et al. Observation of the charge symmetry breaking  $d + d \rightarrow {}^4\text{He} + \pi^0$  reaction near threshold. *Phys. Rev. Lett.*, **91**:142302, 2003.
- [54] U. van Kolck, J. A. Niskanen, and G. A. Miller. Charge symmetry violation in  $pn \rightarrow d\pi^0$  as a test of chiral effective field theory. *Phys. Lett. B*, **493**:65–72, 2000.
- [55] A. Gårdestig et al. Survey of charge symmetry breaking operators for  $dd \rightarrow \alpha\pi^0$ . *Phys. Rev. C*, **69**:044606, 2004.
- [56] D. S. Koltun and A. Reitan. Production and absorption of  $S$ -wave pions at low energy by two nucleons. *Phys. Rev.*, **141**(4):1413–1418, 1966.
- [57] H. O. Meyer, M. A. Ross, R. E. Pollock, A. Berdoz, F. Dohrmann, J. E. Goodwin, M. G. Minty, H. Nann, P. V. Pancella, S. F. Pate, B. v. Przewoski, T. Rinckel, and F. Sperisen. Total cross section for  $p + p \rightarrow p + p + \pi^0$  near threshold measured with the Indiana Cooler. *Phys. Rev. Lett.*, **65**:2846–2849, 1990.
- [58] G. A. Miller and P. U. Sauer. Total cross-section for  $p + p \rightarrow p + p + \pi^0$  near threshold. *Phys. Rev. C*, **44**:1725–1727, 1991.
- [59] J. A. Niskanen. Energy dependence of the  $pp \rightarrow (pp) S$ -wave  $\pi^0$  total cross-section. *Phys. Lett. B*, **289**:227–232, 1992.
- [60] C. Hanhart, J. Haidenbauer, O. Krehl, and J. Speth. Role of the delta isobar in the reaction  $NN \rightarrow NN\pi$  near threshold. *Phys. Lett. B*, **444**:25–31, 1998.
- [61] T. S. H. Lee and D. O. Riska. Short range exchange contributions to the cross-section for  $pp \rightarrow pp\pi^0$  near threshold. *Phys. Rev. Lett.*, **70**:2237–2240, 1993.
- [62] C. J. Horowitz, H. O. Meyer, and David K. Griegel. Role of heavy meson exchange in pion production near threshold. *Phys. Rev. C*, **49**:1337–1346, 1994.
- [63] E. Hernandez and E. Oset. Off-shell  $\pi N$  amplitude and the  $pp \rightarrow pp\pi^0$  reaction near threshold. *Phys. Lett. B*, **350**:158–162, 1995.

- [64] C. Hanhart, J. Haidenbauer, A. Reuber, C. Schutz, and J. Speth. The reaction  $pp \rightarrow pp\pi^0$  near threshold. *Phys. Lett. B*, **358**:21–26, 1995.
- [65] C. Hanhart, J. Haidenbauer, M. Hoffmann, U.-G. Meißner, and J. Speth. The reactions  $pp \rightarrow pp\pi^0$  and  $pp \rightarrow d\pi^+$  at threshold: The role of the isoscalar  $\pi N$  scattering amplitude. *Phys. Lett. B*, **424**:8–14, 1998.
- [66] C. Hanhart, J. Haidenbauer, O. Krehl, and J. Speth. Polarization phenomena in the reaction  $NN \rightarrow NN\pi$  near threshold. *Phys. Rev. C*, **61**:064008, 2000.
- [67] U. van Kolck, G. A. Miller, and D. O. Riska. Meson exchange and pion rescattering contributions to the cross section for  $pp \rightarrow pp\pi^0$ . *Phys. Lett. B*, **388**:679–685, 1996.
- [68] M. T. Peña, D. O. Riska, and A. Stadler. Nucleon resonance effects in  $pp \rightarrow pp\pi^0$  near threshold. *Phys. Rev. C*, **60**:045201, 1999.
- [69] C. J. Horowitz. Role of heavy meson exchange in near threshold  $NN \rightarrow d\pi$ . *Phys. Rev. C*, **48**:2920–2925, 1993.
- [70] J. A. Niskanen. Comment on 'role of heavy meson exchange in near threshold  $NN \rightarrow d\pi$ '. *Phys. Rev. C*, **53**:526–528, 1996.
- [71] B. Y. Park, F. Myhrer, J. R. Morones, T. Meissner, and K. Kubodera. Chiral perturbation approach to the  $pp \rightarrow pp\pi^0$  reaction near threshold. *Phys. Rev. C*, **53**:1519–1531, 1996.
- [72] V. Dmitrasinovic, K. Kubodera, F. Myhrer, and T. Sato. A next-to-next-to leading-order  $pp \rightarrow pp\pi^0$  transition operator in chiral perturbation theory. *Phys. Lett. B*, **465**:43–54, 1999.
- [73] S.-I. Ando, T.-S. Park, and D.-P. Min. Threshold  $pp \rightarrow pp\pi^0$  up to one-loop accuracy. *Phys. Lett. B*, **509**:253–262, 2001.
- [74] C. Hanhart, G. A. Miller, F. Myhrer, T. Sato, and U. van Kolck. Toy model for pion production in nucleon nucleon collisions. *Phys. Rev. C*, **63**:044002, 2001.
- [75] A. Motzke, C. Elster, and C. Hanhart. Toy model for pion production 2: The role of three particle singularities. *Phys. Rev. C*, **66**:054002, 2002.
- [76] V. Malafaia and M. T. Peña. Pion re-scattering in  $\pi^0$  production. *Phys. Rev. C*, **69**:024001, 2004.
- [77] Y. Kim, I. Danchev, K. Kubodera, F. Myhrer, and T. Sato. Use of  $V_{\text{low-k}}$  in a chiral-perturbation-theory description of the  $pp \rightarrow pp\pi^0$  reaction. *Phys. Rev. C*, **73**:025202, 2006.
- [78] V. Bernard, N. Kaiser, and U.-G. Meißner. Novel approach to pion and eta production in proton proton collisions. *Eur. Phys. J. A*, **4**:259–275, 1999.
- [79] C. Hanhart, U. van Kolck, and G. A. Miller. Chiral three-nucleon forces from  $p$ -wave pion production. *Phys. Rev. Lett.*, **85**:2905–2908, 2000.

- [80] P. N. Deepak, J. Haidenbauer, and C. Hanhart. Partial-wave analysis of  $\vec{p}\vec{p} \rightarrow pp\pi^0$  data. *Phys. Rev. C*, **72**:024004, 2005.
- [81] V. Lensky, V. Baru, A. Kudryavtsev, J. Haidenbauer, C. Hanhart, and U.-G. Meißner. Towards a field theoretic understanding of  $NN \rightarrow NN\pi$ . *Eur. Phys. J. A*, **27**:37–45, 2006.
- [82] V. Lensky, V. Baru, A. Kudryavtsev, J. Haidenbauer, C. Hanhart, and U.-G. Meißner. Precision calculation of  $\gamma d \rightarrow \pi^+ nn$  within chiral perturbation theory. *Eur. Phys. J. A*, **26**:107–123, 2005.
- [83] A. Nogga and C. Hanhart. Can one extract the  $\pi$  neutron scattering length from  $\pi$  deuteron scattering? *Phys. Lett. B*, **634**:210–213, 2006.
- [84] R. Haag. Quantum field theories with composite particles and asymptotic conditions. *Phys. Rev.*, **112**:669–673, 1958.
- [85] H. Lehmann, K. Symanzik, and W. Zimmermann. On the formulation of quantized field theories. *Nuovo Cim.*, **1**:205–225, 1955.
- [86] D. A. Hutcheon et al. Measurements of  $NN \rightarrow d\pi$  very near threshold. 1. The  $np \rightarrow d\pi^0$  cross-section. *Nucl. Phys. A*, **535**:618–636, 1991.
- [87] R. Machleidt. The high-precision, charge-dependent Bonn nucleon-nucleon potential (CD-Bonn). *Phys. Rev. C*, **63**:024001, 2001.
- [88] R. B. Wiringa, V. G. J. Stoks, and R. Schiavilla. Accurate nucleon-nucleon potential with charge-independence breaking. *Phys. Rev. C*, **51**:38–51, 1995.
- [89] J. Haidenbauer, K. Holinde, and M. B. Johnson. Coupled-channel potential for nucleons and Deltas. *Phys. Rev. C*, **48**:2190–2200, 1993.
- [90] C. Hajduk and P. U. Sauer. Effect of the Delta (1236) isobar on the three nucleon bound states. *Nucl. Phys. A*, **322**:329–348, 1979.
- [91] C. Hajduk, P. U. Sauer, and W. Struve. Properties of the three nucleon bound states with virtual Delta isobar excitation. *Nucl. Phys. A*, **405**:581–605, 1983.
- [92] P. Heimberg et al. Measurement of the  $pp \rightarrow d\pi^+$  cross-section and analyzing power at threshold. *Phys. Rev. Lett.*, **77**:1012–1015, 1996.
- [93] M. Drochner et al. The  $p+p \rightarrow \pi^+ + d$  reaction close to threshold at COSY. *Nucl. Phys. A*, **643**:55–82, 1998.
- [94] P. Hauser et al. New precision measurement of the pionic deuterium S-wave strong interaction parameters. *Phys. Rev. C*, **58**:1869–1872, 1998.
- [95] H. Machner and J. Niskanen. Charge independence studied in  $NN \rightarrow d\pi$  reactions. *Nucl. Phys. A*, **776**:172–188, 2006.

- [96] I. S. Gerstein, R. Jackiw, S. Weinberg, and B. W. Lee. Chiral loops. *Phys. Rev. D*, **3**:2486–2492, 1971.
- [97] V. Bernard, N. Kaiser, and U.-G. Meißner. Chiral corrections to the S-wave pion–nucleon scattering lengths. *Phys. Lett. B*, **309**:421–425, 1993.
- [98] P. N. Deepak and G. Ramachandran. Singlet and triplet differential cross sections for  $pp \rightarrow pp\pi^0$ . *Phys. Rev. C*, **65**(2):027601, 2002.
- [99] W. W. Daehnick et al. Spin correlations in  $\vec{p}\vec{p} \rightarrow pn\pi^+$  pion production near threshold. *Phys. Rev. C*, **65**:024003, 2002.
- [100] B. von Przewoski et al. Measurement of spin correlation coefficients in  $\vec{p}\vec{p} \rightarrow d\pi^+$ . *Phys. Rev. C*, **61**:064604, 2000.
- [101] M. Daum et al. The reaction  $np \rightarrow pp\pi^-$  from threshold up to 570 MeV. *Eur. Phys. J. C*, **23**:43–59, 2002.
- [102] M. Daum et al. Analysing powers for the reaction  $np \rightarrow pp\pi^-$  and for  $np$  elastic scattering from 270 MeV to 570 MeV. *Eur. Phys. J. C*, **25**:55–65, 2002.
- [103] E. C. Booth, B. Chasan, J. Comuzzi, and P. Bosted.  ${}^2H(\gamma, \pi^+)nn$  total cross section from threshold to  $\Delta E = 22$  MeV. *Phys. Rev. C*, **20**:1217–1220, 1979.
- [104] A. Gårdestig and D. R. Phillips. Using chiral perturbation theory to extract the neutron neutron scattering length from  $\pi^-d \rightarrow nn\gamma$ . *Phys. Rev. C*, **73**:014002, 2006.
- [105] M. I. Levchuk, M. Schumacher, and F. Wissmann. The reaction  ${}^2H(\gamma, \pi^0)np$  in the threshold region. *Nucl. Phys. A*, **675**:621–636, 2000.
- [106] M. Benmerrouche and E. Tomusiak.  $\gamma d \rightarrow \pi^0 d$  reaction in the threshold region. *Phys. Rev. C*, **58**:1777–1789, 1998.
- [107] M. P. Rekaló and E. Tomasi-Gustafsson. Considerations on rescattering effects for threshold photo- and electro-production of  $\pi^0$  on deuteron. *Phys. Rev. C*, **66**:015203, 2002.
- [108] V. E. Tarasov, V. V. Baru, and A. E. Kudryavtsev. Near-threshold amplitude of pion–deuteron scattering: One-loop contributions. *Phys. Atom. Nucl.*, **63**:801–811, 2000.
- [109] F. Myhrer. Validity of the impulse approximation in meson - nucleus scattering. *Nucl. Phys. A*, **241**:524–532, 1975.
- [110] G. Fåldt. Binding corrections and the pion - deuteron scattering length. *Phys. Scripta*, **16**:81–86, 1977.
- [111] O. D. Dalkarov, V. M. Kolybasov, and V. G. Ksenzov. Nonadiabatic effects in nuclear reactions and the problem of determination of the proton electromagnetic form-factor in the nonphysical region. *Nucl. Phys. A*, **397**:498, 1983.

- [112] S. R. Beane, V. Bernard, T. S. H. Lee, U.-G. Meißner, and U. van Kolck. Neutral pion photoproduction on deuterium in baryon chiral perturbation theory to order  $q^4$ . *Nucl. Phys. A*, **618**:381–401, 1997.
- [113] N. M. Kroll and M. A. Ruderman. A theorem on photomeson production near threshold and the suppression of pairs in pseudoscalar meson theory. *Phys. Rev.*, **93**:233–238, 1954.
- [114] V. Bernard, N. Kaiser, and U.-G. Meißner. Threshold pion photoproduction in chiral perturbation theory. *Nucl. Phys. B*, **383**:442–496, 1992.
- [115] V. Bernard, N. Kaiser, J. Gasser, and U.-G. Meißner. Neutral pion photoproduction at threshold. *Phys. Lett. B*, **268**:291–295, 1991.
- [116] E. Korkmaz et al. Measurement of the  $\gamma p \rightarrow \pi^+ n$  reaction near threshold. *Phys. Rev. Lett.*, **83**:3609–3612, 1999.
- [117] H. W. Fearing, T. R. Hemmert, R. Lewis, and C. Unkmeir. Radiative pion capture by a nucleon. *Phys. Rev. C*, **62**(5):054006, 2000.
- [118] O. Hanstein, D. Drechsel, and L. Tiator. Multipole analysis of pion photoproduction based on fixed  $t$  dispersion relations and unitarity. *Nucl. Phys. A*, **632**:561–606, 1998.
- [119] D. B. Kaplan, M. J. Savage, and M. B. Wise. Two-nucleon systems from effective field theory. *Nucl. Phys. B*, **534**:329–355, 1998.
- [120] S. R. Beane, V. Bernard, E. Epelbaum, U.-G. Meißner, and D. R. Phillips. The  $S$ -wave pion nucleon scattering lengths from pionic atoms using effective field theory. *Nucl. Phys. A*, **720**:399–415, 2003.
- [121] J. Haidenbauer and W. Plessas. On separable approximations of two-body interactions. *Phys. Rev. C*, **27**:63–70, 1983.
- [122] J. Haidenbauer and W. Plessas. Separable representation of the Paris nucleon–nucleon potential. *Phys. Rev. C*, **30**:1822–1839, 1984.
- [123] C. R. Howell et al. Toward a resolution of the neutron-neutron scattering-length issue. *PLB*, **444**:252, 1998.
- [124] D. E. González Trotter, F. Salinas, Q. Chen, A. S. Crowell, W. Glöckle, C. R. Howell, C. D. Roper, D. Schmidt, I. Šlaus, H. Tang, W. Tornow, R. L. Walter, H. Witała, and Z. Zhou. New measurement of the  $^1S_0$  neutron-neutron scattering length using the neutron-proton scattering length as a standard. *Phys. Rev. Lett.*, **83**:3788–3791, 1999.
- [125] V. Huhn et al. New investigation of the neutron neutron and neutron proton final state interaction in the  $nd$  breakup reaction. *Phys. Rev. C*, **63**:014003, 2001.
- [126] C. Tzara and N de Botton. Internal Report DPhN/HE 78/06. Technical report, Saclay, 1978.

- [127] U.-G. Meißner, U. Raha, and A. Rusetsky. The pion nucleon scattering lengths from pionic deuterium. *Eur. Phys. J. C*, **41**:213–232, 2005.
- [128] G. A. Miller, B. M. K. Nefkens, and I. Šlaus. Charge symmetry, quarks and mesons. *Phys. Rept.*, **194**:1–116, 1990.
- [129] B. Gabioud et al.  $nn$  scattering parameters  $a_{nn}$  and  $r_{nn}$  from the photon spectrum of the reaction  $\pi^-d \rightarrow \gamma nn$ . *Nucl. Phys. A*, **420**:496–524, 1984.
- [130] O. Schori et al. Measurement of the neutron-neutron scattering length  $a_{nn}$  with the reaction  $\pi^-d \rightarrow nn\gamma$  in complete kinematics. *Phys. Rev. C*, **35**:2252–2257, 1987.
- [131] V. Huhn, L. Wätzold, Ch. Weber, A. Siepe, W. von Witsch, H. Witała, and W. Glöckle. New attempt to determine the  $nn$  scattering length with the  ${}^2H(n, np)n$  reaction. *Phys. Rev. Lett.*, **85**:1190–1193, 2000.
- [132] D. E. Gonzalez Trotter, F. Salinas Meneses, W. Tornow, C. R. Howell, Q. Chen, A. S. Crowell, C. D. Roper, R. L. Walter, D. Schmidt, H. Witala, W. Glockle, H. Tang, Z. Zhou, and I. Šlaus. Neutron-deuteron breakup experiment at  $e_n = 13$  mev: Determination of the  ${}^1S_0$  neutron-neutron scattering length  $a_{nn}$ . *Phys. Rev. C*, **73**:034001, 2006.
- [133] R. Machleidt and H. Mütter. Charge symmetry breaking of the nucleon-nucleon interaction:  $\rho - \omega$  mixing versus nucleon mass splitting. *Phys. Rev. C*, **63**:034005, 2001.
- [134] A. Nogga, A. Kievsky, H. Kamada, W. Glöckle, L.E. Marcucci, S. Rosati, and M. Viviani. Three-nucleon bound states using realistic potential models. *Phys. Rev. C*, **67**:034004, 2003.
- [135] A. Gårdestig and D. R. Phillips. How low-energy weak reactions can constrain three-nucleon forces and the neutron-neutron scattering length. *Phys. Rev. Lett.*, **96**:232301, 2006.
- [136] A. Gasparyan, J. Haidenbauer, C. Hanhart, and K. Miyagawa.  $\Lambda n$  scattering length from the reaction  $\gamma d \rightarrow K^+ \Lambda n$ . *EPJA*, 2007.
- [137] A. Gårdestig. Chiral  $\mathcal{O}(Q^4)$  two-body operators for  $s$ -wave pion photoproduction on the  $NN$  system. *Phys. Rev. C*, **74**:017001, 2006.
- [138] D. Chatellard et al. X-ray spectroscopy of the pionic deuterium atom. *Nucl. Phys. A*, **625**:855–872, 1997.
- [139] D. Gotta et al. PSI experiment R-06.03; D. Gotta, private communications.
- [140] M. Döring, E. Oset, and M. J. Vicente Vacas. S-wave pion nucleon scattering length from  $\pi N$ , pionic hydrogen and deuteron data. *Phys. Rev. C*, **70**:045203, 2004.



- [141] M. Pavon Valderrama and E. Ruiz Arriola. Renormalization of the deuteron with one pion exchange. *Phys. Rev. C*, **72**:054002, 2005.
- [142] M. Pavon Valderrama and E. Ruiz Arriola. Pion deuteron scattering and chiral expansions. 2006. arXiv:nucl-th/0605078.
- [143] L. Platter and D. R. Phillips. Deuteron matrix elements in chiral effective theory at leading order. *Phys. Lett. B*, **641**:164–170, 2006.
- [144] U.-G. Meißner, U. Raha, and A. Rusetsky. Isospin-breaking corrections in the pion deuteron scattering length. *Phys. Lett. B*, **639**:478–482, 2006.
- [145] A. W. Thomas and R. H. Landau. Pion - deuteron and pion - nucleus scattering: a Review. *Phys. Rept.*, **58**:121, 1980.
- [146] V. L. Highland et al. Branching ratios for stopped pions in deuterium. *Nucl. Phys. A*, **365**:333, 1981.
- [147] K. A. Brückner. Energy levels of  $\pi$ -mesonic atoms. *Phys. Rev.*, **98**(3):769–771, 1955.
- [148] I. R. Afnan and A. W. Thomas. Faddeev approach to pion production and pion deuteron scattering. *Phys. Rev. C*, **10**:109–125, 1974.
- [149] T. Mizutani and D. S. Koltun. Coupled channel theory of pion - deuteron reaction applied to threshold scattering. *Annals Phys.*, **109**:1–40, 1977.
- [150] T. E. O. Ericson, B. Loiseau, and A. W. Thomas. Determination of the pion nucleon coupling constant and scattering lengths. *Phys. Rev. C*, **66**:014005, 2002.
- [151] V. V. Baru and A. E. Kudryavtsev.  $\pi N$  scattering lengths from an analysis of new data on pionic hydrogen and deuterium atoms. *Phys. Atom. Nucl.*, **60**:1476, 1997.
- [152] B. Borasoy and H. W. Griebhammer. Pion deuteron scattering length in effective field theory. *Int. J. Mod. Phys. E*, **12**:65–80, 2003.
- [153] S. R. Beane and M. J. Savage. Pions in the pionless effective field theory. *Nucl. Phys. A*, **717**:104–113, 2003.
- [154] D. J. Thouless. In *Proc. Phys. Soc. (London)*, volume 69. 1956.
- [155] B. K. Jennings. On the  $P(11)$  problem in  $\pi$  - deuteron scattering. *Phys. Lett. B*, **205**:187, 1988.
- [156] H. Garcilazo and T. Mizutani. In  *$\pi NN$  Systems*. World Scientific, Singapore, 1990.
- [157] C. Hanhart and K. Nakayama. On the treatment of  $NN$  interaction effects in meson production in  $NN$  collisions. *Phys. Lett. B*, **454**:176–180, 1999.

- [158] T. E. O. Ericson and A. N. Ivanov. Dispersive e. m. corrections to  $\pi N$  scattering lengths. *Phys. Lett. B*, **634**:39–47, 2006.
- [159] J. Gasser, A. Rusetsky, and I. Scimemi. Electromagnetic corrections in hadronic processes. *Eur. Phys. J. C*, **32**:97–114, 2003.
- [160] V. B. Berestetsky, E. M. Lifshitz, and L. P. Pitaevsky. *Quantum Electrodynamics (Landau and Lifshitz Course of Theoretical Physics, Vol. 4)*. Pergamon Press, Oxford, UK, 1982.
- [161] R. M. Rockmore. Charge asymmetry of the  $\pi d$  scattering length. *Phys. Lett. B*, **356**:153–156, 1995.
- [162] <http://higs.tunl.duke.edu/>.
- [163] C. Hanhart. *Pion-Produktion in Proton-Proton-Stößen*. PhD thesis, Universität Bonn, 1997. (Forschungszentrum Jülich Report Jül-3476, 1997).
- [164] D. A. Varshalovich, A. N. Moskalev, and V. K. Khersonskii. *Quantum Theory of Angular Momentum*. World Scientific, 1988.
- [165] N. Ya. Vilenkin. *Special Functions and the Theory of Group Representations*. American Mathematical Society, 1983.
- [166] I. M. Gel'fand, R. A. Minlos, and Z. Ya. Shapiro. *Representations of the rotation and Lorentz groups and their applications*. MacMillan, 1963.
- [167] A. F. Nikiforov and V. B. Uvarov. *Special Functions of Mathematical Physics*. Birkhauser, 1988.
- [168] M. Lacombe, B. Loiseau, R. Vinh Mau, J. Cote, P. Pires, and R. de Tournell. Parameterization of the deuteron wave function of the Paris  $NN$  potential. *Phys. Lett. B*, **101**:139–140, 1981.